Linear Stability Analysis of Viscous and Nanofluid Flows in Horizontal/Vertical Channels

A Thesis Submitted to
NATIONAL INSTITUTE OF TECHNOLOGY WARANGAL, (T.S.)
for the award of the degree of
DOCTOR OF PHILOSOPHY
IN
MATHEMATICS

BY
DIPAK BARMAN
(Roll No. 717158)

UNDER THE SUPERVISION OF
Prof. D. SRINIVASACHARYA

DEPARTMENT OF MATHEMATICS
NATIONAL INSTITUTE OF TECHNOLOGY
WARANGAL - 506 004, INDIA

JUNE 2021

C E R T I F I C A T E

This is to certify that the thesis entitled " **Linear Stability Analysis of Viscous and Nanofluid Flows in Horizontal/Vertical Channels** " submitted to National Institute of Technology Warangal, for the award of the degree of ***Doctor of Philosophy***, is the bonafide research work done by **Mr. DIPAK BARMAN** under my supervision. The contents of this thesis have not been submitted elsewhere for the award of any degree.

Dr. D. Srinivasacharya
Professor
Department of Mathematics
National Institute of Technology Warangal
Telangana State, INDIA

.

DECLARATION

This is to certify that the work presented in the thesis entitled **" Linear Stability Analysis of Viscous and Nanofluid Flows in Horizontal/Vertical Channels"**, is a bonafide work done by me under the supervision of **Prof. D. SRINIVASACHARYA** and has not been submitted elsewhere for the award of any degree.

I declare that this written submission represents my ideas in my own words and where others' ideas or words have been included, I have adequately cited and referenced the original sources. I also declare that I have adhered to all principles of academic honesty and integrity and have not misrepresented or fabricated or falsified any idea / data / fact /source in my submission. I understand that any violation of the above will be a cause for disciplinary action by the Institute and can also evoke penal action from the sources which have thus not been properly cited or from whom proper permission has not been taken when needed.

Dipak Barman

Roll No. 717158

Date:_____

Dedicated to

My Parents, Teachers
&
Sri Sri Swami Nigamananda Saraswati Paramahansa Dev

ACKNOWLEDGEMENTS

It is a rare privilege and boon that I could associate myself with Dr. D. Srinivasacharya, Professor of Mathematics, National Institute of Technology Warangal, India, for pursuing my research work. I sincerely extend my gratitude to him for his invaluable guidance and constant encouragement throughout the preparation of this thesis and his involvement and meticulous supervision while my work was in progress. With his inimitable qualities as a good teacher, he chiseled my path towards perfection. Ever since I met him, he has been a perpetual source of motivation, inspiration, encouragement and enlightenment. He is responsible for making the period of my research work as an educative and enjoyable learning experience. The thesis would not have seen the light of the day without his unrelenting support and cooperation. I deem it a privilege to have worked under his amiable guidance. My vocabulary is inadequate to express my gratitude.

I am grateful to Prof. G. Radhakrishnamacharya (Retd.), Prof. Y. N. Reddy, Prof. K.N.S. Kasi Viswanadham, Prof. J. V. Ramana Murthy and Prof. Debashis Dutta, Department of Mathematics, National Institute of Technology Warangal for their help and support throughout my research period.

I thank the members of the Doctoral Scrutiny Committee, Dr. J. Pranitha, Dr. Ch. Ramreddy, Department of Mathematics, National Institute of Technology Warangal and Dr. S. Srinath, Department of Chemical Engineering, National Institute of Technology Warangal for their valuable suggestions, moral support and encouragement while my work was in progress.

I place on record my gratitude to Dr. P. Muthu (Head) and all other faculty members of the Department of Mathematics, National Institute of Technology Warangal for their constant encouragement. Also, I thank the office staff.

I express my cordial thanks to Prof. N. V. Ramana Rao, Director, National Institute of Technology, Warangal for awarding me Institute Fellowship (MHRD, GoI) to carry out my research work. I thank him for his kind support and encouragement at every stage of this endeavor.

I express my sincere thanks and gratitude to Prof. D. A. S. Rees, Department of Mechanical Engineering, University of Bath, United Kingdom and Prof. Jitesh S. B. Gajjar, School of Mathematics, The University of Manchester, United Kingdom for their valuable suggestions to enrich my research.

I owe my special thanks to Dr. T. Pradeepa, Dr. M. Varun Kumar, Dr. Venkata Rao, Dr. P. Jagadeeshwar, Dr. G. Nithish Kumar, Dr. G. Venkata Suman, Dr. P. Naveen, Dr. I. Sreenath, Dr. G. Shiva Kumar, for their support. I thank Mr. Omprakash, Mr. Ramana, Mr. Abhinav, and all other research colleagues in the Department of Mathematics, National Institute of Technology Warangal and my friends, who helped me during my Ph.D for being cooperative and also for making my stay in the NITW campus fruitful and enjoyable every moment.

My deepest gratitude to my Parents, Sri. Dwijen Barman and Smt. Chabi Barman, brother, Mr. Pankaj Barman, and other family members for their continuous support and constant encouragement over the years. All of their love and affection have been motivating force behind what I am today.

My sincere thanks to Sri. Monotosh Chakravarty for his constant support and encouragement throughout my career.

Finally, last but not the least, I would like to thank Binandita Barman for her continuous support and encouragement throughout my Ph.D. journey.

. Dipak Barman

A B S T R A C T

The study of convective transport through porous media has been a fascinating and prominent topic during recent years because of its relevance in a wide range of industrial and engineering applications. Further, the convective instability in a fluid-saturated porous layer heated from below had been an area that attracted the interest of researchers over many years under different physical conditions. It has many applications in geophysics, food processing, oil reservoir modelling, the building of thermal insulations and nuclear reactors. The prophecy of the instability mechanism of incompressible viscous and nanofluid flow through a porous medium is very important because of its practical applications in engineering. A viscous fluid is a fluid that flows like water - its stress versus the rate of strain curve is linear and passes through the origin. Nanofluids are prepared by the uniform dispersion and suspension of nanometer-sized metallic particles into conventional heat transfer fluids such as water, oil, or ethylene glycol. The main aim of the thesis is to investigate the linear stability analysis of incompressible viscous and nanofluid flow in a horizontal/vertical channel filled with a porous medium.

This thesis consists of four parts and twelve chapters. Part - I consists of a single chapter (Chapter-1), which provides an introduction to the concepts of viscous fluid, nanofluid and porous medium and a review of the pertinent literature.

Part-II contains four chapters (Chapters 2, 3, 4 and 5). Chapter - 2 deals with the impact of variable gravity on the stability of the viscous fluid saturated porous layer using Darcy law due to the combined effects of the Soret parameter, vertical throughflow and viscous dissipation. In Chapter - 3, the influence of viscous dissipation, vertical throughflow and variable gravity field on the stability in a horizontal porous layer filled with a viscous fluid using the Brinkman model is examined. Chapter - 4 considers the effect of variable gravity on the onset of convection in a porous horizontal channel filled with viscous fluid subjected to third kind boundary conditions. In Chapter - 5, the influence of variable gravity, vertical throughflow and local thermal non-equilibrium (LTNE) on the stability in a horizontal porous channel is presented.

Part-III contains six chapters (Chapters 6, 7, 8, 9, 10 and 11). Chapter - 6 analyzes the linear stability of the nanofluid flow in a vertical porous channel. Chapter - 7 explores the impact of the transverse magnetic effect on the instability mechanism of double-diffusive convection in a vertical channel filled with nanofluid. In Chapter - 8, the effect of local thermal non-equilibrium on the stability of nanofluid flow in a vertical channel filled with a porous medium is examined. Chapter - 9 presents the local thermal non-equilibrium effect

on the convective instability in a vertical channel filled with nanofluid in the presence of the transverse magnetic field. In Chapter - 10, the effect of varying gravity field on the onset of convection in a horizontal porous channel filled with a nanofluid under free-free, rigid-free, and rigid-rigid boundaries is considered. The onset of convection in a non-Darcy horizontal porous layer filled with nanofluid due to the viscous dissipation effect is discussed in Chapter - 11.

In all the above chapters, the non-linear governing equations and their associated boundary conditions are initially cast into dimensionless form by using a suitable set of non-dimensional transformations and convert them system of linear ordinary differential equations by using linear stability analysis along with normal mode technique. The resulting system of ordinary differential equations is solved using either *bvp4c* routine in MATLAB or Chebyshev spectral collocation method. The influence of pertinent parameters on the onset of convection is presented through graphs and in tabular form. Moreover, the pattern of the streamlines, isotherms and isonanoconcentrations are plotted at a critical level over one period for some problems.

Part - IV consists of a single chapter (Chapter - 12), which gives a summary and overall conclusions and scope for future work.

NOMENCLATURE

a	overall wave number
B	strength of the magnetic field
B_0, B_1	Biot numbers
$\mathbf{B}_0$	uniform magnetic field
c	wave speed
c_{p}	specific heat at constant pressure
C	concentration
C_1, C_2	constant concentrations
D	mass diffusivity
Da	Darcy number
D_{B}	Brownian diffusion coefficient
D_{CT}	Soret type diffusivity
D_{f}	Dufour parameter
D_{S}	solutal diffusivity
D_{T}	thermophoretic diffusion coefficient
D_{TC}	Dufour type diffusivity
$\mathbf{g}$	gravitational acceleration
g_0	reference gravity
Ge	Gebhart number
$\mathrm{g}(z)$	variable gravity function
h	interphase heat transfer coefficient
H	heat transfer parameter
Ha	Hartmann number
$\mathbf{j}$	current
k	thermal conductivity
K	permeability
L	layer thickness
Le	Lewis number
Le_{m}	modified Lewis number
Ln	thermo-solutal Lewis number
N_{A}	modified diffusivity ratio
N_{B}	modified particle density increment
N_{HP}	Nield number for the fluid/particle interface
N_{HS}	Nield number for the fluid/solid-matrix interface
p	pressure
Pr	Prandtl number
Pr_{m}	modified Prandtl number
q_0	constant heat flux
Q	throughflow parameter
Re	Reynolds number
Ra	Rayleigh number

Rm	basic density Rayleigh number
Rn	concentration Rayleigh number
Rs	solutal Rayleigh number
Sr	Soret parameter
t	time
T	temperature
T_1, T_2	constant temperatures
T_m	reference temperature
$\mathbf{u}$	Darcy velocity
$\mathbf{v}$	Nanofluid velocity
V_0	basic velocity
Va	Vadasz number
W_c	upward throughflow
(u, v, w)	velocity components along x, y and z directions
(x, y, z)	Cartesian coordinates

Greek symbols

α	streamwise wave number
α_f	thermal diffusivity for fluid phase
α_nf	thermal diffusivity for nanofluid
α_m	thermal diffusivity of the porous medium
β	spanwise wave number
β_C	solutal expansion coefficient
β_T	thermal expansion coefficient
γ_m	heat capacity ratio
$\gamma_\mathrm{P}, \gamma_\mathrm{S}$	modified thermal capacity ratios
δ	small disturbance parameter
ϵ	porosity
ε_m	thermal diffusivity ratio
$\varepsilon_\mathrm{P}, \varepsilon_\mathrm{S}$	modified thermal diffusivity ratios
η	growth rate
λ	gravity variation parameter
Λ	viscosity ratio
μ	dynamic viscosity
$\tilde{\mu}$	effective dynamic viscosity
ν	kinematic viscosity
ρ	density
ρ_f	density for the fluid
ρ_p	particle density
$(\rho c)_\mathrm{f}$	heat capacity of the fluid
$(\rho c)_\mathrm{p}$	heat capacity of the particle material
$(\rho c)_\mathrm{s}$	heat capacity of the solid-matrix material
σ	thermal capacity ratio
σ_1	electric conductivity
ϕ	volume fraction
ϕ_1, ϕ_2	constant volume fractions

ψ	stream function
ω	angular frequency

Superscripts

$*$	dimensionless variable
$'$	perturbation variable
tr	transpose of a matrix

Subscripts

0	basic solution
c	critical
f	fluid phase
p	particle phase
s	solid phase
H	horizontal component

Contents

[1] Published in "***International Communications in Heat and Mass Transfer***" 120, ID No. 105050, 2021

[2] Published in "***Journal of Porous Media***" 24(6), 1-13, 2021

[3] Communicated in "***Indian Journal of Physics***"

[4] Communicated in "***International Communications in Heat and Mass Transfer***"

[5] Published in "***Heat Transfer***" 50(4), 3220-3239, 2021

[6] Communicated in "***Journal of Porous Media***"
[7] Accepted in "***Journal of Heat Transfer***"

[8] Communicated in "***Special Topics & Reviews in Porous Medium - An international journal***"
[9] Published in "***Computational Thermal Sciences: An International Journal***", 13(6), 1-17, 2021
[10] Communicated in "***Thermal Science and Engineering Progress***"

Part I

INTRODUCTION

Chapter 1

Preliminaries and Review

1.1 Introduction

Convective transport in porous media has gained prominence in recent years due to its numerous applications in mechanical, chemical, and civil engineering. These applications include migration of moisture in fibrous insulation, the spreading of chemical pollutants in saturated soil, the extraction of geothermal energy, food processing and storage, geophysical systems, underground disposal of nuclear or non-nuclear waste, electro-chemistry, thermal insulation of buildings, metallurgy, the design of pebble-bed nuclear reactors, the cooling system of electronic devices, etc. For the past several decades, many researchers have studied convective heat and mass transfer in porous media under various physical conditions.

Engineered suspensions of nanoparticles in liquids, known recently as nanofluids, have attracted the attention of many researchers due to their potential to improve heat transfer rates in engineering systems, while lowering, or possibly removing, the erosion, sedimentation, and clogging issues that crippled previous solid-liquid mixtures with larger particles. Nanofluids can be employed in a variety of technical applications, including the automobile industry, medicinal applications, power plant cooling systems, and computer systems. The convection due to heated/cooled objects of various geometries under different physical conditions in a nanofluid saturated porous medium yields one of the most important scenarios for heat and mass transfer theory and thus is of considerable theoretical and practical interest.

In the mathematical study of a physical system, the concept of stability has a major impact on development. Stability characteristics can be a critical consideration for the practical application of many technical systems, as demonstrated by real-world examples. Stability is important in engineering constructions (bridges, plates, shells structures under pressure loading or unloading by flowing fluids), high-speed vehicles, truck-trailer combinations, railway trains, and hydrodynamics challenges, to name a few. The response of laminar flow to a small amplitude perturbation is referred to as hydrodynamic stability. A flow is characterised as stable if it returns to its previous (laminar) state after a period of time and remains in that state, whereas it is characterised as unstable if it transitions into a different state. Over the last few decades, researchers have used a linearized stability analysis to solve many of their hydrodynamic and hydromagnetic stability problems in different geometries using diverse fluid models.

1.2 Newtonian Fluids

A Newtonian fluid is one in which the viscous stresses generated from its flow are linearly proportional to the local strain rate, or the rate at which its deformation changes over time, at every point. A fluid is Newtonian if the tensors describing viscous stress and strain rate are related by a constant viscosity tensor that is dependent on basic thermodynamic variables such as temperature and pressure but independent of flow parameters such as shear rate and time. Newtonian fluids are the simplest mathematical models of fluids that account for viscosity. Fluids such as water, oil or ethylene glycol all are Newtonian.

1.3 Nanofluids

Conventional heat transfer fluids like water, ethylene glycol, and oil have relatively low thermal conductivities when compared to the thermal conductivity of solids. Hence, an innovative way of improving the thermal conductivities of fluids is to suspend small solid particles, such as nanometre- or nanometre-sized particles, into the conventional fluids. A nanofluid is a mixture of a regular fluid with a very small amount of suspended metallic or metallic oxide nanoparticles or nanotubes [36]. Nanoparticle materials may be taken as oxide ceramics (Al_2O_3, CuO), metal carbides (SiC), nitrides (AlN, SiN) or metals (Al, Cu) etc. Base fluids may be water, ethylene or tri-ethylene–glycols and other coolants, oil and other lubricants, bio-fluids and polymer solutions. Nanofluids exhibit exceptionally high thermal

conductivity, as well as a significant change in properties such as viscosity and specific heat when compared to the base fluid. During the past decade, the study of nanofluids has attracted immense enthusiasm from researchers in view of its exceptional applications in electronics, communication, high-power X-rays, computing technologies, medicine, lasers, scientific measurement, optical devices, material processing and material synthesis [26, 39, 74].

Several models and methods for studying the convective flows of nanofluids have been proposed by various authors. Two models namely, the Tiwari-Das model [111] and the Buongiorno model [25] are more frequently used by several researchers to investigate the heat transfer enhancement by very fine particles suspended in a fluid. Tiwari and Das developed a model to analyze the behaviour of nanofluids by taking the volumetric fraction of nanoparticles into consideration. Buongiorno considered seven slip mechanisms, namely, inertia, Brownian diffusion, thermophoresis, diffusiophoresis, magnus effect, fluid drainage, and gravity that can produce a relative velocity between nanoparticles and the base fluid. In the absence of turbulent effects, he concluded that only Brownian diffusion and thermophoresis are important slip mechanisms in nanofluids. Based on this observation, Buongiorno proposed a mathematical model for the nanofluid based on these effects. **Brownian motion** refers to the arbitrary movement of nanoparticles within the base fluid. This is caused by continuous collisions between nanoparticles and base fluid molecules. The phenomenon of particle diffusion under the influence of a temperature gradient is known as **thermophoresis** and is the "particle" equivalent of the renowned Soret effect for gaseous or liquid mixtures.

The basic equations of continuity, momentum and energy and nanoparticle concentration for this model are given by

$$\nabla \cdot \mathbf{v} = 0, \tag{1.1}$$

$$\rho_{\mathrm{f}} \left(\frac{\partial \mathbf{v}}{\partial t} + \mathbf{v} \cdot \nabla \mathbf{v} \right) = \rho_{\mathrm{f}} \mathbf{g} - \nabla p + \mu \, \nabla^2 \mathbf{v}, \tag{1.2}$$

$$\left(\frac{\partial T}{\partial t} + \mathbf{v} \cdot \nabla T \right) = \alpha_{\mathrm{nf}} \nabla^2 T + \sigma \left[D_{\mathrm{B}} \, \nabla \phi \cdot \nabla T + \frac{D_{\mathrm{T}}}{T_{\mathrm{m}}} \, \nabla T \cdot \nabla T \right], \tag{1.3}$$

$$\left(\frac{\partial \phi}{\partial t} + \mathbf{v} \cdot \nabla \phi \right) = D_{\mathrm{B}} \, \nabla^2 \phi + \frac{D_{\mathrm{T}}}{T_{\mathrm{m}}} \, \nabla^2 T. \tag{1.4}$$

where $\mathbf{v}$ is the velocity vector, T is the temperature of the nanofluid, ϕ is the nanoparticle volume fraction, D_{B} is the Brownian diffusion coefficient, D_{T} is the thermophoretic diffusion coefficient, T_{m} is the reference temperature, μ is the viscosity of the fluid, $\mathbf{g}$ is the gravita-

tional acceleration, $\alpha_{\rm nf}$ is the thermal diffusivity for nanofluid, and $\sigma = (\rho c)_{\rm p}/(\rho c)_{\rm f}$ is the ratio between heat capacity of nanofluid and nanoparticles.

1.4 Porous Medium

A porous medium is a solid matrix that contains holes, either connected or unconnected, that are dispersed inside the medium on a regular or random basis, provided that such holes occur frequently in the medium. If these pores are saturated with fluid, the solid matrix containing the fluid is referred to as a fluid-saturated porous medium. Fluid flow in a saturated porous material is only possible when some of the pores are connected.

To analyse the motion of fluids through porous media, a thorough knowledge of the governing equations for fluid flow through porous media is required. Because of the complex structure of porous media, several models have been proposed to describe the mathematical and physical aspects of porous media. Among these the Darcy model, and a series of its modifications, attained much acceptance.

Darcy Model

Darcy [38] was the first to present the governing equation for fluid motion in a vertical porous column. It is a balancing act of viscous force, gravitational force, and pressure gradient. In mathematical form, it is given as

$$\mathbf{u} = -\frac{K}{\mu}\left(\nabla P - \rho\,\mathbf{g}\right), \tag{1.5}$$

where $\mathbf{u}$ is the space averaged velocity (or Darcian velocity), K is the (intrinsic) permeability of the medium, μ is the coefficient of viscosity, P is the pressure, ρ is the density of the fluid and $\mathbf{g}$ is the gravitational acceleration. The above law appears to provide good agreement with experimental results for one-dimensional flows and low porosity systems. Because this model does not account for inertial effects, it is only applicable to seepage flows, i.e., flows with a low Reynolds number ($O(Re) < 1$).

Darcy-Forchheimer Model

In 1901, Forchheimer [47] carried out experiments and postulated that inertial effects can be accounted for by including a velocity squared term in the momentum equation. The modification to the Darcy's equation is

$$\left[1 + \frac{\rho\, c_{\mathrm{F}}\, \sqrt{K}}{\mu}|\mathbf{u}|\right] \mathbf{u} = -\frac{K}{\mu}\left[\nabla P - \rho \mathbf{g}\right], \tag{1.6}$$

where c_{F} is the dimensionless form drag coefficient and it varies with the nature of the porous medium. Darcy and Forchheimer coefficients include both the fluid properties and the microstructure of the porous medium. A number of experimental works have confirmed the model's validity.

Darcy-Brinkman Model

Brinkman [24] has corrected Darcy's equation with the addition of the Laplace term under the assumption that flow through an isotropic porous medium with high permeability must reduce to viscous flow in the limit. Brinkman recognised the importance of accounting for the viscous force exerted by a flowing fluid on a dense swarm of spherical particles embedded in a porous mass and added the term $\tilde{\mu}\,\nabla^2\mathbf{u}$ to balance the pressure gradient. Here $\tilde{\mu}$ is the effective viscosity given by $\tilde{\mu} = \mu(1 - 2.5(1-\epsilon))$. The validity of the Brinkman model is restricted to the high porosity medium (as confirmed by the experiments). Its governing equation is given by

$$-\left[\nabla P - \rho \mathbf{g}\right] = \frac{\mu}{K}\mathbf{u} - \tilde{\mu}\nabla^2\mathbf{u}. \tag{1.7}$$

Several other models are found in the literature related to porous media, the validity and limitations of these models are well discussed in Nield and Bejan [78].

1.5 Basic Terminology

Oberbeck-Boussinesq Approximation

The fluid density relies linearly on temperature and concentration differences for adequately small isobaric temperature and concentration changes ([112]). A convenient and simple way

to define the density difference $\rho - \rho_\infty$ in the buoyancy part of the momentum equation for nanofluids is given by

$$\rho = \phi\rho_{\mathrm{p}} + (1-\phi)\rho_{\mathrm{f0}}[1 - \beta_{\mathrm{T}}(T - T_0)], \tag{1.8}$$

where ρ_{p} is the nanoparticle density, ϕ is the nanoparticle volume fraction, T_0 is the reference temperature and ρ_{f0} is the fluid density at reference temperature at some point in the medium, β_{T} is the coefficient of thermal expansion. The Eq. (1.8) is an approximation for the variation of the density, and it is known as the Oberbeck-Boussinesq approximation, which states that

- Except for density in the momentum equation, all variations in fluid properties can be simply neglected.
- The density is considered to vary with the temperature only and its variations can be ignored everywhere except where they give rise to buoyancy force.

If the density ρ varies linearly with T over the range of values of the physical quantities encountered in the transport process, β_{T} in Eq. (1.8) are given by

$$\beta_{\mathrm{T}} = -\frac{1}{\rho}\left(\frac{\partial\rho}{\partial T}\right)_{\mathrm{p,C}}.$$

Convection

Convection is a mechanism in which the movement of fluid from one region to the other region because of density differences. The difference in density produces buoyancy forces when acted upon by gravity. Lighter, less dense fluid intends to rise in comparison to heavier fluid, while heavier fluid strives to sink in comparison to its lighter surroundings. When there is a horizontal component to the local temperature gradient, like a non-horizontal uniform layer of fluid is enclosed between two plane surfaces held at distinct but constant temperatures, the density variations drive the fluid motion directly. Free convection occurs when there is no motivating force, such as an applied pressure gradient. When the uniform layer of fluid is horizontal, no buoyancy forces occur since the temperature gradient vector is parallel to the gravity vector, and thus no flow occurs. However, if the layer is heated from below, the fluid would be susceptible to instability, and convective motion occurs if the buoyancy forces are good enough to withstand the viscous dissipative forces that act to keep the fluid in place.

Local Thermal Non-Equilibrium (LTNE)

Local thermal equilibrium (LTE) occurs when the temperature and rate of heat flux at the interface between the solid and fluid phases are in equilibrium. Thus, it is assumed that there is no heat transfer between the two phases. Generally, the assumption of LTE is valid if one of the phases dominates or if the characteristic length scale of the porous medium is small. This supposition is not appropriate for a large temperature change amongst the phases or high-speed flows. The solid and fluid phases having significantly different temperatures and the porous medium is said to be in Local Thermal Non-Equilibrium (LTNE). In such a situation, the fluid temperature fluctuates quickly with a location on a nano-scale particle and the system becomes quite complicated. Hence, separate temperature equations for solid particle and fluid phases to represent local thermal non-equilibrium (LTNE) are needed. Nield and Bejan [78] gave the simplest form of the heat transport equation as

$$(1-\epsilon)(\rho c)_{\mathrm{s}}\frac{\partial T_{\mathrm{s}}}{\partial t} = (1-\epsilon)\nabla \cdot k_{\mathrm{s}}\nabla T_{\mathrm{s}} + h(T_{\mathrm{f}} - T_{\mathrm{s}}), \tag{1.9}$$

$$\epsilon(\rho c_{\mathrm{p}})_{\mathrm{f}}\left[\frac{\partial T_{\mathrm{f}}}{\partial t} + \mathbf{u}\cdot\nabla T_{\mathrm{f}}\right] = \epsilon\nabla \cdot k_{\mathrm{f}}\nabla T_{\mathrm{f}} + h(T_{\mathrm{s}} - T_{\mathrm{f}}), \tag{1.10}$$

where h is the inter-phase heat transfer coefficient, ∇T is the temperature gradient and ϵ is the porosity of the porous medium. The subscripts s and f refer to the solid and fluid phases respectively. The specific heat of the solid is denoted by c, c_{p} is the specific heat at constant pressure of the fluid and k is the thermal conductivity.

Hydrodynamic Stability

A physical system is said to be stable when it returns to its original state after being perturbed in some way. To analyse a system's stability, it is subjected to arbitrary small perturbations, and the system's response to these perturbations is evaluated. To be of the permanent type, an equilibrium state or steady flow must not only satisfy the governing equations but also be stable against arbitrary small perturbations.

Hydrodynamic stability concerns the stability and instability of motions of fluids. Hydrodynamic stability theory determines the reaction of a steady motion of a fluid (base flow) to small disturbances. The stability of fluid flow is determined by the growth rate of disturbances. If the disturbances grow in time, the flow is considered unstable. Conversely, the flow is considered stable if all the possible disturbances that it can be subjected to decay in

time. The origins of this theory can be traced back to the nineteenth century to Helmholtz, Kelvin, Rayleigh, and Reynolds.

Method of Normal Mode

The method of normal modes is equivalent to superimposing infinitesimal perturbations on base flow. In doing so, the linearized equations that govern the perturbations can be derived. The fluid system is considered unstable if at least one eigenvalue of the resulting linear operator exists in the right half of the complex plane. And the eigenvector associated with the most unstable eigenvalue (the most unstable mode of disturbance) is expected to dominate the form of the instability. Finding the eigenvalues and the eigenvectors is very challenging due to the large dimensions of the linear operator. The problem can be simplified if some assumptions about the base flow and the nature of disturbances are made.

1.6 Literature Review

Thermal instability theory has stimulated significant attention and has been identified as a fundamental problem in many areas of fluid dynamics. For a horizontal fluid layer cooled from above and heated from below, the effect of buoyancy can become a dominant force driving a possible convective instability. Bénard [17] provided a detailed description of the development of convective flow. Rayleigh [89] was the first to develop an analytical perspective to the problem to establish the criteria that delineate the breakdown of the basic state. As a consequence of these works the thermal instability convection driven by buoyancy is called **Rayleigh-Bénard convection**. Chandrasekhar [32] explained in detail, the thermal instability of a Newtonian fluid, under varying assumptions of hydrodynamics and hydromagnetics. As a result, several theoretical and experimental research has been conducted to demonstrate various facts about thermal convection.

Thermal instability in a porous medium is a phenomenon that can occur in a variety of situations. It has many applications in geophysics, food processing, the building of thermal insulations, oil reservoir modelling, and nuclear reactors [51, 97]. The porous media analogue of Rayleigh-Bénard convection in a clear fluid is the Darcy-Bénard problem. It is the prototypical problem for thermoconvective stability in porous media. The fluid flow and heat transport in porous media was initially studied by Horton and Rogers [58] and Lapwood [66]. These researches are based on the Darcy law, which ignores inertial forces and solid bound-

ary effects. Hence, this problem is also known as the Horton - Rogers - Lapwood (HRL) problem. The Darcy–Bénard problem was formulated for a horizontal fluid-saturated porous layer in a motionless state, bounded by two horizontal, isothermal, and impermeable walls maintained at different temperatures. Since then, several investigators have studied extensively the instability mechanism of viscous fluid flows in a horizontal porous layer via diverse physical situations. A detailed and comprehensive survey of the work on fluid convection in porous media is presented in a book by Nield and Bejan [78].

It is known that the assumption of a uniform gravity field is not valid for large-scale convection phenomenon that arises in the climate, atmosphere, sea or mantle of the earth [57, 67, 110]. In such a situation, the gravitational field changes with elevation from its surface and some parts of the fluid layers may show a more stable nature and another part more unstable. To overcome this problem, it is necessary to consider the variable gravity field that depends on the height of the earth's surface . The nonlinear variation of gravity field with depth (parabolic, binomial and exponential) can occurs in sedimentary basins, epeirogenic and orogenic movements of the Earth's crust and crustal structures ([37, 103, 101]). The existence of elevated gravity levels varying with distance, during the formation of crystals grown from the molten phase in a furnace placed at the arm extremity of a centrifuge, have been reported by Rodot *et al.* [92]. Rao *et al.* [120] compared the exponential, binomial and parabolic functions and found that the parabolic model fits more closely with most crustal structures. Pradhan and Samal [87] were the first to analyze the instability mechanism between two horizontal plates under the action of varying gravity field and they noticed that the value of the variable gravity parameter plays an important role on the convection motion. Alex *et al.* [6] considered internal heat source and inclined temperature gradient on the instability mechanism for inconstant varying gravity field and later extension of this work has been reported in an anisotropic porous region by Alex and Patil [5]. They concluded that when the variable gravity parameter is nonnegative, an increase in heat generation destabilises the system, and when it is negative, the reverse effect occurs. Harfash [53, 54] studied the effect of variable gravity field on the three-dimensional simulations for convection an anisotropic region with nonhomogeneous porosity and thermal diffusivity and inside a porous medium with the internal heat source. Their results reveal that the linear threshold accurately predicts on the onset of instability in the basic steady state. They also observed found as the Rayleigh number approaches the linear threshold, the time required to attain the basic steady state increases significantly. Harfash and Alshara [56] analyzed the impact of variable gravity and chemical reaction on the double-diffusive convection in a porous medium in the presence of a traverse magnetic field. They concluded that gravity and

magnetic fields have a considerable stabilising impact. Roy and Murthy [94] investigated the effect of the variable gravity field and viscous dissipation on the free convection in a horizontal porous layer. They found a significant decrease in the value of the critical horizontal Rayleigh number when the modified variable gravity parameter is changed from -1 to 1. Mahajan and Tripathi [71] examined the influence of spatially varying gravity, temperature and concentration on the linear and non-linear stability analysis of a chemically reacting fluid layer. Yadav [124, 125] considered the effect of the variable gravity field and rotation on the onset convection in a porous layer and the thermal instability in an anisotropic porous layer. The results demonstrated that both the rotation parameter and the gravity variation parameter prevent convection from arriving. The measurement of convection cells decreases as the rotation and gravity variation parameters are increased.

The effect of throughflow has been considered by several researchers for the reason that it gives the possibility to control the convective instability. The first investigation on the Rayleigh instability of convection was carried out by Wooding [122] under the influence of throughflow in a porous medium and this study was followed by Sutton [109] and Chen [33]. Later, Vanishree [119] considered the effect of internal heat generation in a variable viscosity liquid saturating an anisotropic porous medium to study the stability analysis in the presence of the throughflow effect. Kuznetsov and Nield [65] examined vertical throughflow effect the stability of an internally heated fluid-saturated porous layer under the local thermal non-equilibrium circumstance and concluded that downward throughflow is destabilizing effect, while upward throughflow is stabilizing effect. Kiran [60] considered the effect of throughflow and gravity modulation on the weakly nonlinear stability analysis of the Darcy-Bénard convection. He demonstrated that throughflow increases heat transport in the upward direction while decreasing it in the downward way. Bhadauria and Singh [22] analyzed the effect of throughflow and G-jitter on the convection in an anisotropic porous medium. They concluded that the throughflow parameter delays chaotic convection, resulting in a reduction in heat transmission in the system. Dubey and Murthy [43, 44] considered the effects of throughflow on the convective instability of horizontal porous layer with inclined thermal and solutal gradients and mixed thermal conditions. They identified that the magnitude of throughflow varies in different flow regimes, which has an impact on stability. Yadav [123] investigated numerically the combined effect of variable gravity field and throughflow on the onset convection in a porous layer. His results indicate that both the throughflow and gravity variation parameters delay the onset of convective motion.

In most of the studies on convection in a fluid-saturated porous medium, the contribution of the viscous dissipation is ignored. However, viscous dissipation has a substantial influence

on the convective flows in a porous medium when the fluid has both high viscosity and low thermal conductivity. The irreversible process through which the work done by a fluid on adjacent layers due to the action of shear forces is transformed into heat is defined as viscous dissipation. The importance of viscous dissipation effect on the natural convection has been discussed firstly by Gebhart [48]. He introduced a new term to study the effect of viscous dissipation which does not depend on the Grashof number and Prandtl number. Later on, Gebhart and Mollendorf [49] investigated the effect of viscous dissipation on external natural convection. Turcotte *et al.* [113] reported the influence of viscous dissipation on finite amplitude Bénard convection. Barletta *et al.* [12] considered horizontal flow in a porous layer induced by viscous dissipation. Barletta and Storesletten [14] discussed the impact of vertical throughflow with viscous dissipation on the convective roll instabilities in a horizontal porous layer. Their findings show that, while the effect of viscous dissipation is generally weak, it is stabilising in the case of downward throughflow and destabilising in the case of upward throughflow. Barletta and Nield [15] studied the thermosolutal convective instability in the presence of viscous dissipation effect. They demonstrated that the combined effects of viscous dissipation and mass diffusion can cause the basic horizontal flow to become unstable. Roy and Murthy [94, 95, 96] investigated the effect of viscous dissipation on the convective instability with variable gravity, in an inclined temperature gradient, horizontal throughflow and Soret effect with double diffusion. Except for some positive values of the Soret parameter, they concluded that the critical Rayleigh number decreases in the presence of viscous dissipation. Dubey and Murthy [45] carried out the influence of viscous dissipation in a Brinkman porous region with throughflow and Soret effect.

The convection of nanofluids based on Buongiorno's model has attracted great interest because of its wide range of applications. Using this model for nanofluid, Tzou [114, 115] analysed the Bénard problem for a nanofluid and found that the critical Rayleigh number is lowered by one or two orders of magnitude than for regular fluids. Nield and Kuznetsov [79] analyzed the thermal instability in a porous medium layer saturated by a nanofluid. They discovered that the inclusion of nanoparticles can lower or increase the critical thermal Rayleigh number by a significant amount, depending on whether the basic nanoparticle distribution is top-heavy or bottom-heavy. Kuznetsov and Nield [64] investigated the thermal instability in porous layer saturated by nanofluid using the Brinkman model and concluded that in the case of a bottom-heavy nanoparticle distribution, oscillatory instability is possible. Bhadauria and Agarwal [21] performed a nonlinear study of natural convection in a nanofluid saturated rotating porous layer. Chand and Rana [29, 30] considered the onset of thermal convection in rotating nanofluid and oscillating convection of nanofluid in the porous medium

and found that stationary convection is possible for both bottom and top-heavy distribution of nanoparticles. Yadav *et al.* [126] considered the boundary and internal heat source effects on the onset of Darcy-Brinkman convection in a porous layer saturated with nanofluid. They noticed that the internal heat source, nanoparticle Rayleigh number, modified diffusivity ratio, and Lewis number have a destabilising effect on the system, whereas Darcy number and porosity have a stabilising effect. Nield and Kuznetsov [82, 83] examined the onset of convection in a nanofluid layer with internal heating and using the revised model. The results showed that the presence of the nanofluid particles leads to increased instability of the system and the effect of the nanoparticles on non-oscillatory convection is destabilizing. Rana and Chand [88] studied the onset of thermal convection in a rotating nanofluid layer saturated with Darcy-Brinkman porous medium. Ahuja and Sharma [3] summarized the studies about the instability of a horizontal nanofluid layer under the impact of various parameters such as rotation, magnetic field, Hall currents and LTNE effects in both porous and non-porous medium.

In recent years, several investigators have analyzed the fluid flow and heat transfer problems by including the transverse magnetic field when the fluid is electrically conducting. Furthermore, due to the effect of magnetic fields on flow control and the efficiency of several systems using electrically conducting fluids, there has been a growing interest in investigating Magnetohydrodynamics (MHD) flow and heat transfer in porous media. The investigation of MHD flow for electrically conducting fluids in a channel has numerous engineering applications, for instance, crystal growth in fluids, purification of molten metals, metal casting, nuclear reactor cooling, microelectronic devices and geothermal energy extractions. Although the effect of magnetic field on the flow of nanofluid saturated porous medium is important, only a few studies have been reported on the stability of fluid flow in a channel in the presence of the transverse magnetic field. Alboussiere *et al.* [4] presented an asymptotic analysis and Davoust *et al.* [40] investigated experimentally the buoyancy-driven convection due to uniform magnetic effect. Yadav *et al.* [127] considered the effect of vertical magnetic field on the onset of convection in an electrically conducting nanofluid layer heated uniformly from below for free–free, rigid–rigid and lower-rigid and upper-free boundaries. The corresponding eigenvalue problem is solved analytically for free–free boundaries and numerically for others two boundaries using Galerkin method. Gupta *et al.* [50] examined the stability analysis for the onset of convection in a nanofluid layer with the magnetic field and found that a magnetic field can stabilise a nanofluid layer in both stationary and oscillatory motions. Harfash [52, 55] studied the effect of magnetic field on the convection in a porous medium with variable gravity and chemical reaction and demonstrated the strong stabilising effect of gravity

and magnetic fields. Hudoba and Molokov [59] studied the effect of transverse magnetic field and internal heat sources on the linear stability of buoyant convective flow through a vertical channel and concluded that the basic flow of liquid metals in high magnetic fields is very stable.

The study of double-diffusive convection in a porous medium is a current topic due to its many applications in the fields of engineering, food processing, bio-engineering and cancer therapy, movement of biological fluid and oceanography. The prospect of heat transfer in the medium cannot narrate exclusively in situations involving more than one solute fields. In such a situation, both heat and mass transfers are required. The combined effects of temperature differences and concentration variation in a saturated porous medium induce the buoyancy forces. Starting from the study of the onset of thermohaline convection in a horizontal layer of the fluid-saturated porous medium by Nield [75], several authors analyzed the double-diffusive convection in a saturated porous medium by considering different effects. Kuznetsov and Nield [63] examined the onset of double-diffusive nanofluid convection in a layer saturated by the porous medium and found that in order for oscillations to occur, two of the buoyancy forces must be in opposite directions. Nield and Kuznetsov [81] considered the onset of double-diffusive convection in a nanofluid layer. Agarwal and Rana [1] analysed the periodic and aperiodic convective stability of double-diffusive nanofluid convection in a rotating porous layer. They concluded that convection in binary nanofluids is delayed compared to ordinary nanofluids. Yadav *et al.* [128] studied the onset of double-diffusive nanofluid convection in a rotating porous medium layer with variations in thermal conductivity and viscosity. Umavathi *et al.* [116] investigated the cross-diffusion effects on the onset of double diffusive convection in nanofluid saturated porous medium. They deduced that the Soret and Dufour parameters, viscosity ratio, and thermal conductivity ratio have a stabilising effect for the stationary mode, whereas the solutal Rayleigh number destabilises the system. Deepika [41] studied the linear and nonlinear stability of double-diffusive convection with the Soret effect and observed that the effect of the Soret parameter on stabilisation or destabilisation is significant for Soret parameters less than 2. Mahajan and Sharma [69] considered the double-diffusive convection in a magnetic nanofluid with cross-diffusion effects. They noticed that in both the gravity and microgravity environments, increasing the values of the Dufour parameter delays the beginning of double-diffusive magnetic nanofluid convection, but increasing the values of the Soret parameter advances it. Dubey and Murthy [46] investigated the onset of double-diffusive convection in a Brinkman porous layer with convective boundary conditions. They found that when the direction of the solute concentration gradient opposes the direction of thermal buoyancy, the Soret parameter has a linearly

destabilising influence on the flow.

Most of the investigations on the convective instability were under the local thermal equilibrium (LTE) mode. This supposition is not appropriate for a large temperature change amongst the phases or high-speed flows. In such a situation, separate temperature equations for solid particle and fluid phases to represent local thermal non-equilibrium (LTNE) are needed. Vadasz [117] proposed that both the phases (fluid phase and particle phase) have a temperature difference. Theories of thermal convection which involve local thermal non-equilibrium effects, including a concentration on microfluidic effect have been well documented in the book by Straughan [108]. The study of LTNE for nanofluid saturated porous media turns to be an important research area due to its interesting applications in microwave heating, cooling and drying of foods, and rapid heat transfer from computer chips via the use of porous metal foams. Several investigators carried out their research on the effect of LTNE on the instability mechanism. Straughan [107] presented global nonlinear stability in porous convection with a thermal non-equilibrium model. Malshetty *et al.* [73] analyzed the double-diffusive convection in porous layer using thermal non-equilibrium model and noticed that small inter-phase heat transfer coefficient has significant effect on the stability of the system. Kuznetsov and Nield [62] studied the onset of convection in a porous layer saturated by nanofluid with LTNE effect. They claimed that the LTNE effect can be significant when the Nield numbers maintain a certain range but remain unimportant for distinctive dilute nanofluids. Nield and Kuznetsov [80] investigated analytically the effect of local thermal non-equilibrium on the onset of convection in a nanofluid layer. Their analysis revealed that while LTNE can have a considerable influence in specific situations, it has a minor effect in a typical dilute nanofluid (with a big Lewis number and a small particle-to-fluid heat capacity ratio). Bhadauria and Agarwal [20] considered the convective transport in a nanofluid saturated porous layer with thermal non-equilibrium model and concluded that convection sets in earlier for LTNE as compared to LTE. Agarwal *et al.* [2] studied the Rayleigh Bénard convection in a nanofluid layer using thermal non-equilibrium model. Barletta and Rees [16] carried out the local thermal non-equilibrium analysis of the thermoconvection instability in an inclined porous layer. The scaling of the Darcy–Rayleigh number with cosine of the inclination angle to the horizontal, which corresponds to the well-known LTE regime, implies a monotonic increase in the stability of the basic flow as the inclination to the horizontal increases. Bera and Khandelwal [19] examined the effect of local thermal non-equilibrium perspective on the stability characteristics of non-isothermal Poiseuille flow in a vertical porous channel. Their findings indicated that the inter-phase heat transfer coefficient (the porosity scaled conductivity ratio) have the effect of stabilising (destabilising) the flow. Celli

et al. [28] discussed the effect of local thermal non-equilibrium on the thermoconvective instability of Horton-Rogers-Lapwood problem with a free surface and conclude that the fluid layer is more stable when the free surface is highly capable of exchanging heat with the external environment. Sharma and Gupta [100] considered the LTNE effect on the nanofluid convection under Hall current. They concluded that, in contrast to the LTE model, the presence of nanoparticles has a significant influence on critical wave number via LTNE parameters. Mahajan and Sharma [70] studied the impact of LTNE on the stability analysis in a magnetic nanofluid layer. They observed that ester-based magnetic nanofluids are more stable than water-based magnetic nanofluids in both gravity and microgravity environments.

1.7 Aim and Scope

The present thesis aims to study the linear stability analysis of incompressible viscous and nanofluid flow in a horizontal/vertical channel filled with a porous medium. The effect of double diffusion, magnetic field, inter-phase heat transfer parameter (LTNE parameter), viscous dissipation, variable gravity, Biot number (convective boundary condition parameter), Soret number, Dufour number on the stability is analyzed numerically. To initiate the work on the stability of the flows in channels, few simple extensions on the viscous fluid-saturated horizontal porous layer with the variable gravity are considered. Hence, the effect of various governing parameters on stability is analysed. In the case of nanofluids, the patterns of the streamlines, isotherms and isonanoconcentrations are analyzed at the critical level. The problems considered in the thesis deal with the unsteady horizontal/vertical porous channels where the walls are maintained by one of the isothermal, heat flux conditions, convective boundary conditions.

1.8 Outline of the Thesis

This thesis consists of four parts and twelve chapters.

Part - I consists of a single chapter, Chapter-1. It deals with the introduction and presents the motivation for the investigations carried out in the thesis. A survey of pertinent literature is presented explaining the significance of the problems considered. The basic equations governing the nanofluid based on the Buongiorno model has been given in this chapter.

Part - II deals with the effect of variable gravity on the stability of viscous fluid in a horizontal channel. This part consists of four chapters (Chapters 2, 3, 4 and 5). In each of these chapters, the governing equations and their associated boundary conditions are initially cast into dimensionless form. The resulting system forms an eigenvalue problem. This system of equations is solved using *bvp4c* routine available in MATLAB software. For solving purpose, the system of higher-order ordinary differential equations is transformed into a system of first-order ordinary differential equations. The normalization condition is used corresponds to non-trivial solutions at $z = 0$. In these chapters, four types of variations viz., linear, quadratic, cubic and exponential, in the gravitational force are considered. As the problems considered are

In Chapter - 2, the impact of variable gravity on the instability mechanism of the viscous fluid-saturated porous layer is studied due to the combined effects of the Soret parameter, vertical throughflow and viscous dissipation. The effect of various parameters viz., solutal Rayleigh number, Lewis number, Gebhart number (viscous dissipation parameter), Soret number and gravity variation parameter on the instability mechanism is shown graphically and analyzed.

Chapter - 3 analyzes the influence of viscous dissipation, vertical throughflow and variable gravity field on the onset of convective instability in a horizontal porous layer filled with a viscous fluid. The Brinkman extended Darcy model is accounted into the momentum equation of the governing flow through the porous layer. The effects of pertinent parameters i.e. non-dimensional throughflow parameter, viscous dissipation, Darcy number and gravity variation parameter on the instability mechanism is discussed for linear, quadratic and exponential varying gravity field.

In Chapter - 4, the effect of variable gravity on the onset of convection in a Brinkman porous medium in an infinite horizontal channel packed with viscous fluid in the presence of third kind boundary conditions is addressed. The breakdown of convection has been identified under the influence of Darcy number, gravity variation parameter, and Biot numbers for linear and quadratic varying gravity fields and presented through graphs. Also, the critical Rayleigh number and corresponding wavenumber are calculated when one boundary maintains constant heat flux while another one attains the isothermal condition.

In Chapter - 5, the effect of variable gravity on the stability analysis has been investigated in a horizontal porous medium with throughflow under a local thermal non-equilibrium (LTNE) situation. The influence of onset of convection due to the governing parameters, such as gravity variation parameter, throughflow parameter, inter-phase heat transfer parameter

and porosity modified conductivity ratio for the above gravity fields. Further, the critical Rayleigh number and corresponding wavenumber are obtained at the limiting cases of LTNE approaches.

Part - III deals with the stability of convective flows in a vertical channel filled with a nanofluid. This part consists of six chapters (Chapters 6, 7, 8, 9, 10 and 11). In all these chapters, The model which incorporates the Brownian motion and thermophoresis is used for nanofluid. The eigenvalue problem for the perturbed state is obtained from a normal mode analysis and solved using the Chebyshev spectral collocation technique.

Chapter - 6 analyzes the linear stability analysis of the nanofluid flow in a vertical porous channel. The basic velocity, temperature and volume fraction profiles have been shown graphically for a typical nanofluid (for which the Lewis number is large). Also, the onset of convection has been discussed graphically for different values of Darcy number, Prandtl number, concentration Rayleigh number, Lewis number, modified diffusivity ratio and modified particle density increment. Further, the pattern of streamlines, isotherms, isonanoconcentrations, eigenfunctions and growth rate have been examined for the governing parameters related to nanofluid at the critical level.

In Chapter - 7, the effect of the transverse magnetic effect on the instability mechanism of double-diffusive convection in a vertical channel filled with nanofluid is considered. The instability boundaries have been investigated for various values of the magnetic effect, solutal Rayleigh number, thermo-solutal Lewis number, Dufour parameter and Soret parameter. Also, patterns of the streamlines, isotherms, isonanoconcentrations, isosolutes and growth rate are shown graphically for various values of Darcy number and Hartmann number (magnetic parameter) under critical situation.

In Chapter - 8, the stability of the flow of nanofluid saturated porous medium in a vertical channel is examined numerically when the fluid, particle and solid-matrix phases are not in local thermal equilibrium (LTE). The impact of the LTNE parameters, namely, inter-phase heat transfer parameters, modified thermal capacity ratios and modified thermal diffusivity ratios between the fluid and particles phases and fluid and solid phases on the breakdown of convection has been disclosed. Further, patterns of the streamlines, isotherms(fluid), isotherms(particle), isotherm(solid-matrix), isonanoconcentrations and eigenfunctions have been presented for Nield numbers(inter-phase heat transfer parameters) at a critical level.

Chapter - 9 presents the local thermal non-equilibrium effect on the convective instability in a vertical channel filled with nanofluid in the presence of the transverse magnetic field. The Buongiorno model is used for the nanofluid and the two-field model is used for the energy

equation each representing the fluid and particle phases separately. The stability region has been discussed for the occurrence of physical parameters Hartmann number, concentration Rayleigh number, modified diffusivity ratio, Lewis number, inter-phase heat transfer parameter and thermal diffusivity ratio. Apart from these, the pattern of streamlines, isotherms and isonanoconcentrations for various values of Hartmann number and inter-phase heat transfer parameter is shown over a period.

Chapter - 10 deals with the variable gravity effect in a horizontal porous channel filled with a nanofluid. The impact of variable (linear, quadratic, cubic and exponential) gravity fields on the stability analysis have been carried out for the governing parameters under free-free, rigid-free, and rigid-rigid boundaries.

In Chapter - 11, the onset of longitudinal convective rolls of a horizontal porous layer filled with nanofluid induced by viscous dissipation is investigated numerically. An infinitely long horizontal porous region has been considered which is bounded by two rigid surfaces. The lower surface is thermally insulated, whereas the upper surface is considered to be isothermal. The Buongiorno model for the nanofluid and the Brinkman-extended Darcy model for porous medium are adopted. The effect of pertinent parameters on the longitudinal convective rolls ia analysed and presented graphically.

Part - IV consists of a single chapter, Chapter - 12, which includes the principal conclusions of the thesis and the directions in which further investigations may be carried out.

In all the above chapters, it is assumed the porous medium is homogeneous and hydrodynamically as well as thermally isotropic.

A list of references is given at the end of the thesis. The references are arranged in alphabetical order. In some of the chapters, details which are already presented in the earlier Chapters are avoided. As a review of the existing literature is presented in the introductory chapter itself, in each of the chapters only a brief introduction to the concerned problem is given. Also, the physical meaning of the various parameters is repeated in each chapter for easy readability.

A considerable part of the work in the thesis is published/accepted for publication in reputed journals. The remaining part is communicated for possible publications. The details are presented below.

List of papers published

1. "Stability of nanofluid flow in a vertical porous channel", ***Special Topics & Reviews in Porous Media — An International Journal***, 11(5):477–491, 2020.

2. "The variable gravity field and viscous dissipation effects on the double diffusive and Soret driven convective instability in a porous layer with throughflow", ***International Communications in Heat and Mass Transfer***, 120, ID No. 105050, 2021.

3. "Linear stability of convection in a vertical channel filled with nanofluid saturated porous medium", ***Heat Transfer***, 50(4):3220-3239, 2021.

4. "The variable gravity field and viscous dissipation effects on the convective instability in a porous layer with throughflow: Brinkman model", ***Journal of Porous Media***, 24(6):1-13, 2021.

5. "The effect of changeable gravity field on the stability of convection in a porous layer filled with nanofluid: Brinkman model", ***Computational Thermal Sciences: An International Journal***, 13(6):1-17, 2021.

List of papers accepted

6. "Effect of local thermal non-equilibrium on the stability of the flow in a vertical channel filled with nanofluid saturated porous medium", ***Journal of Heat Transfer***.

List of papers communicated

7. "Local thermal non-equilibrium effect on the convective instability in a vertical channel filled with nanofluid in the presence of transverse magnetic field", ***Special Topics & Reviews in Porous Media — An International Journal***.

8. "Linear stability of double diffusive convection in a vertical channel filled with a nanofluid saturated porous medium in the presence of transverse magnetic field", ***Journal of Porous Media***.

9. "Effect of variable gravity on the onset of convection in a Brinkman porous medium under convective boundary conditions", ***Indian Journal of Physics***.

10. "The effect of local thermal non-equilibrium on the stability analysis due to the presence of variable gravity field with throughflow", ***International Communications in Heat and Mass Transfer***.

11. "Linear stability of longitudinal convective rolls in a non-Darcy porous layer filled with nanofluid due to viscous dissipation effect", ***Thermal Science and Engineering Progress***.

Part II

STABILITY OF VISCOUS FLOW IN A POROUS HORIZONTAL CHANNEL WITH VARIABLE GRAVITY

Chapter 2

The variable gravity field and viscous dissipation effects on the double diffusive and Soret driven convective instability in a porous layer with throughflow [1]

2.1 Introduction

The convection with double diffusion in a porous medium has gained more attention owing to its many applications in the areas of food processing, geophysics, chemical science, engineering and nuclear industries, movement of biological fluid, cancer therapy and oceanography. The prospect of heat transfer in the medium cannot narrate exclusively in conditions containing at least one solute fields. In this type of situations, heat and mass transfers together are required. The cumulative impact of concentration and temperature differences in a fluid-saturated porous matrix induces the buoyancy forces. Nield [75] initiated the first investigation on the instability mechanism of convection in a horizontal fluid saturated porous layer with double diffusion. Several authors analyzed the double diffusion convection in a fluid-saturated porous layer by incorporating different effects in their study. Nield and Bejan [78] and Vafai [118] presented a prevalent literature on the double-diffusive convection

[1] Published in "***International Communications in Heat and Mass Transfer***" 120, ID No. 105050, 2021

in porous matrix.

It is well known that viscous dissipation has great importance in mixed or natural convection processes. The viscous dissipation effects may also be present a significant role in stronger gravitational fields. Gebhart [48] investigated the viscous dissipation effect in natural convection under two type of boundary conditions. This dissipation number does not depend on the Grashof number and Prandtl number. Several investigators analysed the effect of viscous dissipation on the convective instabilities in a porous channel/layer.

Several researchers were attracted to the study of the influence of vertical throughflow as it contributes to the chance to regulate convective instability. Wooding [122] was the first to consider the throughflow in a porous medium. Later, it was extended by Sutton [109], Chen [33] and Nield [77] and Nield and Kuznetsov [82]. The variation of gravity with height is taken into account in large-scale convection problems as it variates the buoyancy force applied by the fluid. This causes a certain section of the fluid layer to be stable and other section unstable. Straughan [106] examined the linear stability of convection in a variable gravity field. Several researchers, Harfash [53] and Yadav [123] examined the variable gravity effects on the convective flow.

In this chapter, we consider the linear stability analysis for the onset of double diffusion convection in the presence of variable gravity, viscous dissipation and vertical throughflow. The influence of these governing parameters on the stability of convection is presented through graphs and tabular form.

2.2 Mathematical Formulation

Consider an incompressible and double diffusive horizontal fluid layer saturated with porous medium of thickness L. The Cartesian co-ordinate system is selected such that $x-$axis is taken along the horizontal direction and $z-$ axis is vertically upwards. The boundary planes of the porous layer are $z = 0$ and $z = L$. The variable gravity $\mathbf{g}(z)$ is acting in the direction of negative $z-$ axis as plotted in Fig. 2.1. The temperatures (T) of the bottom and top layers are taken as T_1 and T_2 $(T_1 > T_2)$ and the corresponding concentrations (C) are as C_1 and C_2 $(C_1 > C_2)$, respectively.

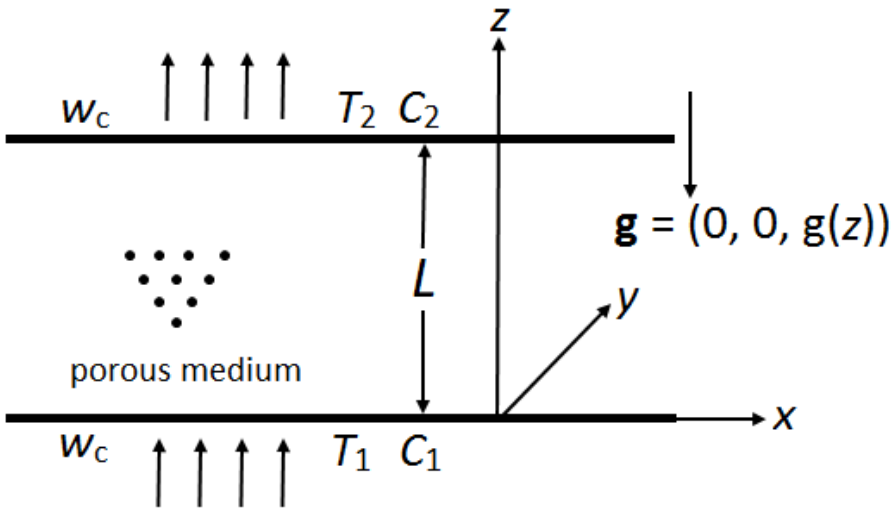

Figure 2.1: Schematic representation of the problem.

The fluid and porous medium are supposed to be in a local thermal equilibrium state. The porous medium is isotropic and homogeneous. The Darcy law for porous medium is employed in the momentum equation. Also, a concurrent mass diffusion that is present due to the concentration difference maintained at the horizontal walls gets effected due to the thermal gradients contributing to the concentration distribution (due to the Soret effect). But the Dufour effect is not considered. The fluid that saturates the porous matrix is assumed to be Newtonian.

Under the above assumptions and invoking Oberbeck-Boussinesq approximation, the equations governing the flow can be written as ([78, 93]):

$$\nabla \cdot \mathbf{u} = 0, \tag{2.1}$$

$$0 = -\nabla p - \frac{\mu}{K}\mathbf{u} - \rho_0[1 - \beta_{\mathrm{T}}(T - T_2) - \beta_{\mathrm{C}}(C - C_2)]\mathrm{g}(z)\hat{\mathbf{e}}_{\mathrm{z}}, \tag{2.2}$$

$$(\rho c)_{\mathrm{m}}\frac{\partial T}{\partial t} + (\rho c)_{\mathrm{f}}\mathbf{u} \cdot \nabla T = k_{\mathrm{m}}\nabla^2 T + \frac{\mu}{K}\mathbf{u} \cdot \mathbf{u}, \tag{2.3}$$

$$\epsilon\frac{\partial C}{\partial t} + \mathbf{u} \cdot \nabla C = D\nabla^2 C + D_{\mathrm{CT}}\nabla^2 T, \tag{2.4}$$

where $\mathbf{u}(= (u, v, w))$ is the Darcy velocity vector. p, μ and K are pressure, dynamic viscosity, and permeability, respectively. ρ_0 is the density of the fluid, $\hat{\mathbf{e}}_{\mathrm{z}}$ is unit vector in the $z-$direction, $(\rho c)_{\mathrm{m}}$ is the heat capacity of the medium, $(\rho c)_{\mathrm{f}}$ is heat capacity of the fluid,

$k_{\rm m}$ and ϵ are the thermal conductivity and porosity of the porous medium, respectively. D is the mass diffusivity and $D_{\rm CT}$ is the Soret coefficient. Also, $\beta_{\rm T}$ and $\beta_{\rm C}$ are thermal and solutal expansion coefficients of the fluid. Here, $\mathrm{g}(z) = \mathrm{g}_0(1 + \lambda G(z))$, where g_0 and λ are the reference gravity and the gravity variation parameter, respectively. The overall heat capacity per unit volume, overall thermal conductivity of the medium are given by ([78])

$$(\rho c)_{\rm m} = (1-\epsilon)(\rho c)_{\rm s} + \epsilon(\rho c_{\rm p})_{\rm f} \quad \text{and} \quad k_{\rm m} = (1-\epsilon)k_{\rm s} + \epsilon k_{\rm f},$$

where the subscripts s, f and m referring to the solid, fluid and porous components, respectively, $c_{\rm p}$ is the specific heat at constant pressure of the fluid.

The conditions on the boundary planes are given by

$$w = W_{\rm c}, \quad T = T_1, \quad C = C_1 \quad \text{at} \quad z = 0, \tag{2.5a}$$

$$w = W_{\rm c}, \quad T = T_2, \quad C = C_2 \quad \text{at} \quad z = L. \tag{2.5b}$$

The non-dimensional variables are defined as

$$\begin{aligned}(x^*, y^*, z^*) = \frac{(x,y,z)}{L}, \quad \mathbf{u}^* = \frac{\mathbf{u}L}{\alpha_{\rm m}}, \quad p^* = \frac{Kp}{\mu\alpha_{\rm m}},\\ t^* = \frac{\alpha_{\rm m} t}{\epsilon L^2}, \quad T^* = \frac{T - T_2}{T_1 - T_2}, \quad C^* = \frac{C - C_2}{C_1 - C_2},\end{aligned} \tag{2.6}$$

where $\alpha_{\rm m} = \dfrac{k_{\rm m}}{(\rho c_{\rm p})_{\rm f}}$ is the thermal diffusivity.

The dimensionless form of Eqs. (2.1)-(2.4), after eliminating pressure term from Eq. (2.2), are (after dropping asterisk)

$$\nabla^2 w = \left(Ra \nabla_{\rm H}^2 T + \frac{Rs}{Le} \nabla_{\rm H}^2 C \right) (1 + \lambda G(z)), \tag{2.7}$$

$$(\gamma \frac{\partial}{\partial t} + \mathbf{u}\cdot\nabla) T = \nabla^2 T + \frac{Ge}{Ra} \mathbf{u}\cdot\mathbf{u}, \tag{2.8}$$

$$(\frac{\partial}{\partial t} + \mathbf{u}\cdot\nabla) C = \frac{1}{Le}\nabla^2 C + Sr \nabla^2 T. \tag{2.9}$$

Here $\nabla_{\rm H}^2 \equiv \dfrac{\partial^2}{\partial x^2} + \dfrac{\partial^2}{\partial y^2}$. The non-dimensional parameters are defied as $Ra = \dfrac{\rho_0 \mathrm{g}_0 \beta_{\rm T} K L (T_1 - T_2)}{\mu \alpha_{\rm m}}$ is the thermal Rayleigh number, $Rs = \dfrac{\rho_0 \mathrm{g}_0 \beta_{\rm C} K L (C_1 - C_2)}{\mu D}$ is the solutal Rayleigh number,

$Le = \dfrac{\alpha_m}{D}$ is the Lewis number, $\gamma = \dfrac{(\rho c)_{\mathrm{m}}}{\epsilon(\rho c_{\mathrm{p}})_{\mathrm{f}}}$ is the heat capacity ratio, $Ge = \dfrac{\beta_{\mathrm{T}} g_0 L}{c_{\mathrm{p}}}$ is the Gebhart number due to viscous dissipation effect and $Sr = \frac{D_{\mathrm{CT}}(T_1 - T_2)}{\alpha_{\mathrm{m}}(C_1 - C_2)}$ is the Soret parameter. The dimensionless conditions on the boundary are

$$w = Q, \quad T = 1, \quad C = 1 \quad \text{at} \quad z = 0, \tag{2.10a}$$

$$w = Q, \quad T = 0, \quad C = 0 \quad \text{at} \quad z = 1, \tag{2.10b}$$

where $Q = \dfrac{W_{\mathrm{c}} L}{\alpha_{\mathrm{m}}}$ is the throughflow parameter.

2.3 Basic state solution

The flow in the basic state is assumed as steady, uni-directional and fully developed and then the velocity, temperature and concentration in basic state are of the form: $\mathbf{u}_0 = (0, 0, Q)$, $T_0 = T_0(z)$ and $C_0 = C_0(z)$, respectively. The solution of the basic state temperature and concentration are, respectively,

$$T_0 = \frac{e^Q + \frac{GeQ}{Ra}}{e^Q - 1} - \frac{(\frac{GeQ}{Ra} + 1)}{e^Q - 1} e^{Qz} + \frac{GeQ}{Ra} z, \tag{2.11}$$

$$\begin{aligned} C_0 = -\tfrac{(e^{QLe} - e^{QLez})}{(1 - e^{QLe})} + \tfrac{SrLe}{(1-Le)(1-e^{QLe})} \left(\tfrac{GeQ}{Ra} + 1\right) \left[\tfrac{e^Q - e^{QLe}}{1 - e^Q} + e^{QLez}\right] \\ - \tfrac{SrLe}{(1-Le)(1-e^Q)} \left(\tfrac{GeQ}{Ra} + 1\right) e^{Qz}. \end{aligned} \tag{2.12}$$

In the basic temperature and concentration profiles given in Eqs. 2.11 and 2.12, both $Q = 0$ and $Le = 1$ are singular points. In the limit $Q \to 0$, the basic temperature profile is a linear function of z (i.e., $T_0 = 1 - z$). The basic concentration profile for $Le = 1$ is obtained as

$$C_0 = \frac{e^Q - e^{Qz}}{e^Q - 1} + \frac{SrQ}{(e^Q - 1)^2} \left(\frac{GeQ}{Ra} + 1\right) \left[\left(e^Q - z e^{Qz}\right) + e^Q e^{Qz}(z - 1)\right]. \tag{2.13}$$

By considering the limit $Q \to 0$ and $Le \to 1$, the basic concentration profile can be obtained as $C_0 = 1 - z$.

2.4 Linear stability analysis

The linear stability analysis is studied by imposing the infinitesimal disturbances in the velocity, temperature, and concentration as given below

$$\mathbf{u} = \mathbf{u}_0 + \delta\mathbf{u}',\ T = T_0(z) + \delta T',\ C = C_0(z) + \delta C', \tag{2.14}$$

where $\delta \ll 1$ is a small disturbance parameter and the prime denotes an infinitesimal disturbance. Substituting Eq. (2.14) into Eqs. (2.7)-(2.9) and neglecting δ^2 and higher order terms, we get the following equations for disturbances.

$$\nabla^2 w' = \left(Ra\nabla_{\mathrm{H}}^2 T' + \frac{Rs}{Le}\nabla_{\mathrm{H}}^2 C' \right)(1 + \lambda G(z)), \tag{2.15}$$

$$\gamma\frac{\partial T'}{\partial t} + (\mathbf{u}'\cdot\nabla)T_0 + (\mathbf{u_0}\cdot\nabla)T' = \nabla^2 T' + \frac{2Ge}{Ra}\mathbf{u_0}\cdot\mathbf{u}', \tag{2.16}$$

$$\frac{\partial C'}{\partial t} + (\mathbf{u}'\cdot\nabla)C_0 + (\mathbf{u_0}\cdot\nabla)C' = \frac{1}{Le}\nabla^2 C' + Sr\nabla^2 T'. \tag{2.17}$$

By applying the usual normal mode form, the disturbances are specified by

$$[w', T', C'] = [\hat{w}(z), \hat{T}(z), \hat{C}(z)]e^{i(a_x x + a_y y) + \eta t}, \tag{2.18}$$

where $a = \sqrt{a_x^2 + a_y^2}$ is wavenumber, and $\eta = \eta_r + i\eta_i$ is a complex parameter, where η_r and η_i are describing the growth rate and angular frequency of the disturbances, respectively.

On substituting Eq. (2.18) into Eqs. (2.15)-(2.17) and by putting $\eta = 0$, we get the following differential equations for neutral stability mode

$$\left(\frac{d^2\hat{w}}{dz^2} - a^2\hat{w}\right) + a^2\left(Ra\hat{T} + \frac{Rs}{Le}\hat{C}\right)(1 + \lambda G(z)) = 0, \tag{2.19}$$

$$-\hat{w}\frac{dT_0}{dz} + \left(\frac{d^2\hat{T}}{dz^2} - Q\frac{d\hat{T}}{dz} - a^2\hat{T}\right) + \frac{2Ge}{Ra}Q\hat{w} = 0, \tag{2.20}$$

$$-\hat{w}\frac{dC_0}{dz} + \left[\frac{1}{Le}\left(\frac{d^2\hat{C}}{dz^2} - a^2\hat{C}\right) - Q\frac{d\hat{C}}{dz}\right] + Sr\left(\frac{d^2\hat{T}}{dz^2} - a^2\hat{T}\right) = 0. \tag{2.21}$$

The associated conditions on the boundary are

$$\hat{w} = \hat{T} = \hat{C} = 0 \quad \text{at} \quad z = 0 \quad \text{and} \quad z = 1. \tag{2.22}$$

2.5 Results and discussion

The Eqs. (2.19)-(2.21) form an eigenvalue problem with Ra as the eigenvalue. This system of equations is solved using *bvp4c* routine in MATLAB. For solving purpose, the system of Eqs. (2.19)-(2.21) is transformed into a system of first order differential equations. The normalization condition $D\hat{w}(0) = 1$ is used corresponds to non-trivial solutions, at $z = 0$. Using the governing parameters (a, Rs, Le, Ge, Sr, Q), the eigenvalue Ra can be obtained. The critical Rayleigh number Ra_c and the corresponding wavenumber a_c are obtained by calculating the minimum of the function $Ra(a)$. The absolute and relative tolerance are taken as 10^{-10} and 10^{-6}, respectively.

In this study, four types of variations viz., linear, quadratic, cubic and exponential, in the gravitational force are considered. The gravity force functions are taken as $G(z) = -z$ (for linear variations and is denoted by Case-A), $G(z) = -z^2$ (for quadratic variations and is denoted by Case-B), $G(z) = -z^3$ (for cubic variations and is denoted by Case-C), and $G(z) = -(e^z - 1)$ (for exponential variations and is denoted by Case-D).

To verify the exactness of our code, the results obtained from the present analysis are compared with the published results of Rionero and Straughan [91] for $Q = 0$ and Yadav [123] for $Q \neq 0$ and presented in Tables 2.1 and 2.2, respectively. The Ra_c and the corresponding α_c are calculated for stationary convection. The parameters Rs, Ge and Sr are taken to be zero for both the studies. Also, we have consider the ratio of thermal and solutal diffusivity as unity. It can be observed from Tables 2.1 and 2.2 that the outcomes are in good accord with the results of Rionero and Straughan [91] and Yadav [123].

The influence of the solutal Rayleigh number, gravity variation parameter, throughflow parameter, Gebhart number, Lewis number, and Soret parameter on the Ra_c and corresponding α_c is computed and results are presented in Figs. 2.2 to 2.6 and also in Tables 2.3 and 2.4.

Fig. 2.2 displays the variation of Ra_c as a function of gravity changeable parameter λ for various values of solutal Rayleigh number Rs for four cases (Case-A, B, C and D) of gravity field variations. It is noticed from this figure that the effect of Rs on the critical Rayleigh

number is not visible for all four cases of gravity variations. Further, it is noticed that the critical Rayleigh number is increasing with an increase in the gravity variation parameter λ. Hence, λ has a stabilizing effect. An improvement of λ imparts a decay in the gravity field and the disturbance in the system regain. This refers to delay the convection. To have a clear understanding of the effect of Rs for fixed values of λ, the critical Rayleigh number and critical wavenumber are computed for different values of λ and Rs and presented in the Table 2.3. It is noticed from this table that critical Rayleigh number Ra_c decreases for increasing the values of Rs. Thus, this factor has a destabilizing effect and the destabilizing rate is very less.

The influence of the throughflow parameter on the instability mechanism is displayed in Fig. 2.3. It is noticed that Ra_{c} enhances with an increase in the value of Q. Thus, Q has a stabilizing effect.

The impact of mass diffusivity and thermal diffusivity on the stability mechanism is portrayed in Fig. 2.4. It is seen that Ra_{c} rises with an improvement in the Lewis number Le. Thus, Le has a stabilizing effect when thermal diffusivity dominates the mass diffusivity and hence delays the convection. Further, an increase in Le augments the rate of heat supply to the system that manages to increase the values of critical Rayleigh number.

Fig. 2.5 demonstrate the effect of viscous dissipation parameter Ge on the variation of critical Rayleigh number. It is perceived that the critical Rayleigh number is decreasing with an increase in the viscous dissipation parameter. The influence of Ge is very less for Case-A and Case-D. Hence, the flow has a destabilizing character in presence of viscous dissipation parameter. This is due to the reason that the work done by a fluid on contiguous layers is converted into heat because of the action of shear forces and this directs to advance the convective motion. The critical value of Ra is calculated against λ for different values of the Soret parameter and plotted in Fig. 2.6 for four cases of gravity force variations. It is observed that the system is becoming stable when $Sr > 0$, as Ra_{c} is growing with an increase in Sr. Further, it is found that the stability of the convection is more for Case - D and instability are more for Case - C.

The impact of the parameters Le, Ge, Sr and λ on a_{c} with $Q = 0.5$ and $Rs = 20$ for four cases (Case A, B, C and D) of gravity variations is presented in the Table 2.4. It is noticed from this table that the critical wavenumber is increasing with a rise value in λ. This increase is more pronounced for the cases A and D. a_{c} increases when Le and Sr increase. The a_{c} has dual nature i.e., increasing and decreasing nature when Ge increases and variation is very less.

Table 2.1: Comparison of Ra_c and a_c^2 of the present analysis with the results of Rionero and Straughan [91] for $Rs = 0$, $Ge = 0$, $Sr = 0$, $Q = 0$ and $Le = 1$.

$G(z)$	λ	Rionero and Straughan [91]		Present results	
		Ra_c	a_c^2	Ra_c	a_c^2
Case-A	0	39.478	9.870	39.478	9.870
	1	77.020	10.209	77.080	10.209
	1.5	132.020	12.314	132.021	12.314
	1.8	189.908	17.198	189.908	17.198
	1.9	212.280	19.477	212.284	19.477
Case-B	0	39.478	9.870	39.478	9.870
	0.2	41.832	9.874	41.832	9.874
	0.4	44.455	9.887	44.455	9.887
	0.6	47.389	9.915	47.389	9.915
	0.8	50.682	9.961	50.682	9.961
	1	54.390	10.034	54.390	10.034
Case-D	0	39.478	9.870	39.478	9.870
	0.1	42.331	9.872	42.331	9.872
	0.2	45.607	9.883	45.607	9.883
	0.3	49.398	9.904	49.398	9.904
	0.4	53.828	9.942	53.828	9.942
	0.5	59.053	10.005	59.053	10.005

Table 2.2: Comparison of Ra_c and a_c of the present analysis with the results of Yadav [123] for $Rs = 0$, $Ge = 0$, $Sr = 0$, $Q = 0.5$, and $Le = 1$.

$G(z)$	λ	Yadav [123]		Present results	
		Ra_c	a_c	Ra_c	a_c
Case-A	0	39.827	3.151	39.828	3.150
	0.6	57.569	3.146	57.571	3.149
	1.2	99.660	3.224	99.664	3.226
Case-B	0	39.827	3.151	39.828	3.150
	0.6	48.469	3.146	48.471	3.142
	1.2	61.088	3.167	61.091	3.167
Case-C	0	39.827	3.151	39.828	3.150
	0.6	44.857	3.146	44.859	3.146
	1.2	51.029	3.153	51.031	3.152
Case-D	0	39.827	3.151	39.828	3.150
	0.6	67.948	3.162	67.951	3.163
	1.2	157.128	3.798	157.133	3.795

Table 2.3: Evaluation of Ra_c and a_c for various values of solutal Rayleigh number (Rs) and gravity variation parameter (λ) when $Le = 10$, $Ge = 1$, $Q = 0.5$ and $Sr = 0.1$ for four cases A, B, C and D.

Rs	λ	Case - A		Case - B		Case - C		Case - D	
		Ra_c	a_c	Ra_c	a_c	Ra_c	a_c	Ra_c	a_c
5	0	38.814	3.103	38.805	3.147	38.815	3.101	38.816	3.098
	0.5	52.603	3.105	45.774	3.103	42.921	3.104	59.950	3.157
	1	79.628	3.158	55.263	3.123	47.789	3.114	114.738	3.398
	1.5	144.185	3.460	68.505	3.179	53.567	3.135	232.312	4.621
15	0	38.782	3.084	38.765	3.145	38.776	3.098	38.765	3.144
	0.5	52.541	3.099	45.715	3.099	42.867	3.100	59.868	3.154
	1	79.575	3.156	55.179	3.119	47.717	3.109	114.572	3.365
	1.5	144.004	3.479	68.389	3.173	53.476	3.130	232.063	4.617
25	0	38.737	3.098	38.726	3.143	38.725	3.144	38.737	3.092
	0.5	52.465	3.144	45.651	3.109	42.802	3.142	59.784	3.153
	1	79.423	3.141	55.095	3.114	47.645	3.104	114.408	3.360
	1.5	143.818	3.479	68.273	3.168	53.385	3.124	231.812	4.630

Table 2.4: Evaluation of a_c for various values of Le, Ge, Sr and λ with $Q = 0.5$ and $Rs = 20$ for four types of gravity variations.

Le	Ge	Sr	λ	Case - A	Case - B	Case - C	Case - D
0.1	1	0.1	0	0.702	0.702	0.701	0.702
			0.4	0.784	0.745	0.727	0.821
			0.8	0.904	0.797	0.755	1.026
			1.6	1.472	0.941	0.822	2.362
1	1	0.1	0	2.111	2.094	2.095	2.109
			0.4	2.267	2.201	2.169	2.329
			0.8	2.437	2.279	2.226	2.628
			1.6	3.206	2.518	2.334	4.473
10	1	0.1	0	3.142	3.144	3.144	3.143
			0.4	3.144	3.143	3.097	3.148
			0.8	3.156	3.106	3.102	3.188
			1.2	3.209	3.132	3.113	3.773
10	0	0.1	0	3.145	3.146	3.146	3.145
			0.4	3.143	3.143	3.143	3.124
			0.8	3.153	3.147	3.144	3.205
			1.2	3.215	3.166	3.151	3.787
10	2	0.1	0	3.142	3.143	3.143	3.142
			0.4	3.144	3.143	3.143	3.091
			0.8	3.159	3.151	3.146	3.229
			1.2	3.234	3.174	3.156	3.758
10	1	0	0	3.117	3.117	3.118	3.117
			0.6	3.066	3.126	3.122	3.094
			1.2	3.181	3.158	3.137	3.760
			1.8	4.117	3.237	3.173	5.341
10	1	-0.5	0	2.876	2.777	2.781	2.873
			0.6	2.973	2.854	2.831	2.956
			1.2	3.089	2.948	2.887	3.698
			1.8	4.066	3.104	2.959	5.302

2.6 Conclusions

The double diffusive convection in a fluid saturated porous layer is studied due to the combined effects of the Soret parameter, vertical throughflow, changeable gravity field with height and viscous dissipation. Four different types (linear, quadratic, cubic and exponential) of gravity field variations are considered for the study. The main conclusions of the linear stability analysis are described in the following:

- The impact of increasing Q, Le, λ and Sr are found to lag the onset of convection, whereas Rs and Ge react to elevate the onset of convective motion.
- The size of the convective cells decreases with rising the effect of gravity field parameter, Lewis number and Soret parameter, while solutal Rayleigh number and Gebhart number has a dual character on the dimension of convection cells.
- It is distinguished that for Case - D the flow is more stable and for Case - C the flow is more unstable.

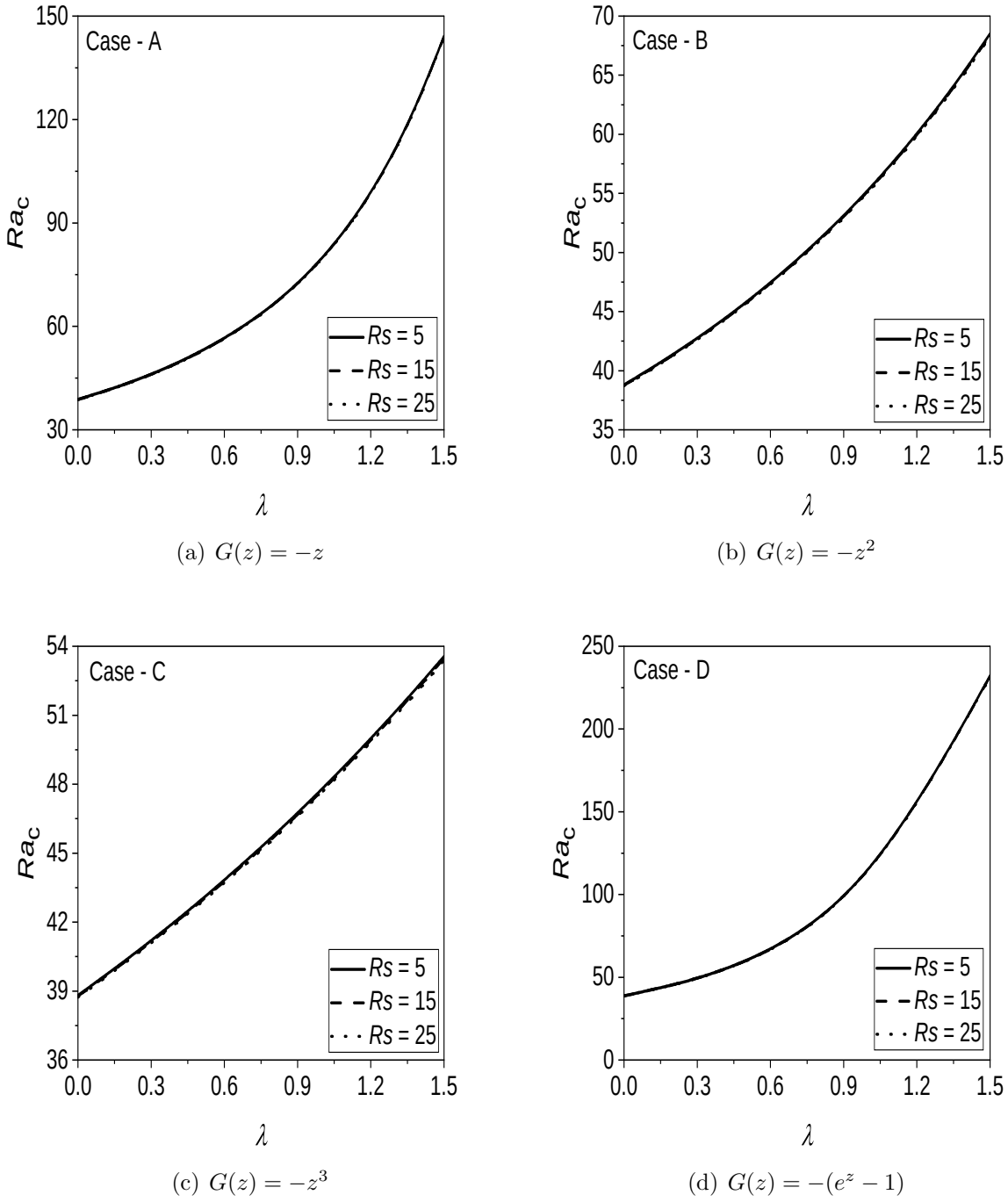

(a) $G(z) = -z$

(b) $G(z) = -z^2$

(c) $G(z) = -z^3$

(d) $G(z) = -(e^z - 1)$

Figure 2.2: Influence of solutal Rayleigh number (Rs) on Ra_c for four cases A, B, C and D when $Q = 0.5$, $Ge = 1$, $Le = 10$ and $Sr = 0.1$.

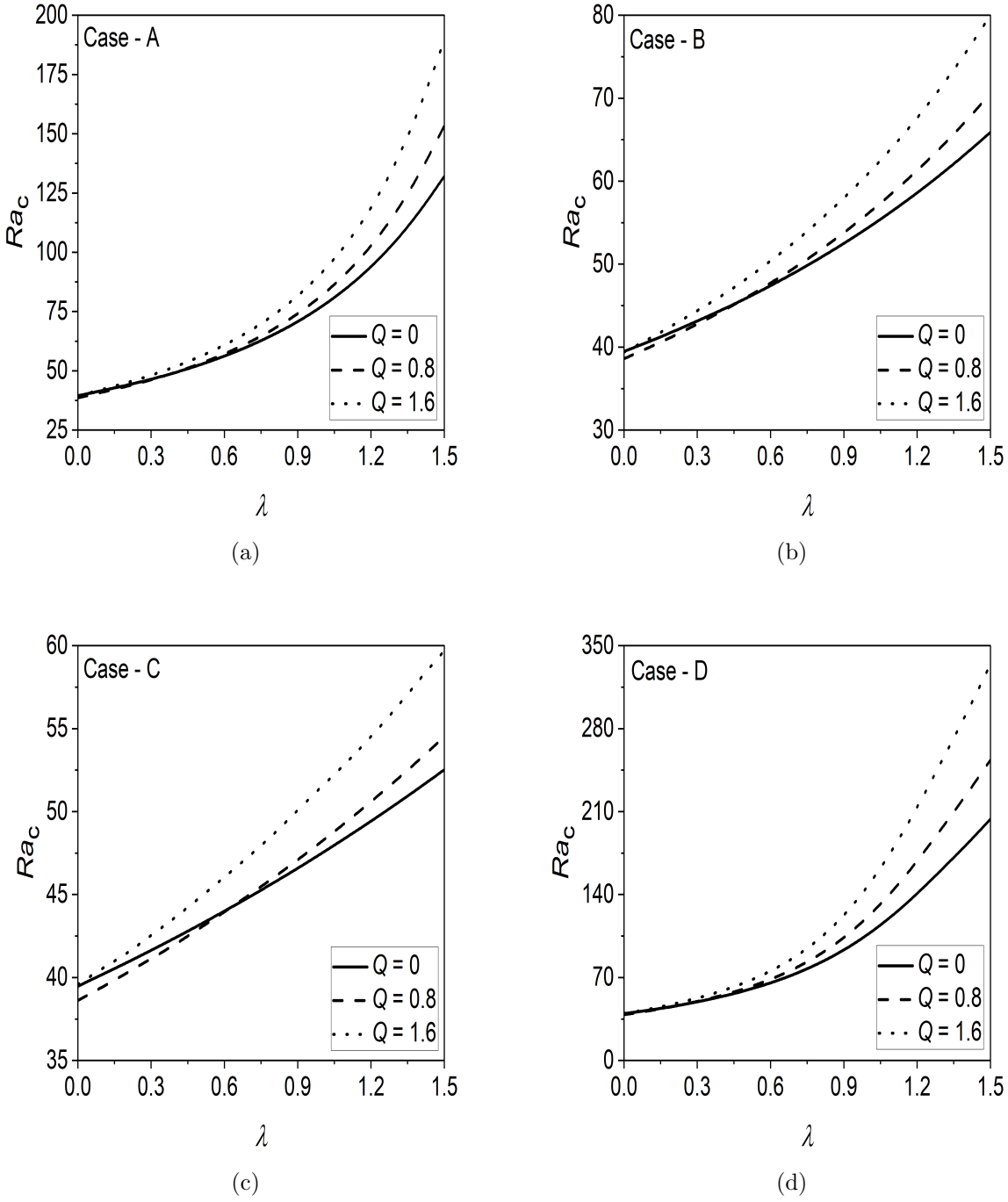

Figure 2.3: Influence of throughflow parameter (Q) on Ra_c for four cases A, B, C and D when $Rs = 20$, $Ge = 1$, $Le = 10$ and $Sr = 0.1$.

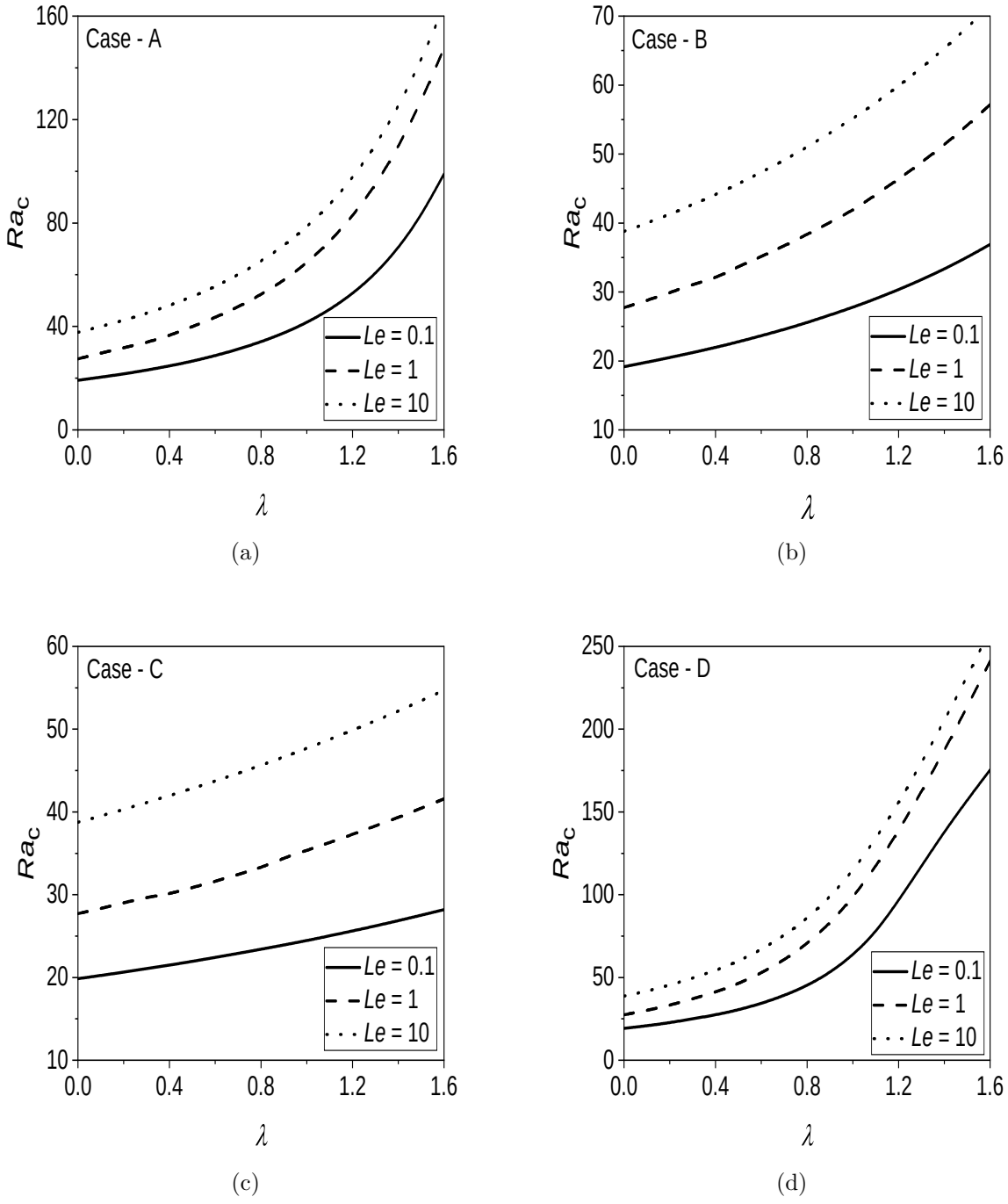

Figure 2.4: Influence of Lewis number (Le) on Ra_c for four cases A, B, C and D when $Q = 0.5$, $Ge = 1$, $Rs = 20$ and $Sr = 0.1$.

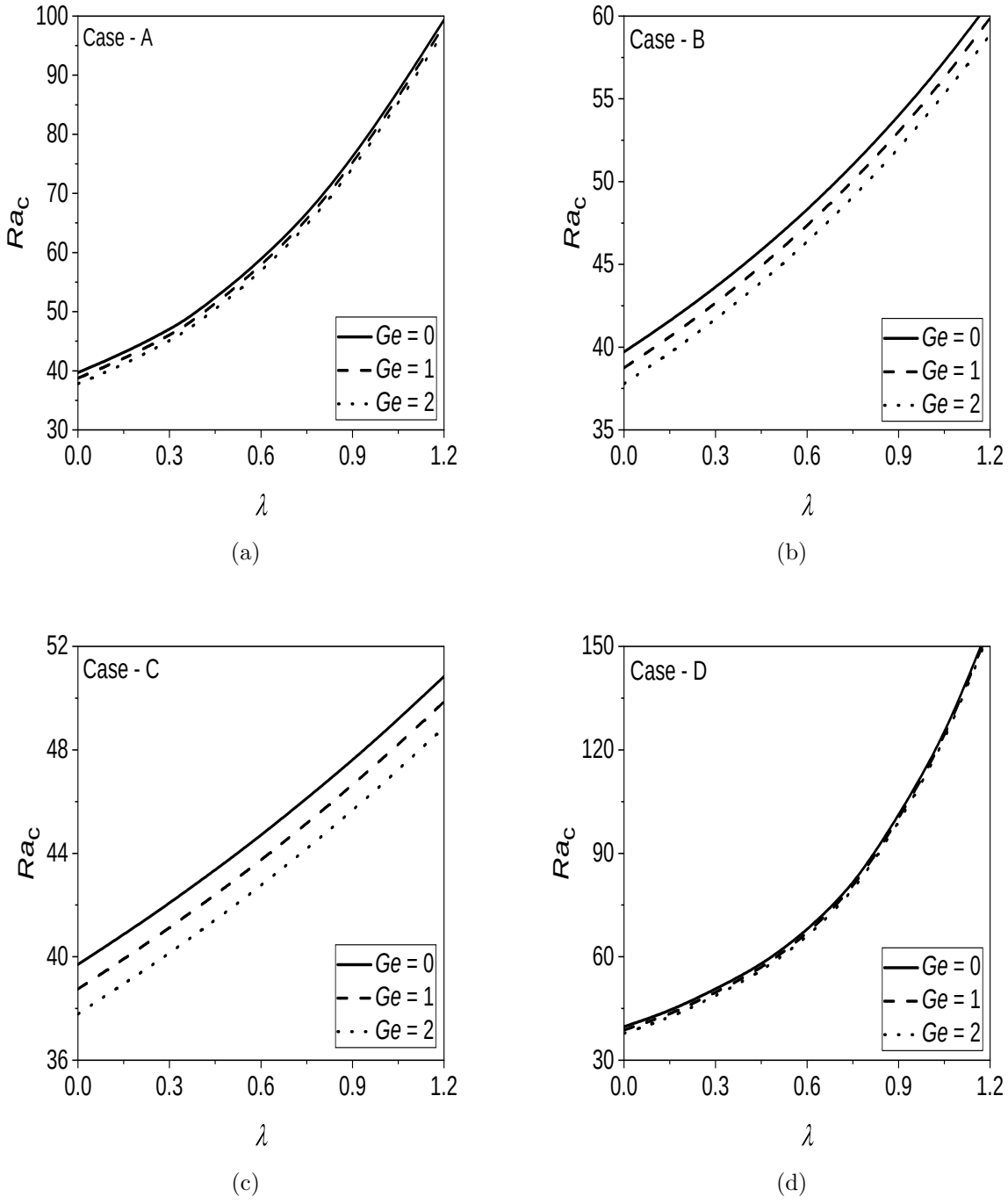

Figure 2.5: Influence of Gebhart number (Ge) on Ra_c for four cases A, B, C and D when $Q = 0.5$, $Rs = 20$, $Le = 10$ and $Sr = 0.1$.

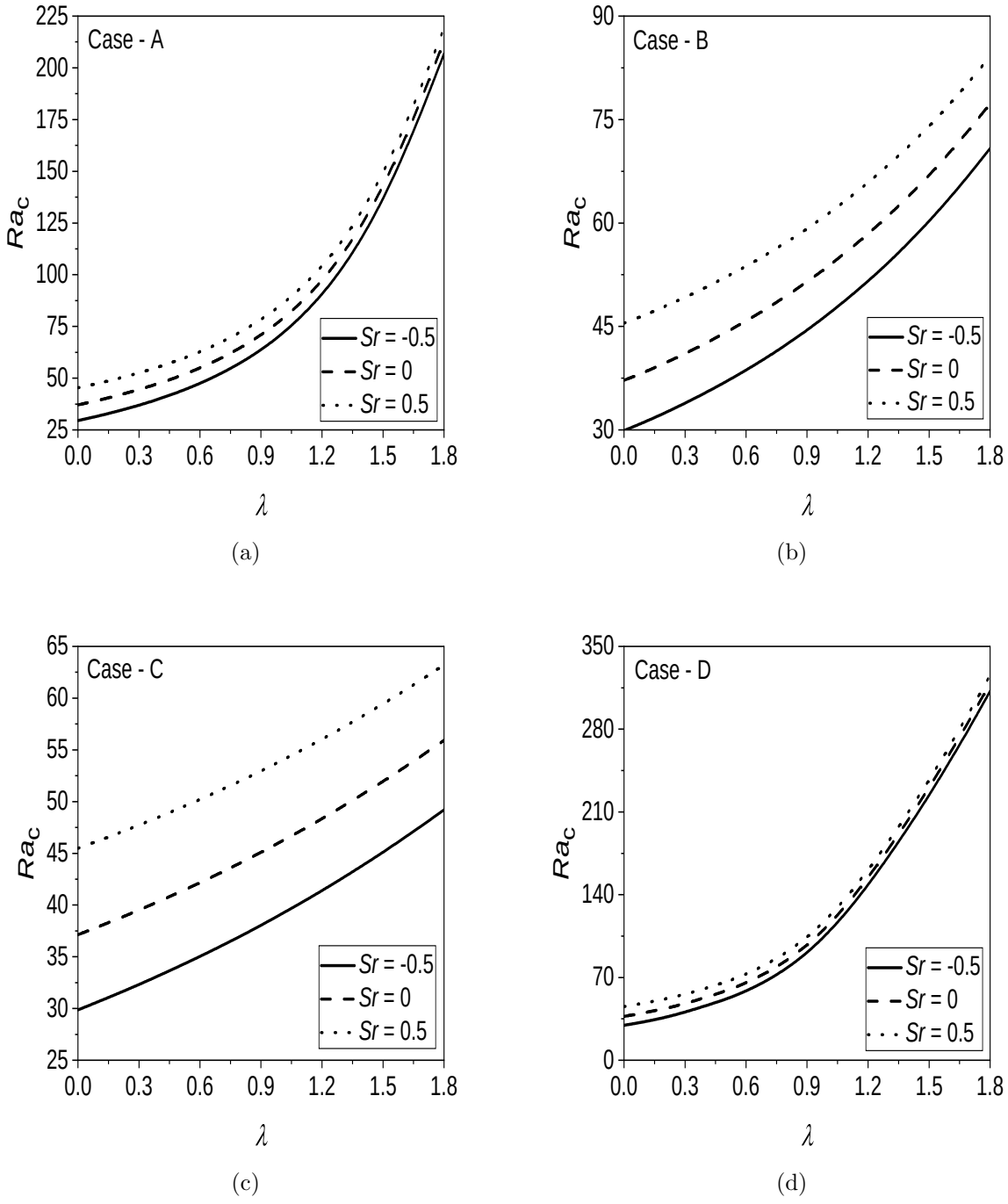

Figure 2.6: Influence of Soret parameter (Sr) on Ra_c for four cases A, B, C and D when $Q = 0.5$, $Rs = 20$, $Le = 10$ and $Ge = 1$.

Chapter 3

The variable gravity field and viscous dissipation effects on the convective instability in a porous layer with throughflow: Brinkman Model [1]

3.1 Introduction

The fluid flow and heat transfer in a horizontal porous layer is a fundamental convection problem due to its several fields of application such as chemical science, geophysics, engineering and nuclear industries, food processing and oceanography. The first investigation on the onset convection in a porous medium was done by Horton and Rogers Jr. [58] and Lapwood [66]. These problems are familiar as Horton–Rogers–Lapwood problem and are based on the Darcy model, which ignores the inertia force effect. A modification to the Darcy model was suggested by Brinkman [24] to model the flows with high porosity and large shear rates. Later, Nield [76] shown that the Brinkman term is more comfortable to study the inertia effect when the porosity of the medium is greater than 0.6. Several authors viz., Postelnicu and Rees [86], Postelnicu [85] and Wang and Tan [121] studied the onset convection in a porous layer using the Brinkman model under different situations. A comprehensive discussion on the thermal convection for Darcy–Brinkman model can be found in Nield and Bejan [78].

[1] Published in "***Journal of Porous Media***" 24(6), 1-13, 2021

In this chapter, the effects of the variable gravity field and viscous dissipation on the convective instability in a porous layer in the presence of throughflow using the Brinkman Model are analyzed by taking the top and bottom layer surfaces are rigid boundaries. The corresponding eigenvalue problem is solved numerically by using *bvp4c* routine in MATLAB.

3.2 Mathematical Formulation

Consider a horizontal porous layer of thickness L saturated with an incompressible viscous fluid. The variable gravity $\mathbf{g}(\mathrm{z})$ is acting in the opposite direction of z–axis as shown in Fig. 2.1. The Brinkman model and Oberbeck-Boussinesq are employed in the momentum equation. Also, the dissipation effect is assumed to be prominent in the medium. Under the above assumptions, the corresponding governing equations can be written as

$$\nabla \cdot \mathbf{u} = 0, \tag{3.1}$$

$$\frac{\rho_0}{\epsilon}\frac{\partial \mathbf{u}}{\partial t} = -\nabla p - \frac{\mu}{K}\mathbf{u} + \tilde{\mu}\nabla^2\mathbf{u} - \rho_0[1-\beta_{\mathrm{T}}(T-T_1)]\mathrm{g}(z)\hat{\mathbf{e}}_{\mathrm{z}}, \tag{3.2}$$

$$(\rho c)_{\mathrm{m}}\frac{\partial T}{\partial t} + (\rho c)\mathbf{u}\cdot\nabla T = k_{\mathrm{m}}\nabla^2 T + \frac{\mu}{K}\mathbf{u}\cdot\left(\mathbf{u} - \frac{K}{\mu}\tilde{\mu}\nabla^2\mathbf{u}\right), \tag{3.3}$$

where μ is the dynamic viscosity, $\tilde{\mu}$ is the effective dynamic viscosity and the remaining quantities are defined in Chapter - 2.

The corresponding boundary conditions are written as

$$w = W_{\mathrm{c}}, \quad \frac{\partial w}{\partial z} = 0, \quad T = T_1, \quad \text{at} \quad z = 0, \tag{3.4a}$$

$$w = W_{\mathrm{c}}, \quad \frac{\partial w}{\partial z} = 0, \quad T = T_2, \quad \text{at} \quad z = L. \tag{3.4b}$$

Using the non-dimensional scheme defined in Eq. (2.6), the dimensionless form of Eqs. (3.1)–(3.3), after eliminating pressure term from Eq. (3.2), are

$$\frac{Da}{Pr_{\mathrm{m}}}\frac{\partial}{\partial t}\left(\nabla^2 w\right) = -\nabla^2 w + \Lambda Da\nabla^4 w + Ra\nabla_{\mathrm{H}}^2 T(1+\lambda G(z)), \tag{3.5}$$

$$\gamma\frac{\partial T}{\partial t} + \mathbf{u}\cdot\nabla T = \nabla^2 T + \frac{GeDa}{Ra}\mathbf{u}\cdot\left(Da^{-1}\mathbf{u} - \Lambda\nabla^2\mathbf{u}\right). \tag{3.6}$$

The non-dimensional parameters are defied as $Da = \dfrac{K}{L^2}$ is the Darcy number, $\Lambda = \dfrac{\tilde{\mu}}{\mu}$ is the

viscosity ratio, and $Pr_{\rm m} = \dfrac{\mu\epsilon^2}{\alpha_{\rm m}\rho_0}$ is the modified Prandtl number. Also, $\Lambda = 1$ has been taken in this study due to a specific measurement of it.
The corresponding dimensionless boundary conditions are

$$w = Q, \quad \frac{\partial w}{\partial z} = 0, \quad T = 1, \quad \text{at} \quad z = 0, \tag{3.7a}$$

$$w = Q, \quad \frac{\partial w}{\partial z} = 0, \quad T = 0, \quad \text{at} \quad z = 1, \tag{3.7b}$$

where $Q = \dfrac{W_{\rm c}L}{\alpha_{\rm m}}$ is the throughflow parameter.

3.3 Basic state solution

Considering the basic state as steady, unidirectional and fully developed and then the basic velocity and the basic temperature are of the form: $\mathbf{u}_0 = (0, 0, Q)$ and $T_0 = T_0(z)$, respectively. The solution of the basic state temperature is

$$T_0 = \frac{e^Q + \frac{Ge}{Ra}Q}{e^Q - 1} - \frac{1 + \frac{Ge}{Ra}Q}{e^Q - 1}e^{Qz} + \frac{Ge}{Ra}Qz. \tag{3.8}$$

3.4 Linear stability analysis

As in Chapter - 2, we impose the infinitesimal disturbances (Eq. (2.14)) on the basic state solution and apply the usual normal mode form for the disturbances (Eq. (2.18)). Substituting Eq. (2.14) into Eqs. (3.5)–(3.6), neglecting δ^2 and higher order terms and then applying Eq. (2.18) into the resulting equations, we obtain the following system of ordinary differential equations for neutral stability modes ($\eta = 0$).

$$Da\left(\frac{d^4\hat{w}}{dz^4} - 2a^2\frac{d^2\hat{w}}{dz^2} + a^4\hat{w}\right) - \left(\frac{d^2\hat{w}}{dz^2} - a^2\hat{w}\right) - a^2Ra\hat{T}\left(1 + \lambda G(z)\right) = 0, \tag{3.9}$$

$$-\frac{dT_0}{dz}\hat{w} + \frac{QGeDa}{Ra}\left[2Da^{-1}\hat{w} - \left(\frac{d^2\hat{w}}{dz^2} - a^2\hat{w}\right)\right] + \left(\frac{d^2\hat{T}}{dz^2} - Q\frac{d\hat{T}}{dz} - a^2\hat{T}\right) = 0, \tag{3.10}$$

where $a = \sqrt{a_x^2 + a_y^2}$ is the resulting wavenumber. The corresponding perturbed boundary conditions are

$$\hat{w} = \frac{d\hat{w}}{dz} = \hat{T} = 0 \quad \text{at} \quad z = 0, 1. \tag{3.11}$$

3.5 Results and discussion

The Eqs. (3.9)–(3.10) define an eigenvalue problem solved using the *bvp4c* routine in MATLAB. In this investigation, three types of gravitational force viz., linear, quadratic and exponential are considered. The gravity force functions are taken as $G(z) = -z$ (for linear variations and is denoted by Case - A), $G(z) = -z^2$ (for quadratic variations and is denoted by Case - B) and $G(z) = -(e^z - 1)$ (for exponential variations and is denoted by Case - C). To confirm the exactness of our code, the results obtained from the present analysis are compared with the results of Rionero and Straughan [91] in absence of throughflow parameter (Q) and Yadav [123] in presence of throughflow parameter (Q) for Cases A, B and C, and tabulated in Tables 3.1 and 3.2, respectively. The critical Rayleigh number and corresponding wavenumber are calculated for stationary convection. The parameters Ge and Da are taken to be zero for both tables. From Tables 3.1 and 3.2, it can be noticed that the results are in good agreement with the results of Rionero and Straughan [91] and Yadav [123]. The effects of viscous dissipation and the gravity variation parameter for the onset of convective rolls are depicted through the results exhibited in Table 3.3 for linear, quadratic and exponential gravity field at $Q = 0.5$ and $Da = 0.1$. The values of Ge are taken as 0, $10^{-5}, 10^{-2}, 10^{-1}$, 0.5 and 1 (Barletta et al. [14]). It is observed that the critical Rayleigh number Ra_c and corresponding wavenumber a_c depend significantly on λ, while they depend weakly on Ge. In the other words, viscous dissipation has a weak destabilizing effect on the Brinkman flow regime. This is because the action of shear forces leads the work done by a fluid on adjacent layers is transformed into heat and it refers to rise the convective motion. The critical Rayleigh number enhances with an increased value of λ and it indicates λ has a stabilizing effect on the flow field. This is happening since the disturbances of the system regain due to the increment of λ which offers a delay in the gravity field. Thus the convective instability is postponing with the augment of λ. The size of the convective cells decreases upon enhancing the value of Ge, while it increases for small values of λ and opposite nature has been observed for large values of λ. Fig. 3.1 reveals the variation of critical Rayleigh number Ra_c and corresponding wavenumber a_c due to the effect of throughflow parameter Q. It may note that the value of Ra_c increases with Q. Therefore, convective motion delays due to the growing value of Q. Since the urgent heat gradients to a boundary layer can modify with the increased value of the throughflow parameter Q and also it can shift where the throughflow is narrated. This indicates that Q stabilizes the flow.

Quantitatively speaking, the value of Ra_c is changed from 357.029 to 380.138, 275.437 to 290.238 and 455.688 to 504.069 (i.e., Ra_c increased 6.5%, 5.4% and 10.5%, respectively) for

linear, quadratic and exponential gravity field variable, respectively, on replacing Q equal to 0 by 1 at $\lambda = 0.8$, $Da = 0.1$ and $Ge = 1$. Further enhancing the value of Q from 1 to 2, Ra_c increased 15.5% (i.e., from 380.138 to 438.951) for linear, 14.3% (i.e., from 290.238 to 331.895) for quadratic gravity field variable and 20.6% (i.e., from 504.069 to 607.737) for exponential field variable. However, when λ replaced by 1.5 the corresponding critical Rayleigh number is changed from 799.911 to 945.649 (i.e., increased approximately 18.2%) and 945.649 to 1230.067 (i.e., increased approximately 30.1%) for linear gravity function, from 362.071 to 396.779 (i.e., increased approximately 9.6%) and 396.779 to 474.024 (i.e., increased approximately 19.5%) for quadratic gravity function and from 1826.612 to 2430.965 (i.e., increased approximately 33%) and 2430.965 to 3508.877 (i.e., increased approximately 44.3%) for exponential gravity function on the stepwise changing of Q from 0 to 1 and 1 to 2, respectively. So, from this quantitative analysis, it can be concluded that the onset of convection can manage via throughflow parameter, i.e., by choosing suitable governing parameter, the onset convection can advance or postpone. The effect of Darcy number Da on the variation of critical Rayleigh number Ra_c and corresponding wavenumber a_c are displayed in the Fig. 3.2 for categories (A) $G(z) = -z$, (B) $G(z) = -z^2$ and (C) $G(z) = -(e^z - 1)$. It is observed that Ra_c increases with growing value of Da, while a_c decreases with augment value of Da. Therefore, the characteristic of enhancing Da delays the arrival of convective motion. Since the viscous effects, as mediated by the Brinkman terms, increase as Da increases, which leads the enhance value of Ra_c, which leads to enhance in the estimate of Ra_c. Also, the dimension of convective cells elevated as in the increase value of Da. In particular, the limiting case of the Darcy flow regime ($Da \to \infty$) without porous medium and in absence of throughflow parameter ($Q = 0$) and viscous dissipation ($Ge = 0$) gives $Ra_c = 1707.765$ and $a_c = 3.116$ for constant gravity variation function ($\lambda = 0$), which matches up to second decimal places with the corresponding exact and well-known results $Ra_c = 1707.762$ and $a_c = 3.117$ for Rayleigh–Bénard convection presented by Chandrasekhar [32]. Further, it is noticed that the system is more stable for exponential varying gravity field, while more unstable for quadratic varying gravity field. When $Da = 0$, the Brinkman flow regime is switching back to the Darcy flow regime. The onset of convection of Darcy flow is addressed by Yadav [123] in absence of viscous dissipation effect. From Table 3.4, it is clear that viscous dissipation has a weak destabilizing effect on the Darcy flow regime also.

Table 3.1: Comparison of Ra_c and a_c^2 between the results obtained by Rionero and Straughan [91] and present results when $Ge = 0$, $Q = 0$ and $Da = 0$ for cases (A) $G(z) = -z$, (B) $G(z) = -z^2$ and (C) $G(z) = -(e^z - 1)$.

$G(z)$	λ	Rionero and Straughan [91]		Present results	
		Ra_c	a_c^2	Ra_c	a_c^2
Case - A	0	39.478	9.870	39.478	9.870
	1	77.020	10.209	77.080	10.209
	1.5	132.020	12.314	132.021	12.314
	1.8	189.908	17.198	189.908	17.198
	1.9	212.280	19.477	212.284	19.477
Case - B	0	39.478	9.870	39.478	9.870
	0.2	41.832	9.874	41.832	9.874
	0.4	44.455	9.887	44.455	9.887
	0.6	47.389	9.915	47.389	9.915
	0.8	50.682	9.961	50.682	9.961
	1	54.390	10.034	54.390	10.034
Case - C	0	39.478	9.870	39.478	9.870
	0.1	42.331	9.872	42.331	9.872
	0.2	45.607	9.883	45.607	9.883
	0.3	49.398	9.904	49.398	9.904
	0.4	53.828	9.942	53.828	9.942
	0.5	59.053	10.005	59.053	10.005

Table 3.2: Comparison of Ra_c and a_c between the results obtained by Yadav [123] and present results when $Ge = 0$ and $Da = 0$ for cases (A) $G(z) = -z$, (B) $G(z) = -z^2$ and (C) $G(z) = -(e^z - 1)$.

$G(z)$	Q	λ	Yadav [123]		Present results	
			Ra_c	a_c	Ra_c	a_c
Case - A	0.5	0	39.827	3.151	39.827	3.151
		0.6	57.569	3.146	57.569	3.146
		1.2	99.660	3.224	99.661	3.224
	1	0	40.873	3.179	40.873	3.179
		0.6	60.071	3.159	60.073	3.159
		1.2	108.160	3.208	108.164	3.208
Case - B	0.5	0	39.827	3.151	39.827	3.151
		0.6	48.469	3.146	48.469	3.146
		1.2	61.088	3.167	61.089	3.167
	1	0	40.873	3.179	40.873	3.179
		0.6	50.462	3.161	50.463	3.161
		1.2	64.938	3.166	64.939	3.166
Case - C	0.5	0	39.827	3.151	39.827	3.151
		0.6	67.948	3.162	67.948	3.162
		1.2	157.128	3.798	157.127	3.798
	1	0	40.873	3.179	40.873	3.179
		0.6	72.051	3.162	72.050	3.162
		1.2	179.933	3.812	179.934	3.812

Table 3.3: Evaluation of Ra_c (in roman) and a_c (in *italic*) for different values of Ge and λ when $Da = 0.1$ and $Q = 0.5$ for cases (A) $G(z) = -z$, (B) $G(z) = -z^2$ and (C) $G(z) = -(e^z - 1)$.

$G(z)$	λ	$Ge = 0$	$Ge = 10^{-5}$	$Ge = 10^{-2}$	$Ge = 10^{-1}$	$Ge = 0.5$	$Ge = 1$
Case - A	0	217.348	217.339	217.330	217.149	216.341	215.331
		3.154	*3.154*	*3.154*	*3.154*	*3.157*	*3.159*
	0.2	242.122	242.122	242.078	241.902	241.108	240.085
		3.153	*3.153*	*3.153*	*3.154*	*3.155*	*3.158*
	0.4	273.143	273.143	273.123	272.941	272.131	271.118
		3.152	*3.152*	*3.152*	*3.153*	*3.154*	*3.157*
	0.6	313.145	313.145	313.125	312.942	312.129	311.114
		3.152	*3.152*	*3.152*	*3.152*	*3.154*	*3.156*
	0.8	366.539	366.539	366.538	366.335	365.519	364.498
		3.152	*3.153*	*3.153*	*3.153*	*3.155*	*3.156*
	1	441.107	441.107	441.087	440.902	440.078	439.054
		3.157	*3.157*	*3.157*	*3.157*	*3.159*	*3.160*
	1.2	551.645	551.645	551.624	551.436	550.601	549.553
		3.169	*3.169*	*3.169*	*3.169*	*3.170*	*3.171*
Case - B	0	217.348	217.339	217.330	217.149	216.341	215.331
		3.154	*3.154*	*3.154*	*3.154*	*3.157*	*3.159*
	0.2	230.619	230.618	230.599	230.417	229.6071	228.596
		3.153	*3.153*	*3.153*	*3.154*	*3.156*	*3.158*
	0.4	245.551	245.550	245.530	245.348	244.538	243.460
		3.152	*3.152*	*3.152*	*3.153*	*3.155*	*3.157*
	0.6	262.466	262.466	262.446	262.263	261.448	260.431
		3.152	*3.152*	*3.152*	*3.152*	*3.154*	*3.156*
	0.8	281.765	281.765	281.744	281.561	280.746	279.727
		3.152	*3.152*	*3.152*	*3.152*	*3.154*	*3.156*
	1	303.959	303.959	303.939	303.754	302.933	301.912
		3.153	*3.153*	*3.153*	*3.153*	*3.155*	*3.157*
	1.2	329.700	329.700	329.679	329.494	328.671	327.642
		3.155	*3.155*	*3.155*	*3.156*	*3.157*	*3.159*
Case - C	0	217.337	217.337	217.330	217.149	216.341	215.332
		3.154	*3.154*	*3.154*	*3.154*	*3.157*	*3.159*
	0.2	252.075	252.075	252.055	251.872	251.062	250.051
		3.153	*3.152*	*3.152*	*3.153*	*3.155*	*3.157*
	0.4	299.670	299.670	299.649	299.467	298.653	297.637
		3.152	*3.152*	*3.152*	*3.152*	*3.154*	*3.156*
	0.6	368.578	368.578	368.557	368.372	367.552	366.527
		3.155	*3.155*	*3.155*	*3.155*	*3.156*	*3.158*
	0.8	476.012	476.012	475.991	475.804	474.968	473.923
		3.166	*3.167*	*3.167*	*3.167*	*3.168*	*3.169*
	1	660.960	660.960	660.938	660.742	659.869	658.776
		3.210	*3.210*	*3.210*	*3.210*	*3.211*	*3.212*
	1.2	1014.252	1014.252	1014.228	1014.003	1013.023	1011.790
		3.372	*3.372*	*3.372*	*3.373*	*3.373*	*3.374*

Table 3.4: Evaluation of Ra_c (in roman) and a_c (in *italic*) for Darcy regime flow at different values of Ge and λ when $Q = 0.5$ for cases (A) $G(z) = -z$, (B) $G(z) = -z^2$ and (C) $G(z) = -(e^z - 1)$.

$G(z)$	λ	$Ge = 10^{-5}$	$Ge = 10^{-2}$	$Ge = 10^{-1}$	$Ge = 0.5$	$Ge = 1$
Case - A	0	39.827	39.821	39.727	39.326	38.825
		3.151	*3.151*	*3.151*	*3.151*	*3.151*
	0.2	44.427	44.417	44.326	43.924	43.424
		3.148	*3.148*	*3.148*	*3.148*	*3.148*
	0.4	50.183	50.173	50.082	49.680	49.176
		3.146	*3.146*	*3.146*	*3.146*	*3.146*
	0.6	57.569	57.559	57.469	57.065	56.562
		3.147	*3.146*	*3.146*	*3.146*	*3.147*
	0.8	67.334	67.324	67.233	66.828	66.321
		3.153	*3.153*	*3.153*	*3.153*	*3.153*
	1	80.697	80.687	80.595	80.188	79.679
		3.173	*3.173*	*3.173*	*3.173*	*3.173*
	1.2	99.661	99.651	99.558	99.148	98.636
		3.224	*3.224*	*3.224*	*3.225*	*3.225*
Case - B	0	39.827	39.821	39.727	39.326	38.825
		3.151	*3.151*	*3.151*	*3.151*	*3.151*
	0.2	42.374	42.364	42.274	41.872	41.370
		3.148	*3.148*	*3.148*	*3.148*	*3.148*
	0.4	45.237	45.227	45.136	44.734	44.231
		3.146	*3.146*	*3.146*	*3.146*	*3.146*
	0.6	48.469	48.459	48.368	47.965	47.461
		3.146	*3.146*	*3.146*	*3.146*	*3.146*
	0.8	52.136	52.126	52.035	51.631	51.126
		3.149	*3.149*	*3.149*	*3.149*	*3.149*
	1	56.314	56.304	56.213	55.807	55.300
		3.155	*3.155*	*3.155*	*3.155*	*3.155*
	1.2	61.089	61.079	60.987	60.581	60.072
		3.167	*3.167*	*3.167*	*3.168*	*3.168*
Case - C	0	39.827	39.821	39.727	39.326	38.825
		3.151	*3.151*	*3.151*	*3.151*	*3.151*
	0.2	46.350	46.340	46.250	45.848	45.345
		3.146	*3.146*	*3.146*	*3.146*	*3.146*
	0.4	55.254	55.244	55.153	54.749	54.244
		3.147	*3.147*	*3.147*	*3.147*	*3.147*
	0.6	67.949	67.939	67.847	67.441	66.933
		3.163	*3.163*	*3.163*	*3.163*	*3.146*
	0.8	86.899	86.889	86.797	86.387	85.875
		3.219	*3.219*	*3.219*	*3.219*	*3.219*
	1	115.855	115.844	115.751	115.336	114.818
		3.389	*3.389*	*3.389*	*3.389*	*3.389*
	1.2	157.131	157.121	157.026	156.607	156.080
		3.798	*3.798*	*3.798*	*3.798*	*3.798*

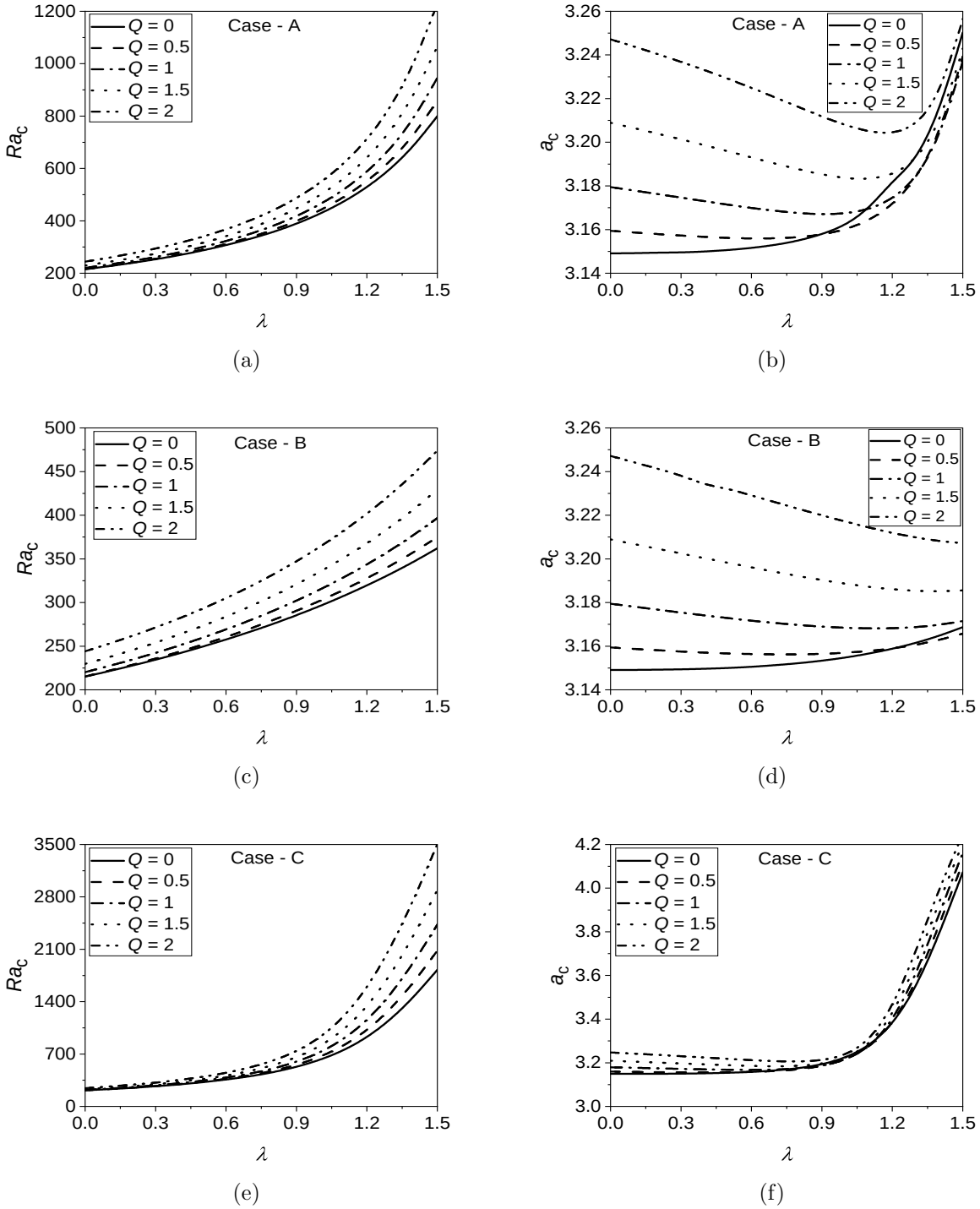

Figure 3.1: Effect of throughflow parameter (Q) on Ra_{c} and a_{c} for cases - A, B and C when $Ge = 1$ and $Da = 0.1$.

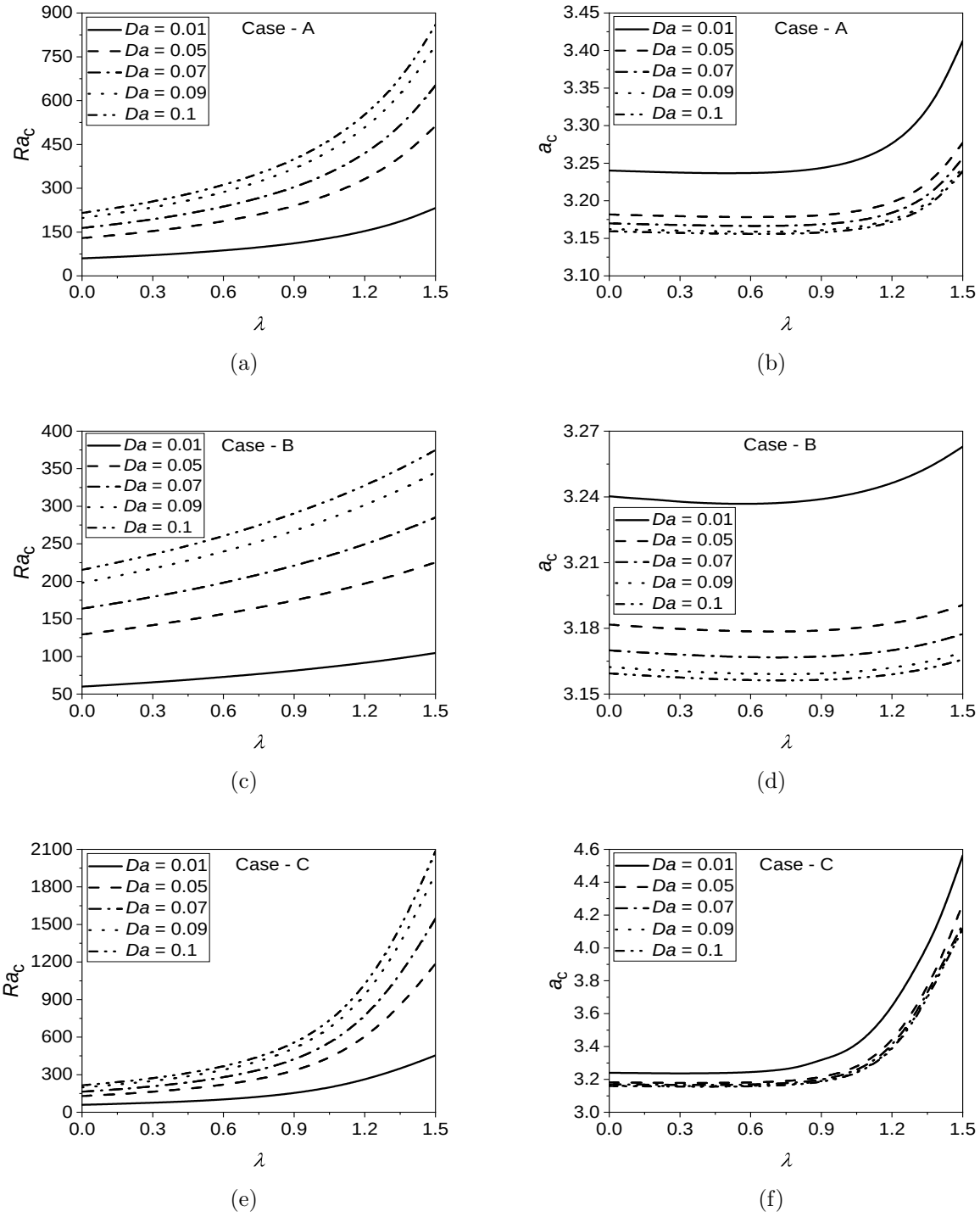

Figure 3.2: Effect of Darcy number (Da) on Ra_c and a_c for cases - A, B and C when $Ge = 1$ and $Q = 0.5$.

3.6 Conclusions

The combined effect of the changeable gravity field, throughflow, viscous dissipation, and Darcy number in a horizontal porous layer has been studied on the onset of convection. Also, the boundaries of the planes are kept at constant temperatures. Linear, quadratic and exponential changeable gravity fields are taken into account in this investigation.

- It is found that the Darcy number, throughflow parameter, and gravity variation parameter have a stabilizing effect. The system is destabilizing due to the effect of viscous dissipation.
- The dimension of the convective cells increases with the rising Darcy number, decreases with the enhancing value of Gebhart number, while the dual character is observed with the increasing magnitudes of throughflow parameter and gravity variation parameter.
- The convective motion postpones very quickly for exponential varying gravity field while advances very quickly for quadratic varying gravity field.
- The critical wavenumber a_c increases monotonically in absence of the vertical throughflow parameter (Q), but it shows a dual nature (first decreases and then increases) in the presence of the vertical throughflow parameter (Q) when λ increases from 0 to 1.5.
- The viscous dissipation has a weak destabilizing effect for the Darcy flow regime also. It is observed that the flow field becomes more stable for the Brinkam model as compared with the Darcy model.

Chapter 4

Effect of variable gravity field on the onset of convection in a Brinkman porous medium under convective boundary conditions [1]

4.1 Introduction

The majority of the investigations on the Darcy-Bénard convection or Horten-Rogers-Lapwood problem were carried out either by using the combination of two Dirichlet boundary conditions at the two boundaries maintained at prescribed temperature or the combination of Neumann (prescribed heat flux) and Dirichlet (Prescribed temperature) thermal boundary conditions at the two boundaries.

Recently, a novel mechanism for the heating process, by providing the heat with a finite capacity to the convecting fluid through the bounding surface, has been attracted by numerous researchers. This type of thermal boundary condition is called convective thermal boundary condition or Robin-type boundary condition and is a mixture of Dirichlet and Neumann thermal boundaries. Robin boundary conditions are the mathematical formulation of Newton's law of cooling where the heat transfer coefficient is utilized. This condition corresponds to the existence of convection heating (or cooling) at the surface and is obtained from the surface energy balance. Investigation of heat transfer with the convective thermal condition has received significant attention in mechanical and design fields, for example, heat exchangers, atomic plants, gas turbines, and so forth. Also, it occurs when a solid substrate is in contact with the fluid at a different temperature and involves relative motion

[1] Communicated in "***Indian Journal of Physics***"

between the fluid and the substrate. In many practical applications involving cooling or heating of the surface, the presence of convective heat exchange between the surface and the surrounding fluid cannot be neglected, and this is a very crucial aspect in the thermal materials processing industries.

Several researchers investigated the Darcy-Bénard convection by invoking the general case of the thermal boundary condition i.e. Robin-type boundary condition by considering the imperfectly conducting boundaries. Storesletten and Barletta [105] studied the onset of convection by assuming the lower boundary as adiabatic while the upper boundary is subject to Robin-type boundary condition which introduced the non-dimensional parameter Bi known as Biot number. They claimed that the onset of convection strongly depends on Bi. Barletta *et al.* [10] discussed the instability mechanism due to the combined effect of free surface and convective boundary condition inside a non-equilibrium regime. Braga *et al.* [23] investigated the stability analysis inside a porous channel where the lower boundary is heated by uniform heat flux and the upper boundary is cooled by external cooling. Dubey and Murthy [45] studied the onset of convection on the Brinkman extended Darcy's model in the presence of convective thermal boundary conditions on the boundaries and extended for double diffusive convection [46].

In this chapter, we investigated the instability mechanism due to the effect of third kind thermal boundary or Robin type boundary conditions in a horizontal porous layer in the presence of linear and quadratic varying gravity fields. The *bvp4c* routine in MATLAB used to calculate the critical Rayleigh number (Ra_{c}) and corresponding wavenumber (a_{c}).

4.2 Mathematical Formulation

Consider an incompressible fluid saturated in a horizontal porous layer of thickness L with rigid, impermeable and thermally conducting boundary planes. The geoetry and coordinate system is shown in Fig. 2.1. The variable gravity $\mathbf{g}(\mathrm{z})$ is acting in the opposite direction of z–axis. There is a basic temperature difference ΔT across the two boundaries. The fluid-saturated porous layer is considered to be heated from below with further heating by some external sources at both the boundaries.

Using the Brinkman extension to the Darcy's law, the governing equations of the flow are

$$\nabla \cdot \mathbf{u} = 0, \tag{4.1}$$

$$\frac{\rho_0}{\epsilon}\frac{\partial \mathbf{u}}{\partial t} = -\nabla p - \frac{\mu}{K}\mathbf{u} + \tilde{\mu}\nabla^2\mathbf{u} + \rho_0 \mathrm{g}\beta_\mathrm{T}(T - T_0)\mathrm{g}(z)\hat{\mathbf{e}}_\mathbf{z}, \tag{4.2}$$

$$(\rho c)_\mathrm{m}\frac{\partial T}{\partial t} + (\rho c)(\mathbf{u}\cdot\nabla T) = k_\mathrm{m}\nabla^2 T. \tag{4.3}$$

All the quantities are defined in Chapter - 2.

$$z = 0: \quad w = 0, \quad \frac{\partial w}{\partial z} = 0, \quad -k_\mathrm{m}\frac{\partial T}{\partial z} + h_0(T - T_0 - \Delta T) = q_0, \tag{4.4a}$$

$$z = L: \quad w = 0, \quad \frac{\partial w}{\partial z} = 0, \quad -k_\mathrm{m}\frac{\partial T}{\partial z} - h_1(T - T_0) = q_0, \tag{4.4b}$$

where $\Delta T = \dfrac{q_0 L}{k_\mathrm{m}}$, q_0 is the constant heat flux at both the boundaries.

Applying the non-dimensional variables given in Eq. (2.6) in the Eqs. (4.1)–(4.4), after eliminating pressure term, we get (by removing asterisk)

$$\frac{Da}{Pr_\mathrm{m}}\frac{\partial}{\partial t}(\nabla^2 w) = -\nabla^2 w + Da\nabla^4 w + Ra\nabla_\mathrm{H}^2 T[1 + \lambda G(z)], \tag{4.5}$$

$$\gamma\frac{\partial T}{\partial t} + \mathbf{u}\cdot\nabla T = \nabla^2 T, \tag{4.6}$$

subject to the boundary conditions

$$z = 0: \quad w = 0, \quad \frac{\partial w}{\partial z} = 0, \quad -\frac{\partial T}{\partial z} + B_0(T - 1) = 1, \tag{4.7a}$$

$$z = 1: \quad w = 0, \quad \frac{\partial w}{\partial z} = 0, \quad -\frac{\partial T}{\partial z} - B_1 T = 1, \tag{4.7b}$$

where $B_0 = \dfrac{h_0 L}{k_\mathrm{m}}$ and $B_1 = \dfrac{h_1 L}{k_\mathrm{m}}$ are the Biot numbers for the lower and upper boundaries, respectively. The other parameters are defined in Chapter - 2.

4.3 Basic state solution

The basic state is considered as time independent, unidirectional and fully developed. The basic velocity and the basic temperature are of the form $\mathbf{u}_0 = (0, 0, 0)$ and $T_0 = T_0(z)$, respectively.

The Eq. (4.6) can be written

$$\frac{d^2 T_0}{dz^2} = 0, \tag{4.8}$$

subject to the boundary conditions

$$z = 0: \quad -\frac{dT_0}{dz} + B_0(T_0 - 1) = 1, \tag{4.9a}$$

$$z = 1: \quad -\frac{dT_0}{dz} - B_1 T_0 = 1. \tag{4.9b}$$

The solution of the basic temperature (after applying boundary conditions Eq. (4.9)) is

$$T_0(z) = 1 - z. \tag{4.10}$$

4.4 Linear stability analysis

As in Chapter - 2 and Chapter - 3, imposing the infinitesimal disturbances on the basic state solution and applying the usual normal mode form for the disturbances, we obtain the following system of ordinary differential equations for neutral stability modes ($\eta = 0$)

$$Da\left(\frac{d^4\hat{w}}{dz^4} - 2a^2\frac{d^2\hat{w}}{dz^2} + a^4\hat{w}\right) - \left(\frac{d^2\hat{w}}{dz^2} - a^2\hat{w}\right) - a^2 Ra\hat{T}\left(1 + \lambda G(z)\right) = 0, \tag{4.11}$$

$$-\frac{dT_0}{dz}\hat{w} + \left(\frac{d^2\hat{T}}{dz^2} - a^2\hat{T}\right) = 0, \tag{4.12}$$

corresponding disturbances boundary conditions are

$$z = 0: \quad \hat{w} = 0, \quad \frac{d\hat{w}}{dz} = 0, \quad -\frac{d\hat{T}}{dz} + B_0\hat{T} = 0, \tag{4.13a}$$

$$z = 1: \quad \hat{w} = 0, \quad \frac{d\hat{w}}{dz} = 0, \quad \frac{d\hat{T}}{dz} + B_1\hat{T} = 0. \tag{4.13b}$$

4.5 Results and discussion

The solutions of the governing Eqs. (4.11)–(4.12) corresponding with boundary conditions Eq. (4.13) is obtained using the *bvp4c* routine in MATLAB. The numerical results of the convective instability in a horizontal porous layer considering the linear ($G(z) = -z$ denoted by Case (A)) and quadratic ($G(z) = -z^2$, denoted by Case (B)) variable gravity field under third kind of thermal boundary conditions are presented graphically. The values of B_0 and B_1 are taken as 0.01, 0.1, 1, 10 and 100 ([46]).

To validate the correctness of our present results, the results obtained from the present analysis are compared with the results of Rionero and Straughan [91] in absence of Q and λ

and $Da \to 0$, $B_0 \to \infty$ and $B_1 \to \infty$ and presented in Table 4.1 for the linear ($G(z) = -z$) and quadratic ($G(z) = -z^2$) varying gravity fields. From this Table 4.1, it can be noticed that the results are in good agreement with the results of Rionero and Straughan [91].

Table 4.2 describes the effect of linear and quadratic varying gravity fields, Darcy number (Da) and Biot numbers B_0 and B_1 for fixed value of $\lambda = 0.5$. It is noticed that the linearly varying gravity field shows a more stabilizing nature compared to the quadratic varying gravity field. As the Darcy number increases, the critical Rayleigh number is also increasing for both linear and quadratic gravity fields. Hence the Darcy number exerts a stabilizing influence on the stationary convection regime. The effect of Biot number at the lower plate i.e. heat served from the lower boundary is to increase the critical Rayleigh number for both linear and quadratic gravity fields. A similar trend is observed for the effect of the Biot number at the upper plate.

Figure 4.1 display the variation of critical Rayleigh number as a function of variable gravity parameter λ for different values of the Biot numbers B_0 and B_1 in different flow regimes. In particular, Figs. 4.1(a), 4.1(c), 4.1(e) and 4.1(g) represents the linearly gravity field and Figs. 4.1(b), 4.1(d), 4.1(f) and 4.1(h) denote quadratic varying gravity field for $Da = 0$, 0.01, 1 and 100, respectively. It is seen from Fig. 4.1 that the preferred mode of instability occurs at $\lambda = 0$ in all the flow regimes represented by the various values of Da. The values of Ra_c increases with an increase in the gravity variation parameter (λ). Hence, the gravity variation parameter has a stabilizing effect. Because the disturbance in the system regain as the gravitational field decreases and this refers to delay the convection. Further, the quantitative response of Ra_c indicates that Da has a stabilizing effect in the Brinkman flow regime, with different combinations of Biot numbers. This is happening because of enhancing the viscous effects. The size of the convective cells shows a dual nature with an increased value of λ and Da. The critical Rayleigh number is increasing with increasing values of B_0 and B_1.

Figures 4.2(a), 4.2(c), 4.2(e) and 4.2(g) display the variation of critical wavenumber for linearly varying gravity field with λ for different values of the Biot numbers B_0 and B_1 for $Da = 0$, 0.01, 1 and 100, respectively. It is observed from these figures that the effect of Biot numbers is to increase a_c. But the effect of gravity varaition parameter is visible only for $\lambda > 1$. Figs. 4.2(b), 4.2(d), 4.2(f) and 4.2(h) denote the variation of critical wavenumber for quadratic varying gravity field with λ for different values of the Biot numbers B_0 and $B_1$for $Da = 0$, 0.01, 1 and 100, respectively. It is observed from these figures that the effect of Biot numbers is to increase critical wavenumber.

The effect of coefficients of external heating on the stability mechanism is depicted for Darcy (represented by Figs. 4.3(a)–4.3(d)) as well as Brinkman (represented by Figs. 4.3(e)–4.3(h)) flow regimes for linear and quadratic varying gravity fields. The variation of critical Rayleigh number shows against B_0 for fixed values of B_1 in all the figures. From the figures, it is observed that Ra_c increases with the increasing values of the coefficient of external heating at the lower boundary for particular values of B_1. Similar nature has been observed for B_1 on Ra_c when B_0 is fixed. And, this scenario has been found for all the flow regimes. Thus, stability of fluid flow increases monotonically with improving values of external heating parameters i.e., for Biot numbers B_0 and B_1.

4.5.1 Limiting case $B_0 = 0$ and $B_1 \to \infty$

In this limiting case the bottom boundary maintains constant heat flux while the isothermal condition attains at the top boundary. In this case, the perturbed boundary conditions as mentioned in the Eq. (4.13) reduces to

$$z = 0: \quad \hat{w} = 0, \quad \frac{d\hat{w}}{dz} = 0, \quad \frac{d\hat{T}}{dz} = 0, \tag{4.14a}$$

$$z = 1: \quad \hat{w} = 0, \quad \frac{d\hat{w}}{dz} = 0, \quad \hat{T} = 0. \tag{4.14b}$$

In this case, $Ra_c = 27.097533091$ and corresponding wavenumber $a_c = 2.326215$ are obtained for $Da = 0$ and $\lambda = 0$, which coincides upto three decimal places with the given outcomes by Murthy [61]. The variation of Ra_c against gravity variation parameter λ has been calculated and presented in the Table 4.3 at $Da = 0.1, 1$ and 10 for linear and quadratic varying gravity fields. From the table, it is observed that the stability of the system increases monotonically with the increasing values of λ for both the gravity fields, at fixed values of Da. Therefore, the impression of growing Da and λ delay the onset of convection, for this limiting case. On the other hand, a_c decreases with an augmenting value of λ for both the gravity fields. This feature shows that size of the convective cells increases due to the rising effect of λ for linear and quadratic varying gravity fields. Further, it is noticed that the size of the cell is more for linearly varying gravity field as compared with a quadratic varying gravity field.

4.5.2 Limiting case $B_0 \to \infty$ and $B_1 = 0$

In this limiting case the top boundary maintains constant heat flux while the isothermal condition attains at the bottom boundary. In this situation, the perturbed boundary conditions as mentioned in the Eq. (4.13) reduces to

$$z = 0: \quad \hat{w} = 0, \quad \frac{d\hat{w}}{dz} = 0, \quad \hat{T} = 0, \tag{4.15a}$$

$$z = 1: \quad \hat{w} = 0, \quad \frac{d\hat{w}}{dz} = 0, \quad \frac{d\hat{T}}{dz} = 0. \tag{4.15b}$$

In this limiting case also, we have calculated the variation of Ra_c and a_c against gravity variation parameter λ for both the gravity fields at different Darcy number and tabulated them in Table 4.4. It is observed that Ra_c increases with increasing λ for both the gravity fields. Further noticed that the corresponding critical wavenumber a_c increases with rising λ. Thus, λ and Da are stabilizing the flow, while the size of the convective cells decreases with the increase of λ for both the gravity fields.

Table 4.1: Comparison of Ra_c and a_c^2 between the results obtained by Rionero and Straughan [91] and present results when $Da \to 0$, $B_0 \to \infty$, $B_1 \to \infty$ for case (A) $G(z) = -z$ and (B) $G(z) = -z^2$.

$G(z)$	λ	Rionero and Straughan [91]		Our results	
		Ra_c	a_c^2	Ra_c	a_c^2
Case - A	0	39.478	9.870	39.478	9.870
	1	77.020	10.209	77.020	10.209
	1.5	132.020	12.314	132.020	12.314
	1.8	189.908	17.198	189.908	17.198
	1.9	212.280	19.477	212.280	19.477
Case - B	0	39.478	9.870	39.478	9.870
	0.2	41.832	9.874	41.832	9.874
	0.4	44.455	9.887	44.455	9.887
	0.6	47.389	9.915	47.389	9.915
	0.8	50.682	9.961	50.682	9.961
	1	54.390	10.034	54.390	10.034

Table 4.2: The values of Ra_c when $\lambda = 0.5$ for both the gravity fields.

			B_1				
Da	$G(z)$	B_0	0.01	0.1	1	10	100
10^{-1}	$-z$	0.01	125.58148	134.72582	162.04568	199.30992	211.96512
		0.1	135.00846	140.72218	165.14441	200.59637	212.65456
		1	164.11154	167.14953	184.31993	216.90255	228.57944
		10	206.38432	208.31143	222.43826	253.62165	266.13728
		100	221.08635	223.06180	237.05021	269.02399	282.06943
	$-z^2$	0.01	109.97342	117.89265	141.93601	173.63881	184.28931
		0.1	118.11583	123.10347	144.49507	175.59078	186.19196
		1	143.37356	146.00852	160.84643	189.61122	199.88708
		10	179.69925	181.51284	193.75990	221.03996	231.95089
		100	192.37502	193.80124	206.29566	234.17609	245.58342
1	$-z$	0.01	1037.73539	1108.45051	1324.98423	1617.97959	1716.79931
		0.1	1110.72270	1155.41131	1348.98032	1636.20276	1734.60152
		1	1343.59514	1365.40172	1503.09563	1766.10670	1863.48553
		10	1680.36613	1696.55593	1810.74251	2065.77954	2168.53320
		100	1800.23553	1816.15445	1929.64276	2190.91989	2298.37757
	$-z^2$	0.01	907.75875	969.69747	1159.13365	1416.03250	1502.85675
		0.1	971.95167	1010.4627	1180.55926	1431.71362	1518.16487
		1	1173.31803	1192.33771	1312.90531	1542.29985	1625.13322
		10	1463.43764	1477.56813	1577.24010	1800.05598	1889.88716
		100	1566.19733	1580.01127	1677.41017	1905.78041	1999.78025
10	$-z$	0.01	10148.63598	10842.72852	12951.71902	15811.74014	16777.52216
		0.1	10865.23112	11299.53571	13185.56943	15989.57541	16951.39274
		1	13131.87849	13344.47513	14688.35959	17255.77976	18207.77162
		10	16418.74773	16576.77491	17691.83923	20185.13644	21205.40749
		100	17588.59674	17743.51019	18853.43932	21408.03137	22458.99485
	$-z^2$	0.01	8878.75200	9485.50123	11330.13394	13837.68340	14686.17000
		0.1	9502.37363	9881.76679	11532.35064	13990.72881	14835.57918
		1	11468.09408	11654.01961	12829.15763	15079.27722	15916.67242
		10	14298.67262	14436.60711	15410.13844	17601.56755	18466.84302
		100	15301.54316	15436.54387	16403.90389	18631.41401	19548.41046

Table 4.3: Critical values of Ra_c and a_c for both gravity fields when $B_0 = 0, B_1 \to \infty$.

		$G(z) = -z$		$G(z) = -z^2$	
Da	λ	Ra_c	a_c	Ra_c	a_c
10^{-1}	0	163.14193	2.54953	163.14193	2.54953
	0.3	189.32185	2.53896	175.93468	2.54080
	0.6	225.32652	2.52580	190.81294	2.53144
	0.9	277.77293	2.50939	208.30376	2.52155
	1.2	360.60369	2.49012	229.11557	2.51130
	1.5	507.76959	2.47532	254.21442	2.50114
1	0	1329.44484	2.55174	1329.44484	2.55174
	0.3	1543.74931	2.54171	1434.32828	2.54345
	0.6	1838.88966	2.52898	1556.37897	2.53440
	0.9	2270.14580	2.51274	1700.13051	2.52468
	1.2	2954.96978	2.49265	1871.60322	2.51438
	1.5	4185.35670	2.47367	2079.07978	2.50382
10	0	12991.59291	2.55190	12991.59291	2.55190
	0.3	15085.62256	2.54188	14016.08122	2.54360
	0.6	17971.44894	2.52922	15209.54907	2.53461
	0.9	22189.56679	2.51302	16615.55391	2.52491
	1.2	28891.74105	2.49282	18293.10658	2.51461
	1.5	40948.37313	2.47343	20323.59226	2.50400

Table 4.4: Critical values of Ra_c and a_c for both the gravity fields when $B_0 \to \infty, B_1 = 0$.

		$G(z) = -z$		$G(z) = -z^2$	
Da	λ	Ra_c	a_c	Ra_c	a_c
10^{-1}	0	163.14193	2.54953	163.14193	2.54953
	0.3	194.51153	2.56131	180.39710	2.56164
	0.6	240.57653	2.58039	201.58524	2.57783
	0.9	314.41744	2.61555	227.76058	2.60230
	1.2	449.63699	2.69533	261.77353	2.63484
	1.5	750.74662	2.94388	307.15061	2.68125
1	0	1328.15107	2.55300	1328.15107	2.55300
	0.3	1584.40793	2.56286	1469.27274	2.56318
	0.6	1958.39301	2.58057	1640.76716	2.57818
	0.9	2557.65573	2.61279	1855.62398	2.59881
	1.2	3656.76477	2.68437	2131.45747	2.62809
	1.5	6139.15761	2.90401	2495.57717	2.67182
10	0	12991.75219	2.55189	12991.75219	2.55189
	0.3	15480.91729	2.56292	14355.95134	2.56320
	0.6	19134.04632	2.58052	16030.52939	2.57808
	0.9	24987.12507	2.61238	18128.36966	2.59848
	1.2	35724.21237	2.68299	20821.67496	2.62745
	1.5	60012.25609	2.89950	24377.90001	2.67056

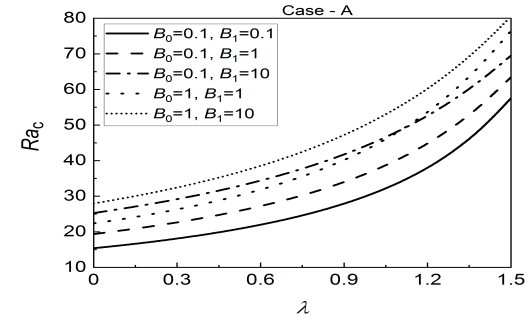

(a) $Da = 0$

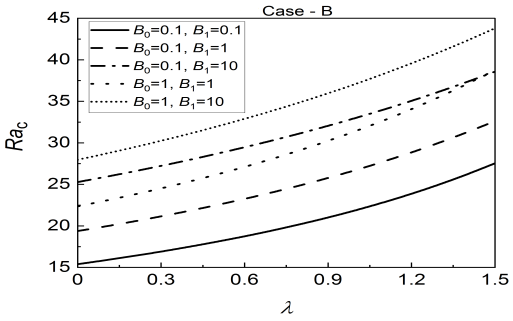

(b) $Da = 0$

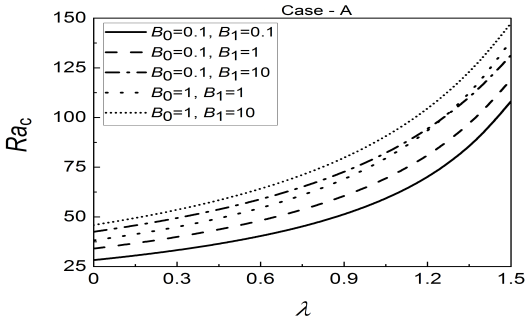

(c) $Da = 10^{-2}$

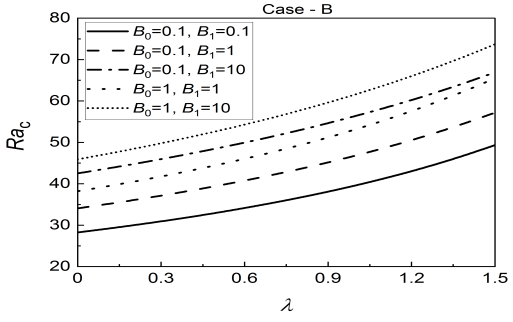

(d) $Da = 10^{-2}$

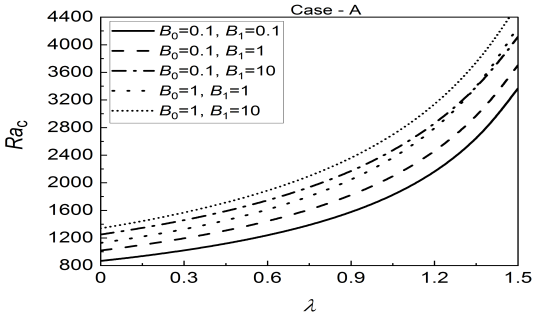

(e) $Da = 1$

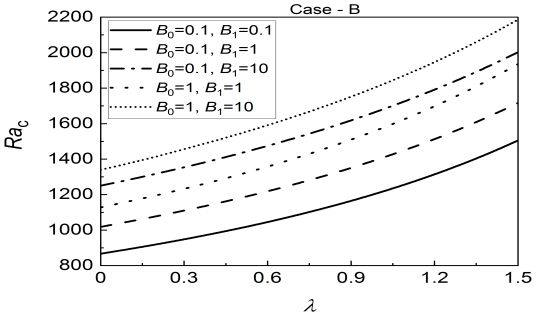

(f) $Da = 1$

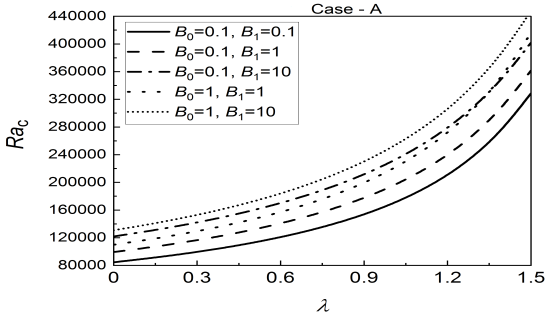

(g) $Da = 10^2$

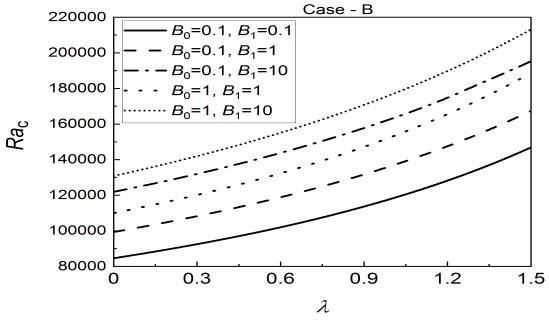

(h) $Da = 10^2$

Figure 4.1: Variations of Ra_c with λ for cases (i) $G(z) = -z$ and (ii) $G(z) = -z^2$ in different flow regimes.

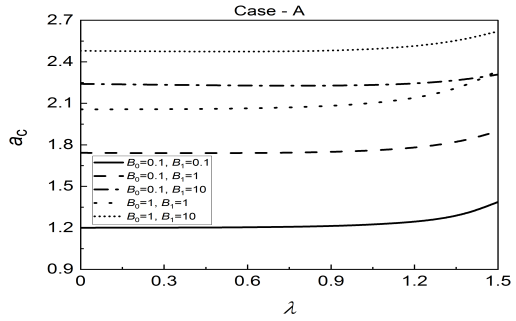

(a) $Da = 0$

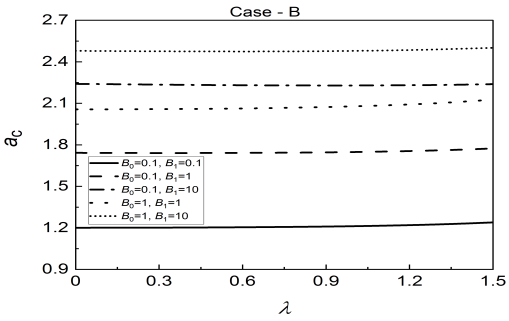

(b) $Da = 0$

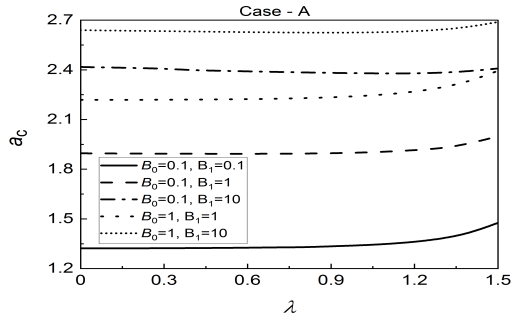

(c) $Da = 10^{-2}$

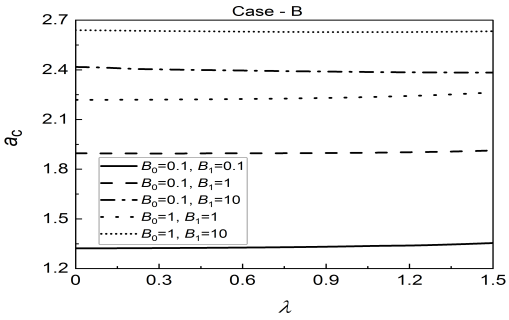

(d) $Da = 10^{-2}$

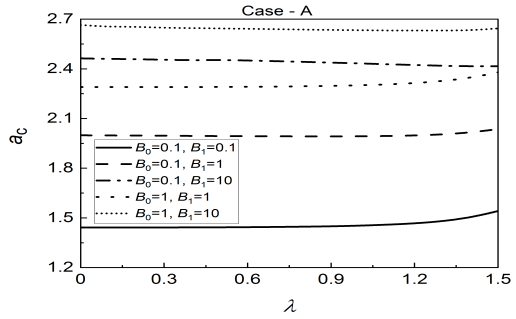

(e) $Da = 1$

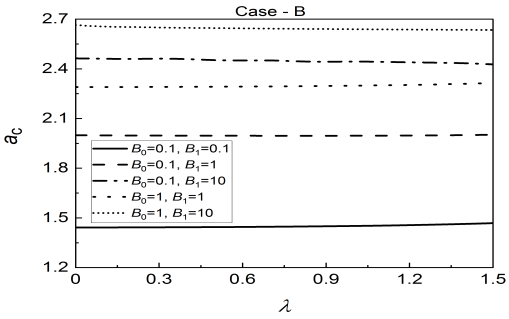

(f) $Da = 1$

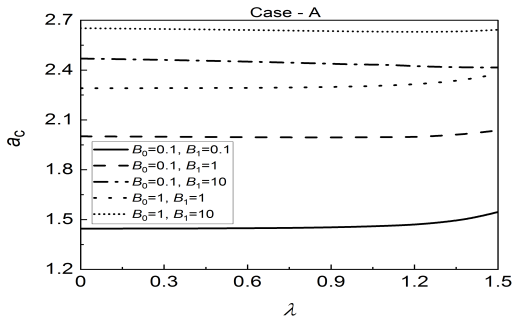

(g) $Da = 10^2$

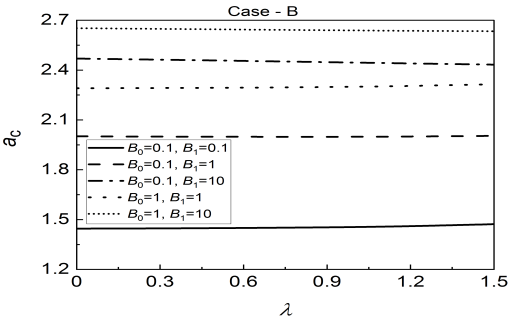

(h) $Da = 10^2$

Figure 4.2: Variations of a_c with λ for cases (i) $G(z) = -z$ and (ii) $G(z) = -z^2$ in different flow regimes.

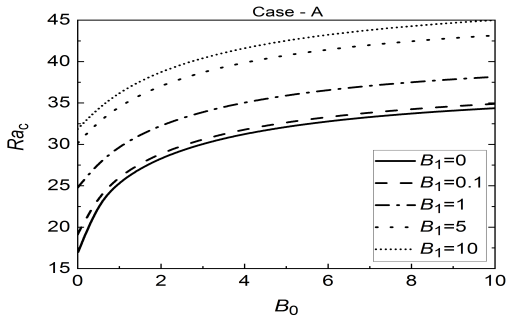

(a) $Da = 0$

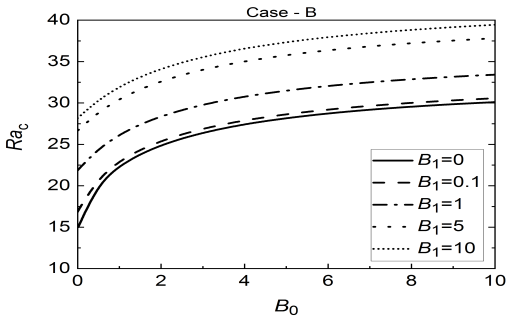

(b) $Da = 0$

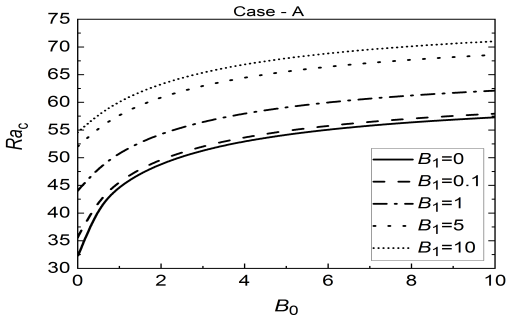

(c) $Da = 10^{-2}$

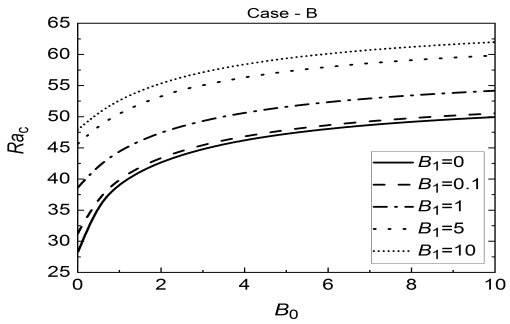

(d) $Da = 10^{-2}$

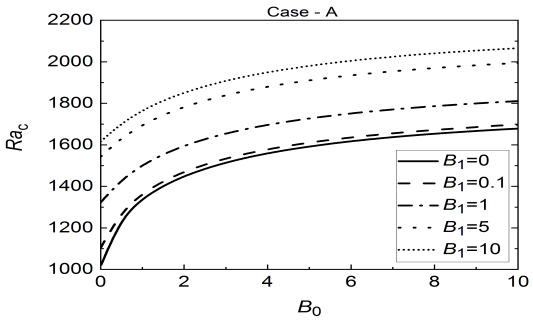

(e) $Da = 1$

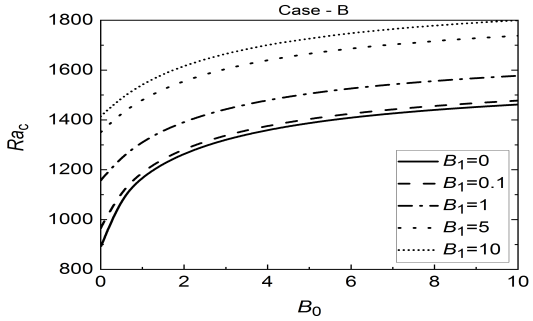

(f) $Da = 1$

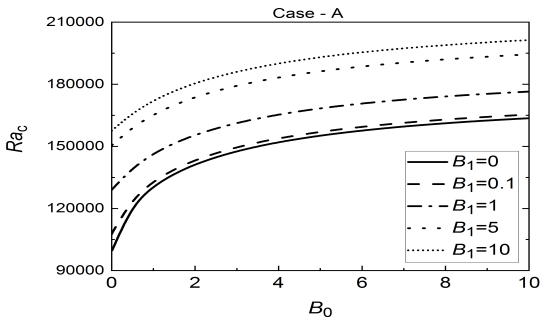

(g) $Da = 10^2$

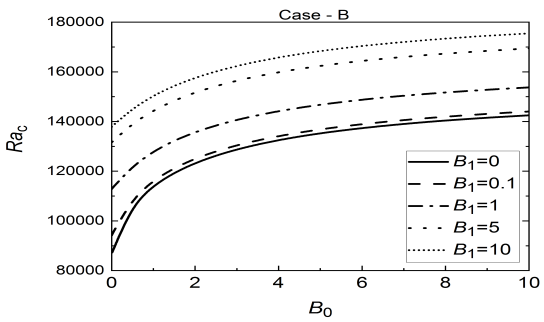

(h) $Da = 10^2$

Figure 4.3: Variations of Ra_c with B_0 and B_1 when $\lambda = 0.5$ for cases A and B in different flow regimes.

4.6 Conclusions

The onset of convection in a horizontal porous layer subjected to external heating on the boundaries under the influence of a changeable gravity field is considered. Two different types (linear and quadratic) of gravity field variations are considered for this investigation. The effect of Da, λ, B_0 and B_1 on the critical Rayleigh number (Ra_c) and corresponding wavenumber (a_c) is analyzed. The main conclusions from this investigation are listed below:

- The convection comes earlier for quadratic varying gravity field compares to linear varying gravity field when the external heat supplies on both the boundaries. The same nature of quadratic varying gravity field has been observed one boundary maintains a constant heat flux while another one is an isothermal condition or external heat supplies from the boundaries exchange their role.
- The gravity variation parameter has a stabilizing effect on the flow in the presence of external heat supplies on the boundaries and both the limiting cases also, in any flow regimes.
- The Brinkman flow regime shows more stability when two the boundaries are subjected to external heating for both the gravity fields.
- The rise in the heat supplied both the boundaries stabilize the flow field. Further, the flow shows more stability when the external heating on the lower boundaries is higher than at the top boundary.
- The stability of the flow increases when the upper boundary maintains constant heat flux and lower one as at isothermal state compare to the lower boundary maintain constant heat flux and upper one as at isothermal state.
- The dimension of the convective cells displays dual nature for the rising effect of Da and λ when two the boundaries are subjected to the external heating for both the gravity fields. But, the cell size decreases due to the augmenting values of B_0 and B_1. On the other hand, the cells size increases when $B_0 = 0$ and $B_1 \to \infty$, but it decreases when $B_0 \to \infty$ and $B_1 = 0$ for both the gravity fields.

Chapter 5

The effect of local thermal non-equilibrium on the stability analysis in the presence of variable gravity field with throughflow [1]

5.1 Introduction

Most of the investigations on Horton–Rogers–Lapwood were under the local thermal equilibrium (LTE) mode. This supposition is not appropriate for a large temperature change amongst the phases or high-speed flows. In this situation, the fluid phase and the solid phase are unable to maintain the identical temperatures. Thus, two different temperature equations needed to represent each phase, which was discussed by Nield and Bejan [78]. The extension of the HRL problem on the instability mechanism has been observed analytically and numerically under the LTNE model by Banu and Rees [9]. Taking into account of LTNE effects, several investigations has been carried out on the stability analysis by accounting additional effects such as double diffusion [73], variable viscosity [102], nanofluid [2, 62], inclined porous layer [16] and free surface [28] etc. The stability characteristic of non-isothermal Poiseuille flow was examined by Bera and Khandelwal [19] in a vertical porous channel due to the impact of LTNE state. Mahajan and Sharma [70] studied the impact of LTNE on the stability analysis in a magnetic nanofluid layer.

[1] Communicated in "***International Communications in Heat and Mass Transfer***"

In this chapter, we study the onset of convection in the presence of both the LTNE and variable gravity effects. This is an extension of the work done by Banu and Rees [9]. Two temperature models have been accounted to address the solid and fluid phases for a porous layer. The resulting eigenvalue problem is solved using the *bvp4c* routine in MATLAB. The critical Rayleigh number (Ra_{c}) is calculated to analyze the breakdown of convection and the impact of governing paramters on Ra_{c} is shown graphically.

5.2 Mathematical Formulation

Consider an incompressible fluid enclosed in a horizontal porous layer of width L, lying in the region $0 \leq x \leq L$, which is heated from below. The geometry and coordinate system is displayed in Fig. 2.1. A changeable gravity force $\mathbf{g}(z)$ is applied in the vertically downward direction. Further, it is assumed that the fluid and solid phases are not in local thermal equilibrium state, which motivated us to consider two-field model for temperatures inside an isotropic porous medium. The Darcy model and the Oberbeck-Boussinesq are employed in the momentum equation. The corresponding governing equations are

$$\nabla \cdot \mathbf{u} = 0, \tag{5.1}$$

$$\frac{\mu}{K}\mathbf{u} = -\nabla p - \rho_{\mathrm{f}}\left[1 - \beta_{\mathrm{T}}(T_{\mathrm{f}} - T_1)\right]\mathrm{g}(z)\hat{\mathbf{e}}_{\mathrm{z}}, \tag{5.2}$$

$$(\rho c)_{\mathrm{f}}\left[\epsilon\frac{\partial T_{\mathrm{f}}}{\partial t} + \mathbf{u}\cdot\nabla T_{\mathrm{f}}\right] = \epsilon k_{\mathrm{f}}\nabla^2 T_{\mathrm{f}} + h(T_{\mathrm{s}} - T_{\mathrm{f}}), \tag{5.3}$$

$$(1-\epsilon)\,(\rho c)_{\mathrm{s}}\frac{\partial T_{\mathrm{s}}}{\partial t} = (1-\epsilon)\,k_{\mathrm{s}}\nabla^2 T_{\mathrm{s}} + h(T_{\mathrm{f}} - T_{\mathrm{s}}), \tag{5.4}$$

where k_{f} and k_{s} are the thermal conductivities of the fluid and solid phases, respectively, and h is the interphase heat transfer coefficient. All other quantities are defined in Chapter - 2.

The corresponding boundary conditions are assumed as

$$z = 0: \quad w = W_{\mathrm{c}}, \quad T_{\mathrm{f}} = T_1, \quad T_{\mathrm{s}} = T_1, \tag{5.5a}$$

$$z = L: \quad w = W_{\mathrm{c}}, \quad T_{\mathrm{f}} = T_2, \quad T_{\mathrm{s}} = T_2, \tag{5.5b}$$

where W_{c} is the constant upward throughflow.

Applying the non-dimensional variables given in Eq. (2.6) in the Eqs. (5.1)-(5.4), after

removing pressure term from Eq. (5.2), are

$$\nabla^2 w = Ra\nabla_{\mathrm{H}}^2 T_{\mathrm{f}}(1 + \lambda G(z)), \tag{5.6}$$

$$\frac{\partial T_{\mathrm{f}}}{\partial t} + \mathbf{u} \cdot \nabla T_{\mathrm{f}} = \nabla^2 T_{\mathrm{f}} + H(T_{\mathrm{s}} - T_{\mathrm{f}}), \tag{5.7}$$

$$\varepsilon_{\mathrm{m}} \frac{\partial T_{\mathrm{s}}}{\partial t} = \nabla^2 T_{\mathrm{s}} + \gamma_{\mathrm{m}} H(T_{\mathrm{f}} - T_{\mathrm{s}}), \tag{5.8}$$

where $H = \dfrac{hL^2}{\epsilon k_{\mathrm{f}}}$ is the interphase heat transfer parameter, $\varepsilon_{\mathrm{m}} = \dfrac{\alpha_{\mathrm{f}}}{\alpha_{\mathrm{s}}}$ is the diffusivity ratio of the fluid and solid phases and $\gamma_{\mathrm{m}} = \dfrac{\epsilon k_{\mathrm{f}}}{(1-\epsilon)k_{\mathrm{s}}}$ is the porosity modified conductivity ratio.

The corresponding dimensionless boundary conditions are

$$z = 0: \quad w = Q, \quad T_{\mathrm{f}} = 1, \quad T_{\mathrm{s}} = 1, \tag{5.9a}$$

$$z = 1: \quad w = Q, \quad T_{\mathrm{f}} = 0, \quad T_{\mathrm{s}} = 0, \tag{5.9b}$$

where $Q = \dfrac{W_{\mathrm{c}} L}{\alpha_{\mathrm{f}}}$ is the throughflow parameter.

5.3 Basic state solution

The equations for the basic state (stationary) are (with temperatures of fluid phase and solid phase varying in the vertical direction)

$$\frac{d^2 T_{\mathrm{f0}}}{dz^2} - Q\frac{dT_{\mathrm{f0}}}{dz} + H\left(T_{\mathrm{s0}} - T_{\mathrm{f0}}\right) = 0, \tag{5.10}$$

$$\frac{d^2 T_{\mathrm{s0}}}{dz^2} + H\left(T_{\mathrm{f0}} - T_{\mathrm{s0}}\right) = 0, \tag{5.11}$$

with corresponding boundary conditions are

$$z = 0: \quad T_{\mathrm{f0}} = 1, \quad T_{\mathrm{s0}} = 1, \tag{5.12a}$$

$$z = 1: \quad T_{\mathrm{f0}} = 0, \quad T_{\mathrm{s0}} = 0. \tag{5.12b}$$

The basic temperature profiles for fluid and solid phases versus z for vertical throughflow (Q) and inter-phase heat transfer parameter (H) are displayed in Fig. 5.1. From these figures, it is observed that the thermal boundary layer decreases with increasing values of H for fluid

phase and while very small variation has been observed for solid phase when H is very large. Further, it is recognized that the gap between fluid phase and solid phase enhances due to the rising impact of the throughflow parameter.

5.4 Linear stability analysis

As in Chapter - 2, imposing the infinitesimal disturbances on the basic state solution and applying the usual normal mode form for the disturbances, we obtain the following system of ordinary differential equations for neutral stability modes ($\eta = 0$)

$$\left(\frac{d^2}{dz^2} - a^2\right)\hat{w} + a^2 Ra\hat{T}_{\mathrm{f}}(1 + \lambda G(z)) = 0, \tag{5.13}$$

$$-\hat{w}\frac{dT_{\mathrm{f0}}}{dz} + \left(\frac{d^2}{dz^2} - a^2 - Q\frac{d}{dz} - H\right)\hat{T}_{\mathrm{f}} + H\hat{T}_{\mathrm{s}} = 0, \tag{5.14}$$

$$\left(\frac{d^2}{dz^2} - a^2 - \gamma_{\mathrm{m}}H\right)\hat{T}_{\mathrm{s}} + \gamma_{\mathrm{m}}H\hat{T}_{\mathrm{f}} = 0, \tag{5.15}$$

where $a = \sqrt{a_x^2 + a_y^2}$ is the overall wavenumber. Also, the perturbed boundary conditions can be converted as

$$\hat{w} = \hat{T}_{\mathrm{f}} = \hat{T}_{\mathrm{s}} = 0, \quad \text{at} \quad z = 0, 1. \tag{5.16}$$

5.5 Results and discussion

The solutions of the governing Eqs. (5.13)-(5.15) corresponding to the boundary conditions Eq. (5.16) is obtained using the *bvp4c* routine in MATLAB.

To verify the exactness of our present results, firstly a comparison has been made between the results given by Rionero and Straughan [91] without throughflow effect (Q) and tabulated in Table 5.1 for cases (A) $G(z) = -z$, (B) $G(z) = -z^2$ and (D) $G(z) = -(e^z - 1)$. Secondly, a comparison has been made between the results given Yadav [123] in presence of throughflow parameter (Q) and it tabulated in Table 5.2 for cases (A) $G(z) = -z$, (B) $G(z) = -z^2$, (C) $G(z) = -z^3$ and (D) $G(z) = -(e^z - 1)$. Finally, another comparison has been made between the results given by Banu and Rees [9] for constant gravity field and tabulated in Table 5.3. The values of Ra_{c} and a_{c} are calculated at stationary convection. From Tables 5.1, 5.2 and 5.3, it is clear that the results are in good agreement.

The main focus of this investigation is to analyze the impact of the local thermal non-equilibrium (LTNE) state on the stability mechanism inside a horizontal porous medium in the presence of a variable gravity field with a vertical throughflow effect. The critical Rayleigh number and corresponding wavenumber are calculated for four types of gravity field deviations: (A) $G(z) = -z$, (B) $G(z) = -z^2$, (C) $G(z) = -z^3$ and (D) $G(z) = -(e^z - 1)$ for various values of throughflow parameter (Q), gravity variation parameter (λ), inter-phase heat transfer parameter (H) and porosity modified conductivity ratio (γ_{m}).

In Figs. 5.2–5.3, the variation of critical Rayleigh number (Ra_{c}) and corresponding wavenumber (a_{c}) with λ is illustrated for different values of H for four types of gravity fields with keeping fix values of $Q = 0.5$ and $\gamma_{\mathrm{m}} = 0.1$, respectively. The gravity variation parameter has a stabilizing impact because the promotion of λ forced to decline the gravity field. Since the system restores its disturbances as the gravitational field decreases and it indicates postponing the convection. On the other hand, it is also recognized that the critical wavenumber increases with λ.

The critical Rayleigh number is calculated with the inter-phase heat transfer parameter H and decorated in the Figs. 5.4(a)–5.4(d) for a long-range of values of γ_{m} when $Q = 0.5$ and $\lambda = 0.2$. From the figures, it is clear that Ra_{c} decreases with increasing values of γ_{m} for all the gravity fields. Also, the impact of H on Ra_{c} is unaffected when $\gamma_{\mathrm{m}} \geq 10$. Thus the impact of rising the conductivity ratio is to destabilize the system. The impact is more manifested for small values of γ_{m}. Further, we have noticed that Ra_{c} is independent of γ_{m} when H is very small. This is happening because the heat transfer between the phases is not giving any contribution on the medium when $H \to 0$ i.e., at local thermal equilibrium (LTE) state. Thus, the convective instability does not affect this situation. On the other hand, it is observed that the variation of critical Rayleigh number is also negligible for all four gravity field when $H \to \infty$. Since, both the phases behave like a single in this situation also. This is because the temperature differs by an amount which is of order 1/H when $H \to \infty$.

Fig. 5.5 envisages the effect of H and γ_{m} on the critical wavenumber a_{c} for linear, quadratic, cubic and exponential varying gravity fields, respectively. It is observed that there is no variation on the critical wavenumber at both the limiting cases of inter-phase heat transfer parameter, i.e., at $H \to 0$ and $H \to \infty$. Further, a_{c} decreases monotonically with the rising effect of porosity modified conductivity ratio, while it increases due to the enhancing values of H for the intermediate values of H. Also, the size of the convective cells is always less than for LTNE state as a_{c} is greater than for LTNE state as compared with LTE state.

In Figs. 5.6(a)–5.6(d), the variation of Ra_c based on the mean properties of the fluid with the inter-phase heat transfer coefficient H with different values of γ_m are portrayed for four types of the gravity fields, respectively. The value of $Ra_c\gamma_m/(1+\gamma_m)$ is independent of the impact of inter-phase heat transfer effect when $H \to \infty$, i.e., LTE state, but it does not converges a common limit for all assigned values of γ_m when the flow is maintained by gravity variable, while Malashetty *et al.* [72] claimed that it has a common limit for LTE case i.e. $4\pi^2$ as $H \to \infty$ for constant gravity. Further, the variation of critical wavenumber is plotted in Fig. 5.7 for a range of values of the parameter γ_m under the influence of the four types of changeable gravity variation. It is observed that the value of a_c enhances with rising the values of H from LTE value when H is small, to its maximum LTNE value for intermediate of H, and finally bounces back to its LTE value for large H. This indicates that a_c converges to its LTE value when $H \to 0$ and $H \to \infty$. Apart from that, it is noticed that a_c attains maximum value for exponential varying gravity field, while it offers minimum value for cubic varying gravity field at the intermediate range of H.

Table 5.4 reveals that the critical Rayleigh number increases with the rising effect of the throughflow parameter (Q), which shows that the throughflow parameter has a stabilizing effect on the flow field. The urgent heat gradients can transfer to a boundary layer at the boundary with the increased value of the throughflow parameter Q, where the throughflow is described. This ensures to postponing of the convection due to the rising effect of Q.

Table 5.1: Comparison of Ra_c and a_c^2 between the results received by Rionero and Straughan [91] and present results when $Q = 0$ and $H = 0$ for linear, quadratic and exponential varying gravity fields.

$G(z)$	λ	Rionero and Straughan [91]		Present results	
		Ra_c	a_c^2	Ra_c	a_c^2
$-z$	0	39.478	9.870	39.478	9.870
	1	77.020	10.209	77.080	10.209
	1.5	132.020	12.314	132.021	12.314
	1.8	189.908	17.198	189.908	17.198
	1.9	212.280	19.477	212.284	19.477
$-z^2$	0	39.478	9.870	39.478	9.870
	0.2	41.832	9.874	41.832	9.874
	0.4	44.455	9.887	44.455	9.887
	0.6	47.389	9.915	47.389	9.915
	0.8	50.682	9.961	50.682	9.961
	1	54.390	10.034	54.390	10.034
$-(e^z - 1)$	0	39.478	9.870	39.478	9.870
	0.1	42.331	9.872	42.331	9.872
	0.2	45.607	9.883	45.607	9.883
	0.3	49.398	9.904	49.398	9.904
	0.4	53.828	9.942	53.828	9.942
	0.5	59.053	10.005	59.053	10.005

Table 5.2: Comparison of Ra_c and a_c between the results obtained by Yadav [123] and present results when $H = 0$ and $Q = 0.5$ for four types of gravity fields.

$G(z)$	λ	Yadav [123]		Present results	
		Ra_c	a_c	Ra_c	a_c
$-z$	0	39.827	3.151	39.827	3.151
	0.6	57.569	3.146	57.569	3.146
	1.2	99.660	3.224	99.661	3.224
$-z^2$	0	39.827	3.151	39.827	3.151
	0.6	48.469	3.146	48.469	3.146
	1.2	61.088	3.167	61.089	3.167
$-z^3$	0	39.827	3.151	39.827	3.151
	0.6	44.857	3.146	44.857	3.146
	1.2	51.029	3.153	51.030	3.153
$-(e^z - 1)$	0	39.827	3.151	39.827	3.151
	0.6	67.948	3.162	67.948	3.162
	1.2	157.128	3.798	157.127	3.798

Table 5.3: Comparison of Ra_c and a_c between the results obtained by Banu and Rees [9] and present results when $\lambda = 0$ and $Q = 0$ for a range values of γ_m.

γ_m	H	Banu and Rees [9]		Present results	
		Ra_c	a_c	Ra_c	a_c
10^2	0.196657	39.67538	3.145507	39.67616	3.145580
10^1	1.905025	41.41133	3.179696	41.41223	3.179778
10^0	15.40310	56.32689	3.451618	56.32990	3.451851
10^{-1}	93.98499	151.28364	4.61538	151.28364	4.615375
10^{-2}	640.7896	764.3386	7.384372	764.3387	7.384373
10^{-3}	5402.725	5739.522	12.69114	5739.522	12.69114
10^{-4}	50828.39	51840.03	22.32576	51840.09	22.32525

Table 5.4: Evaluation of Ra_c and a_c for different values vertical throughflow parameter (Q), inter-phase heat transfer parameter (H) and gravity variation parameter (λ) when $\gamma_m = 0.1$.

Q	H	λ	$G(z) = -z$		$G(z) = -z^2$		$G(z) = -z^3$		$G(z) = -(e^z - 1)$	
			Ra_c	a_c	Ra_c	a_c	Ra_c	a_c	Ra_c	a_c
0	0.1	0	39.693	3.151	39.693	3.151	39.693	3.151	38.816	3.151
		0.5	52.758	3.156	46.112	3.154	43.403	3.152	59.348	3.171
		1	77.456	3.204	54.660	3.176	47.738	3.163	106.746	3.430
	1	0	41.461	3.219	41.461	3.219	41.461	3.219	41.461	3.219
		0.5	55.098	3.224	48.158	3.223	45.332	3.221	61.953	3.241
		1	80.785	3.276	57.053	3.246	49.844	3.232	110.739	3.513
	10	0	57.079	3.699	57.079	3.699	57.079	3.699	57.079	3.699
		0.5	75.740	3.708	66.223	3.705	62.362	3.702	84.868	3.736
		1	109.891	3.794	78.079	3.744	68.402	3.722	144.871	4.124
	100	0	156.404	4.614	156.404	4.614	156.404	4.614	156.404	4.614
		0.5	206.766	4.662	180.973	4.649	170.627	4.635	229.409	4.774
		1	291.112	5.010	210.545	4.799	185.877	4.711	351.404	5.871
1	0.1	0	41.070	3.187	41.070	3.187	41.070	3.187	41.070	3.187
		0.5	56.008	3.169	48.811	3.170	45.727	3.173	64.444	3.166
		1	86.405	3.176	59.647	3.167	51.353	3.167	129.451	3.385
	1	0	42.750	3.251	42.750	3.251	42.750	3.251	42.750	3.251
		0.5	58.217	3.236	50.745	3.237	47.553	3.239	66.867	3.235
		1	89.430	3.249	57.053	3.237	53.321	3.234	132.303	3.475
	10	0	57.916	3.714	57.916	3.714	57.916	3.714	57.916	3.714
		0.5	78.178	3.710	68.215	3.709	64.038	3.709	88.849	3.726
		1	116.986	3.771	81.962	3.733	71.158	3.718	160.731	4.115
	100	0	156.711	4.617	156.711	4.617	156.711	4.617	156.711	4.617
		0.5	208.632	4.649	182.421	4.639	171.762	4.629	232.751	4.751
		1	297.313	4.974	213.756	4.778	188.034	4.697	362.934	5.852
2	0.1	0	45.238	3.298	45.238	3.298	45.238	3.298	45.238	3.298
		0.5	63.367	3.255	55.120	3.257	51.403	3.263	74.814	3.227
		1	103.274	3.213	69.728	3.222	59.150	3.234	171.059	3.406
	1	0	46.675	3.352	46.675	3.352	46.675	3.352	46.675	3.352
		0.5	65.173	3.312	56.700	3.314	52.909	3.320	76.672	3.288
		1	105.350	3.249	71.380	3.285	60.683	3.294	170.373	3.500
	10	0	60.501	3.767	60.501	3.767	60.501	3.767	60.501	3.767
		0.5	83.048	3.745	72.353	3.746	67.724	3.748	95.816	3.748
		1	128.301	3.781	88.691	3.754	76.319	3.746	183.987	4.148
	100	0	157.633	4.628	157.633	4.628	157.633	4.628	157.633	4.628
		0.5	211.338	4.643	184.616	4.636	173.604	4.629	237.100	4.735
		1	304.885	4.946	217.924	4.763	191.016	4.689	376.471	5.843

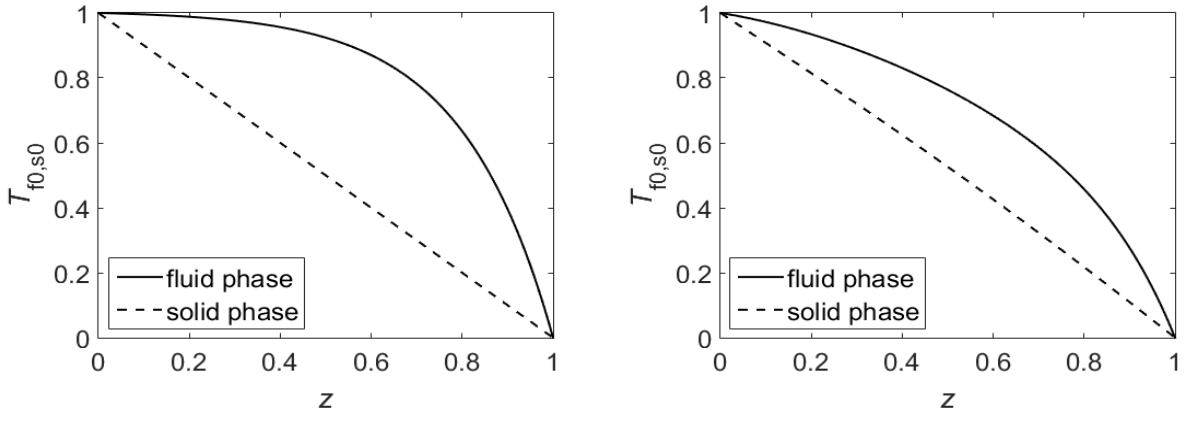

(a) $Q = 5, H = 0.01$

(b) $Q = 5, H = 10$

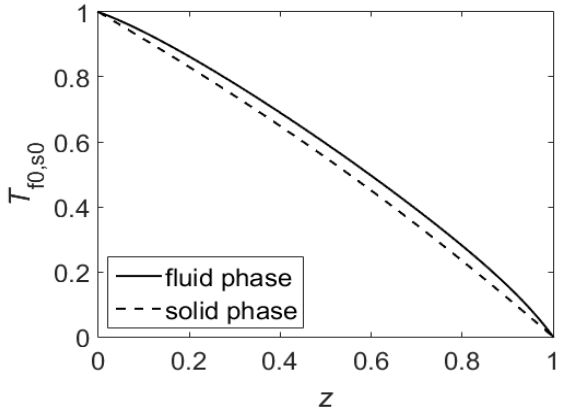

(c) $Q = 5, H = 100$

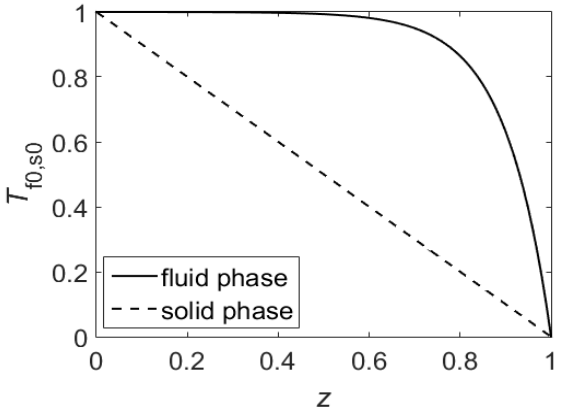

(d) $Q = 10, H = 0.01$

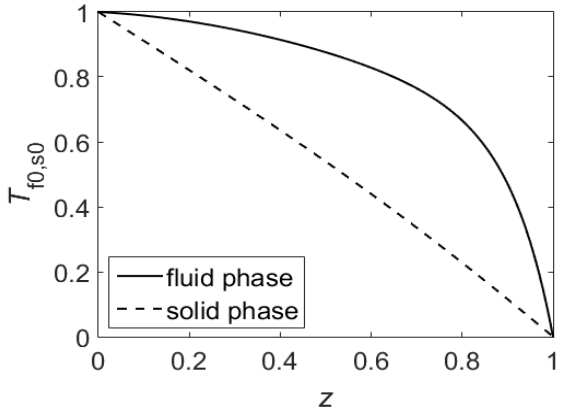

(e) $Q = 10, H = 10$

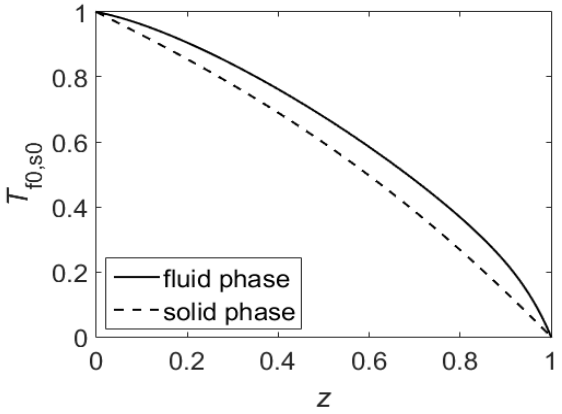

(f) $Q = 10, H = 100$

Figure 5.1: Basic temperature profile of fluid and solid phases for various values of H and Q at $\gamma_{\mathrm{m}} = 0.1$.

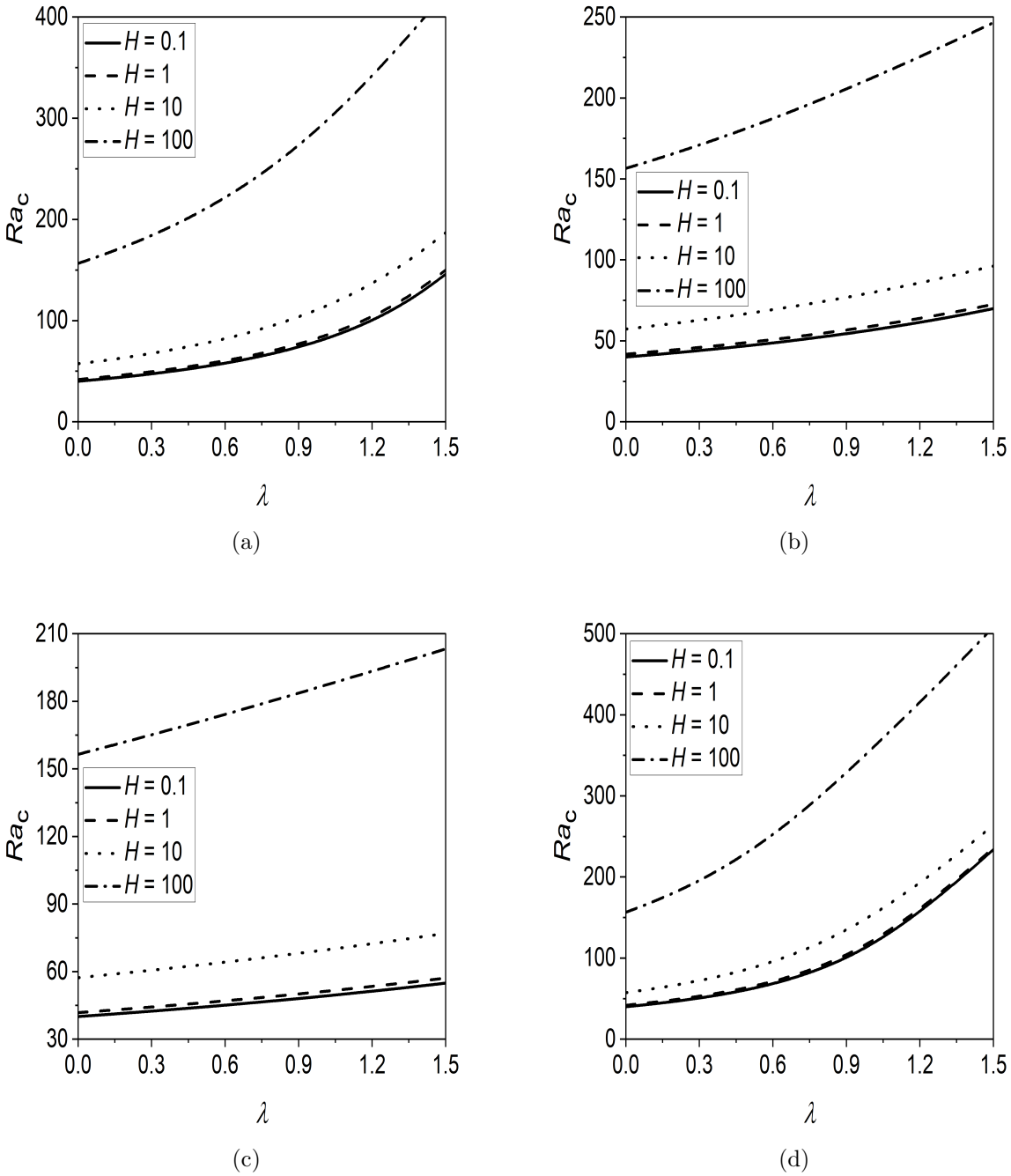

Figure 5.2: Effect of inter-phase heat transfer parameter (H) on Ra_c for (a) $G(z) = -z$, (b) $G(z) = -z^2$, (c) $G(z) = -z^3$ and (d) $G(z) = -(e^z - 1)$ when $Q = 0.5$ and $\gamma_m = 0.1$.

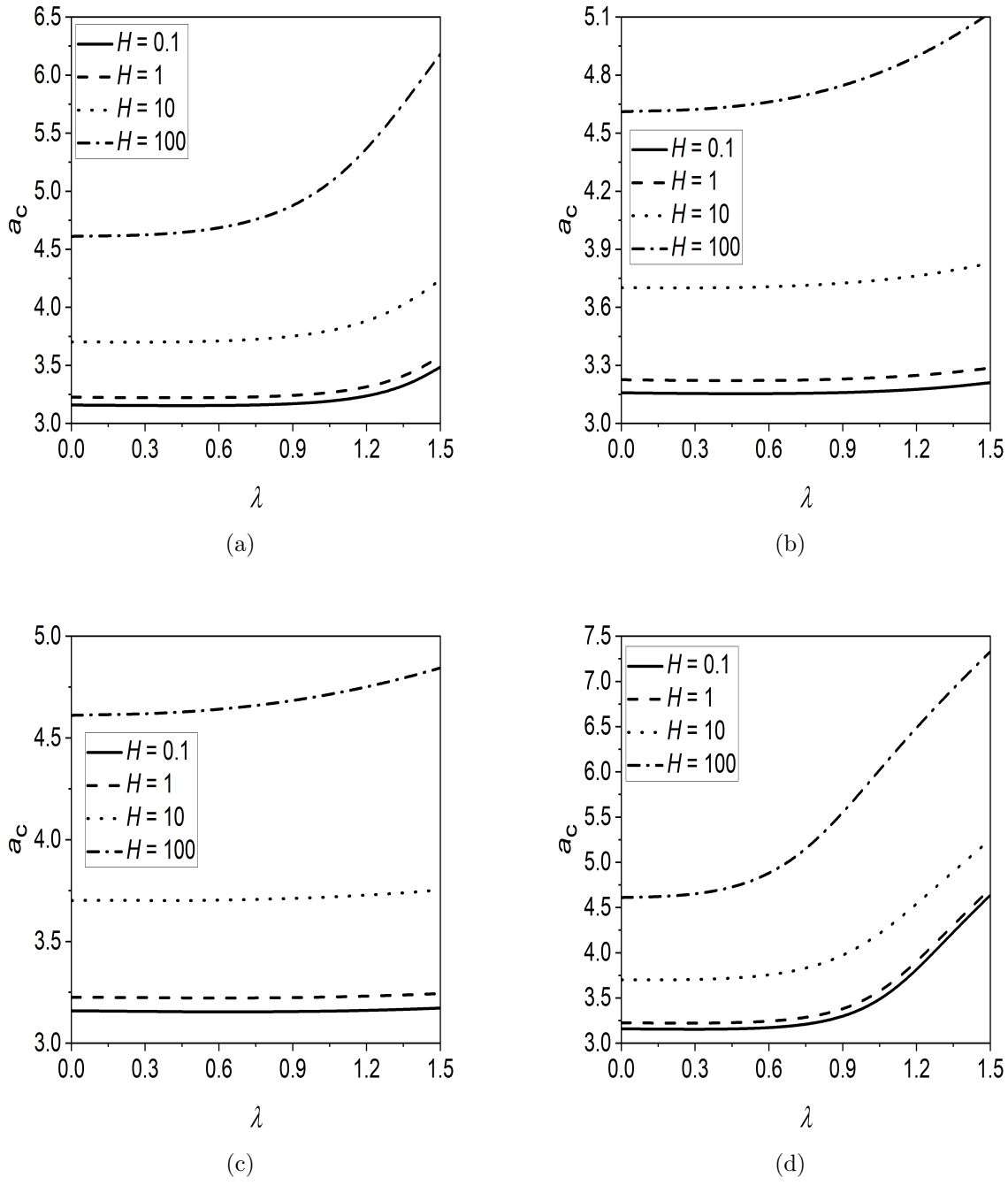

Figure 5.3: Effect of inter-phase heat transfer parameter (H) on a_c for (a) $G(z) = -z$, (b) $G(z) = -z^2$, (c) $G(z) = -z^3$ and (d) $G(z) = -(e^z - 1)$ when $Q = 0.5$ and $\gamma_m = 0.1$.

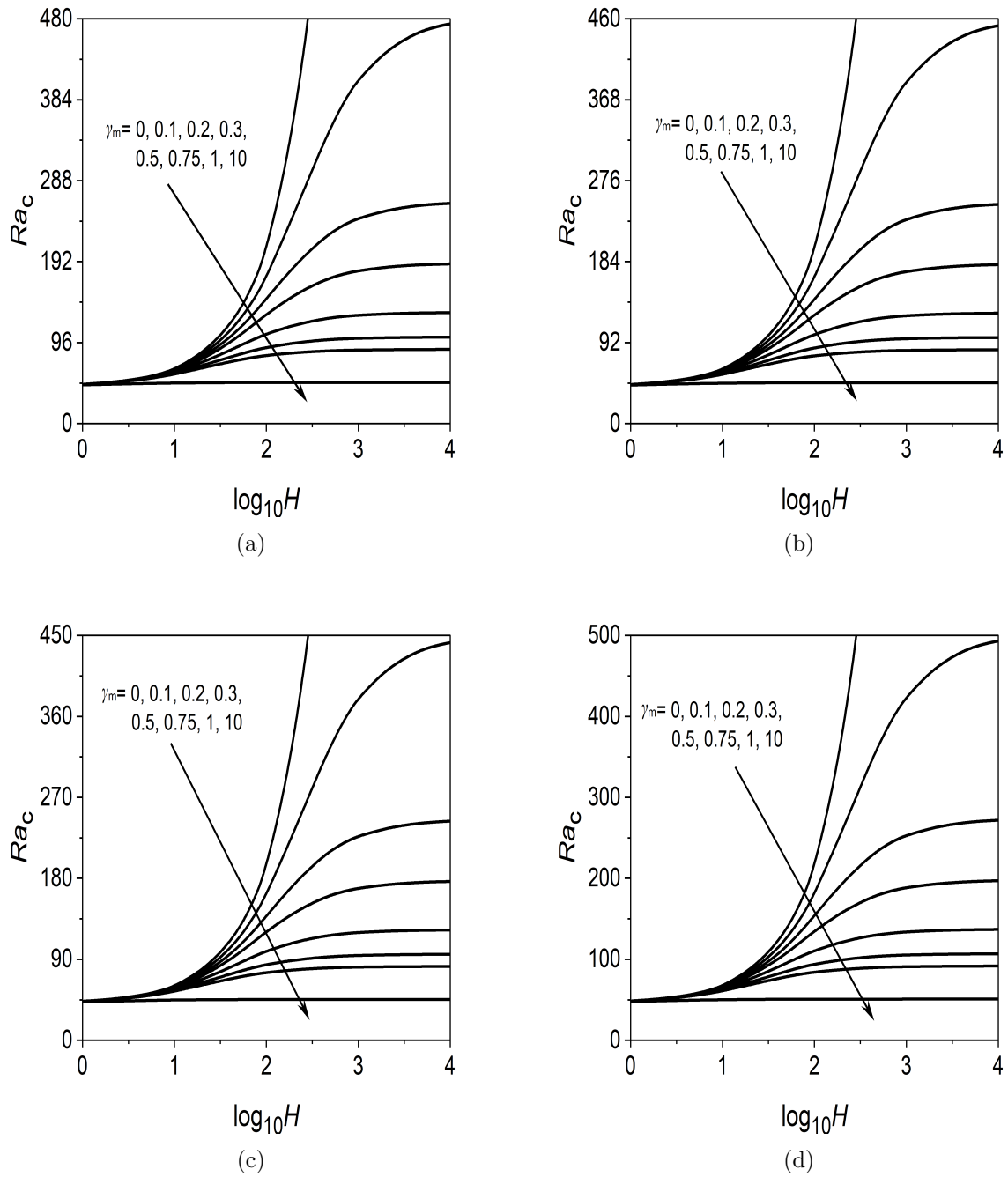

Figure 5.4: Effect of porosity modified conductivity ratio (γ_{m}) on Ra_{c} for (a) $G(z) = -z$, (b) $G(z) = -z^2$, (c) $G(z) = -z^3$ and (d) $G(z) = -(e^z - 1)$ when $Q = 0.5$ and $\lambda = 0.2$.

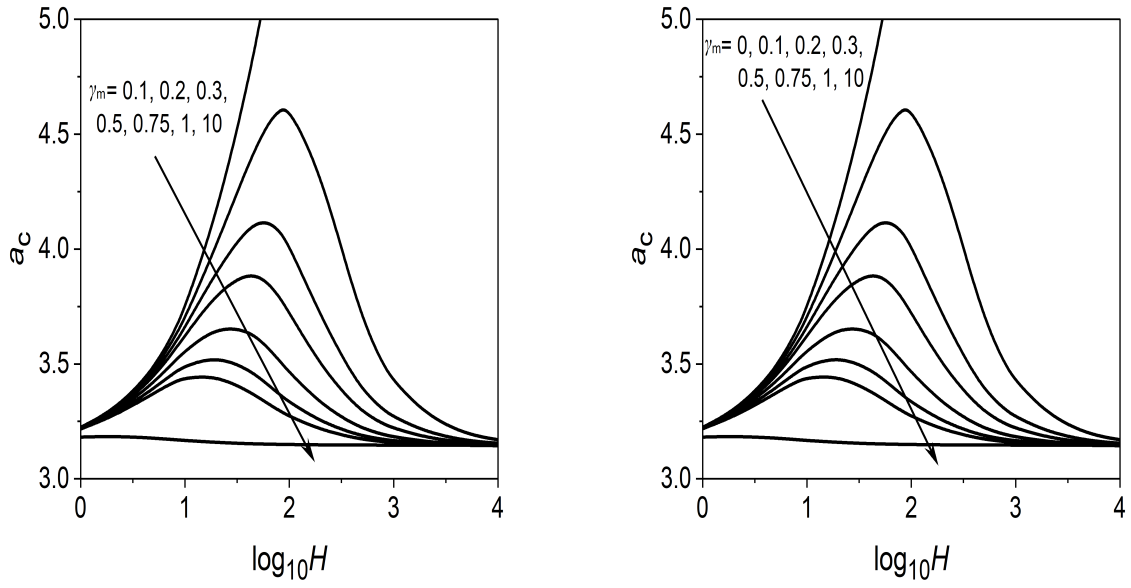

(a)

(b)

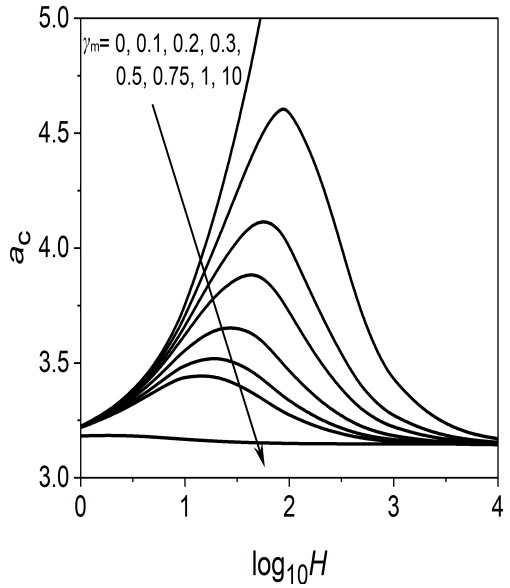

(c)

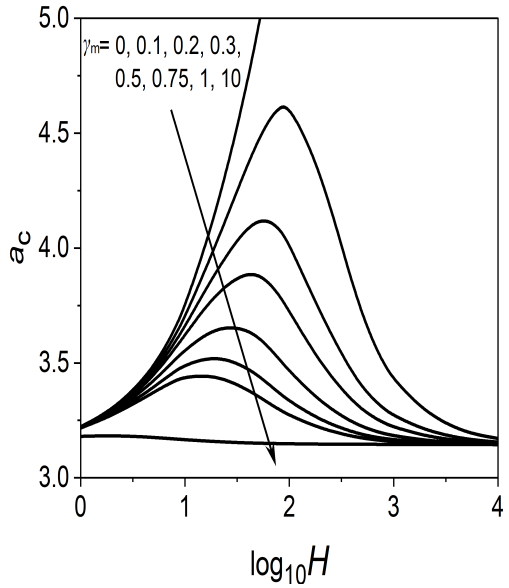

(d)

Figure 5.5: Effect of porosity modified conductivity ratio (γ_{m}) on a_{c} for (a) $G(z) = -z$, (b) $G(z) = -z^2$, (c) $G(z) = -z^3$ and (d) $G(z) = -(e^z - 1)$ when $Q = 0.5$ and $\lambda = 0.2$.

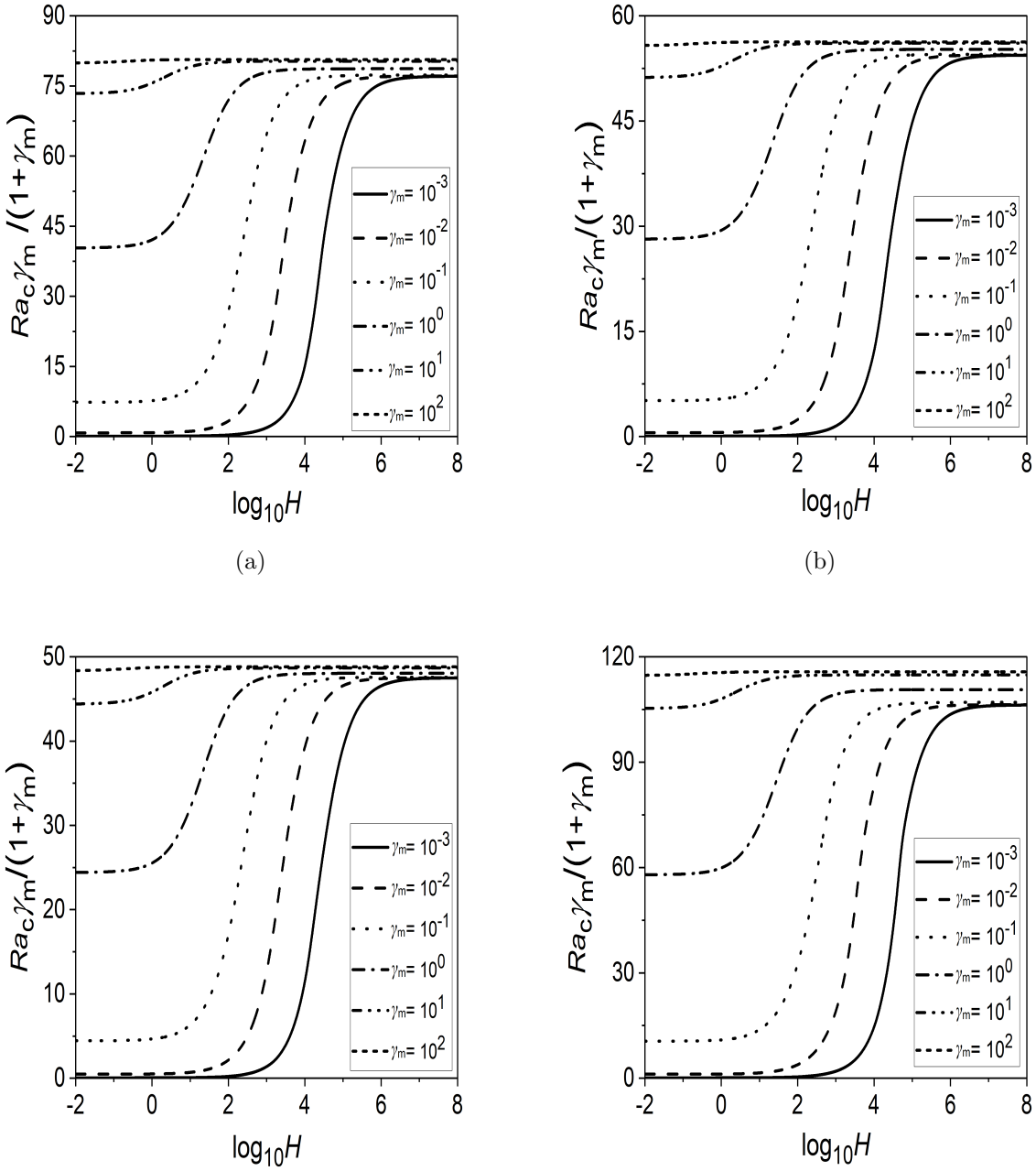

Figure 5.6: Effect of porosity modified conductivity ratio (γ_{m}) on a_{c} for (a) $G(z) = -z$, (b) $G(z) = -z^2$, (c) $G(z) = -z^3$ and (d) $G(z) = -(e^z - 1)$ when $Q = 0.5$ and $\lambda = 1$.

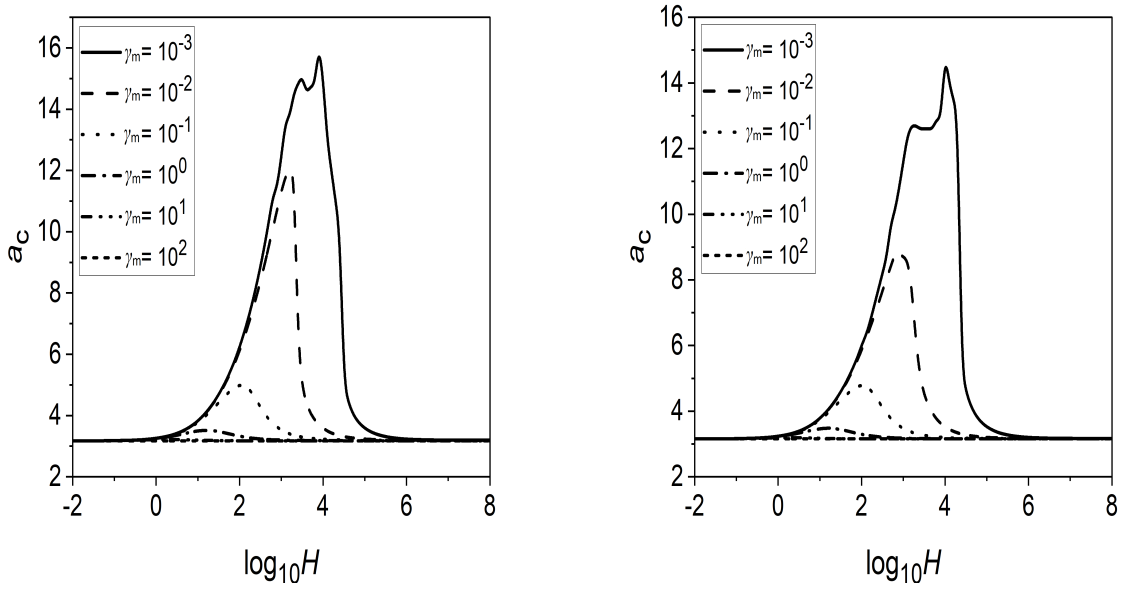

(a) (b)

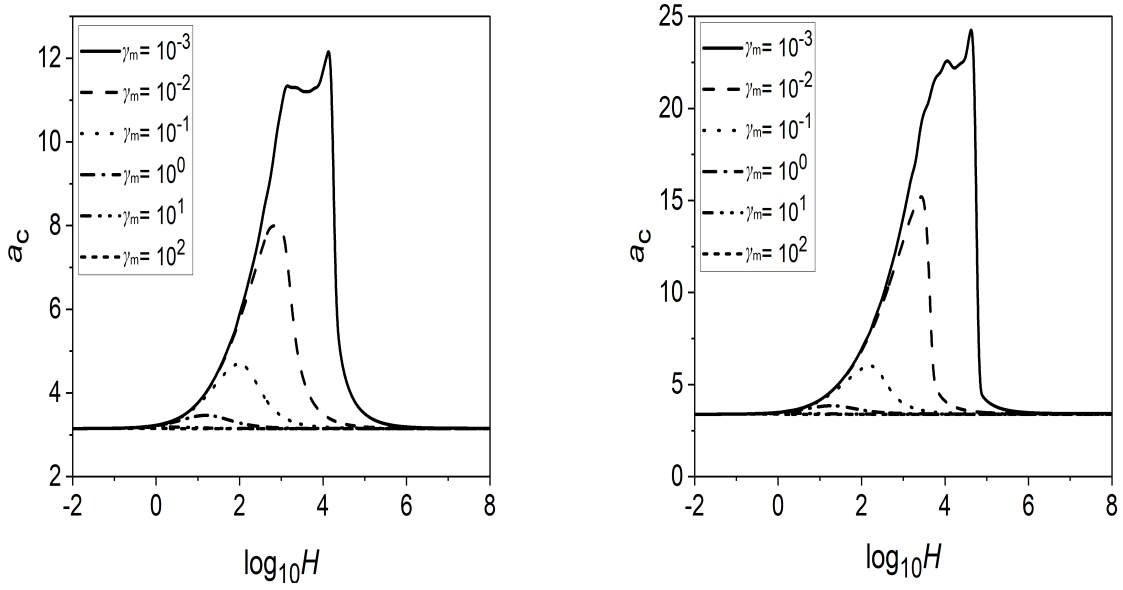

(c) (d)

Figure 5.7: Effect of porosity modified conductivity ratio (γ_{m}) on a_{c} for (a) $G(z) = -z$, (b) $G(z) = -z^2$, (c) $G(z) = -z^3$ and (d) $G(z) = -(e^z - 1)$ when $Q = 0.5$ and $\lambda = 1$.

5.6 Conclusions

The onset of convection in a horizontal porous layer is investigated numerically for the variable gravity field with height and vertical throughflow effects under non-equilibrium conditions. Linear, quadratic, cubic and exponential varying gravity fields have been taken to study for the above consideration.

- The system acts like an LTE model when inter-phase heat transfer parameter H converges both the limiting cases, i.e. $H \to 0$ and $H \to \infty$, while H shows the stabilizing nature inside the intermediate range.
- The effect of the gravity variation parameter and the vertical throughflow parameter is to improve the stability of the system. On the other hand, the impact of rising the porosity modified conductivity ratio (γ_{m}) is to destabilize the system.
- Ra_{c} is independent of H when $\gamma_{\mathrm{m}} \geq 10$. Also, the system is more stable for exponential varying gravity field, while more unstable for cubic varying gravity field.
- The variation of critical wavenumber keeps constant for both the limiting cases, i.e. $H \to 0$ and $H \to \infty$, while it maintains more value as compared with LTE value inside the intermediate values of H. Also, the size of the cell reduces for enhancing the values of gravity variation parameter when the throughflow effect is ignored, otherwise, it shows dual nature.
- The effect of vertical throughflow on the cell size shows dual nature, while it increases with the porosity modified conductivity ratio.
- The dimension of the convective cells is more for cubic varying gravity field and very less for exponential varying gravity field and remains the same when the flow is independent of the throughflow effect.

Part III

STABILITY OF NANOFLUID FLOW IN A POROUS VERTICAL CHANNEL

Chapter 6

Linear stability of convection in a vertical channel filled with nanofluid saturated porous medium [1]

6.1 Introduction

A new class of heat transfer fluids, called nanofluids, can be prepared by mixing metal or metallic oxide (Cu, Al_2O_3, CuO) nanoparticles in the base fluid such as water, oil, ethylene glycol etc. [36]. The resultant nanofluids are anticipated to demonstrate high thermal conductivity compared to those of usual heat transfer fluids. The nanofluids have diverse applications, ranging from laser-assisted drug delivery to the electronic chip cooling. After examining the impact of seven slip mechanisms of suspended nanoparticles, a mathematical model for nanofluid was proposed by Buongiorno [25] based on the Brownian motion and thermophoresis effects. Convection in nanofluid using the Buongiorno's model was studied by Tzou [115], Kuznetsov and Nield [63, 64], Nield and Kuznetsov [79, 81], Yadav *et al.* [127], Chand and Rana [29, 30]. Shankar *et al.* [98] investigated the influence of the magnetic field on the instability of mixed convection in a differentially heated vertical layer.

For the last few decades, several authors have analyzed the stability of the flow in vertical channels. Bera and Khalili [18] studied the stability of convection in a vertical channel occupied with an anisotropic porous medium with zero temperature and zero heat flux condition. Chen [34] analyzed the stability of convection in a vertical channel filled with a porous medium with the Darcy-Brinkman-Forchheimer model. Sharma *et al.* [99] studied amplitude analysis of non-isothermal parallel flow in a vertical channel filled with a highly

[1] Published in "***Heat Transfer***" 50(4), 3220-3239, 2021

permeable porous medium.

In this chapter, we investigate the linear stability of the flow in a vertical channel filled with a nanofluid saturated porous medium. The Brinkman model [24] for the flow in a porous medium and the Buongiorno model [25] for the nanofluid are the basis to the present study. A linear stability analysis is done by adopting normal modes. The resulting eigenvalue problem for small disturbance is solved using the Chebyshev spectral collocation methods. The numerical solution that is obtained is analyzed graphically by varying the governing parameters.

6.2 Mathematical Formulation

Consider an incompressible unsteady convection flow in a long vertical channel of width $2L$ filled with nanofluid saturated porous medium. Assume that the nanofluid is modelled by the Buongiorno [25] model. The Cartesian coordinate system is chosen in such a way that the y-axis is taken along vertically upward direction through the center line of the channel and the $x-$axis makes right angles to vertical plates as shown in Fig. 6.1. Let $\hat{\mathbf{e}}_\mathbf{x}$, $\hat{\mathbf{e}}_\mathbf{y}$ and $\hat{\mathbf{e}}_\mathbf{z}$ be the unit vector along $x-$, $y-$ and $z-$ direction. The gravitational acceleration $\mathbf{g} = -\mathrm{g}\hat{\mathbf{e}}_\mathbf{y}$, is oriented in the opposite direction of the vertical $y-$axis. The plates of the channel are at $x = -L$ and $x = L$, respectively. The constant temperatures T_1 and T_2 ($T_1 > T_2$) are maintained at the left and right walls, respectively. Also, the corresponding nanoparticles volume fractions ϕ_2 at the left wall and ϕ_1 at the right wall are constant.

The thermo-physical properties of the fluid are assumed to be constant except for the density variations in the buoyancy force term in the momentum equation which is satisfied by the Oberbeck-Boussinesq approximation. It is assumed that the fluid and porous medium are everywhere in a local thermal equilibrium state, the porous medium is homogeneous and hydro-dynamically as well as thermally isotropic. The flow within the porous region is governed by Brinkman's [24] equation.

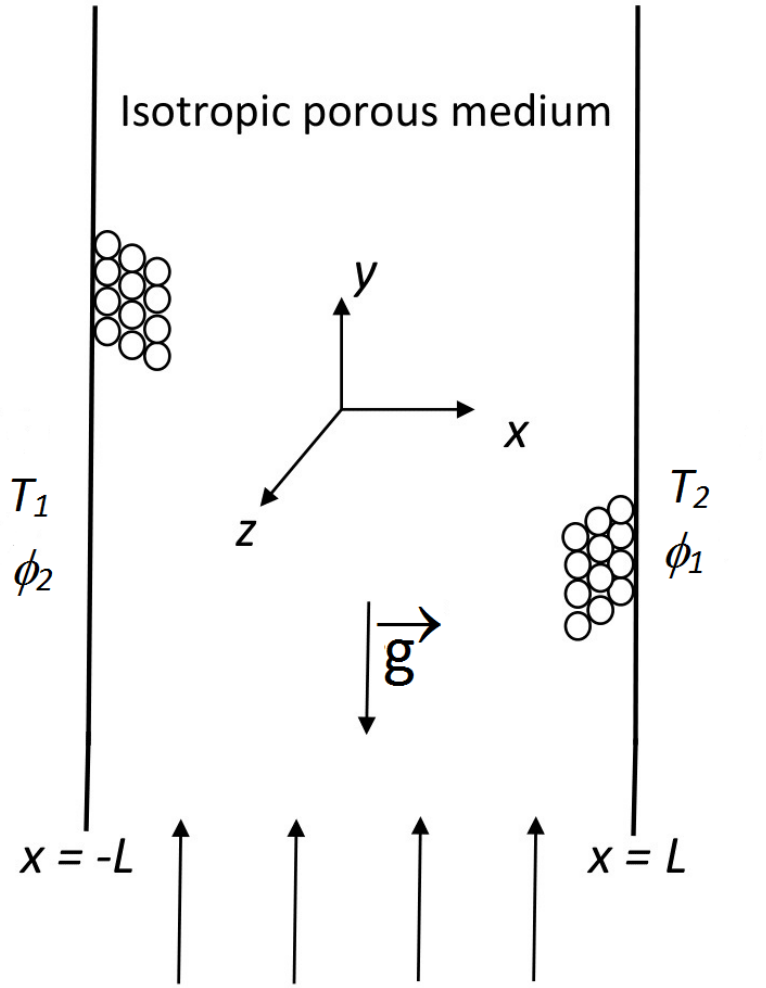

Figure 6.1: Schematic representation of the problem.

With the above assumptions, the equations of mass, momentum, energy and volume fraction of nanofluid in porous medium are

$$\nabla \cdot \mathbf{u} = 0, \tag{6.1}$$

$$\rho_{\mathrm{f}} \left(\frac{1}{\epsilon} \frac{\partial \mathbf{u}}{\partial t} + \frac{1}{\epsilon^2} (\mathbf{u} \cdot \nabla) \mathbf{u} \right) = -\nabla p + \tilde{\mu} \nabla^2 \mathbf{u} - \frac{\mu}{K} \mathbf{u} + [\phi \rho_{\mathrm{p}} + (1 - \phi) \rho_{\mathrm{f}} \{1 - \beta_{\mathrm{T}} (T - T_1] \mathbf{g}, \tag{6.2}$$

$$(\rho c)_{\mathrm{m}} \frac{\partial T}{\partial t} + (\rho c)_{\mathrm{f}} \mathbf{u} \cdot \nabla T = k_{\mathrm{m}} \nabla^2 T + \epsilon (\rho c)_{\mathrm{p}} \left[D_{\mathrm{B}} \nabla \phi \cdot \nabla T + \frac{D_{\mathrm{T}}}{T_1} \nabla T \cdot \nabla T \right], \tag{6.3}$$

$$\frac{\partial \phi}{\partial t} + \frac{1}{\epsilon}\mathbf{u}\cdot\nabla\phi = D_{\mathrm{B}}\nabla^2\phi + \frac{D_{\mathrm{T}}}{T_1}\nabla^2 T, \tag{6.4}$$

where ϕ is the volume fraction of the nanoparticles, ρ_{f} is the density of the base flow, ρ_{p} is the density of the nanoparticles, $(\rho c)_{\mathrm{p}}$ is the heat capacity of the nanoparticles, D_{B} is the Brownian diffusion coefficient and D_{T} is the thermophoretic diffusion coefficient of nanoparticles. The remaining quantities are defined in Chapter - 2.
The boundary conditions are

$$x = -L: \ \mathbf{u} = 0, \ T = T_1, \ \phi = \phi_2, \tag{6.5a}$$

$$x = L: \ \mathbf{u} = 0, \ T = T_2, \ \phi = \phi_1. \tag{6.5b}$$

Introducing non-dimensional scheme is defined as follows

$$\begin{gathered}(x^*, y^*, z^*) = \frac{(x, y, z)}{L}, \quad \mathbf{u}^* = \frac{\mathbf{u}L}{\alpha_{\mathrm{m}}}, \quad p^* = \frac{Kp}{\mu\alpha_{\mathrm{m}}}, \\ t^* = \frac{\alpha_{\mathrm{m}} t}{\sigma L^2}, \quad T^* = \frac{T - T_1}{T_2 - T_1}, \quad \phi^* = \frac{\phi - \phi_1}{\phi_2 - \phi_1},\end{gathered} \tag{6.6}$$

and

$$\alpha_{\mathrm{m}} = \frac{k_{\mathrm{m}}}{(\rho c_{\mathrm{p}})_{\mathrm{f}}}, \quad \text{and} \quad \sigma = \frac{(\rho c_{\mathrm{p}})_{\mathrm{m}}}{(\rho c_{\mathrm{p}})_{\mathrm{f}}}, \tag{6.7}$$

where α_{m} and σ are thermal diffusivity of porous medium and thermal capacity ratio, respectively.

Substituting the non-dimenisonal variables Eq. (6.6) in Eqs. (6.1)-(6.5) and dropping asterisk, we get

$$\nabla\cdot\mathbf{u} = 0, \tag{6.8}$$

$$\frac{1}{Va}\left[\frac{1}{\sigma}\frac{\partial \mathbf{u}}{\partial t} + \frac{1}{\epsilon}(\mathbf{u}\cdot\nabla)\mathbf{u}\right] = -\nabla p + \Lambda Da\nabla^2\mathbf{u} - \mathbf{u} + RaT\hat{\mathbf{e}}_{\mathbf{y}} - Rn\phi\hat{\mathbf{e}}_{\mathbf{y}} - Rm\hat{\mathbf{e}}_{\mathbf{y}}, \tag{6.9}$$

$$\frac{\partial T}{\partial t} + \mathbf{u}\cdot\nabla T = \nabla^2 T + \frac{N_{\mathrm{B}}}{Le}\nabla\phi\cdot\nabla T + \frac{N_{\mathrm{A}}N_{\mathrm{B}}}{Le}\nabla T\cdot\nabla T, \tag{6.10}$$

$$\frac{1}{\sigma}\frac{\partial \phi}{\partial t} + \frac{1}{\epsilon}\mathbf{u}\cdot\nabla\phi = \frac{1}{Le}\nabla^2\phi + \frac{N_{\mathrm{A}}}{Le}\nabla^2 T, \tag{6.11}$$

The dimensionless boundary conditions are

$$x = -1: \ \mathbf{u} = 0, \ T = 0, \ \phi = 1, \tag{6.12a}$$

$$x = 1: \ \mathbf{u} = 0, \ T = 1, \ \phi = 0. \tag{6.12b}$$

In the above the non-dimensional parameters are $Va = \frac{\epsilon Pr}{Da}$ is the Vadasz number, $Rn =$

$\frac{(\rho_{\mathrm{p}}-\rho_{\mathrm{f}})(\phi_2-\phi_1)\mathrm{g}KL}{\mu\alpha_{\mathrm{m}}}$ is concentration Rayleigh number, $Rm = \frac{[\rho_{\mathrm{p}}\phi_1+\rho_{\mathrm{f}}(1-\phi_1)]\mathrm{g}KL}{\mu\alpha_{\mathrm{m}}}$ is the basic-density Rayleigh number, $N_{\mathrm{A}} = \frac{D_{\mathrm{T}}(T_2-T_1)}{D_{\mathrm{B}}T_1(\phi_2-\phi_1)}$ is the modified diffusivity ratio, $N_{\mathrm{B}} = \frac{\epsilon(\rho C)_{\mathrm{p}}}{(\rho C)_{\mathrm{f}}}(\phi_2-\phi_1)$ is the modified particle density increment, $\Lambda = \frac{\tilde{\mu}}{\mu}$ is the ratio of effective viscosity to the fluid viscosity and $Le = \frac{\alpha_{\mathrm{m}}}{D_{\mathrm{B}}}$ is the Lewis number.

In the present study, we have taken the viscosity ratio $\Lambda = 1$ and thermal capacity ratio $\sigma = 1$, to avoid too many parameter studies.

6.3 Basic state solution

The flow in the basic state is assumed as steady, unidirectional and fully developed and is described by $\mathbf{u_0} = (0, V_0(x), 0)$ is the basic velocity vector, $T_0 = T_0(x)$ is the basic temperature, $\phi_0 = \phi_0(x)$ is the basic volume fraction and $p_0 = p_0(y)$ is the basic pressure. Under these conditions, the governing Eqs. (6.8)-(6.11) reduce to

$$\frac{d^2V_0}{dx^2} - \frac{1}{Da}V_0 = \frac{1}{Da}\frac{dp_0}{dy} - \frac{Ra}{Da}T_0 + \frac{Rn}{Da}\phi_0 + \frac{Rm}{Da}, \tag{6.13}$$

$$\frac{d^2T_0}{dx^2} + \frac{N_{\mathrm{B}}}{Le}\frac{d\phi_0}{dx}\frac{dT_0}{dx} + \frac{N_{\mathrm{A}}N_{\mathrm{B}}}{Le}\left(\frac{dT_0}{dx}\right)^2 = 0, \tag{6.14}$$

$$\frac{d^2\phi_0}{dx^2} + N_{\mathrm{A}}\frac{d^2T_0}{dx^2} = 0, \tag{6.15}$$

The corresponding boundary conditions are:

$$x = -1: \ V_0 = 0, \ T_0 = 0, \ \phi_0 = 1, \tag{6.16a}$$

$$x = 1: \ V_0 = 0, \ T_0 = 1, \ \phi_0 = 0. \tag{6.16b}$$

Integrating the Eq. (6.15) and incorporating the boundary condition Eq. (6.16), we get ϕ_0 in terms of T_0 as formed by

$$\phi_0 = -N_{\mathrm{A}}T_0 - \left(\frac{1-N_{\mathrm{A}}}{2}\right)x + \left(\frac{1+N_{\mathrm{A}}}{2}\right). \tag{6.17}$$

Substituting this into Eq. (6.14) and solving the resulting differential equation in T_0, we get

$$T_0 = \frac{1 - e^{-\frac{(1-N_{\mathrm{A}})N_{\mathrm{B}}}{2Le}(1+x)}}{1 - e^{-\frac{(1-N_{\mathrm{A}})N_{\mathrm{B}}}{Le}}}. \tag{6.18}$$

According to Buongiorno [25] for most nanofluids investigated so far Le is large, of order $10^2 - 10^3$, N_{B} is of order $10^{-1} - 10^{-3}$ while N_{A} is not greater than about 10 [64]. A good approximation of T_0, therefore, is

$$T_0 = \frac{1+x}{2}, \tag{6.19}$$

and approximation for ϕ_0 is

$$\phi_0 = \frac{1-x}{2}. \tag{6.20}$$

A comparison of the solutions has been made for exact and approximate basic temperature and volume fraction profiles and presented in the Fig. 6.2 for $N_{\mathrm{A}} = 5,\ N_{\mathrm{B}} = 0.02$ and $Le = 500$. From these figures, it is observed that the solutions are exactly matches with the approximate solution for basic temperature and basic volume fraction, respectively. Hence, the approximate solutions of the basic temperature and volume fraction has been taken for further discussions.

Now, using the Eqs. (6.19) and (6.20) into the Eq. (6.13) with the help of the global mass conservation (i.e. $\int_{-1}^{1} V_0 dx = 2$) and incorporating the boundary conditions Eq. (6.16), the basic velocity is obtained as

$$V_0 = s\left[1 - \frac{\cosh(x/\sqrt{Da})}{\cosh(1/\sqrt{Da})}\right] + \left(\frac{Ra + Rn}{2}\right)\left[x - \frac{\sinh(x/\sqrt{Da})}{\sinh(1/\sqrt{Da})}\right], \tag{6.21}$$

where $s = \dfrac{\sinh(2/\sqrt{Da})}{\sinh(2/\sqrt{Da}) - \sqrt{Da}(\cosh(2/\sqrt{Da}) - 1)}$.

The basic velocity profiles are shown in Fig. 6.3 for different values of Da and Ra.

6.4 Linear stability analysis

The linear stability is studied by imposing the infinitesimal disturbances on the basic state flow. Hence, the velocity, temperature, volume fraction and pressure fields can be written as

$$(\mathbf{u}, T, \phi, p) = (\mathbf{u}_0, T_0(x), \phi_0(x), p_0(y)) + (\mathbf{u}', T', \phi', p'), \tag{6.22}$$

where the prime denotes an infinitesimal disturbance. By substituting Eq. (6.22) into Eqs. (6.8)-(6.11) and neglecting nonlinear terms, we get following linearized perturbed equations

$$\nabla \cdot \mathbf{u}' = 0, \tag{6.23}$$

$$\frac{1}{Va}\left[\frac{\partial \mathbf{u}'}{\partial t}+\frac{1}{\epsilon}\{(\mathbf{u}'\cdot\nabla)\mathbf{u}_0+(\mathbf{u}_0\cdot\nabla)\mathbf{u}'\}\right]=-\nabla p'+Da\nabla^2\mathbf{u}'-\mathbf{u}'+RaT'\hat{\mathbf{e}}_\mathbf{y}-Rn\phi'\hat{\mathbf{e}}_\mathbf{y}, \quad (6.24)$$

$$\frac{\partial T'}{\partial t}+u'\frac{dT_0}{dx}+V_0\frac{\partial T'}{\partial y}=\nabla^2T'+\frac{N_\mathrm{B}}{Le}\left[\frac{d\phi_0}{dx}\frac{\partial T'}{\partial x}+\frac{dT_0}{dx}\frac{\partial \phi'}{\partial x}\right]+\frac{2N_\mathrm{A}N_\mathrm{B}}{Le}\frac{dT_0}{dx}\frac{\partial T'}{\partial x}, \quad (6.25)$$

$$\frac{\partial \phi'}{\partial t}+\frac{1}{\epsilon}\left[u'\frac{d\phi_0}{dx}+V_0\frac{\partial \phi'}{\partial y}\right]=\frac{1}{Le}\nabla^2\phi'+\frac{N_\mathrm{A}}{Le}\nabla^2T'. \quad (6.26)$$

By applying the usual normal mode form [42], the disturbances are given by

$$(\mathbf{u}',T',\phi',p')=(\hat{\mathbf{u}}(x),\hat{T}(x),\hat{\phi}(x),\hat{p}(x))e^{i(\alpha y+\beta z-\alpha ct)}, \quad (6.27)$$

where α and β are real and represent the wavenumber in streamwise (y) and spanwise (z) directions, and $c=c_r+ic_i$ is a wavespeed. The growth or decay of the disturbance depends on the sign of c_i. For $c_i<0$, the disturbances are stable, $c_i=0$, the disturbances are neutrally stable and $c_i>0$, the disturbances are unstable.

On substituting Eq. (6.27) into the governing Eqs. (6.23)-(6.26), linearized disturbance equations become

$$Da\left[\frac{d^4\hat{u}}{dx^4}-2(\alpha^2+\beta^2)\frac{d^2\hat{u}}{dx^2}+(\alpha^2+\beta^2)^2\hat{u}\right]-\frac{i\alpha}{Va}\left(\frac{1}{\epsilon}V_0-c\right)\left[\frac{d^2\hat{u}}{dx^2}-(\alpha^2+\beta^2)\hat{u}\right]$$
$$+\frac{i\alpha}{\epsilon Va}\frac{d^2V_0}{dx^2}\hat{u}-\left[\frac{d^2\hat{u}}{dx^2}-(\alpha^2+\beta^2)\hat{u}\right]-i\alpha Ra\frac{d\hat{T}}{dx}+i\alpha Rn\frac{d\hat{\phi}}{dx}=0, \quad (6.28)$$

$$\frac{\beta}{\epsilon Va}\frac{dV_0}{dx}\hat{u}+\frac{i\alpha}{Va}\left(\frac{1}{\epsilon}V_0-c\right)\hat{\eta}-Da\left[\frac{d^2\hat{\eta}}{dx^2}-(\alpha^2+\beta^2)\hat{\eta}\right]+\hat{\eta}-\beta Ra\hat{T}+\beta Rn\hat{\phi}=0, \quad (6.29)$$

$$\frac{dT_0}{dx}\hat{u}+i\alpha(V_0-c)\hat{T}-\left[\frac{d^2\hat{T}}{dx^2}-(\alpha^2+\beta^2)\hat{T}\right]-\frac{N_\mathrm{B}}{Le}\left(\frac{d\phi_0}{dx}+2N_\mathrm{A}\frac{dT_0}{dx}\right)\frac{d\hat{T}}{dx}$$
$$-\frac{N_\mathrm{B}}{Le}\frac{dT_0}{dx}\frac{d\hat{\phi}}{dx}=0, \quad (6.30)$$

$$\frac{1}{\epsilon}\frac{d\phi_0}{dx}\hat{u}+i\alpha\left(\frac{1}{\epsilon}V_0-c\right)\hat{\phi}-\frac{1}{Le}\left[\frac{d^2\hat{\phi}}{dx^2}-(\alpha^2+\beta^2)\hat{\phi}\right]-\frac{N_\mathrm{A}}{Le}\left[\frac{d^2\hat{T}}{dx^2}-(\alpha^2+\beta^2)\hat{T}\right]=0, \quad (6.31)$$

where $\hat{\mathbf{u}}(x)=(\hat{u},\hat{v},\hat{w})$ and $\hat{\eta}=\beta\hat{v}-\alpha\hat{w}$.

The corresponding boundary conditions are

$$\hat{u}=\frac{d\hat{u}}{dx}=\hat{\eta}=\hat{T}=\hat{\phi}=0 \quad \text{at} \quad x=\mp 1. \quad (6.32)$$

6.5 Numerical solution

The system of differential equations Eqs. (6.28)-(6.31) along with their boundary conditions Eq. (6.32) form a generalized eigenvalue problem with complex disturbance wave speed as the eigenvalue and is solved using Chebyshev spectral collocation method [27]. To solve the eigenvalue problem using the Chebyshev spectral collocation method on $[-1,1]$, first the interval $[-1,1]$ is descritized using the following $N+1$ Gauss-Lobatto collocation points

$$x_j = \cos\frac{\pi j}{N}, \quad j = 0,1,2,...,N. \tag{6.33}$$

Next, the unknown functions $\hat{u}$, $\hat{\eta}$, $\hat{T}$ and $\hat{\phi}$ are approximated at the collocation points as follows

$$\begin{aligned} \hat{u}(x) &\approx \sum_{k=0}^{N} \hat{u}(x_k)T_k(x_j), \qquad \hat{\eta}(x) \approx \sum_{k=0}^{N} \hat{\eta}(x_k)T_k(x_j), \\ \hat{T}(x) &\approx \sum_{k=0}^{N} \hat{T}(x_k)T_k(x_j), \quad \hat{\phi}(x) \approx \sum_{k=0}^{N} \hat{\phi}(x_k)T_k(x_j), \quad j = 0,1,...,N, \end{aligned} \tag{6.34}$$

where T_k is the k^{th} Chebyshev polynomial defined by $T_k(x) = \cos(k\cos^{-1}x)$.

The $\mathbf{m}^{th}$ order of differentiation of the unknown functions at the collocation points are represented as

$$\begin{aligned} \frac{d^{\mathbf{m}}\hat{u}}{dx^{\mathbf{m}}} &= \sum_{k=0}^{J} \mathbf{D}^{\mathbf{m}}_{\mathbf{kj}}\hat{u}(\xi_k), \qquad \frac{d^{\mathbf{m}}\hat{\eta}}{dx^{\mathbf{m}}} = \sum_{k=0}^{J} \mathbf{D}^{\mathbf{m}}_{\mathbf{kj}}\hat{\eta}(\xi_k), \\ \frac{d^{\mathbf{m}}\hat{T}}{dx^{\mathbf{m}}} &= \sum_{k=0}^{J} \mathbf{D}^{\mathbf{m}}_{\mathbf{kj}}\hat{T}(\xi_k), \qquad \frac{d^{\mathbf{m}}\hat{\phi}}{dx^{\mathbf{m}}} = \sum_{k=0}^{J} \mathbf{D}^{\mathbf{m}}_{\mathbf{kj}}\hat{\phi}(\xi_k) \end{aligned} \tag{6.35}$$

where the elements of Chebyshev spectral differentiation matrix $\mathbf{D}$ are given by

$$\mathbf{D}_{jk} = \begin{cases} \frac{2N^2+1}{6}, & j = k = 0, \\ \frac{c_j}{c_k}\frac{(-1)^{j+k}}{x_j - x_k}, & j \neq k;\ j,k = 0,1,2,...,N, \\ -\frac{x_k}{2(1-x_k^2)}, & j = k;\ j,k = 1,2,3,...,N-1, \\ -\frac{2N^2+1}{6}, & j = k = N. \end{cases} \tag{6.36}$$

where

$$c_j = \begin{cases} 2, & j = 0 \ or \ N, \\ 1, & Otherwise \end{cases}$$

Substituting Eqs. (6.34) - (6.35) into Eqs. (6.28)-(6.31), we obtain the following $(4N+4)\times$

$(4N+4)$ eigenvalue problem:

$$\mathbf{A}X = c\mathbf{B}X \tag{6.37}$$

with

$$\mathbf{A} = \begin{bmatrix} A_{11} & \mathbf{0} & A_{13} & A_{14} \\ A_{21} & A_{22} & A_{23} & A_{24} \\ A_{31} & \mathbf{0} & A_{33} & A_{34} \\ A_{41} & \mathbf{0} & A_{43} & A_{44} \end{bmatrix}, \quad \mathbf{B} = \begin{bmatrix} B_{11} & \mathbf{0} & \mathbf{0} & \mathbf{0} \\ \mathbf{0} & B_{22} & \mathbf{0} & \mathbf{0} \\ \mathbf{0} & \mathbf{0} & B_{33} & \mathbf{0} \\ \mathbf{0} & \mathbf{0} & \mathbf{0} & B_{44} \end{bmatrix} \quad \text{and} \quad X = \begin{bmatrix} \hat{u} \\ \hat{\eta} \\ \hat{T} \\ \hat{\phi} \end{bmatrix}.$$

Here c is the complex eigenvalue, X is the representation of the complex eigenfunction, and $\mathbf{A}$ and $\mathbf{B}$ are the square complex matrices.
where

$$A_{11} = Da[\mathbf{D}_4 - 2(\alpha^2+\beta^2)\mathbf{D}_2 + (\alpha^2+\beta^2)^2\mathbf{I}] - \left(\frac{i\alpha}{\epsilon Va}V_0 + 1\right)(\mathbf{D}_2 - (\alpha^2+\beta^2)\mathbf{I}) + \frac{i\alpha}{\epsilon Va}\frac{d^2V_0}{dx^2}\mathbf{I},$$

$$A_{13} = -i\alpha Ra\mathbf{D}_1, \quad A_{14} = i\alpha Rn\mathbf{D}_1, \quad A_{21} = \frac{\beta}{\epsilon Va}\frac{dV_0}{dx}\mathbf{I},$$

$$A_{22} = \frac{i\alpha}{\epsilon Va}V_0\mathbf{I} - Da[\mathbf{D}_2 - (\alpha^2+\beta^2)\mathbf{I}] + \mathbf{I}, \quad A_{23} = -\beta Ra\mathbf{I}, \quad A_{24} = \beta Rn\mathbf{I}, \quad A_{31} = \frac{dT_0}{dx}, \mathbf{I}$$

$$A_{33} = i\alpha V_0 - (\mathbf{D}_2 - (\alpha^2+\beta^2)\mathbf{I}) - \frac{2N_{\mathrm{A}}N_{\mathrm{B}}}{Le}\frac{dT_0}{dx}\mathbf{D}_1 - \frac{N_{\mathrm{B}}}{Le}\frac{d\phi_0}{dx}\mathbf{D}_1, \quad A_{34} = -\frac{N_{\mathrm{B}}}{Le}\frac{dT_0}{dx}\mathbf{D}_1,$$

$$A_{41} = \frac{1}{\epsilon}\frac{d\phi_0}{dx}\mathbf{I}, \quad A_{43} = -\frac{N_{\mathrm{A}}}{Le}(\mathbf{D}_2 - (\alpha^2+\beta^2)\mathbf{I}), \quad A_{44} = \frac{i\alpha}{\epsilon}V_0 - \frac{1}{Le}(\mathbf{D}_2 - (\alpha^2+\beta^2)\mathbf{I}),$$

$$B_{11} = -\frac{i\alpha}{Va}(\mathbf{D}_2 - (\alpha^2+\beta^2)\mathbf{I}), \quad B_{22} = \frac{i\alpha}{Va}\mathbf{I}, B_{33} = i\alpha\mathbf{I}, B_{44} = i\alpha\mathbf{I}.$$

Here $\mathbf{D}_1$ and $\mathbf{D}_2$ are obtained from usual first and second Chebyshev derivative matrices $\mathbf{D}$ and $\mathbf{D}^2 = \mathbf{D} \times \mathbf{D}$ after imposing the boundary conditions $\hat{u}(\pm 1) = 0$. $\mathbf{D}_4$ is the fourth derivative matrix imposing the clamped boundary conditions $\hat{u}(\pm 1) = \hat{u}_x(\pm 1) = 0$ and given by

$$\mathbf{D}_4 = \left[diag(1-x^2)\mathbf{D}^4 - 8diag(x)\mathbf{D}^3 - 12\mathbf{D}^2\right] diag(1/(1-x^2)),$$

$V_0 = \mathrm{diag}[V_0(x_j)]$, $T_0 = \mathrm{diag}[T_0(x_j)]$, $\phi_0 = \mathrm{diag}[\phi_0(x_j)]$, $\mathbf{I}$ and $\mathbf{0}$ are $(N+1)\times(N+1)$ identity and zeros matrices, respectively. Also diag [ ] means that the entries are placed on the main diagonal of an $(N+1)\times(N+1)$ matrix with the rest of the entries being zero.

To check the convergence, the code written to solve the eigenvalue problem Eq. (**??**) is executed by changing the number of collocation points (N) and the least stable eigenvalues obtained are presented in the Table 6.1 for randomly selected values for various parameters. It is apparent from this table that the least stable eigenvalue attain convergence criterion of

10^{-7} for $N \geq 51$. There is no change in the results with an increase of N. The same tendency is witnessed for other values of parameters. Hence, $N = 51$, is adopted to implement the numerical calculations.

The results obtained from the present analysis are compared with the results of an isothermal channel flow without a porous medium. The critical Reynolds number $Re_{\rm c}$ and critical wavenumber α_c for the isothermal channel are obtained as $Re_{\rm c} = 3848.278$ (in this paper $1/Pr$) and $\alpha_{\rm c} = 1.0205$ from the present analysis by setting $Rn = 0$, $\epsilon = 1$, $\beta = 0$, $Da = 10^6$, $N_{\rm A} = 0$, $N_{\rm B} = 0$ and $Le = 10^6$. These values are in good agreement with those given by Orszag [84].

6.6 Results and discussion

The present work analyses of linear stability of a convective flow in a vertical channel filled with nanofluid saturated by porous medium. The effect of the governing parameters i.e., Rn, ϵ, Pr, $N_{\rm A}$, $N_{\rm B}$ and Le on the critical Rayleigh number $Ra_{\rm c}$ and critical wavenumber $\alpha_{\rm c}$ is presented graphically through Figs. 6.5 to 6.10. A logarithmic scale is used along the horizontal axis to display all the instability boundaries. Throughout the numerical investigation, the range for the parameter $N_{\rm A}$ is considered as $1 \leq N_A \leq 10$, the values of Le are taken as 100, 300, 500, $N_{\rm B}$ is taken as very small values 0.002, 0.02, 0.2, the values of the porosity parameter are taken as 0.6, 0.7, 0.8 and the values for Rn are taken as 15, 30, 60 which are not against the physical requirements. The effect of Prandtl number (Pr) on the stability of the flow is emphasized by taking three different values of Pr as (0.7, 1 and 7). As in the case of viscous fluid, Ra_c is computed for several values of spanwise wavenumber (β) to scrutinize the dimension of least stable mode and displayed in Fig. 6.4. It is observed that the computational results ensure the Squire's theorem [104] for nanofluid also, i.e., the least stable mode is 2-dimensional. Therefore, we have taken $\beta = 0$ in the rest of the discussions.

The effect of the Prandtl number Pr on the instability boundaries is presented in the Fig. 6.5 for various values of Da for $Rn = 15$, $\epsilon = 0.6$, $Le = 500$, $N_{\rm A} = 8$ and $N_{\rm B} = 0.02$. It is noticed from Fig. 6.5(a) that the critical Rayleigh number is increasing with an increase in the value of Darcy number Da, which indicates that permeability has a stabilizing effect. For small values of the Darcy number ($Da < 1$), the variation of $Ra_{\rm c}$ is slow and smooth. A rapid increase in $Ra_{\rm c}$ is observed for $Da > 1$. As Darcy number increases, the permeability of the porous medium increase. For small values of Darcy number, noticeable flow resistance in the porous medium is observed. This flow resistance decreases with increasing the permeability

and the flow is accelerated in a porous medium, indicates the contribution of viscous forces contained in the momentum equation. Further, it is noticed that an increase in momentum diffusivity in terms of Pr increases the critical Rayleigh number. Hence, the influence of the Prandtl number is to stabilize the system. Fig. 6.5(b) displays the impact of Pr for α_c on critical wavenumber in the $(\log_{10}Da, \alpha_c)$-plane for different values of Da. It is seen from Fig. 6.5(b) that the critical wavenumber is increasing with the increase in the value of Da. This increase is drastic for $Da < 1$ and then it is smooth and slow. The impact of Pr on the critical wavenumber profile is very small when $Da < 1$, but after that it is significant.

Fig. 6.6 depicts the variation of Ra_c and α_c with the Darcy number Da for the different values of Rn for $Pr = 7$, $\epsilon = 0.6$, $Le = 500$, $N_A = 8$ and $N_B = 0.02$. It is seen from Fig. 6.6(a) that the variation in Ra_c is visible for $Rn = 60$ when $Da < 0.3$. As Rn increases, the variation in the critical Rayleigh number is very small for the remaining values of Da. Similarly, the effect of Rn in α_c is not significant except for $Da < 0.3$ when $Rn = 60$ as plotted in Fig. 6.6(b). The critical wavenumber is increasing with an increase in Rn for $Da < 3$. To have a clear understanding on the effect of Rn for fixed values of Da, the critical Rayleigh number and critical wavenumber are computed for different values of Da and Rn and presented in the Table 6.2. It is noticed from this table that critical Rayleigh number Ra decreases for rising the values of Rn. Thus, this factor has a destabilizing effect on the medium. It is observed that enhancing the value of Rn has a dual effect on the dimension of the convective cells.

The instability boundaries as a functions of the permeability parameter Da and the porosity (ϵ) parameter is plotted in Fig. 6.7 for $Pr = 7$, $Rn = 15$, $Le = 500$, $N_A = 8$ and $N_B = 0.02$. It is understood from the Fig. 6.7(a) that an increase of porosity ϵ tends to increase the critical Rayleigh number Ra_c. Since porosity is a fraction of the volume of voids over the total volume which is a measure of the void spaces in the porous medium. As porosity increases, the volume of the voids increase and hence the porosity has a stabilizing effect. It is noticed from Fig. 6.7(b) that there is a small variation in α_c for increase in the value of the porosity parameter.

The variation in the critical value of Rayleigh number and critical wavenumber with Da for different value of Le is displayed in Fig. 6.8 for $Pr = 7$, $Rn = 15$, $\epsilon = 0.6$, $N_A = 8$ and $N_B = 0.02$. It is observed from Fig. 6.8(a) that the variation of critical Rayleigh number with the Lewis number is not visible. Also, Fig. 6.8(b) shows that the impact of Le on α_c is very small. For fixed values of Da and β, streamwise critical wavenumber α_c and critical value of the Rayleigh number Ra_c are computed for different values of Le and presented in Table 6.3. It is perceived from this table that Ra_c is increasing slightly with an increase

in Lewis number, whereas α_c is decreasing when $\beta = 0$. This signifies that Le is mild on the stability of the flow. This is because an increment in the values Le directs rising in the Brownian diffusion of nanoparticles which supports the power of disturbance in the system. Thus, the effect of rising Le is to postpone the convection. Also, it is observed that Ra_c increases and α_c decreases with the increased values of β.

Fig. 6.9 presents the influence of the modified diffusivity ratio N_A on the instability boundaries for $Pr = 7$, $Rn = 15$, $\epsilon = 0.6$, $Le = 500$ and $N_B = 0.02$. It is noticed from Fig. 6.9(a) that there is no visible effect of the modified diffusivity ratio on Ra_c. Further, the influence of N_A on α_c is also negligible as displayed in Fig. 6.9(b). This is may be due to the restriction of N_A values which does not variate much Brownian motion and thermophoresis of nanoparticles to support the disturbance in the present study.

The influence of modified particle density ratio N_B on Ra_c and α_c is shown in Fig. 6.10 for $Pr = 7$, $Rn = 15$, $\epsilon = 0.6$, $Le = 500$ and $N_A = 8$. It is seen from Fig. 6.10(a) that the influence of modified particle density ratio N_B on the critical Rayleigh number Ra_c is almost negligible. In addition, the effect of N_B on α_c is also negligible as shown in Fig. 6.10(b). Therefore, N_B does not affect the stability. This is because the term N_B is containing as a function of $\frac{N_B}{Le}$ in the governing equation and which is very small, of order 10^{-3} to 10^{-6} pointing to almost no contribution of the nanoparticle flux in the thermal energy conversation.

To focus more attention on the instability mechanism due to the effect of nanofluid parameters, we plotted the variations in the growth rate at the neighbourhood ($Ra_c = Ra_c(1 + 0.01)$) in the Fig. 6.11 for different values of Le, N_A and N_B. From Fig. 6.11(a), it is seen that there is a small variation of the growth rate for increasing values of Le but no variation for increasing values of N_A and N_B as plotted in Fig. 6.11(b) and 6.11(c), respectively. Also, from Figs. 6.11(a)-6.11(c), it is observed that the disturbances of the growth rate are decreasing with an increase in permeability.

The influence of Lewis number on the instability boundary curve in Fig. 6.8 is more enlightened by means of the plots of eigenfunctions at the critical position and Fig. 6.12 presents the eigenfunctions for $Le = 100$ and $Le = 500$ at $Da = 0.1$, $Pr = 7$, $Rn = 15$, $N_A = 8$, $N_B = 0.02$ and $\epsilon = 0.6$ at the critical level. From this figure, it is noted that the magnitude of the eigenfunctions for the velocities are more than the magnitude of the eigenfunctions for the temperature and volume fraction. It is observed from the Figs. 6.12(a) and 6.12(b) that magnitude of the eigenfunctions of the velocities disturbances in the x-direction and y-direction decreases when Lewis number increases. But, the variation of the

magnitude of the eigenfunctions of temperature and volume fraction are almost negligible due to the effect of Le, as depicted in Figs. 6.12(c) and 6.12(d).

Apart from the variations of Ra_c and α_c with different parameters, to understand the dynamics of the flow field and variation in the pattern of temperature and volume fraction the contour plots for streamlines, isotherms and isonanoconcentration at critical level are drawn and illustrated in Figs. 6.13 - 6.16 with varing values of permeability parameter (Da), Lewis number (Le), modified diffusivity ratio (N_A) and modified particle density increment (N_B) for fixed values of the other parameters $Rn = 15$, $Pr = 7$, $\epsilon = 0.6$. In the case of streamline contour, the positive contours are associated with anti-clockwise rotation, whereas, the negative contours are associated with clockwise rotation and for the case isotherms and isonanoconcentrations contour, solid lines indicate the positive contours while dashed line exhibits the negative contours. In the following, we have discussed the flow dynamics in below.

Fig. 6.13 exhibits the streamlines, isotherms and isonanoconcentrations for various values of the Darcy number for fixed values of $N_A = 8$, $N_B = 0.02$ and $Le = 500$ over one period. From Figs. 6.13(a) - 6.13(c), it is observed that the flow is mainly controlled by two asymmetric cells, where one cell (primary cell) is rotating clockwise direction and the other cell (secondary cell) is rotating anticlockwise direction. The shape of the inner cells of this bi-cellular structure is changing with an increase in the Darcy number. Further, it is noticed that the primary cell pushes the secondary cell in upwards direction in the vertical channel as the value of the Darcy number increase. The pattern of the isotherms are almost the same and spread the whole channel over a period for all values of Da shown in Figs. 6.13(d) - 6.13(f). This is because the transfer of the temperature receives mainly by diffusion, indicating to disturbances into flow configuration. The isonanoconcentration lines for the flow in a vertical channel are depicted in Figs. 6.13(g) - 6.13(i) and shows a two-cell structure with each cell on either side to the centre of the channel. These figures reveal that the isonanoconcentration lines are more concentrated in the centre of the channel over a period for different values of permeability. Further, it is noticed that the size of the convective cells reduce as the Darcy number rises.

The influence of Lewis number in the pattern of streamlines, isotherms and isonanoconcentrations for $Da = 10^{-1}$, $N_A = 8$ and $N_B = 0.02$ is plotted in Fig. 6.14 over a period. From Figs. 6.14(a) - 6.14(c), it is noticed that the flow is controlled by bi-cellular patterns where one cell (primary cell) has full structure but another one (secondary cell) has half structure. It is noticed that the streamline pattern looks like moving downwards slowly the vertical channel as the value of Le enhances due to small variation of critical eigenvalue value. The

shape of the inner cells in each of the bi-cellular structure is changed with increasing the potency of the Lewis number. The isotherms of the flow are portrayed in Figs. 6.14(d) - 6.14(f). Here also the isotherms are looking like shifting downwards slowly the vertical channel as Le increases. The isotherms occupy the large part of the channel. The variation of the isonanoconcentration contours is plotted in Figs. 6.14(g)-6.14(i) and observed that patterns are dense at the centre of the channel. The magnitude of the stream function, isotherms and isonanoconcentration reduce indicating the system becoming more stable with augmenting value in the Lewis number.

The deviation of streamlines, isotherms and isonanoconcentrations at the critical level for various values of the modified diffusivity ratio N_{A} and modified particle density increment N_{B} in the Figs. 6.15 and 6.16, respectively, over a period. From Figs. 6.15 and 6.16, it is cleared that the patterns of streamlines, isotherms and isonanoconcentrations are looking like same, as we have seen in Figs. 6.13 and 6.14. Further, it is noticeable that there are no changes in shape or size or shiftiness of cells of the lines with the rising the effect of both the parameters. This is because the variation of N_{A} and N_{B} does not affect on the onset of convection as we have disclosed in Figs. 6.9 and 6.10.

Table 6.1: Convergence of the least stable eigenvalue by Chebyshev collocation method. Here $Da = 1$, $Pr = 7$, $Ra = 100$, $Rn = 15$, $\epsilon = 0.6$, $N_{\mathrm{A}} = 8$, $N_{\mathrm{B}} = 0.2$, $Le = 500$, $\alpha = 1$, $\beta = 0$.

N	Least stable eigenvalue
30	7.254272433915-0.116633842910i
35	7.254500877193-0.117015950398i
40	7.254526715361-0.117063301305i
45	7.254526825573-0.117066975141i
50	7.254526952722-0.117067639985i
51	7.254526831391-0.117067549380i
55	7.254526857357-0.117067503970i
60	7.254526835407-0.117067533337i

Table 6.2: Critical values of α and Ra for different values of Rn and Da at $Le = 500$, $\epsilon = 0.6$, $Pr = 7$, $N_{\mathrm{A}} = 8$ and $N_{\mathrm{B}} = 0.02$.

Da	Rn	α_{c}	Ra_{c}
0.1	15	0.9631	1430.805
	30	0.9542	1427.007
	60	1.6700	587.623
1	15	1.3424	3037.209
	30	1.3406	3032.995
	60	1.3369	3024.707
10	15	1.3819	25253.439
	30	1.3821	25248.012
	60	1.3817	25237.248

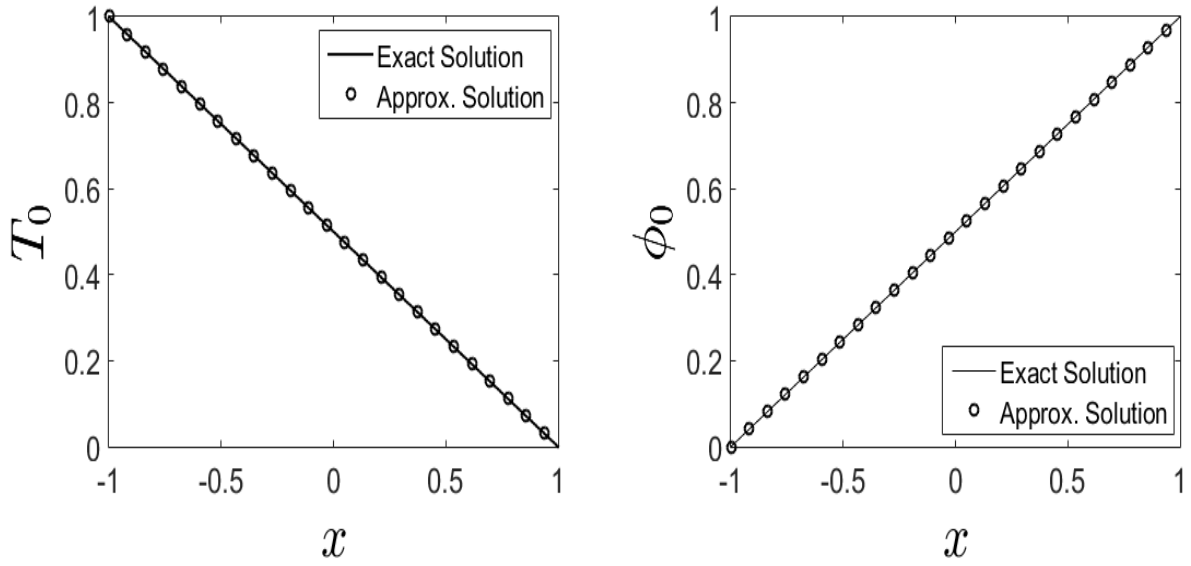

(a) Basic temperature profile

(b) Basic volume fraction profile

Figure 6.2: Comparision of basic temperature and volume fraction profiles.

Table 6.3: Critical values of α and Ra for different values of Le and β at $Rn = 15$, $\epsilon = 0.6$, $Pr = 7$, $N_{\mathrm{A}} = 8$ and $N_{\mathrm{B}} = 0.02$.

Da	β	Le	α_{c}	Ra_{c}
0.1	0	100	0.9645	1418.198
	0	300	0.9632	1428.58
	0	500	0.9631	1430.805
	0.5	500	0.902	1649.284
	1	500	0.7273	2915.056
1	0	100	1.343	3030.343
	0	300	1.3425	3035.799
	0	500	1.3424	3037.209
	0.5	500	1.2951	3263.854
	1	500	1.1423	4203.374
10	0	100	1.3824	25247.08
	0	300	1.3823	25252.12
	0	500	1.3819	25253.44
	0.5	500	1.3361	27021.49
	1	500	1.1894	34195.04

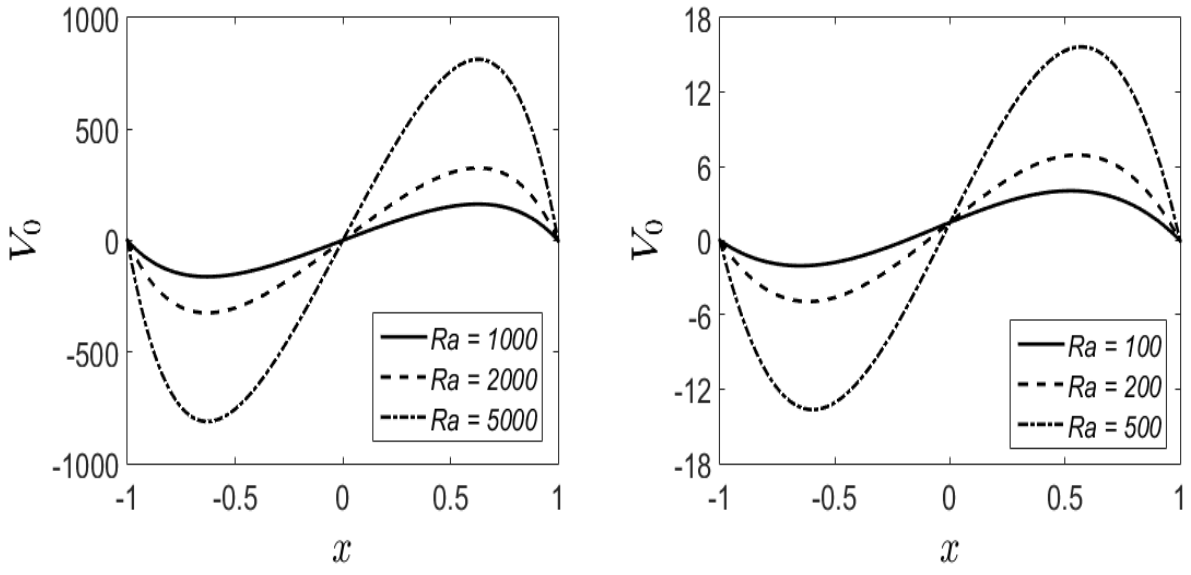

(a) $Da = 10^{-1}$

(b) $Da = 1$

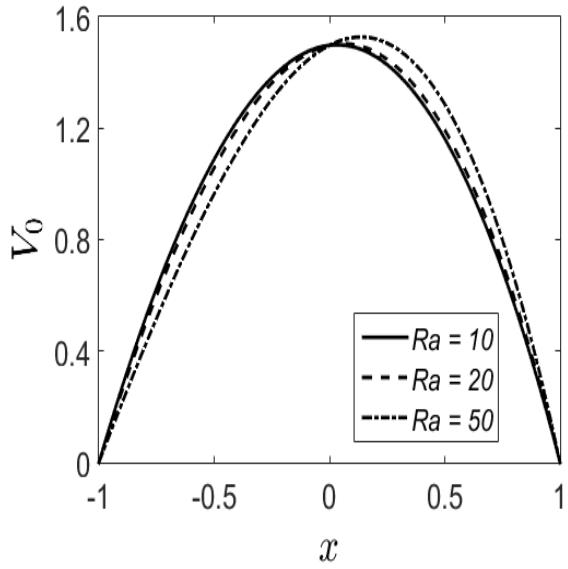

(c) $Da = 10$

Figure 6.3: Basic velocity profiles when $DaRa = 100, 200$ and 500 at $Rn = 2$.

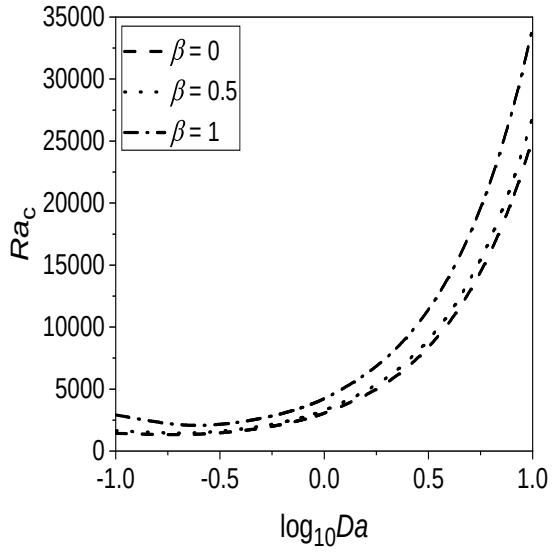

Figure 6.4: Instabilities boundaries in $(\log_{10}Da, Ra_{\rm c})$-plane for different values of β, when $Pr = 7, Rn = 15, \epsilon = 0.6, Le = 500, N_{\rm A} = 8$ and $N_{\rm B} = 0.02$.

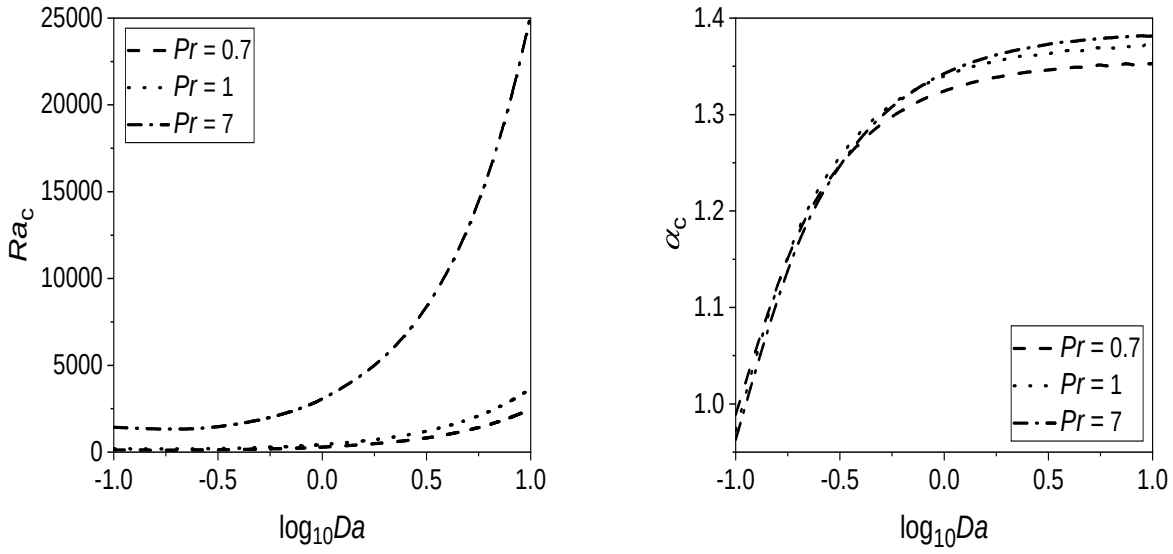

Figure 6.5: Instabilities boundaries in (a) $((\log_{10}Da, Ra_{\rm c}), Ra_{\rm c})$-plane and (b) $((\log_{10}Da, \alpha_{\rm c})$-plane for different values of Pr when $Rn = 15, \epsilon = 0.6, Le = 500, N_{\rm A} = 8$ and $N_{\rm B} = 0.02$.

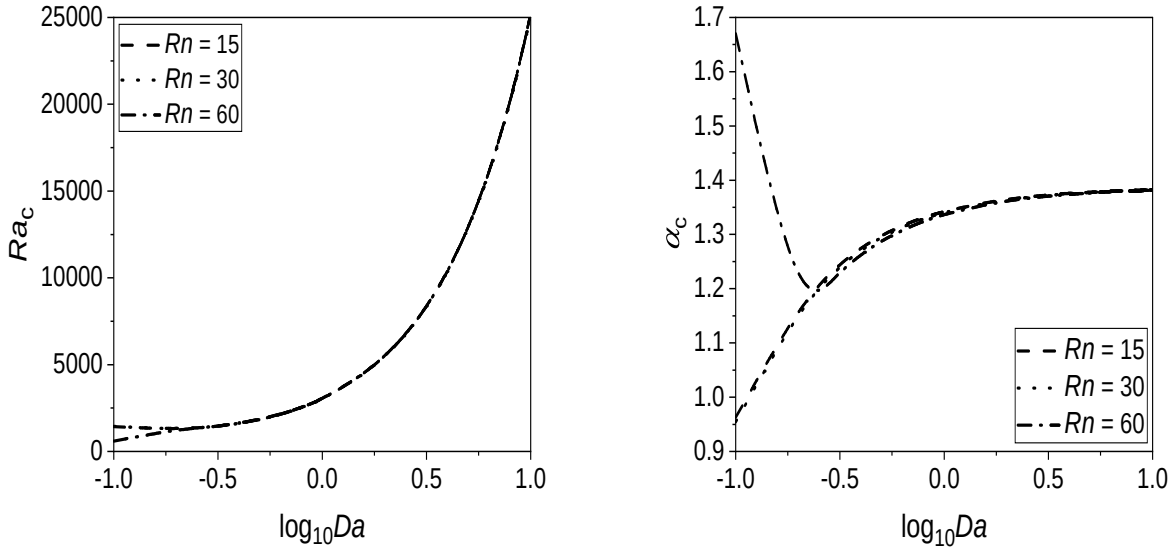

(a) (b)

Figure 6.6: Instabilities boundaries in (a) $((\log_{10}Da, Ra_{\rm c})$-plane and (b) $(\log_{10}Da, \alpha_{\rm c})$-plane for different values of Rn when $Pr = 7, \epsilon = 0.6, Le = 500, N_{\rm A} = 8$ and $N_{\rm B} = 0.02$.

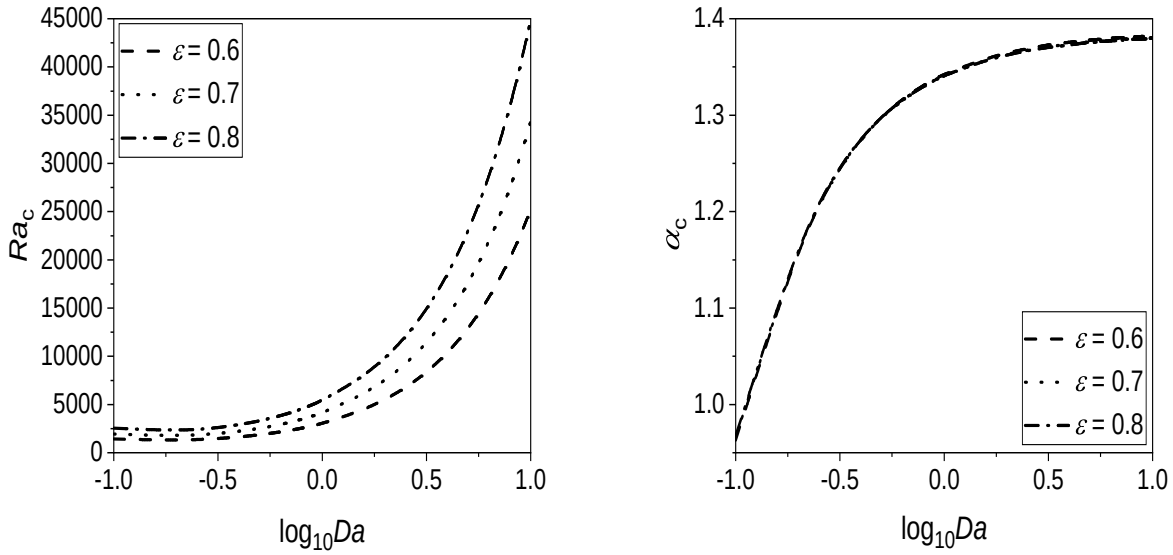

(a) (b)

Figure 6.7: Instabilities boundaries in (a) $(\log_{10}Da, Ra_{\rm c})$-plane and (b) $(\log_{10}Da, \alpha_{\rm c})$-plane for different values of ϵ when $Pr = 7, Rn = 15, Le = 500, N_{\rm A} = 8$ and $N_{\rm B} = 0.02$.

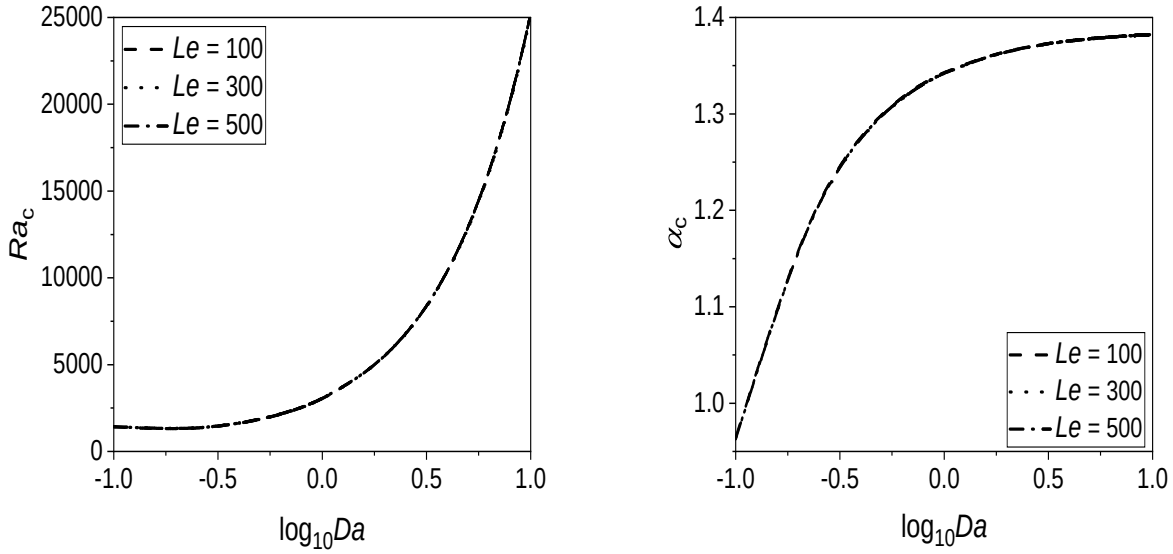

(a) (b)

Figure 6.8: Instabilities boundaries in (a) $(\log_{10}Da, Ra_c)$-plane and (b) $(\log_{10}Da, \alpha_c)$-plane for different values of Le when $Pr = 7, Rn = 15, \epsilon = 0.6, N_A = 8$ and $N_B = 0.02$.

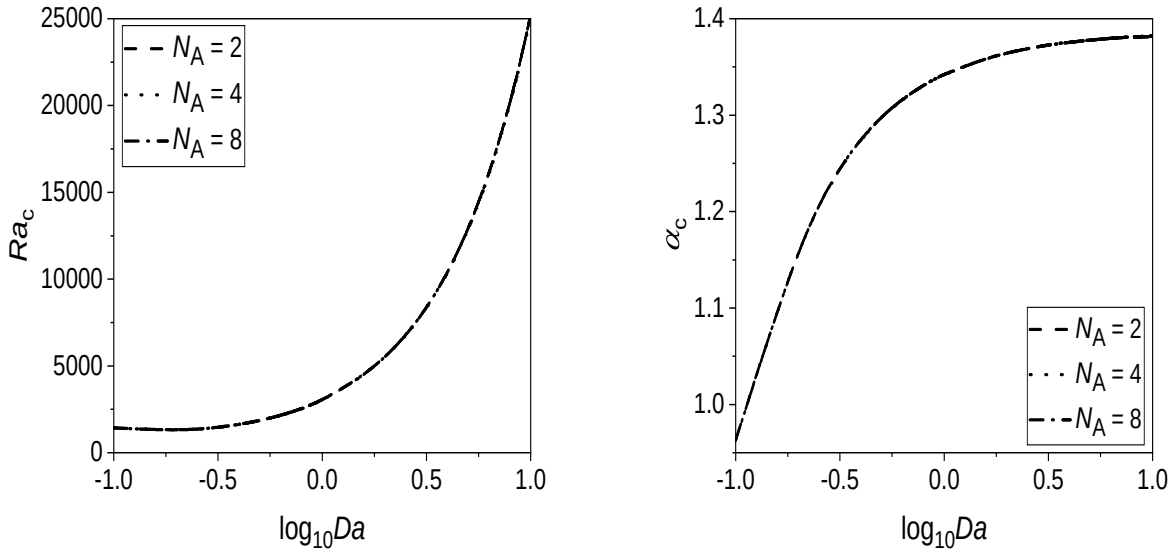

(a) (b)

Figure 6.9: Instabilities boundaries in (a) $(\log_{10}Da, Ra_c)$-plane and (b) $(\log_{10}Da, \alpha_c)$-plane for different values of N_A when $Pr = 7, Rn = 15, \epsilon = 0.6, Le = 500$ and $N_B = 0.02$.

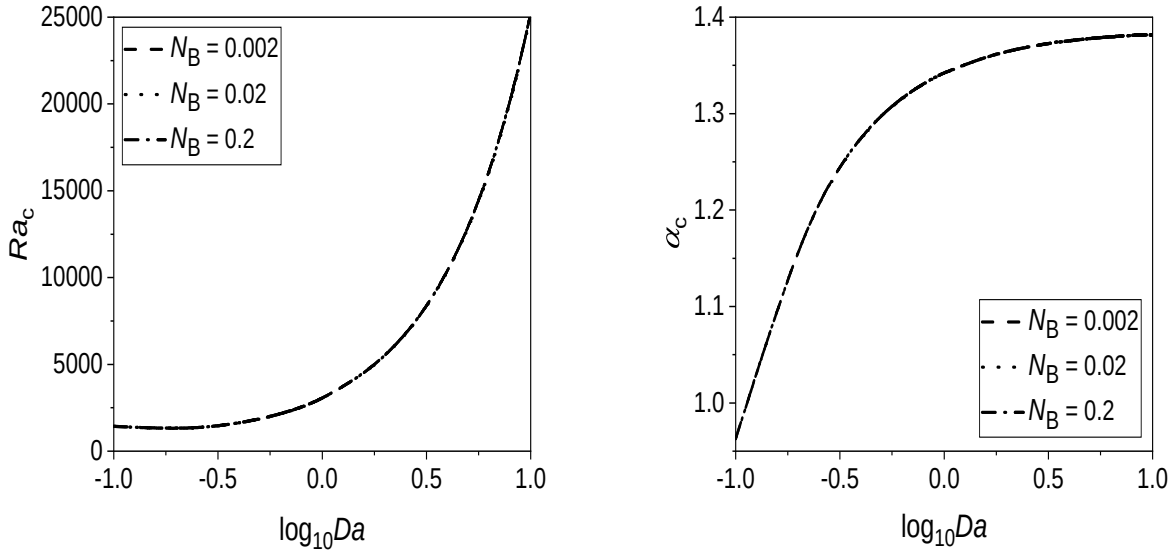

(a) (b)

Figure 6.10: Instabilities boundaries in (a) $(\log_{10}Da, Ra_c)$-plane and (b) $(\log_{10}Da, \alpha_c)$-plane for different values of N_B when $Pr = 7, Rn = 15, \epsilon = 0.6, Le = 500$ and $N_A = 8$.

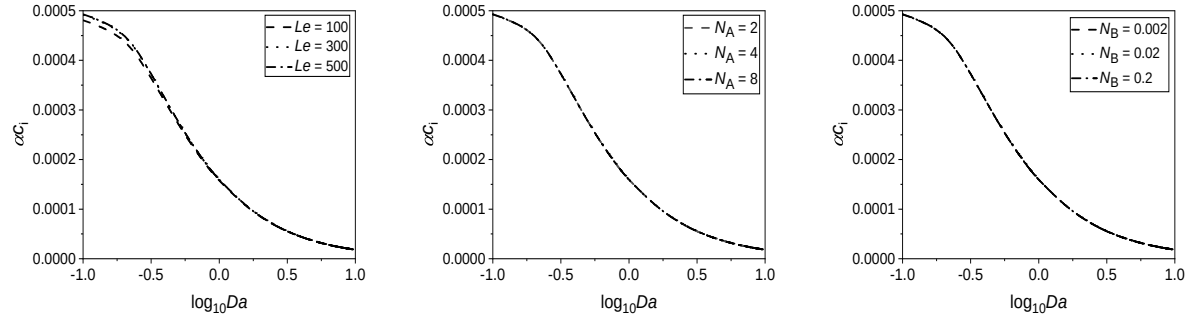

(a) (b) (c)

Figure 6.11: Growth rate (αc_i) as a function of Da for (a) Le (at $N_A = 8$ and $N_B = 0.02$), (b) N_A (at $Le = 500$ and $N_B = 0.02$) and (c) N_B (at $Le = 500$ and $N_A = 8$) when $Pr = 7$, $Rn = 15$ and $\epsilon = 0.6$.

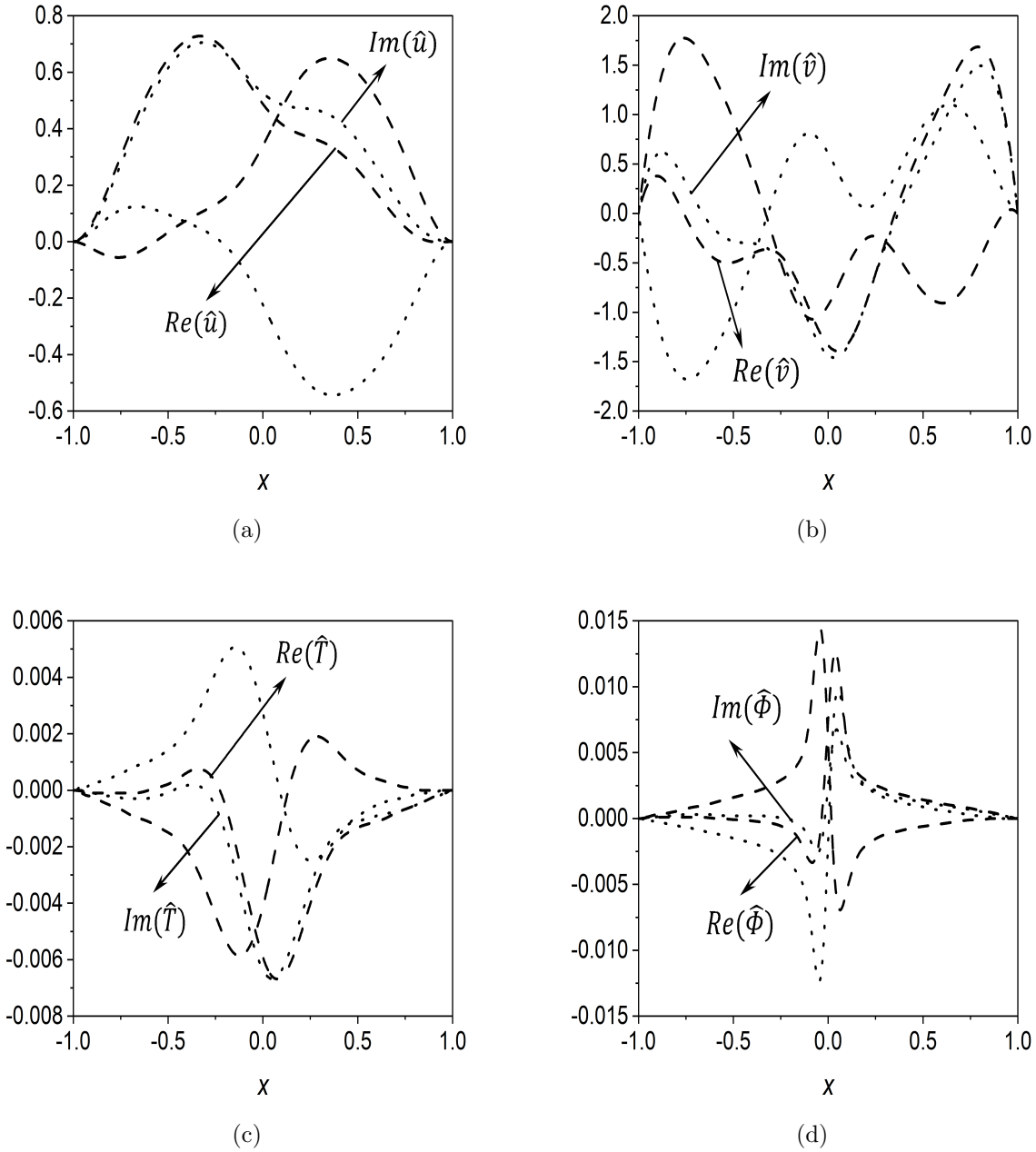

Figure 6.12: Eigenfunctions of (a) $\hat{u}$, (b) $\hat{v}$, (c) $\hat{T}$ and (d) $\hat{\phi}$ for $Le = 100$ ('–'), and $Le = 500$ ('$\cdots$') when $Pr = 7$, $Da = 10^{-1}$, $Rn = 15$, $\epsilon = 0.6$, $N_{\mathrm{A}} = 8$ and $N_{\mathrm{B}} = 0.02$.

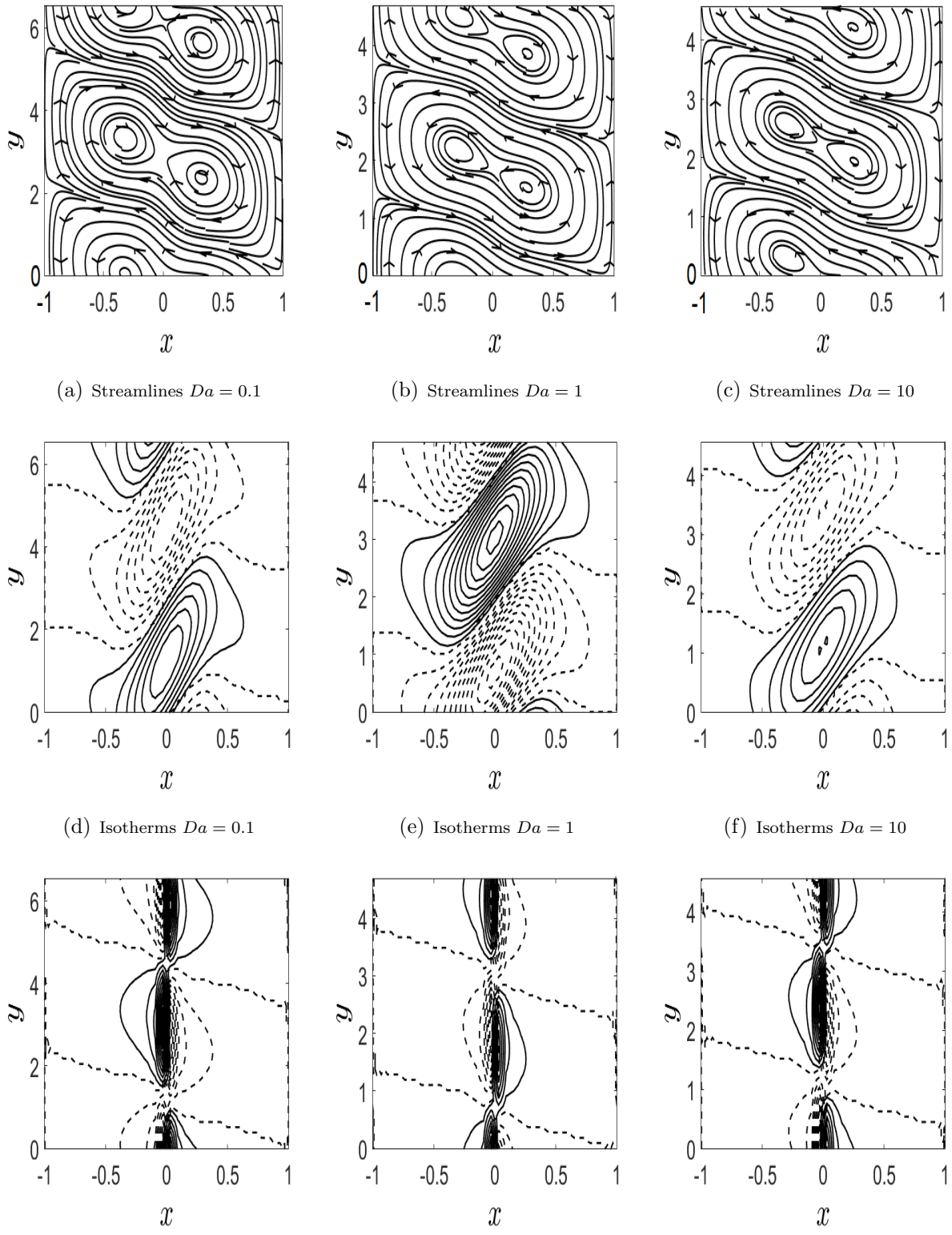

(a) Streamlines $Da = 0.1$ (b) Streamlines $Da = 1$ (c) Streamlines $Da = 10$

(d) Isotherms $Da = 0.1$ (e) Isotherms $Da = 1$ (f) Isotherms $Da = 10$

(g) Isonanoconcentrations $Da = 0.1$ (h) Isonanoconcentrations $Da = 1$ (i) Isonanoconcentrations $Da = 10$

Figure 6.13: The disturbance of streamlines ((a) to (c)), isotherms ((d) to (f)) and isonanoconcentrations ((g) to (i)) for various values of Darcy number (Da) over one period when $Pr = 7$, $Rn = 15$, $\epsilon = 0.6$, $Le = 500$, $N_{\mathrm{A}} = 8$ and $N_{\mathrm{B}} = 0.02$.

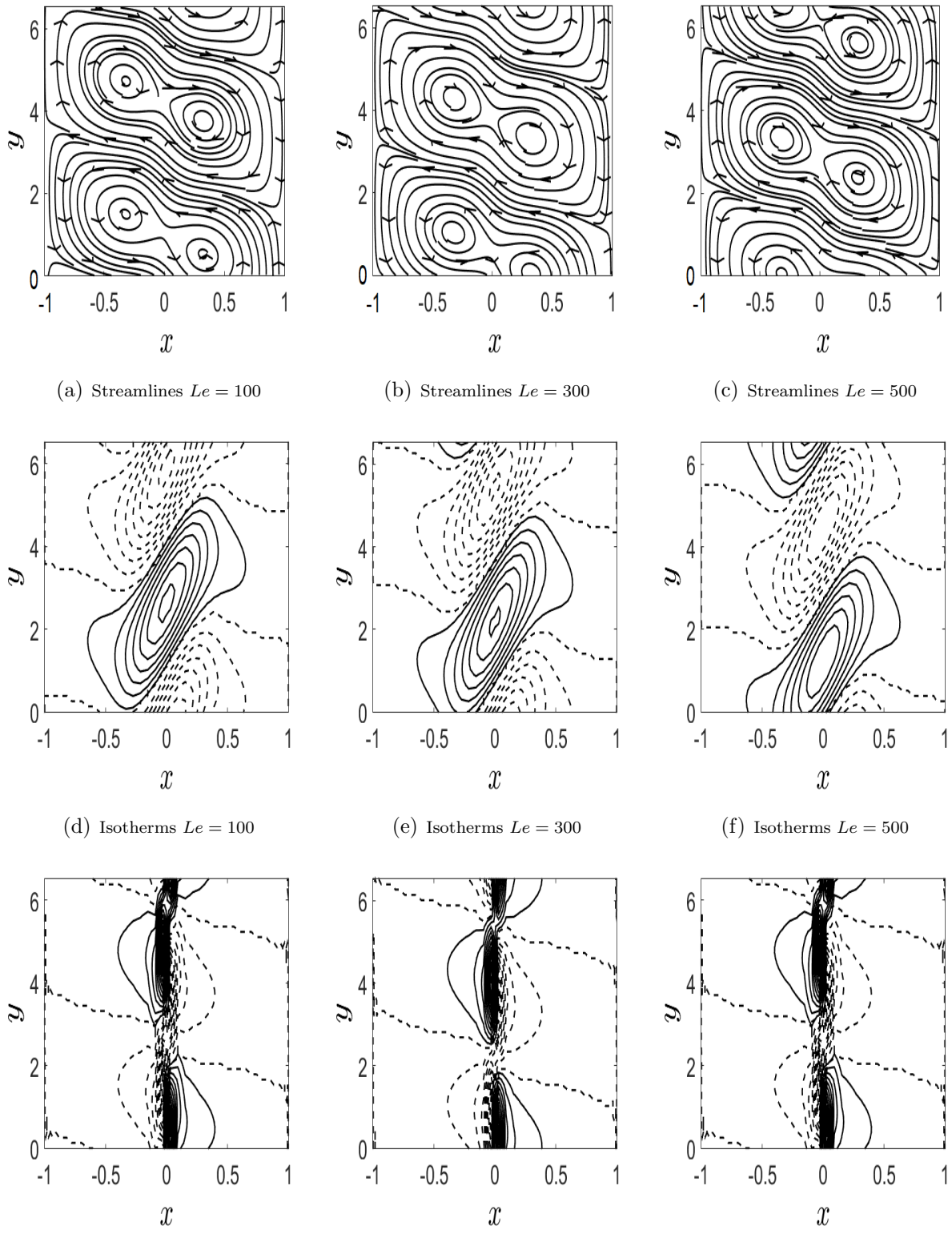

(a) Streamlines $Le = 100$ (b) Streamlines $Le = 300$ (c) Streamlines $Le = 500$

(d) Isotherms $Le = 100$ (e) Isotherms $Le = 300$ (f) Isotherms $Le = 500$

(g) Isonanoconcentrations $Le = 100$ (h) Isonanoconcentrations $Le = 300$ (i) Isonanoconcentrations $Le = 500$

Figure 6.14: The disturbance of streamlines ((a) to (c)), isotherms ((d) to (f)) and isonanoconcentrations ((g) to (i)) for various values of Lewis number (Le) over one period when $Pr = 7$, $Rn = 15$, $\epsilon = 0.6$, $Da = 0.1$, $N_{\mathrm{A}} = 8$ and $N_{\mathrm{B}} = 0.02$.

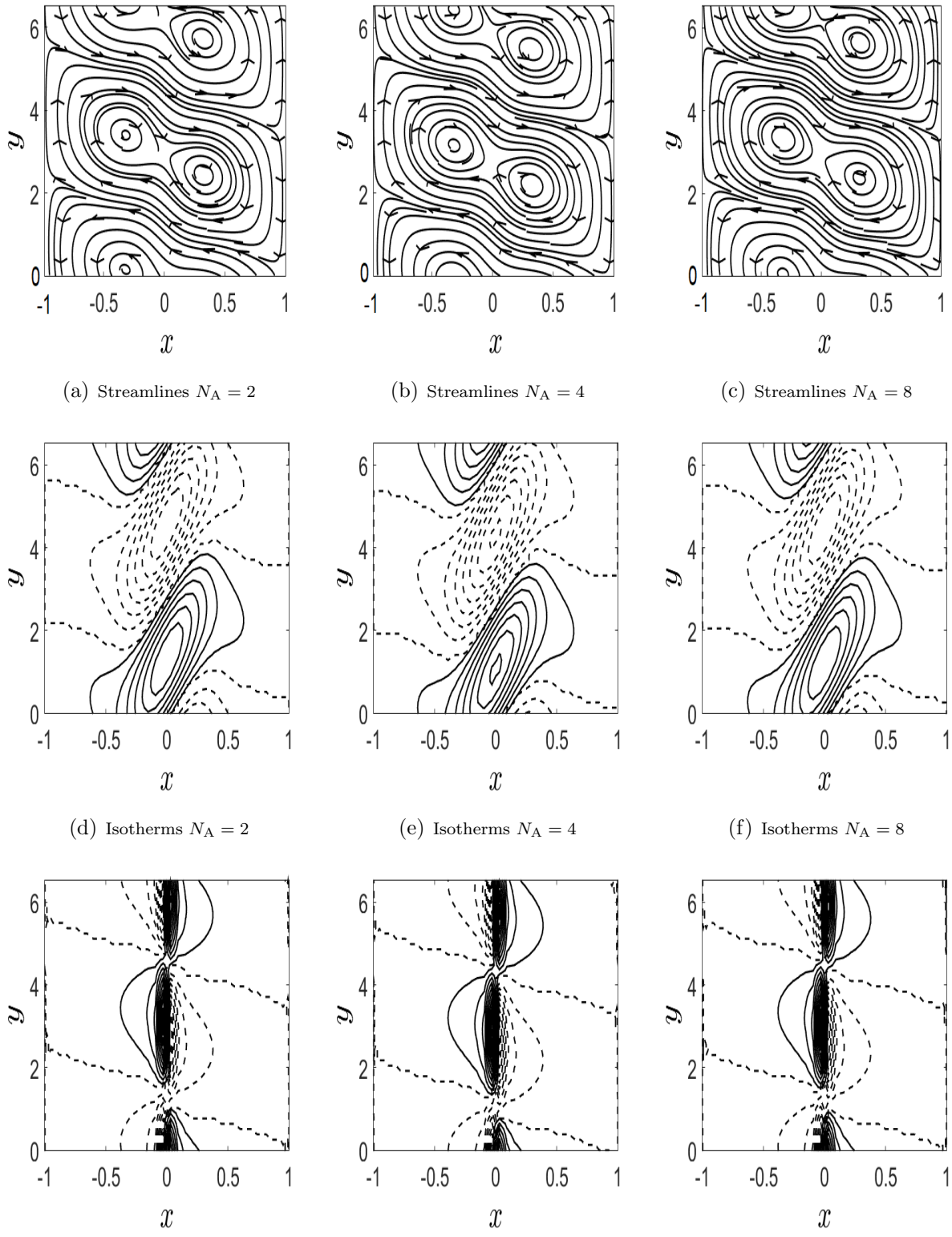

(a) Streamlines $N_{\mathrm{A}} = 2$ (b) Streamlines $N_{\mathrm{A}} = 4$ (c) Streamlines $N_{\mathrm{A}} = 8$

(d) Isotherms $N_{\mathrm{A}} = 2$ (e) Isotherms $N_{\mathrm{A}} = 4$ (f) Isotherms $N_{\mathrm{A}} = 8$

(g) Isonanoconcentrations $N_{\mathrm{A}} = 2$ (h) Isonanoconcentrations $N_{\mathrm{A}} = 4$ (i) Isonanoconcentrations $N_{\mathrm{A}} = 8$

Figure 6.15: The disturbance of streamlines ((a) to (c)), isotherms ((d) to (f)) and isonanoconcentrations ((g) to (i)) for various values of modified diffusivity ratio (N_{A}) over one period when $Pr = 7$, $Rn = 15$, $\epsilon = 0.6$, $Da = 0.1$, $Le = 500$ and $N_{\mathrm{B}} = 0.02$.

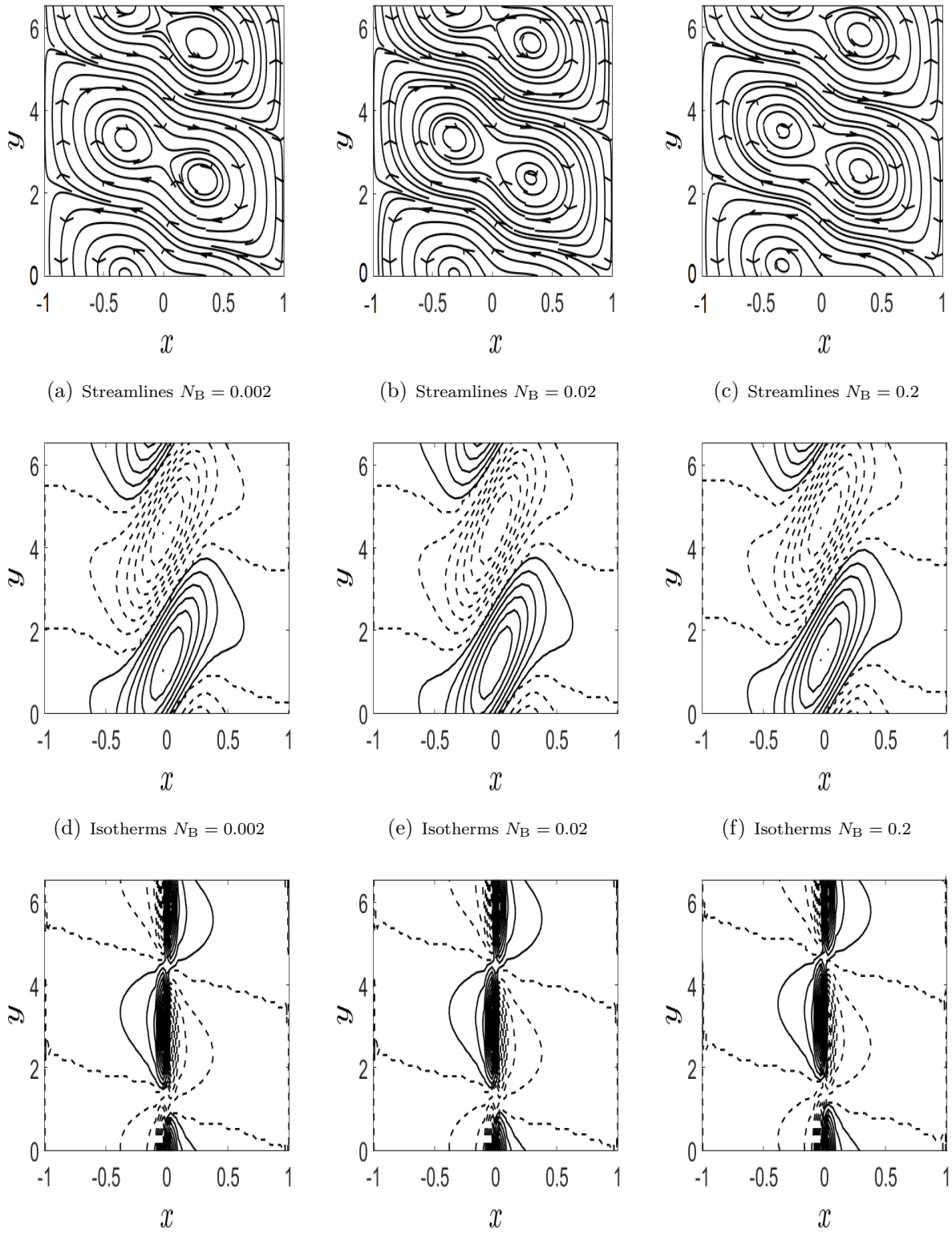

(a) Streamlines $N_{\mathrm{B}} = 0.002$ (b) Streamlines $N_{\mathrm{B}} = 0.02$ (c) Streamlines $N_{\mathrm{B}} = 0.2$

(d) Isotherms $N_{\mathrm{B}} = 0.002$ (e) Isotherms $N_{\mathrm{B}} = 0.02$ (f) Isotherms $N_{\mathrm{B}} = 0.2$

(g) Isonanoconcentrations $N_{\mathrm{B}} = 0.002$ (h) Isonanoconcentrations $N_{\mathrm{B}} = 0.02$ (i) Isonanoconcentrations $N_{\mathrm{B}} = 0.2$

Figure 6.16: The disturbance of streamlines ((a) to (c)), isotherms ((d) to (f)) and isonanoconcentrations ((g) to (i)) for various values of modified particle density increment (N_{B}) over one period when $Pr = 7$, $Rn = 15$, $\epsilon = 0.6$, $Da = 0.1$, $Le = 500$ and $N_{\mathrm{A}} = 8$.

6.7 Conclusions

In this study, we have investigated the instability mechanism of the nanofluid flow in a vertical channel which is filled with a porous medium. The eigenvalue problem solved numerically using the spectral method. The main observations from the obtained results are:

- The critical Rayleigh number increases when the values of Pr, Da, ϵ and Le increase, it decreases with rising the value of Rn, it remains same for the enhancing values of N_{A} and N_{B}.
- The effects of increasing Pr, Da, ϵ and Le delay the onset of convection, Rn advances the convective motion while N_{A} and N_{B} do not change the stability of the system.
- The dimension of the convective cells reduces on enhancing Da, increases on rising Le, duals character on gaining Pr, Rn and ϵ, while remains same on growing N_{A} and N_{B}.

Chapter 7

Linear stability of double diffusive convection in a vertical channel filled with nanofluid saturated porous medium in the presence of transverse magnetic field [1]

7.1 Introduction

The study of double-diffusive convection in a porous medium is an active research area due to its many applications in the fields of chemical science, engineering and nuclear industries, food processing, geophysics, bio-engineering and cancer therapy, movement of biological fluid, oceanography. The prospect of heat transfer in the medium cannot narrate exclusively in situations involving one or more solute fields. In such conditions, both heat and mass transfers are needed to be considered. The buoyancy forces are induced by the combined effects of temperature and concentration differences in a saturated porous medium.

In recent years, several investigators have analyzed the nanofluid flow and heat transfer problems by including in the presence of transverse of magnetic field when the fluid is electrically conducting. In addition, there has been a renewed interest in studying MHD flow and heat transfer in porous media due to the effect of magnetic fields on flow control and on the performance of many systems using electrically conducting fluids. The study of MHD flow for an electrically conducting nanofluid in channels has important applications in

[1] Communicated in "***Journal of Porous Media***"

many engineering problems crystal growth in fluids, purification of molten metals, the metal casting, nuclear reactor cooling, microelectronic devices and geothermal energy extractions. Although the effect of magnetic field on the flow of the nanofluid saturated porous medium is important, very little attention has been given in literature [7, 8]. Only few studies have been reported to analyze the stability of the fluid flow in a channel in the presence of transverse magnetic filed. Hudoba and Molokov [59] studied the effect of internal heat sources and a transverse magnetic field of a buoyancy convective flow in a vertical channel. The interesting phenomenon of elevator convection modes in vertical ducts with imposed magnetic field and mean flow directed downwards was investigated by Lin and Zikanov [68].

The majority of the works reported deal with the stability in a horizontal porous layer saturated by nanofluid. As per the author's knowledge, no work has been done in a vertical channel filled with nanofluid saturated porous medium. Further, the stability characteristics of double-diffusive convective nanofluid saturated porous medium in a vertical channel with the effect a transverse magnetic field has not been studied.

In this chapter, we study the effect of transverse magnetic field in a vertical channel filled with saturated porous medium for double diffusion convection for Darcy-Brinkman model.

7.2 Mathematical Formulation

Consider an incompressible, unsteady and double diffusive nanofluid flow in a vertical porous channel of width $2L$ bounded by two impermeable and perfectly thermally conducting walls as shown in Fig. 6.1. Both the left wall ($x = -L$) and right wall ($x = L$) exchange heat between the internal and external fluid environment, with the reference temperatures T_1 and T_2, respectively, with the former being the greater. The volume fraction at the left and right wall are taken as ϕ_2 and ϕ_1 and the corresponding solute concentrations are as C_1 and C_2, respectively. A uniform magnetic field $\mathbf{B_0} = B\hat{\mathbf{e}}_\mathbf{x}$, where B is the strength of the magnetic field, is applied normal to the channel. The magnetic Reynolds number is assumed to be small so that the induced magnetic field can be neglected in comparison with the applied magnetic field. Hence, the governing equations for double diffusive convection can be written as

$$\nabla \cdot \mathbf{u} = 0, \tag{7.1}$$

$$\rho_{\mathrm{f}}\left(\frac{1}{\epsilon}\frac{\partial \mathbf{u}}{\partial t}+\frac{1}{\epsilon^2}(\mathbf{u}\cdot\nabla)\mathbf{u}\right)=-\nabla p+\tilde{\mu}\nabla^2\mathbf{u}-\frac{\mu}{K}\mathbf{u}+\mathbf{j}\times\mathbf{B_0}$$
$$+\left\{\phi\rho_{\mathrm{p}}+(1-\phi)\rho_{\mathrm{f}}\left[1-\beta_{\mathrm{T}}(T-T_1)-\beta_{\mathrm{C}}(C-C_1)\right]\right\}\mathbf{g}, \tag{7.2}$$

$$(\rho c)_{\mathrm{m}}\frac{\partial T}{\partial t}+(\rho c)_{\mathrm{f}}\mathbf{u}\cdot\nabla T=k_{\mathrm{m}}\nabla^2 T+\epsilon(\rho c)_{\mathrm{p}}\left[D_{\mathrm{B}}\nabla\phi\cdot\nabla T+\frac{D_{\mathrm{T}}}{T_2}\nabla T\cdot\nabla T\right]+(\rho c)_{\mathrm{f}}D_{\mathrm{TC}}\nabla^2 C, \tag{7.3}$$

$$\frac{\partial\phi}{\partial t}+\frac{1}{\epsilon}\mathbf{u}\cdot\nabla\phi=D_{\mathrm{B}}\nabla^2\phi+\frac{D_{\mathrm{T}}}{T_2}\nabla^2 T, \tag{7.4}$$

$$\frac{\partial C}{\partial t}+\frac{1}{\epsilon}\mathbf{u}\cdot\nabla C=D_{\mathrm{S}}\nabla^2 C+D_{\mathrm{CT}}\nabla^2 T, \tag{7.5}$$

where D_{S} is the solutal diffusivity for the porous medium, D_{TC} is a diffusivity of Dufour type and D_{CT} is a diffusivity of Soret. The second last term in the momentum equation is due to imposition of a transverse magnetic field, where $\mathbf{B_0}=B\hat{\mathbf{e}}_{\mathbf{x}}$ is the magnetic induction field and $\mathbf{j}$ is the current. The relation between them is given by

$$\mathbf{j}\times\mathbf{B_0}=\sigma_1(\mathbf{u}\times B\hat{\mathbf{e}}_{\mathbf{x}})\times B\hat{\mathbf{e}}_{\mathbf{x}}, \tag{7.6}$$

where σ_1 is the electric conductivity.

The corresponding boundary conditions are written as

$$x=-L:\ \mathbf{u}=0,\ T=T_1,\ \phi=\phi_2,\ C=C_1, \tag{7.7a}$$

$$x=L:\ \mathbf{u}=0,\ T=T_2,\ \phi=\phi_1,\ C=C_2. \tag{7.7b}$$

Substituting the non-dimensional variables given in Eq. (6.6) in the governing Eqs. (7.1)-(7.5), the boundary conditions Eq. (7.7) and dropping asterisk, we get

$$\nabla\cdot\mathbf{u}=0, \tag{7.8}$$

$$\frac{1}{Va}\left[\frac{1}{\sigma}\frac{\partial\mathbf{u}}{\partial t}+\frac{1}{\epsilon}(\mathbf{u}\cdot\nabla)\mathbf{u}\right]=-\nabla p+\Lambda Da\nabla^2\mathbf{u}-\mathbf{u}+DaHa^2(\mathbf{u}\times\hat{\mathbf{e}}_{\mathbf{x}})\times\hat{\mathbf{e}}_{\mathbf{x}}$$
$$+RaT\hat{\mathbf{e}}_{\mathbf{y}}-Rn\phi\hat{\mathbf{e}}_{\mathbf{y}}+\frac{Rs}{Ln}C\hat{\mathbf{e}}_{\mathbf{y}}-Rm\hat{\mathbf{e}}_{\mathbf{y}}, \tag{7.9}$$

$$\frac{\partial T}{\partial t}+\mathbf{u}\cdot\nabla T=\nabla^2 T+\frac{N_{\mathrm{B}}}{Le}\nabla\phi\cdot\nabla T+\frac{N_{\mathrm{A}}N_{\mathrm{B}}}{Le}\nabla T\cdot\nabla T+D_{\mathrm{f}}\nabla^2 C, \tag{7.10}$$

$$\frac{1}{\sigma}\frac{\partial\phi}{\partial t}+\frac{1}{\epsilon}\mathbf{u}\cdot\nabla\phi=\frac{1}{Le}\nabla^2\phi+\frac{N_{\mathrm{A}}}{Le}\nabla^2 T, \tag{7.11}$$

$$\frac{1}{\sigma}\frac{\partial C}{\partial t}+\frac{1}{\epsilon}\mathbf{u}\cdot\nabla C=\frac{1}{Ln}\nabla^2 C+Sr\nabla^2 T, \tag{7.12}$$

$$x = -1: \ \mathbf{u} = 0, \ T = 0, \ \phi = 1, \ C = 0, \tag{7.13a}$$

$$x = 1: \ \mathbf{u} = 0, \ T = 1, \ \phi = 0, \ C = 1. \tag{7.13b}$$

where $Ha = BL\sqrt{\frac{\sigma_1}{\mu}}$ is the magnetic parameter (Hartmann number), $Rs = \frac{\rho_{\mathrm{f}} g \beta_{\mathrm{C}} KL(C_2 - C_1)}{\mu D_{\mathrm{S}}}$ is the familiar solutal Rayleigh number, $Ln = \frac{\alpha_{\mathrm{m}}}{D_{\mathrm{S}}}$ is the thermo-solutal Lewis number. $D_{\mathrm{f}} = \frac{D_{\mathrm{TC}}(C_2 - C_1)}{\alpha_{\mathrm{m}}(T_2 - T_1)}$ is the Dufour parameter and $Sr = \frac{D_{\mathrm{CT}}(T_2 - T_1)}{\alpha_{\mathrm{m}}(C_2 - C_1)}$ is the Soret parameter. To avoid too many parameter studies, we have taken the viscosity ratio $\Lambda = 1$ and thermal capacity ratio $\sigma = 1$.

7.3 Basic state solution

The flow in the basic state is assumed as steady, unidirectional and fully developed and is defined as $\mathbf{u}_0 = (0, V_0(x), 0)$ is the basic velocity vector, $T_0 = T_0(x)$ is the basic temperature, $\phi_0 = \phi_0(x)$ is the basic volume fraction, $C_0 = C_0(x)$ is the basic concentration and $p_0 = p_0(y)$ is the basic pressure. With these assumptions, the governing Eqs. (7.8)-(7.12) are reduced into the following set of coupled ordinary differential equations:

$$\frac{d^2 V_0}{dx^2} - \left(\frac{1}{Da} + Ha^2\right) V_0 = \frac{1}{Da}\frac{dp_0}{dy} - \frac{Ra}{Da} T_0 + \frac{Rn}{Da}\phi_0 - \frac{Rs}{DaLn} C_0 + \frac{Rm}{Da}, \tag{7.14}$$

$$\frac{d^2 T_0}{dx^2} + \frac{N_{\mathrm{B}}}{Le}\frac{d\phi_0}{dx}\frac{dT_0}{dx} + \frac{N_{\mathrm{A}} N_{\mathrm{B}}}{Le}\left(\frac{dT_0}{dx}\right)^2 + D_{\mathrm{f}}\frac{d^2 C_0}{dx^2} = 0, \tag{7.15}$$

$$\frac{d^2 \phi_0}{dx^2} + N_{\mathrm{A}}\frac{d^2 T_0}{dx^2} = 0, \tag{7.16}$$

$$\frac{1}{Ln}\frac{d^2 C_0}{dx^2} + Sr\frac{d^2 T_0}{dx^2} = 0, \tag{7.17}$$

The solution of the base flow Eqs. (7.14)-(7.17) admits the boundary conditions:

$$x = -1: \ V_0 = 0, \ T_0 = 0, \ \phi_0 = 1, \ C_0 = 0, \tag{7.18a}$$

$$x = 1: \ V_0 = 0, \ T_0 = 1, \ \phi_0 = 0, \ C_0 = 1. \tag{7.18b}$$

Proceeding as in Chapter - 6, we get basic solutions as

$$T_0 = \frac{1 + x}{2}, \qquad \phi_0 = \frac{1 - x}{2} \quad \text{and} \quad C_0 = \frac{1 + x}{2}. \tag{7.19}$$

Table 7.1: Minimum values of Ra for point of inflection and backflow at $Rs = 200, Rn = 10$ and $Ln = 40$.

Ha	Da	Ra_i	Ra_b
1	10^1	72	192
	10^0	-4	8
	10^{-1}	-19	-10
2	10^1	142	265
	10^0	3	16
	10^{-1}	-19	-9
3	10^1	257	388
	10^0	15	28
	10^{-1}	-20	-8

$$V_0 = s\left[1 - \frac{\cosh(mx)}{\cosh(m)}\right] + \frac{1}{2m^2 Da}\left(Ra + \frac{Rs}{Ln} + Rn\right)\left[x - \frac{\sinh(mx)}{\sinh(m)}\right], \tag{7.20}$$

where $m = \sqrt{\frac{1}{Da} + Ha^2}$ and $s = m\left(\frac{\sinh(2m)}{m(\sinh(2m)) - \cosh(2m) + 1}\right)$.

The basic velocity profiles with Ra for the different values of Da and Ha with $Rs = 200$, $Rn = 10$ and $Ln = 40$ are shown in Fig. 7.1 by fixing the division of Ra and Da as constants at 5, 10 and 15. Figs. 7.1(a)-7.1(c) depicts the variation of basic velocity profile for three different values of $Ha = 1, 2$ and 3 for the fixed value $Da = 10^1$. From Figs. 7.1(b) and 7.1(c), it is noticed that the velocity profile has no point of inflection as well as back flow (or, negative flow) but Fig. 7.1(a) contains point of inflection without backflow for $Ra = 150$. The velocity profiles for the fixed value of $Da = 1$, different values $Ra = 5$, $Ra = 10$ and $Ra = 15$ are presented at $Ha = 1, Ha = 2$ and $Ha = 3$ in Fig. 7.1(d)-7.1(f), respectively. It is observed that the velocity profile possesses the point of inflection only at $Ra = 15$ for $Ha = 3$ shown in Fig. 7.1(f), but 7.1(d) and 7.1(e) contain point of inflection for all values of Ra, whereas backflow contains only at $Ra = 10$ and $Ra = 15$ for $Ha = 1$. At $Da = 10^{-1}$, the basic velocity profile possesses the point of inflection as well as back flow for all values of Ra at different values of Ha, which are shown in Figs. 7.1(g)-7.1(i). The above discussion gives the indication that the Darcy number effect and magnetic effect in the momentum equation has significant impact on the flow regime. The possibility for the instability in the basic flow is the sustenance of the inflection points in the velocity profiles. Hence, the minimum integer value of Rayleigh number (Ra) for which the inflection points (Ra_i) and back flow (Ra_b) appear in the flow field for the values of Ha and Da are presented Table 7.1.

In the literature [35], it has been noticed that the point of inflection is a potential for

instability in the velocity profile, because of that we are very much interest to know the minimum of Rayleigh number (Ra) for which non-Darcy flow will have a point of inflection for a particular value of Darcy number Da. For this, the minimum value of Ra has been calculated for different values of Da in the Table 7.1 for which the back flow and point of inflection appear in the flow regime. Here, Ra_i and Ra_b denote the respective minimum values of for which point of inflection and back flow appear in the velocity profile.

7.4 Linear stability analysis

As in Chapter - 6, imposing the infinitesimal disturbances (δ) on the basic state solutions, neglecting δ^2 and higher order terms and then using the usual normal mode form [42] to express infinitesimal disturbances of corresponding field variables, and eliminating pressure terms from the resulting equations, the linearized stability equations become

$$Da\left[\frac{d^4\hat{u}}{dx^4}-2(\alpha^2+\beta^2)\frac{d^2\hat{u}}{dx^2}+(\alpha^2+\beta^2)^2\hat{u}\right]-\frac{i\alpha}{\epsilon Va}V_0\left[\frac{d^2\hat{u}}{dx^2}-(\alpha^2+\beta^2)\hat{u}\right]+\frac{i\alpha}{\epsilon Va}\frac{d^2V_0}{dx^2}\hat{u}$$
$$-\left[\frac{d^2\hat{u}}{dx^2}-(\alpha^2+\beta^2)\hat{u}\right]-DaHa^2\frac{d^2\hat{u}}{dx^2}-i\alpha Ra\frac{d\hat{T}}{dx}+i\alpha Rn\frac{d\hat{\phi}}{dx}-i\alpha\frac{Rs}{Ln}\frac{d\hat{C}}{dx}$$
$$=-\frac{i\alpha c}{Va}\left[\frac{d^2\hat{u}}{dx^2}-(\alpha^2+\beta^2)\hat{u}\right], \quad (7.21)$$

$$\frac{\beta}{\epsilon Va}\frac{dV_0}{dx}\hat{u}+\frac{i\alpha}{\epsilon Va}V_0\hat{\eta}-Da\left[\frac{d^2\hat{\eta}}{dx^2}-(\alpha^2+\beta^2)\hat{\eta}\right]+\hat{\eta}+DaHa^2\hat{\eta}-\beta Ra\hat{T}+\beta Rn\hat{\phi}$$
$$-\beta\frac{Rs}{Ln}\hat{C}=\frac{i\alpha c}{Va}\hat{\eta}, \quad (7.22)$$

$$\frac{dT_0}{dx}\hat{u}+i\alpha V_0\hat{T}-\left[\frac{d^2\hat{T}}{dx^2}-(\alpha^2+\beta^2)\hat{T}\right]-\frac{N_B}{Le}\frac{dT_0}{dx}\left(\frac{d\hat{\phi}}{dx}+2N_A\frac{d\hat{T}}{dx}\right)-\frac{N_B}{Le}\frac{d\phi_0}{dx}\frac{d\hat{T}}{dx}$$
$$-D_f\left[\frac{d^2\hat{C}}{dx^2}-(\alpha^2+\beta^2)\hat{C}\right]=i\alpha c\hat{T}, \quad (7.23)$$

$$\frac{1}{\epsilon}\frac{d\phi_0}{dx}\hat{u}+\frac{i\alpha}{\epsilon}V_0\hat{\phi}-\frac{1}{Le}\left[\frac{d^2\hat{\phi}}{dx^2}-(\alpha^2+\beta^2)\hat{\phi}\right]-\frac{N_A}{Le}\left[\frac{d^2\hat{T}}{dx^2}-(\alpha^2+\beta^2)\hat{T}\right]=i\alpha c\hat{\phi}, \quad (7.24)$$

$$\frac{1}{\epsilon}\frac{dC_0}{dx}\hat{u}+\frac{i\alpha}{\epsilon}V_0\hat{C}-\frac{1}{Ln}\left[\frac{d^2\hat{C}}{dx^2}-(\alpha^2+\beta^2)\hat{C}\right]-Sr\left[\frac{d^2\hat{T}}{dx^2}-(\alpha^2+\beta^2)\hat{T}\right]=i\alpha c\hat{C}, \quad (7.25)$$

where $\hat{\mathbf{u}}(x)=(\hat{u},\hat{v},\hat{w})$ and $\hat{\eta}=\beta\hat{v}-\alpha\hat{w}$.

The associated boundary conditions for non-permeable rigid walls are no-slip condition for the velocity disturbance and the isothermal condition for the temperature, volume fraction and concentration disturbances are given by

$$\hat{u} = \frac{d\hat{u}}{dx} = \hat{\eta} = \hat{T} = \hat{\phi} = \hat{C} = 0 \quad \text{at} \quad x = \mp 1. \tag{7.26}$$

7.5 Results and discussion

The system of differential equations (7.21)-(7.25) along with their boundary conditions at the walls Eq. (7.26) form a generalized eigenvalue problem with complex disturbance wave speed as the eigenvalue and solved using Chebyshev spectral collocation method.

To examine the convergence, the least stable eigenvalues are calculated by switching the number of grid points (N) and tabulated them in the Table 7.2 for arbitrarily chosen values of governing parameters. This table shows that the least stable eigenvalue achieve convergence requirement of 10^{-7} for $N \geq 51$. The results are consistent for increasing values of N. The same tendency has been observed for other governing parameter values. As a result, the numerical computations have been performed with $N = 51$.

The results obtained from the present analysis are verified by comparing with the published results of an isothermal channel flow without porous medium. The critical Reynolds number Re_{c} and critical wavenumber α_c for the isothermal channel are obtained as $Re_{\mathrm{c}} = 3848.278$ (in this paper $1/Pr$) and $\alpha_{\mathrm{c}} = 1.0205$ from the present analysis by setting $Ra = 0$, $Rn = 0$, $Rs = 0$, $Ha = 0$, $Da = 10^6$, $\beta = 0$, $\epsilon = 1$, $N_{\mathrm{A}} = 0$, $N_{\mathrm{B}} = 0$, $Le = 10^7$, $Sr = 0$, $D_{\mathrm{f}} = 0$ and $Ln = 10^7$. These values are in good agreement with those given by Orszag [84].

The double-diffusive convective instabilities in a vertical channel filled with nanofluid saturated porous medium by considering the effect of a transverse magnetic field is governed by several parameters Pr, Da, Ha, Rn, Rs, Ln, ϵ, N_{A}, N_{B}, Le, D_{f} and Sr. In this study, a special attention is given to analyze the influence Darcy number (Da), the magnetic parameter (Hartmann number Ha), solutal Rayleigh number (Rs), thermo-solutal Lewis number (Ln), Soret parameter (Sr) and Dufour parameter (D_{f}) on the instability of the flow. The values of the remaining parameters are fixed as $\epsilon = 0.6$, $Rn = 10$, $Pr = 7$, $N_{\mathrm{A}} = 8$, $N_{\mathrm{B}} = 0.2$ and $Le = 1000$. As in the case of viscous fluid, here we have also examined the dimension of the least stable mode by calculating Ra_c for various values of spanwise wavenumber (β) in the (Ha, Ra_c)-plane. It has been observed that the numerical results follow the Squire's theorem [104] for nanofluid also, i.e., least stable mode is two dimensional as it displayed in

Fig. 7.2. Therefore, we have been taken $\beta = 0$ in the rest of the conversations. Also, the results obtained for the critical Rayleigh number (Ra_c) and critical wavenumber (α_c) with other parameters are presented graphically.

The combined effect of the magnetic field and permeability parameter (Darcy number) on the instability boundaries is presented in (Ha, Ra_c) and (Ha, α_c) planes in the Fig. 7.3 for various values of Da with fixing the other parameters i.e., $Rs = 200$, $Ln = 40$, $Sr = 0.3$ and $D_f = 0.04$. It is observed from Fig. 7.3(a) that the critical Rayleigh number is increasing with an increase in the value of Darcy number Da, which indicates that permeability has a stabilizing effect. For small values of Darcy number, the porous layer is considered to be less permeable to fluid penetration and consequently the fluid experiences a pronounced large resistance as it flows through the porous matrix. This results in hindering flow activities in the porous region. Further, it is noticed that an increase in the magnetic parameter increases the critical Rayleigh number. Hence, the influence of the magnetic field is to stabilize the system. It is well known that the initiation of a magnetic field is perpendicular to the flow direction has a trend to generate the drag known as the Lorentz force. As a result, a great deal of energy is used by the system to overcome this resistance and hence convection is delayed giving rise to a stabilizing effect. Thus magnetic field can be effectively used to regulate convection in a nanofluid saturated porous medium. Fig. 7.3(b) reveals that the critical wavenumber decreases with an increase in Ha for fixed Darcy number. But, the critical wavenumber increases with the permeability and increasing rate is very less when Da goes from 1 to 10 compared to Da changes from 0.1 to 1.

For various values of solutal Rayleigh number, the critical Rayleigh number (Ra_c) and the corresponding critical wavenumber are plotted in Fig. 7.4 with the Hartmann number (Ha) when $Da = 0.1$, $Ln = 40$, $Sr = 0.3$ and $D_f = 0.04$. From this, it is observed that there is no visible effect of the solutal Rayleigh number on the critical Rayleigh number but a very small variation on the critical wavenumber. The critical wavenumber decreases with an increase in the values of Rs and this decreasing rate is very small. Therefore, the influence of solutal Rayleigh number on the instability boundaries is almost insignificant.

Fig. 7.5 displays the variation of the critical Rayleigh number and critical wavenumber plotted against the magnetic parameter for different values of Ln with $Da = 10^{-1}$, $Rs = 200$, $Sr = 0.3$ and $D_f = 0.04$. It is seen from 7.5(a) that the critical Rayleigh number decreases with an increase in the values of thermo-solutal Lewis number (Ln). Thus, Ln has a destabilizing effect. When the Lewis number is increased, the heat is more than that of solute, and therefore, it destabilizes the system. The wavenumber is increasing with an increase of Ln as depicted in Fig. 7.5(b). It is interesting to note that for $Ha > 2.7$, the

variation of the critical wavenumber is not significant.

The influence of Soret parameter (Sr) on the critical Rayleigh number and critical wavenumber is presented in Fig. 7.6 when $Da = 10^{-1}$, $Rs = 200$, $Ln = 40$ and $D_{\mathrm{f}} = 0.04$. It is observed from Fig. 7.6(a) that the critical Rayleigh number decreases with an increase in the value of Sr but the decreasing rate is very small. Therefore, the Soret parameter has a destabilizing effect of the flow field when the nanofluid flow in a vertical channel. The physical interpretation is that the Soret effect enhances the density gradient of solute, which leads to a convective instability at fixed temperature differences. On the other hand, there is a visible variation of the critical wavenumber (α_{c}) for the effect of the Soret parameter to the Hartmann number. Fig. 7.6(b) reveals that α_{c} increases when Sr increasing from -0.5 to 0 in the whole range of Ha and this trend continues when Sr increases from 0 to 0.5 up to $Ha < 2.3$ and after that it has decreasing nature.

Fig. 7.7 depicts the patterns of the critical Rayleigh number and the critical wavenumber against Hartmann number for the different effect of the Dufour parameter (D_{f}) by fixing the values of Da, Rs, Ln and Sr at 10^{-1}, 200, 40 and 0.3, respectively. From Fig. 7.7(a), it is visible that the critical Rayleigh number decreases with the increase in the value of Dufour parameter. Thus, it gives the conclusion that the Dufour parameter (D_{f}) has a destabilizing effect on the system. The critical wavenumber is increasing with the increase in the Dufour parameter as portrayed in Fig. 7.7(b).

The variations in the growth rate in the neighbourhood ($Ra_{\mathrm{c}} = Ra_{\mathrm{c}}(1 + 0.01)$) of the critical point is plotted in Fig. 7.8 for different values of the permeability parameter to understand instability mechanism more clearly, when $Rs = 200$, $Ln = 40$, $Sr = 0.3$ and $D_{\mathrm{f}} = 0.04$. From Fig. 7.8, it is clear that disturbances of the growth rate decrease with an increase in the magnetic parameter. Further, it is noticed that the growth rate is also decreasing with the increase in Da. This is because the impacts of rising both the parameters postpone the onset of convective motion. From Figs. 7.8(a)-7.8(c), it is observed that the curve of the growth rate is smooth nature for all values of Darcy number (Da).

The variation in the pattern of the streamlines, isotherms, isonanoconcentrations and isosolutes at the critical level for various values of the Darcy number (Da) and the Hartmann number (Ha) are displayed in Figs. 7.9 and 7.10 with $Rs = 200$, $Ln = 40$, $Sr = 0.3$ and $D_{\mathrm{f}} = 0.04$. Fig. 7.9 exhibits the streamlines, isotherms, isonanoconcentrations and isosolutes for various values of the Darcy number with fixing $Ha = 2$. From Figs. 7.9(a)-7.9(c), it is observed that the flow is mainly controlled by a bi-cellular structure (two asymmetric cells), where one cell (primary cell) is rotating clockwise direction and the other cell (secondary cell)

is rotating anticlockwise direction. The shape of the inner cells of this bi-cellular structure is changing with an increase in the Darcy number. Further, it is noticed that the primary cell pushes the secondary cell in upwards direction in the vertical channel as the value of the Darcy number increase. Figs. 7.9(d)-7.9(f) shows that the pattern of the isotherms are almost the same and spread the whole channel over a period for all values of Da. Since, the transfer of the disturbance temperature takes place mainly by diffusion, leading to a more stable flow configuration. The isonanoconcentration lines and isosolute for the flow in a vertical channel are depicted in Figs. 7.9(g)-7.9(i) and Figs. 7.9(j)-7.9(l), respectively. These figures reveal that the isonanoconcentration lines and isosolute lines are more concentrated in the centre of the channel over a period for different values of permeability. It is noticed that the isonanoconcentration lines and isosoultes lines have also a two-cell structure with each cell on either side to the centre of the channel. Further, it is observed that the size of the cells is decreasing as the Darcy number is increasing.

The influence of magnetic parameter on the pattern of streamlines, isotherms, isonanoconcentrations and isosolutes for $Da = 0.1$, is shown in Fig. 7.10. From Figs. 7.10(a) - 7.10(c), it is noticed that the flow is controlled by bi-cellular patterns where one cell (primary cell) has full structure but another one (secondary cell) has half structure. It is noticed that the streamline pattern looks like moving downwards the vertical channel as the value of the magnetic parameter Ha increase. The shape of the inner cells in each of the bi-cellular structure is changed with increasing of the strength of magnetic field. The isotherms of the flow are presented in Figs. 7.10(d) - 7.10(f). Here also the isotherms are looking like shifting downwards the vertical channel as the Hartmann number Ha increase. The isotherms occupies the large part of the channel for all values of Ha. The iso-nanoconcentration contours and isosolutes of the flow are depicted in Figs. 7.10(g)-7.10(i) and 7.10(j)- 7.10(l). The variation of the isonanoconcentration contours and isosolutes with the increasing values of the magnetic parameter are similar. Both the patterns are dense at the centre of the channel. The magnitude of the stream function, isotherms, isonanoconcentration and isosolutes reduce indicating the system becoming more stable with augmenting value in the Hartmann number.

Table 7.2: Convergence of the least stable eigenvalue by Chebyshev collocation method. Here $Da = 0.1$, $Ha = 2$, $Pr = 7$, $Ra = 10$, $Rn = 10$, $Rs = 200$, $Ln = 40$, $\epsilon = 0.6$, $N_{\mathrm{A}} = 8$, $N_{\mathrm{B}} = 0.2$, $Le = 1000$, $Sr = 0.5$, $D_{\mathrm{f}} = 0.04$, $\alpha = 1$ and $\beta = 0$.

N	Least stable eigenvalue
30	7.485859172934-0.043104194212i
40	7.486328518031-0.043192358007i
45	7.486321875150-0.043187337026i
50	7.486321164723-0.043187583713i
51	7.486321141281-0.043187659108i
55	7.486321134844-0.043187629962i
60	7.486321156386-0.043187653330i

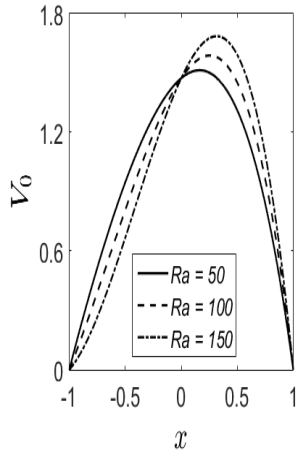

(a) $Da = 0.1, Ha = 1$

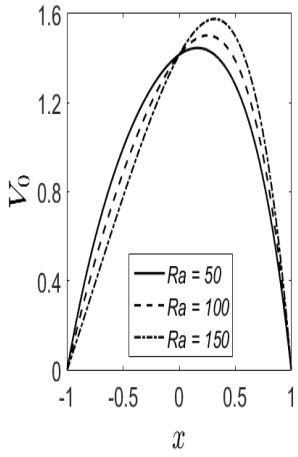

(b) $Da = 0.1, Ha = 2$

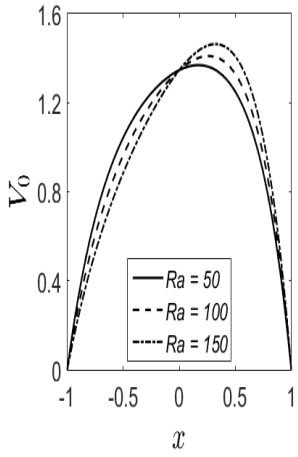

(c) $Da = 0.1, Ha = 3$

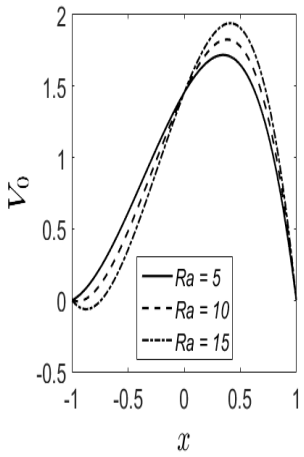

(d) $Da = 1, Ha = 1$

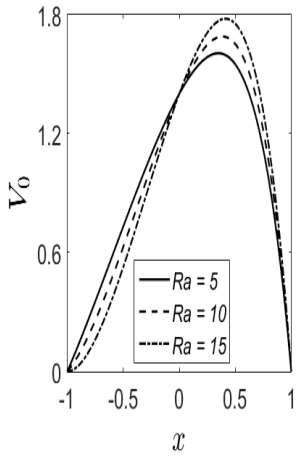

(e) $Da = 1, Ha = 2$

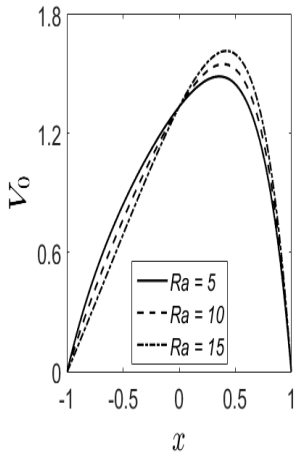

(f) $Da = 1, Ha = 3$

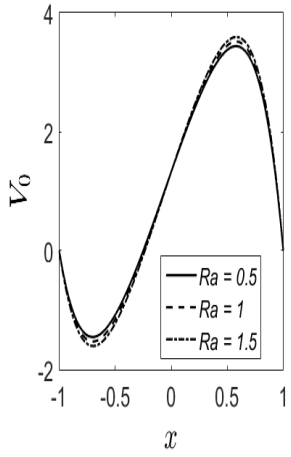

(g) $Da = 10, Ha = 1$

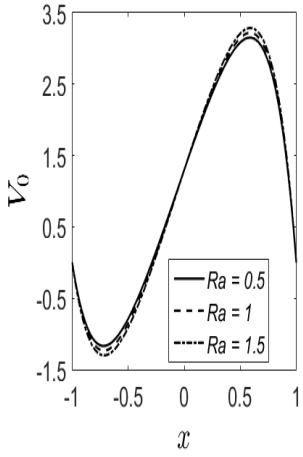

(h) $Da = 10, Ha = 2$

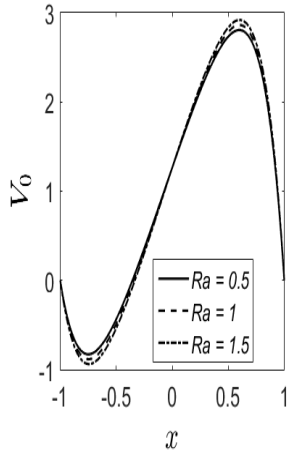

(i) $Da = 10, Ha = 3$

Figure 7.1: Basic velocity profiles for $Rs = 200$, $Rn = 10$ and $Ln = 40$.

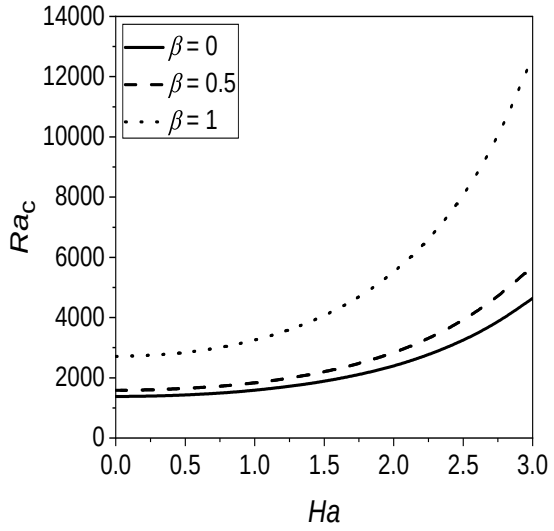

Figure 7.2: Instabilities boundaries in (Ha, Ra_{c})-plane for different values of β, when $Da = 0.1,\ Pr = 7, Rn = 10, \epsilon = 0.6, Rs = 200, Le = 1000, N_{\mathrm{A}} = 8,\ N_{\mathrm{B}} = 0.2,\ Ln = 40, Sr = 0.3$ and $D_{\mathrm{f}} = 0.04$.

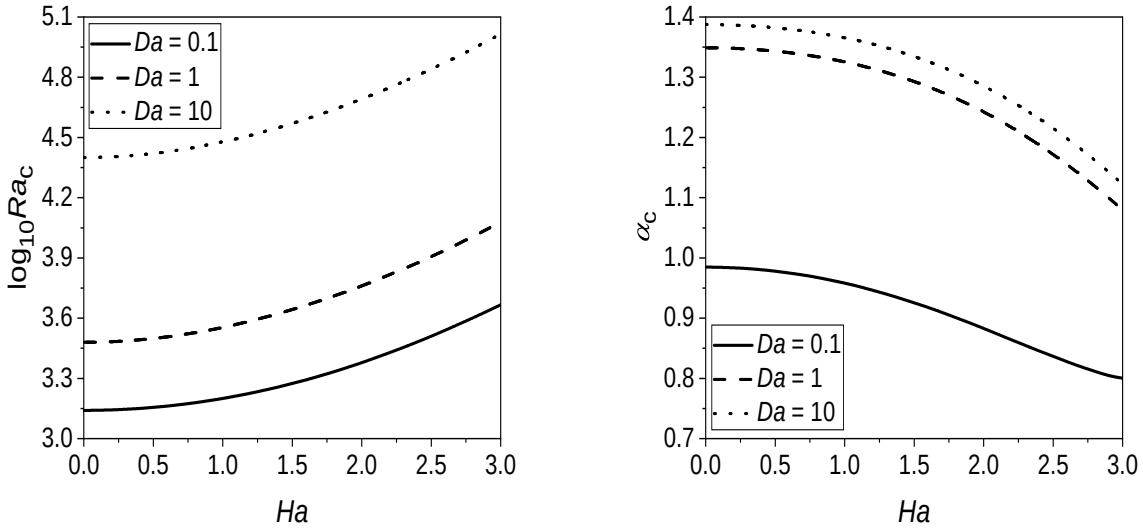

(a) (b)

Figure 7.3: Instabilities boundaries in (a) (Ha, Ra_{c})-plane and (b) $(Ha, \alpha_{\mathrm{c}})$-plane for different values of Da when $Rs = 200,\ Ln = 40,\ Sr = 0.3,\ D_{\mathrm{f}} = 0.04$.

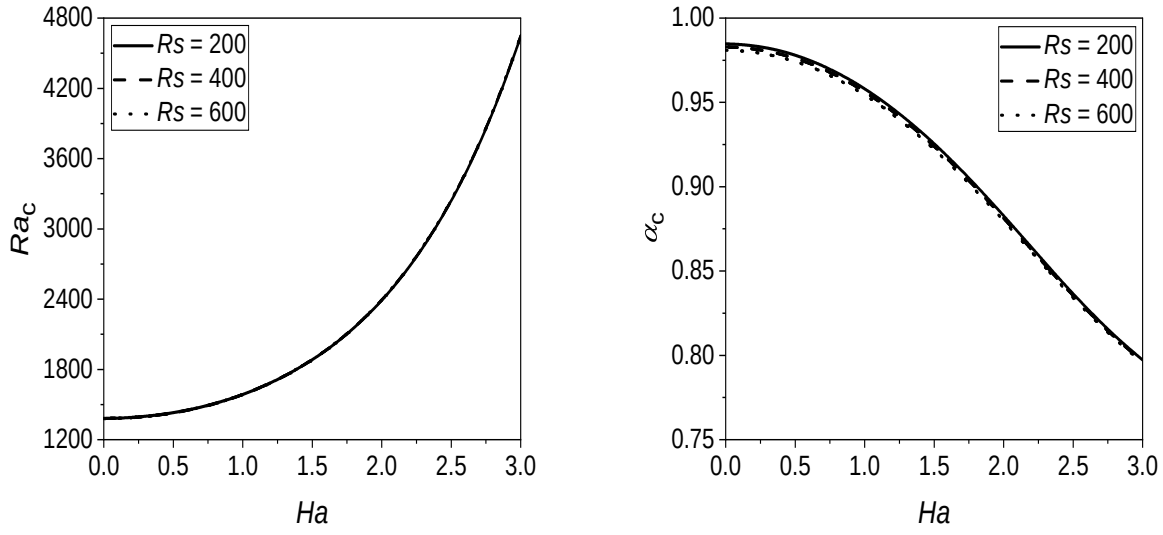

(a) (b)

Figure 7.4: Instabilities boundaries in (a) (Ha, Ra_{c})-plane and (b) $(Ha, \alpha_{\mathrm{c}})$-plane for different values of Rs when $Da = 0.1$, $Ln = 40$, $Sr = 0.3$, $D_{\mathrm{f}} = 0.04$.

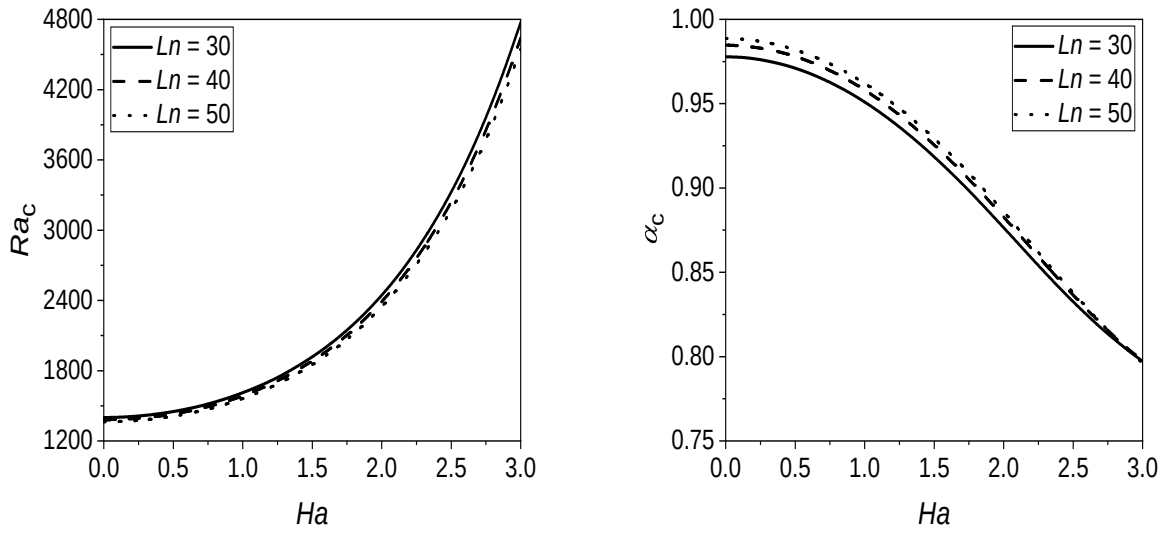

(a) (b)

Figure 7.5: Instabilities boundaries in (a) (Ha, Ra_{c})-plane and (b) $(Ha, \alpha_{\mathrm{c}})$-plane for different values of Ln when $Da = 0.1$, $Rs = 200$, $Sr = 0.3$, $D_{\mathrm{f}} = 0.04$.

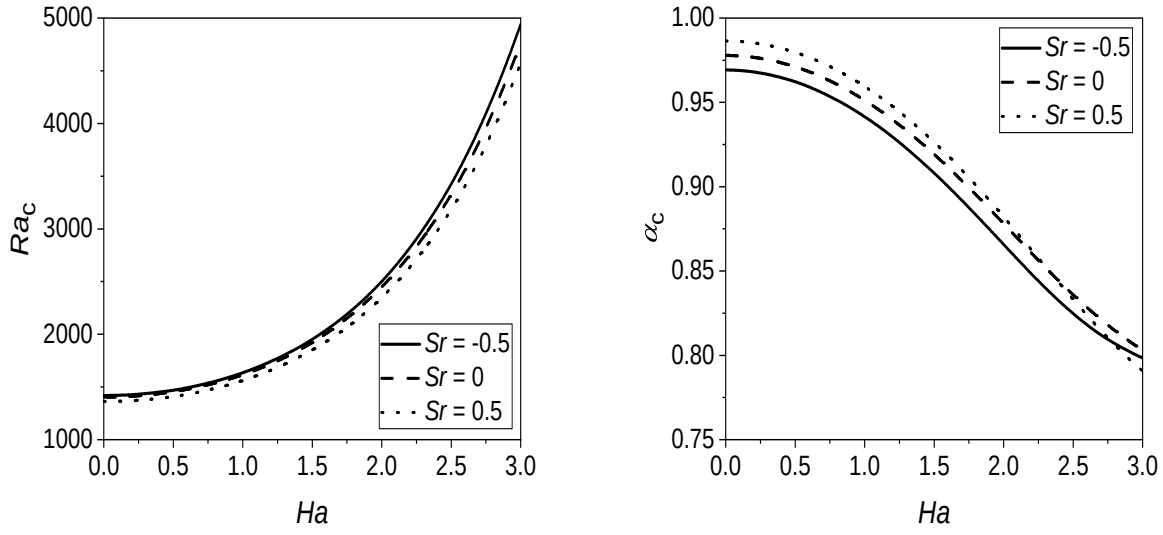

(a) (b)

Figure 7.6: Instabilities boundaries in (a) (Ha, Ra_c)-plane and (b) (Ha, α_c)-plane for different values of Sr when $Da = 0.1$, $Rs = 200$, $Ln = 40$, $D_f = 0.04$.

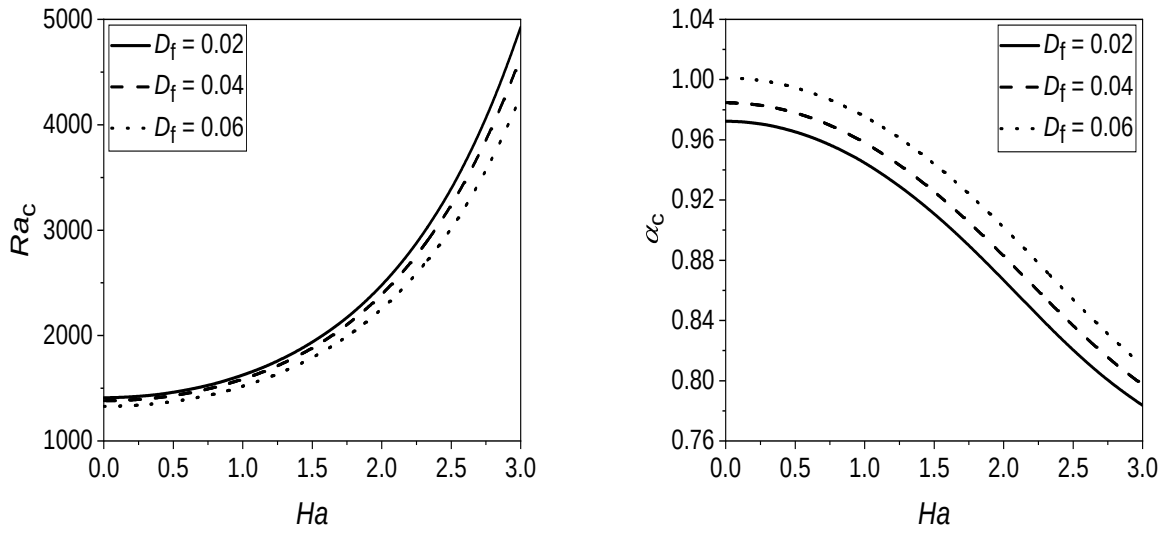

(a) (b)

Figure 7.7: Instabilities boundaries in (a) (Ha, Ra_c)-plane and (b) (Ha, α_c)-plane for different values of D_f when $Da = 0.1$, $Rs = 200$, $Ln = 40$, $Sr = 0.3$.

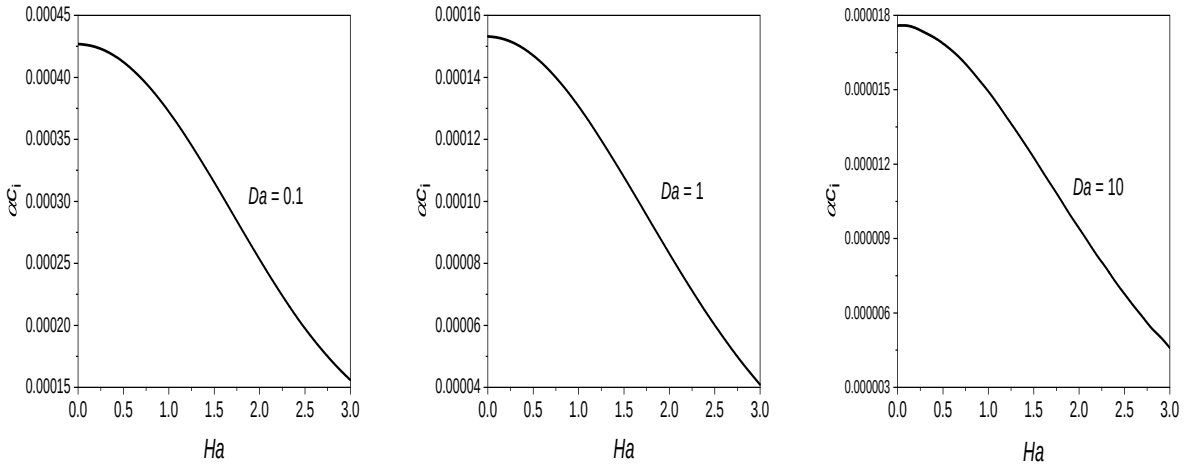

(a) (b) (c)

Figure 7.8: Growth rate (αc_i) as a function of Ha for (a) $Da = 0.1$, (b) $Da = 1$ and (c) $Da = 10$.

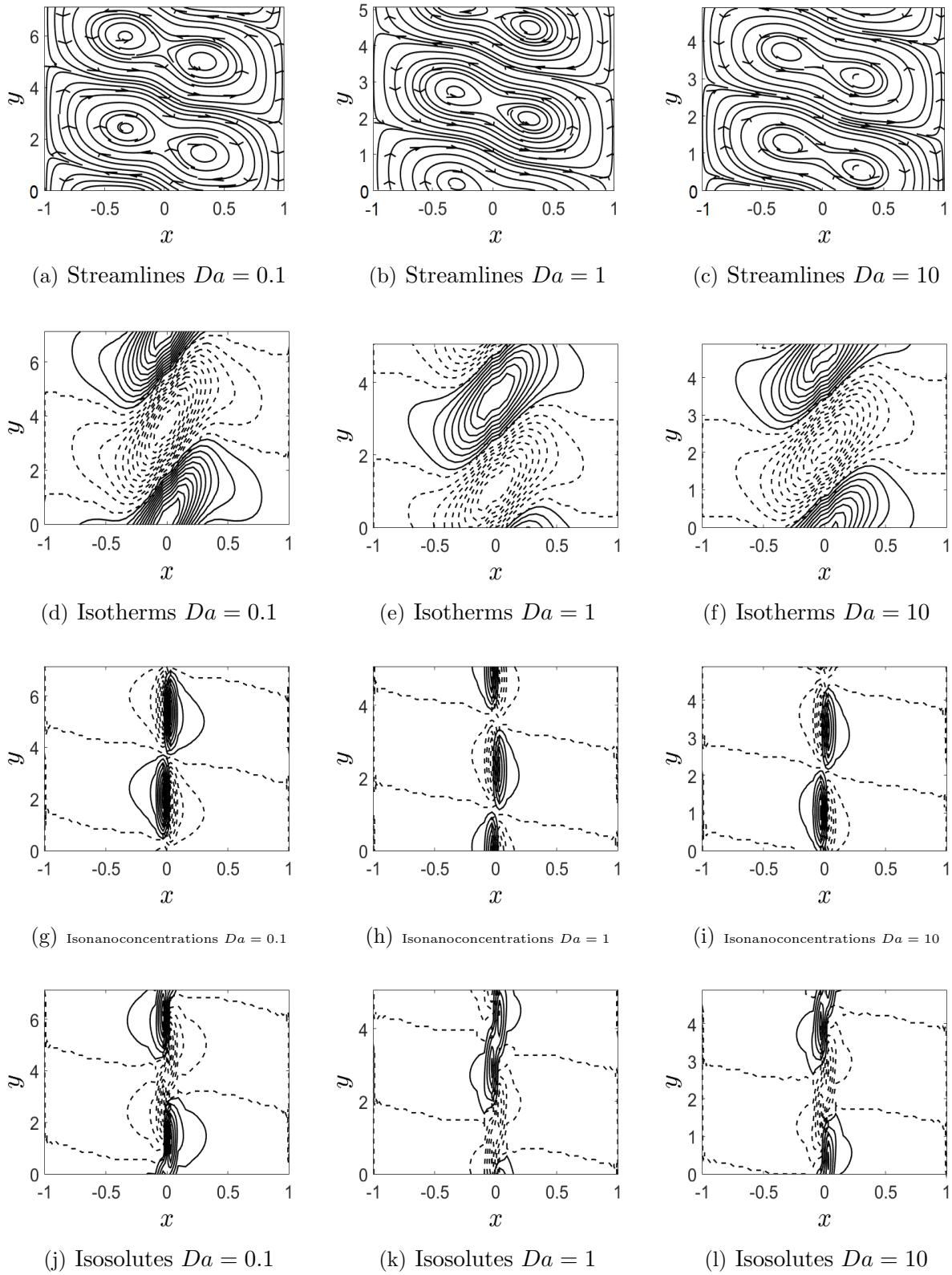

(a) Streamlines $Da = 0.1$ (b) Streamlines $Da = 1$ (c) Streamlines $Da = 10$

(d) Isotherms $Da = 0.1$ (e) Isotherms $Da = 1$ (f) Isotherms $Da = 10$

(g) Isonanoconcentrations $Da = 0.1$ (h) Isonanoconcentrations $Da = 1$ (i) Isonanoconcentrations $Da = 10$

(j) Isosolutes $Da = 0.1$ (k) Isosolutes $Da = 1$ (l) Isosolutes $Da = 10$

Figure 7.9: The disturbance of streamlines ((a) to (c)), isotherms ((d) to (f)), isonanoconcentrations ((g) to (i)) and isosolutes ((j) to (l)) for various values of Darcy number (Da) over one period.

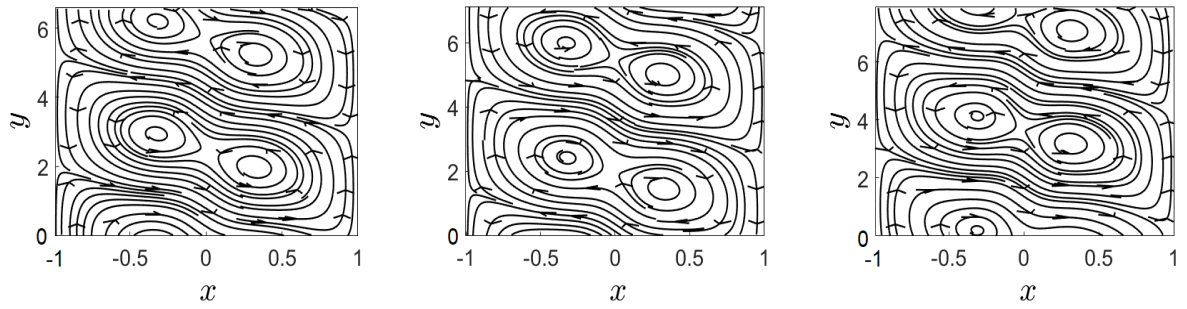

(a) Streamlines $Ha = 1$ (b) Streamlines $Ha = 2$ (c) Streamlines $Ha = 3$

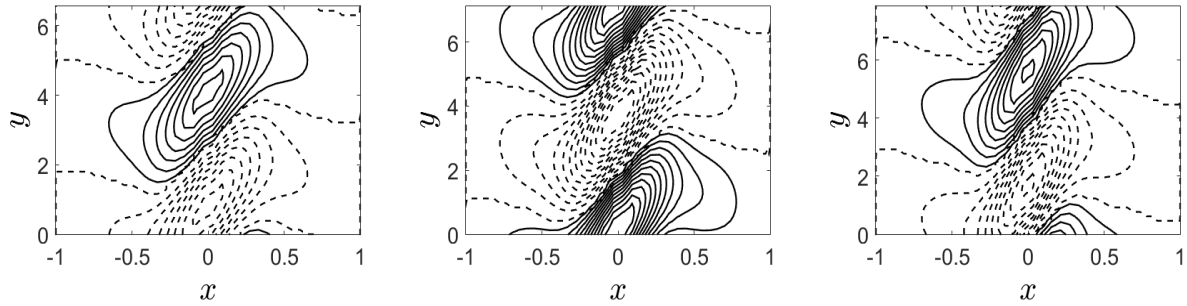

(d) Isotherms $Ha = 1$ (e) Isotherms $Ha = 2$ (f) Isotherms $Ha = 3$

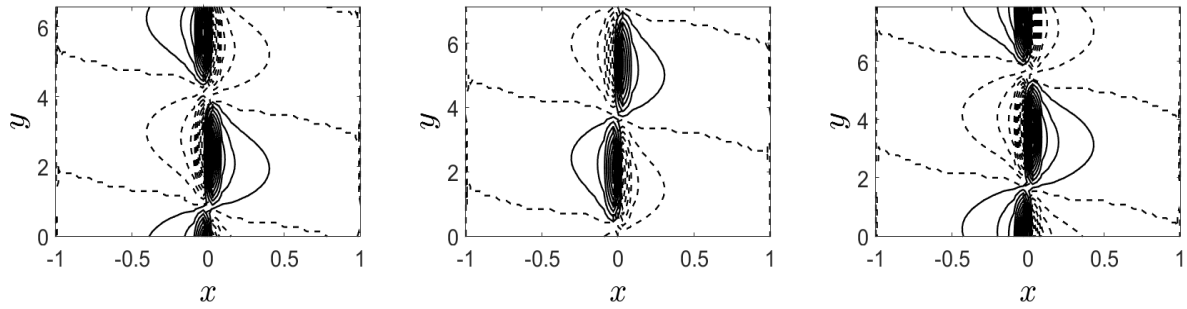

(g) Isonanoconcentrations $Ha = 1$ (h) Isonanoconcentrations $Ha = 2$ (i) Isonanoconcentrations $Ha = 3$

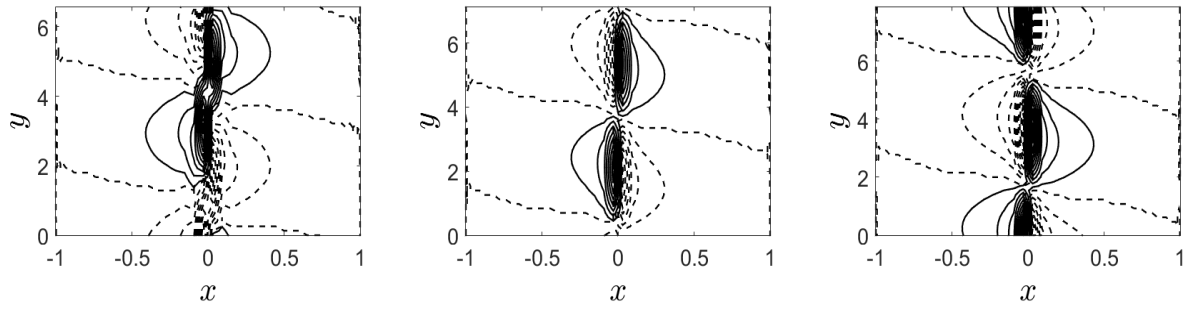

(j) Isosolutes $Ha = 1$ (k) Isosolutes $Ha = 2$ (l) Isosolutes $Ha = 3$

Figure 7.10: The disturbance of streamlines (a) to (c), isotherms (d) to (f), isonanoconcentrations (g) to (i) and isosolutes (j) to (l) for various values of Hartmann number (Ha) over one period.

7.6 Conclusions

The linear stability of double-diffusive convective with a transverse magnetic effect in a vertical channel filled with a nanofluid saturated porous medium for Brinkman-extended Darcy model is examined. The influence of the Hartmann number (Ha) is studied numerically with the Chebyshev spectral collocation method. The critical Rayleigh number and critical wavenumber are calculated and the results displayed graphically for various values of Da, Rs, Ln, Sr and D_{f} against Ha. The main observations from the obtained results are:

- The stability of the fluid is emphasized with an increase in the value of the magnetic parameter. Thus, the Hartmann number (Ha) has a stabilizing effect on the flow field.
- Permeability of the medium has a stabilizing effect on the flow regime and it increases rapidly when permeability increases. Thus, impacts of rising Da postpone the onset of convection.
- The effect of the solutal Rayleigh number (Rs) on the stability of the system is not significant but it dual effect on the size of convection cells.
- Thermo-solutal Lewis number (Ln), Soret parameter (Sr) and Dufour parameter (D_{f}) have destabilizing nature of the flow in a vertical channel. Hence, the effects of increasing these parameters are to advance the onset of convective motion in the flow field.
- The dimension of the convective cells is becoming more with the rising effect of Ha and Rs, becoming less for the enhancing effect of D_{f}, while it is showing a dual character with rising the effect of Ln and Sr.

Chapter 8

Effect of local thermal non-equilibrium on the stability of the flow in a vertical channel filled with nanofluid saturated porous medium [1]

8.1 Introduction

The majority of the theoretical studies available in the literature have been observed by considering LTE between the fluid, particle and porous medium. The study of LTNE state for nanofluid is found to be a significant research area due to its interesting applications in cooling and drying of foods, microwave heating and rapid heat transfer etc. Nield and Bejan [78] discussed LTNE model for fluid phase and solid-matrix in the temperature equation, instead of using the LTE model. Bera and Khandelwal [19] analyzed the instability of non-isothermal Poiseuille flow in a vertical porous channel under the influence of LTNE state. Recently, Mahajan and Sharma [70] discussed the effect of LNTE on the onset of convection in a magnetic nanofluid layer.

From the literature survey, it is noticed that the stability characteristics of a nanofluid in a vertical channel under LTNE state between fluid and particle phases and fluid and solid-matrix phases has not been studied.

In this chapter, we analyzes the effect of LTNE on the stability of convection in a nanofluid flow through a vertical channel occupied with porous medium. A linear stability analysis is carried out by adopting normal modes. Then, the system of differential equations for

[1] Accepted in "***Journal of Heat Transfer***"

small disturbance is solved entirely using the spectral method. The computational results are analyzed graphically for diverse values of the governing LTNE parameter.

8.2 Mathematical Formulation

Consider an incompressible, unsteady nanofluid flow in a vertical channel of width $2L$ bounded by two impermeable and perfectly thermally conducting walls. The schematic representation of the problem is displayed in Fig. 6.1. The LTNE state between fluid, particle and solid-matrix phases is assumed. The three-temperature model is considered. Three heat transport equations are thus considered, one for each of the three phases.

Applying Oberbeck-Boussinesq approximation and Darcy-Brinkman model for the flow in the porous medium, the governing equations of the flow are:

$$\nabla \cdot \mathbf{u} = 0, \tag{8.1}$$

$$\rho_{\mathrm{f}}\left(\frac{1}{\epsilon}\frac{\partial \mathbf{u}}{\partial t} + \frac{1}{\epsilon^2}(\mathbf{u}\cdot\nabla)\mathbf{u}\right) = -\nabla p + \tilde{\mu}\nabla^2\mathbf{u} - \frac{\mu}{K}\mathbf{u} + \left[\phi\rho_{\mathrm{p}} + (1-\phi)\rho_{\mathrm{f}}\{1-\beta_{\mathrm{T}}(T_{\mathrm{f}}-T_1)\}\right]\mathbf{g}, \tag{8.2}$$

$$(1-\phi_1)(\rho c)_{\mathrm{f}}\epsilon\left(\frac{\partial T_{\mathrm{f}}}{\partial t} + \frac{1}{\epsilon}\mathbf{u}\cdot\nabla T_{\mathrm{f}}\right) = \epsilon(1-\phi_1)k_{\mathrm{f}}\nabla^2 T_{\mathrm{f}} + (1-\phi_1)\epsilon(\rho c)_{\mathrm{p}} \times \left[D_{\mathrm{B}}\nabla\phi\cdot\nabla T_{\mathrm{f}} + \frac{D_{\mathrm{T}}}{T_1}\nabla T_{\mathrm{f}}\cdot\nabla T_{\mathrm{f}}\right] - h_{\mathrm{fp}}(T_{\mathrm{f}}-T_{\mathrm{p}}) - h_{\mathrm{fs}}(T_{\mathrm{f}}-T_{\mathrm{s}}), \tag{8.3}$$

$$\epsilon\phi_1(\rho c)_{\mathrm{p}}\left(\frac{\partial T_{\mathrm{p}}}{\partial t} + \frac{1}{\epsilon}\mathbf{u}\cdot\nabla T_{\mathrm{p}}\right) = \epsilon\phi_1 k_{\mathrm{p}}\nabla^2 T_{\mathrm{p}} + h_{\mathrm{fp}}(T_{\mathrm{f}}-T_{\mathrm{p}}), \tag{8.4}$$

$$(1-\epsilon)(\rho c)_{\mathrm{s}}\frac{\partial T_{\mathrm{s}}}{\partial t} = (1-\epsilon)k_{\mathrm{s}}\nabla^2 T_{\mathrm{s}} + h_{\mathrm{fs}}(T_{\mathrm{f}}-T_{\mathrm{s}}), \tag{8.5}$$

$$\frac{\partial \phi}{\partial t} + \frac{1}{\epsilon}\mathbf{u}\cdot\nabla\phi = D_{\mathrm{B}}\nabla^2\phi + \frac{D_{\mathrm{T}}}{T_2}\nabla^2 T_{\mathrm{f}}, \tag{8.6}$$

where subscripts 'f', 'p' and 's' refers to fluid, particle and solid phases. T_{f}, T_{p}, and T_{s} are temperatures in three phases, h_{fp} and h_{fs} are the inter-phase heat transfer coefficients between the fluid and particles phases and fluid and solid phases, respectively.

The corresponding boundary conditions are written as

$$x = -L: \ \mathbf{u} = 0, \ T_{\mathrm{f}} = T_1, \ T_{\mathrm{p}} = T_1, \ T_{\mathrm{s}} = T_1, \ \phi = \phi_2, \tag{8.7a}$$

$$x = L: \ \mathbf{u} = 0, \ T_{\mathrm{f}} = T_2, \ T_{\mathrm{p}} = T_2, \ T_{\mathrm{s}} = T_2, \ \phi = \phi_1. \tag{8.7b}$$

The non-dimensional scheme is defined by

$$\begin{aligned} &(x^*, y^*, z^*) = \frac{(x, y, z)}{L}, \quad (u^*, v^*, w^*) = \frac{(u, v, w)L}{\alpha_{\mathrm{f}}}, \quad p^* = \frac{Kp}{\mu\alpha_{\mathrm{f}}}, \quad t^* = \frac{\alpha_{\mathrm{f}} t}{L^2}, \\ &T_{\mathrm{f}}^* = \frac{T_{\mathrm{f}} - T_1}{T_2 - T_1}, \quad T_{\mathrm{p}}^* = \frac{T_{\mathrm{p}} - T_1}{T_2 - T_1}, \quad T_{\mathrm{s}}^* = \frac{T_{\mathrm{s}} - T_1}{T_2 - T_1}, \quad \phi^* = \frac{\phi - \phi_1}{\phi_2 - \phi_1}, \end{aligned} \tag{8.8}$$

where $\alpha_{\mathrm{f}} = \dfrac{k_{\mathrm{f}}}{(\rho c)_{\mathrm{f}}}$ is the thermal diffusivity of porous medium.
Substituting the non dimensional variables given in Eq. (8.8) in the governing Eqs. (8.1)-(8.6), the boundary conditions Eq. (8.7) and dropping asterisk, we get

$$\nabla \cdot \mathbf{u} = 0, \tag{8.9}$$

$$\frac{1}{Va}\left[\frac{\partial \mathbf{u}}{\partial t} + \frac{1}{\epsilon}(\mathbf{u} \cdot \nabla)\mathbf{u}\right] = -\nabla p + \Lambda Da \nabla^2 \mathbf{u} - \mathbf{u} + Ra T_{\mathrm{f}} \hat{e}_{\mathrm{y}} - Rn\phi \hat{e}_{\mathrm{y}} - Rm \hat{e}_{\mathrm{y}}, \tag{8.10}$$

$$\frac{\partial T_{\mathrm{f}}}{\partial t} + \frac{1}{\epsilon}\mathbf{u} \cdot \nabla T_{\mathrm{f}} = \nabla^2 T_{\mathrm{f}} + \frac{N_{\mathrm{B}}}{Le}\nabla\phi \cdot \nabla T_{\mathrm{f}} + \frac{N_{\mathrm{A}} N_{\mathrm{B}}}{Le}\nabla T_{\mathrm{f}} \cdot \nabla T_{\mathrm{f}} - N_{\mathrm{HP}}(T_{\mathrm{f}} - T_{\mathrm{p}}) - N_{\mathrm{HS}}(T_{\mathrm{f}} - T_{\mathrm{s}}), \tag{8.11}$$

$$\frac{\partial T_{\mathrm{p}}}{\partial t} + \frac{1}{\epsilon}\mathbf{u} \cdot \nabla T_{\mathrm{p}} = \varepsilon_{\mathrm{P}} \nabla^2 T_{\mathrm{p}} + \gamma_{\mathrm{P}} N_{\mathrm{HP}}(T_{\mathrm{f}} - T_{\mathrm{p}}), \tag{8.12}$$

$$\frac{\partial T_{\mathrm{s}}}{\partial t} = \varepsilon_{\mathrm{S}} \nabla^2 T_{\mathrm{s}} + \gamma_{\mathrm{S}} N_{\mathrm{HS}}(T_{\mathrm{f}} - T_{\mathrm{s}}), \tag{8.13}$$

$$\frac{\partial \phi}{\partial t} + \frac{1}{\epsilon}\mathbf{u} \cdot \nabla \phi = \frac{1}{Le}\nabla^2 \phi + \frac{N_{\mathrm{A}}}{Le}\nabla^2 T_{\mathrm{f}}, \tag{8.14}$$

$$x = -1: \ \mathbf{u} = 0, \ T_{\mathrm{f}} = 0, \ T_{\mathrm{p}} = 0, \ T_{\mathrm{s}} = 0, \ \phi = 1, \tag{8.15a}$$

$$x = 1: \ \mathbf{u} = 0, \ T_{\mathrm{f}} = 1, \ T_{\mathrm{p}} = 1, \ T_{\mathrm{s}} = 1, \ \phi = 0. \tag{8.15b}$$

where $N_{\mathrm{HP}} = \dfrac{h_{\mathrm{fp}} L^2}{\epsilon(1-\phi_1)k_{\mathrm{f}}}$ and $N_{\mathrm{HS}} = \dfrac{h_{\mathrm{fs}} L^2}{\epsilon(1-\phi_1)k_{\mathrm{f}}}$ are the inter-phase heat transfer parameters called as Nield number([117]), $\gamma_{\mathrm{P}} = \dfrac{(1-\phi_1)}{\phi_1}\dfrac{(\rho c)_{\mathrm{f}}}{(\rho c)_{\mathrm{p}}}$ and $\gamma_{\mathrm{S}} = \dfrac{\epsilon(1-\phi_1)}{(1-\epsilon)}\dfrac{(\rho c)_{\mathrm{f}}}{(\rho c)_{\mathrm{s}}}$ are modified thermal capacity ratios and $\varepsilon_{\mathrm{P}} = \dfrac{k_{\mathrm{p}}}{k_{\mathrm{f}}}\dfrac{(\rho c)_{\mathrm{f}}}{(\rho c)_{\mathrm{p}}}$ and $\varepsilon_{\mathrm{S}} = \dfrac{k_{\mathrm{s}}}{k_{\mathrm{f}}}\dfrac{(\rho c)_{\mathrm{f}}}{(\rho c)_{\mathrm{s}}}$ are modified thermal diffusivity ratios, respectively. To avoid too many parameter studies, the viscosity ratio (Λ) is taken as

constant 1.

8.3 Basic state solution

The flow in the basic state is assumed as steady, unidirectional and fully developed and is permit a solution of the form: $\mathbf{u_0} = (0, V_0(x), 0)$ is the basic velocity vector, $T_{\mathrm{f0}} = T_{\mathrm{f0}}(x)$ is the basic temperature for fluid phase, $T_{\mathrm{p0}} = T_{\mathrm{p0}}(x)$ is the basic temperature for particle phase, $T_{\mathrm{s0}} = T_{\mathrm{s0}}(x)$ is the basic temperature for solid phase, $\phi_0 = \phi_0(x)$ is the basic volume fraction and $p_0 = p_0(y)$ is the basic pressure. Under these situations, the governing Eqs. (8.9)-(8.14) reduce to

$$\frac{d^2V_0}{dx^2} - \frac{1}{Da}V_0 = \frac{1}{Da}\frac{dp_0}{dy} - \frac{Ra}{Da}T_{\mathrm{f0}} + \frac{Rn}{Da}\phi_0 + \frac{Rm}{Da}, \tag{8.16}$$

$$\frac{d^2T_{\mathrm{f0}}}{dx^2} + \frac{N_{\mathrm{B}}}{Le}\frac{d\phi_0}{dx}\frac{dT_{\mathrm{f0}}}{dx} + \frac{N_{\mathrm{A}}N_{\mathrm{B}}}{Le}\left(\frac{dT_{\mathrm{f0}}}{dx}\right)^2 + N_{\mathrm{HP}}(T_{\mathrm{p0}} - T_{\mathrm{f0}}) + N_{\mathrm{HS}}(T_{\mathrm{s0}} - T_{\mathrm{f0}}) = 0, \tag{8.17}$$

$$\varepsilon_{\mathrm{P}}\frac{d^2T_{\mathrm{p0}}}{dx^2} + \gamma_{\mathrm{P}}N_{\mathrm{HP}}(T_{\mathrm{f0}} - T_{\mathrm{p0}}) = 0, \tag{8.18}$$

$$\varepsilon_{\mathrm{S}}\frac{d^2T_{\mathrm{s0}}}{dx^2} + \gamma_{\mathrm{S}}N_{\mathrm{HS}}(T_{\mathrm{f0}} - T_{\mathrm{s0}}) = 0, \tag{8.19}$$

$$\frac{d^2\phi_0}{dx^2} + N_{\mathrm{A}}\frac{d^2T_{\mathrm{f0}}}{dx^2} = 0. \tag{8.20}$$

The associated boundary conditions are:

$$x = -1: \ V_0 = 0, \ T_{\mathrm{f0}} = 0, \ T_{\mathrm{p0}} = 0, \ T_{\mathrm{s0}} = 0, \ \phi_0 = 1, \tag{8.21a}$$

$$x = 1: \ V_0 = 0, \ T_{\mathrm{f0}} = 1, \ T_{\mathrm{p0}} = 1, \ T_{\mathrm{s0}} = 1, \ \phi_0 = 0. \tag{8.21b}$$

As explained in Chapter - 6, solutions of the Eqs. (8.17)-(8.20) and Eq. (8.16) with boundary conditions Eq. (8.21) are

$$T_{\mathrm{f0}} = T_{\mathrm{p0}} = T_{\mathrm{s0}} = \frac{1+x}{2} \quad \text{and} \quad \phi_0 = \frac{1-x}{2}, \tag{8.22}$$

$$V_0 = s\left[1 - \frac{\cosh(x/\sqrt{Da})}{\cosh(1/\sqrt{Da})}\right] + \left(\frac{Ra+Rn}{2}\right)\left[x - \frac{\sinh(x/\sqrt{Da})}{\sinh(1/\sqrt{Da})}\right], \tag{8.23}$$

where $s = \dfrac{\sinh(2/\sqrt{Da})}{\sinh(2/\sqrt{Da}) - \sqrt{Da}(\cosh(2/\sqrt{Da}) - 1)}$.

8.4 Linear stability analysis

As in Chapter - 6, imposing the infinitesimal disturbances (δ) on the basic state solutions, neglecting δ^2 and higher order terms and then using the usual normal mode form to express infinitesimal disturbances of corresponding field variables, and eliminating pressure terms from the resulting equations, the linearized stability equations become

$$Da\left[\frac{d^4\hat{u}}{dx^4}-2(\alpha^2+\beta^2)\frac{d^2\hat{u}}{dx^2}+(\alpha^2+\beta^2)^2\hat{u}\right]-\frac{i\alpha}{Va}\left(\frac{1}{\epsilon}V_0-c\right)\left[\frac{d^2\hat{u}}{dx^2}-(\alpha^2+\beta^2)\hat{u}\right]$$
$$+\frac{i\alpha}{\epsilon Va}\frac{d^2V_0}{dx^2}\hat{u}-\left[\frac{d^2\hat{u}}{dx^2}-(\alpha^2+\beta^2)\hat{u}\right]-i\alpha Ra\frac{d\hat{T}_{\rm f}}{dx}+i\alpha Rn\frac{d\hat{\phi}}{dx}=0, \quad (8.24)$$

$$\frac{\beta}{\epsilon Va}\frac{dV_0}{dx}\hat{u}+\frac{i\alpha}{Va}\left(\frac{1}{\epsilon}V_0-c\right)\hat{\eta}-Da\left[\frac{d^2\hat{\eta}}{dx^2}-(\alpha^2+\beta^2)\hat{\eta}\right]+\hat{\eta}-\beta Ra\hat{T}_{\rm f}+\beta Rn\hat{\phi}=0, \quad (8.25)$$

$$\frac{1}{\epsilon}\frac{dT_{\rm f0}}{dx}\hat{u}+i\alpha(\frac{1}{\epsilon}V_0-c)\hat{T}_{\rm f}-\left[\frac{d^2\hat{T}_{\rm f}}{dx^2}-(\alpha^2+\beta^2)\hat{T}_{\rm f}\right]-\frac{N_{\rm B}}{Le}\left(\frac{d\phi_0}{dx}+2N_{\rm A}\frac{dT_{\rm f0}}{dx}\right)\frac{d\hat{T}_{\rm f}}{dx}$$
$$-\frac{N_{\rm B}}{Le}\frac{dT_{\rm f0}}{dx}\frac{d\hat{\phi}}{dx}-N_{\rm HP}(\hat{T}_{\rm p}-\hat{T}_{\rm f})-N_{\rm HS}(\hat{T}_{\rm s}-\hat{T}_{\rm f})=0, \quad (8.26)$$

$$\frac{1}{\epsilon}\frac{dT_{\rm p0}}{dx}\hat{u}+i\alpha(\frac{1}{\epsilon}V_0-c)\hat{T}_{\rm p}-\varepsilon_{\rm P}\left[\frac{d^2\hat{T}_{\rm p}}{dx^2}-(\alpha^2+\beta^2)\hat{T}_{\rm p}\right]-\gamma_{\rm P}N_{\rm HP}(\hat{T}_{\rm f}-\hat{T}_{\rm p})=0, \quad (8.27)$$

$$i\alpha c\hat{T}_{\rm s}+\varepsilon_{\rm S}\left[\frac{d^2T_{\rm s}}{dx^2}-(\alpha^2+\beta^2)\hat{T}_{\rm s}\right]+\gamma_{\rm S}N_{\rm HS}(\hat{T}_{\rm f}-\hat{T}_{\rm s})=0, \quad (8.28)$$

$$\frac{1}{\epsilon}\frac{d\phi_0}{dx}\hat{u}+i\alpha\left(\frac{1}{\epsilon}V_0-c\right)\hat{\phi}-\frac{1}{Le}\left[\frac{d^2\hat{\phi}}{dx^2}-(\alpha^2+\beta^2)\hat{\phi}\right]-\frac{N_{\rm A}}{Le}\left[\frac{d^2\hat{T}_{\rm f}}{dx^2}-(\alpha^2+\beta^2)\hat{T}_{\rm f}\right]=0, \quad (8.29)$$

where $\hat{\mathbf{u}}(x)=(\hat{u},\hat{v},\hat{w})$ and $\hat{\eta}=\beta\hat{v}-\alpha\hat{w}$.
The associated conditions on the boundary are

$$\hat{u}=\frac{d\hat{u}}{dx}=\hat{\eta}=\hat{T}_{\rm f}=\hat{T}_{\rm p}=\hat{T}_{\rm s}=\hat{\phi}=0 \quad \text{at} \quad x=\mp 1. \quad (8.30)$$

8.5 Results and discussion

The system of Eqs. (8.24)-(8.29) along with Eq. (8.30) form a generalized eigenvalue problem with complex disturbance wave speed as the eigenvalue and solved using Chebyshev spectral collocation method ([27]).

To examine the convergence, the least stable eigenvalues are calculated by switching the number of grid points (N) and tabulated them in the Table 8.1 for arbitrarily chosen values of governing parameters. This table shows that the least stable eigenvalue achieve convergence requirement of 10^{-7} for $N \geq 51$. The results are consistent for increasing values of N. The same tendency has been observed for other governing parameter values. As a result, the numerical computations have been performed with $N = 51$.

The results obtained from the present analysis are verified by comparing with the published results of channel flow with equal temperatures at the walls and in the absence of a porous medium for local thermal equilibrium. The critical Reynolds number Re_{c} and critical wavenumber α_{c} for the isothermal channel are obtained as $Re_{\mathrm{c}} = 3848.278$ (in this paper $1/Pr$) and $\alpha_{\mathrm{c}} = 1.0205$ from the present analysis by setting $Ra = 0$, $Rn = 0$, $Da = 10^6$, $\beta = 0$, $\epsilon = 1$, $N_{\mathrm{A}} = 0$, $N_{\mathrm{B}} = 0$, $Le = 10^7$, $N_{\mathrm{HP}} = 0$, $N_{\mathrm{HS}} = 0$, $\varepsilon_{\mathrm{P}} = 1$ and $\varepsilon_{\mathrm{S}} = 1$. These values are in good agreement with those given by Orszag [84].

The effect of LTNE state on the instability mechanism studied in a vertical channel filled with nanofluid saturated porous medium. The flow is governed by fourteen parameters, namely, $Ra, Rn, Da, Pr, \varepsilon, N_{\mathrm{A}}, N_{\mathrm{B}}, Le$ (related to LTE state), N_{HP}, N_{HS}, γ_{P}, γ_{S}, ε_{P} and ε_{S} namely, inter-phase heat transfer parameters N_{HP} and N_{HS}, modified thermal capacity ratios γ_{P} and γ_{S} and modified thermal diffusivity ratios ε_{P} and ε_{S} are also added in the governing parameters list.

As the number of parameters are more, the analysis is simplified to focus on the effect of LTNE parameters only. Therefore the LTE parameters fixed at $Da = 0.5$, $Pr = 7$, $Rn = 10$, $\epsilon = 0.6$, $N_{\mathrm{A}} = 8$, $N_{\mathrm{B}} = 0.02$ and $Le = 100$ for the rest of discussions. The dimension of the least stable mode is studied by computing the critical Rayleigh number for integer and non-integer values of spanwise wavenumber (β) in the $(N_{\mathrm{HP}}, Ra_{\mathrm{c}})$ and $(N_{\mathrm{HS}}, Ra_{\mathrm{c}})$-planes and presented in Fig. 8.1. From this figure, it is clarified that the computational results conform the Squire's theorem [104] for LTNE state, i.e., least stable mode is two dimensional. Therefore, in the entire section, β has been taken to zero.

The variation of critical Rayleigh number (Ra_{c}) and critical wavenumber (α_{c}) calculated as functions of Nield numbers N_{HP} and N_{HS} for different LTNE parameters and plotted in Figs. 8.2–8.7. Since, an increase in the values of N_{HP} and N_{HS} rises the heat-release from fluid to solid and fluid to nanoparticle or vice-versa, respectively, the variation of Rayleigh number is significant up to a certain value of N_{HP} or N_{HS} and further than that all the three phases have nearly the identical temperatures and operate as a single phase, i.e., local thermal equilibrium state will be attained. This is because, the temperature differ by an

amount which is of order 1/(inter-phase heat transfer parameters) when $N_{\mathrm{HP}} \to \infty$ and $N_{\mathrm{HS}} \to \infty$.

The influence of N_{HP} and N_{HS} on the critical Rayleigh number Ra_{c} and critical wavenumber wavenumber α_{c} with is presented Figs. 8.2 and 8.3 for different values of Nield numbers for fluid/solid-matrix and fluid/particle inter-phases, respectively. Fig. 8.2(a) indicates that the critical Rayleigh number reduces with N_{HP}, but rises due to the rising effect of N_{HS}. The same characteristic of Ra_{c} has been observed in the Fig. 8.3(a) for the impact of inter-phase heat transfer parameters. Further, it is observed that the variation of Ra_{c} is insignificant when N_{HP} and N_{HS} are very small. This is happening because, at $N_{\mathrm{HP}} \to 0, N_{\mathrm{HS}} \to 0$, i.e., occurrence of heat transfer between fluid/nanoparticle and fluid/solid-matrix inter-phases are almost zero. Thus, the convective instability does not affected in this situation. Also, it is recognized that the variation of the critical Rayleigh number is almost uniform when $N_{\mathrm{HP}} \to \infty$ and $N_{\mathrm{HS}} \to \infty$. Therefore, the system behaves like LTE state for both the limiting cases for N_{HP} and N_{HS}. Further, it is distinguished that the system converges to destabilize for the intermediate values of N_{HP}, while opposite nature for the system has been recorded for the intermediate values of N_{HS}. After that, the variation of critical wavenumber are displayed in Figs. 8.2(b) and 8.3(b) for the effect of N_{HP} and N_{HS}, respectively. We observe that alternation of α_{c} is almost negligible when $N_{\mathrm{HP}} \to 0$ and $N_{\mathrm{HS}} \to 0$, and when $N_{\mathrm{HP}} \to \infty$ and $N_{\mathrm{HS}} \to \infty$. Therefore, α_{c} approaches to its LTE value for both the limiting case, i.e., $N_{\mathrm{HP}} \to 0, N_{\mathrm{HS}} \to 0$ and $N_{\mathrm{HP}} \to \infty, N_{\mathrm{HS}} \to \infty$. It is noticed that α_{c} decreases firstly up to certain value of N_{HP} and after that it increases very quickly in the intermediate value of N_{HP}, as shown Fig. 8.2(b). This is may be happen due to the domination of heat transfer of fluid/ particle by fluid/solid-matrix. But, α_{c} decreases monotonically in the intermediate value of N_{HS}, as displayed in Fig. 8.3(b). Further noticed that, α_{c} decreases with N_{HS}, while reverse trends has been noted for the effect of N_{HP}.

Figs. 8.4 and 8.5 are presented the impact of modified thermal capacity ratios, γ_{P} and γ_{S} on the critical Rayleigh number and corresponding wavenumber with inter-phase heat transfer parameters by fixing the other governing parameters. It is noticed that Ra_{c} increases with γ_{P} as shown in Figs. 8.4(a) and 8.4(b), while it decreases with γ_{S} as portrayed in Figs. 8.5(a) and 8.5(b). Thus, γ_{P} has a stabilizing effect, while the system is destabilize due to the rising effect of γ_{S}. Also, α_{c} increases with γ_{P} as pictured in Figs. 8.4(c) and 8.4(d), while it has dual nature for the effect of γ_{S} as captured in Figs. 8.5(c) and 8.5(d).

The influence of the modified thermal diffusivity ratios, ε_{P} and ε_{S}, on Ra_{c} and corresponding α_{c} are depicted in the Figs. 8.6 and 8.7 with inter-phase heat transfer parameters, respectively. It is seen that Ra_{c} increases with the modified thermal diffusivity ratios except

in the plane (N_{HP}, Ra_{c}) as displayed in Fig. 8.7(a). This may be the reason that the impact of ε_{S} does not affect the instability boundary when the system absorbed more heat between fluid/particle inter-phase as compared with fluid/solid-matrix inter-phase. The corresponding wavenumber increases with the enhancing values of the modified thermal diffusivity ratios, as shown in Figs. 8.6(c)–8.6(d) and 8.7(c)–8.7(d).

The impact of Nield number N_{HP} on the instability boundary curve in Figs. 8.2 and 8.4–8.7 are more highlighted by means of the plots of eigenfunctions at the critical position and Fig. 8.8 presents the eigenfunctions for $N_{\mathrm{HP}} = 1, 10$ and 100 at $\gamma_{\mathrm{P}} = 0.04$, $\gamma_{\mathrm{S}} = 0.01$, $\varepsilon_{\mathrm{P}} = 0.7$, $\varepsilon_{\mathrm{S}} = 0.2$ and $N_{\mathrm{HS}} = 50$. From the figures, it is observed that magnitude of the eigenfunctions for the velocities are more than the magnitude of the eigenfunctions for the all three temperature phases and volume fraction. It is noticed from the Figs. 8.8(a), 8.8(b), 8.8(d) and 8.8(e) that magnitude of the eigenfunctions of the velocities disturbances in the x-direction, y-direction and temperature disturbances for fluid and solid phases, respectively, decreases when N_{HP} increases. Also, magnitude of the eigenfunctions of the temperature disturbances for fluid phase increases when N_{HP} increases as displayed in Fig. 8.8(c). But, the variation of the magnitude of the eigenfunctions of volume fraction are almost negligible due to the effect N_{HP}, as depicted in Fig. 8.8(f).

The influence of Nield number N_{HS} on the instability boundary curve in Figs. 8.3–8.7 are more enlightened by means of the plots of eigenfunctions at the critical position and Fig. 8.9 presents the eigenfunctions for $N_{\mathrm{HS}} = 1, 10$ and 100 at $\gamma_{\mathrm{P}} = 0.04$, $\gamma_{\mathrm{S}} = 0.01$, $\varepsilon_{\mathrm{P}} = 0.7$, $\varepsilon_{\mathrm{S}} = 0.2$ and $N_{\mathrm{HP}} = 100$. Here also, it is observed that magnitude of the eigenfunctions for the velocities are more than the magnitude of the eigenfunctions for the all three temperature phases and volume fraction. It is noticed from the Figs. 8.9(a), 8.9(b) and 8.9(e) that magnitude of the eigenfunctions of the velocities disturbances in the x-direction, y-direction and temperature disturbances for solid phase, respectively, increases when N_{HP} increases. Also, magnitude of the eigenfunctions of the temperature disturbances for fluid and particle phases decreases when N_{HP} increases as displayed in Figs. 8.9(c) and 8.9(d). But, the variation of the magnitude of the eigenfunctions of volume fraction are almost negligible due to the effect N_{HP}, as depicted in Fig. 8.9(f).

Apart from the variations of critical Ra and critical α_{c} with different parameters, to understand the dynamics of the flow field and behaviour of the patterns of temperature and volume fraction are demonstrated by means of the contour plots of streamlines, isotherms and isonanoconcentration at critical level is plotted in Figs. 8.10–8.11 with different values of inter-phase heat transfer parameters or Nield numbers N_{HP} and N_{HS} for fixed values of other parameters $\gamma_{\mathrm{P}} = 0.04$, $\gamma_{\mathrm{S}} = 0.01$, $\varepsilon_{\mathrm{P}} = 0.7$ and $\varepsilon_{\mathrm{S}} = 0.2$.

In the case of streamline contour, the positive contours are concomitant with clockwise rotation, whereas, the negative contours are concerned with anti-clockwise rotation and for the case isotherms and isonanoconcentrations contour, solid lines indicate the positive contours while dashed line exhibits the negative contours.

Fig. 8.10 illustrates the pattern of streamlines, isotherms and isonanoconcentrations for various values of N_{HP} for $N_{\mathrm{HS}} = 50$ over one period. From Figs. 8.10(a)–8.10(c), it is observed that the flow is mainly controlled (two asymmetric cells), where one cell (primary cell) is rotating clockwise direction and the other cell (secondary cell) is rotating anticlockwise direction. The shape of the inner cells of this bi-cellular structure is changing with the increasing values of the heat transfer parameter for fluid/nanoparticle inter-phase. Further, it is noticed that the primary cell pushes the secondary cell in upwards direction in the vertical channel as the value of N_{HP} increases. The pattern of the isotherms for fluid, nanoparticle and solid-matrix phases are almost the same over a period for all values of N_{HP} shown in Figs. 8.10(d)–8.10(l). This is because the transfer of the temperature receives mainly by diffusion, indicating to disturbances into flow configuration. The isonanoconcentration lines for the flow in a vertical channel are depicted in Figs. 8.10(m)–8.10(o) and shows that a two-cell structure is spreading in the middle portion of the channel over a period for different values of N_{HP}. Also, we did not observe any significant variation in the isonanoconcentration pattern due to the effect of N_{HP}. Further, it is noticed that the size of the convective cells reduces as the inter-phase heat transfer parameter for fluid/nanoparticle rises.

The influence of the fluid/solid-matrix inter-phase Nield number (N_{HS}) in the pattern of streamlines, isotherms and isonanoconcentrations for $N_{\mathrm{HP}} = 100$ is displayed in Fig. 8.11 over a period. From Figs. 8.11(a)–8.11(c), it is noticed that the flow is controlled by bi-cellular patterns where one cell (primary cell) has full structure but another one (secondary cell) has half structure. It is noticed that the streamline pattern looks like moving downwards the vertical channel as the value of N_{HS} enhances due to variation of critical eigenvalue value. The shape of the inner cells in each of the bi-cellular structure is changed with increasing the potency of the heat transfer parameter for fluid/solid-matrix phases. The pattern of the isotherms for fluid, nanoparticle and solid-matrix phases are portrayed in Figs. 8.11(d)–8.11(l) are looking like shifting downwards in the vertical channel N_{HS} increases. Since, the transmission of the disturbance temperature occurs primarily by diffusion, directing to a more stable flow configuration. The variation of the isonanoconcentration contours is plotted in Figs. 8.11(g)-8.11(i) and observed that patterns are dense at the middle portion of the channel. The magnitude of the stream function, isotherms and isonanoconcentration reduce indicating the system becoming more stable with augmenting the value of N_{HS}.

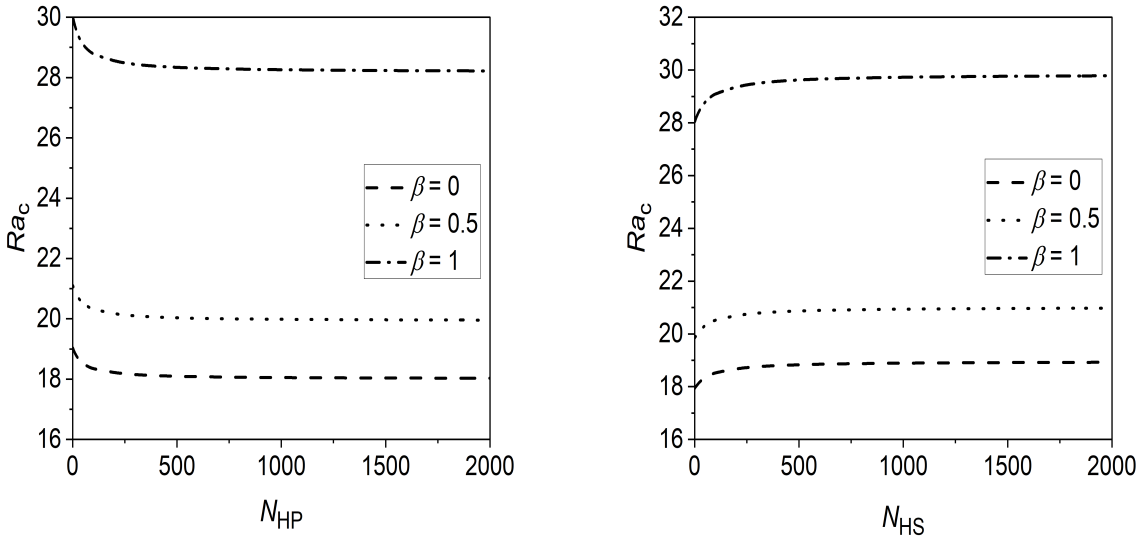

(a) (b)

Figure 8.1: Instabilities boundaries in (a) $(N_{\rm HP}, Ra_{\rm c})$-plane at $N_{\rm HS} = 50$ and (b) $(N_{\rm HS}, Ra_{\rm c})$-plane at $N_{\rm HP} = 100$ for different values of β when $\gamma_{\rm P} = 0.04$, $\gamma_{\rm S} = 0.01$, $\varepsilon_{\rm P} = 0.7$ and $\varepsilon_{\rm S} = 0.2$.

Table 8.1: Convergence of the eigenvalue for least stable mode by Chebyshev collocation method. Here $Da = 0.5$, $Pr = 7$, $Ra = 20$, $Rn = 10$, $\epsilon = 0.6$, $N_{\rm A} = 8$, $N_{\rm B} = 0.02$, $Le = 100$, $N_{\rm HP} = 100$, $N_{\rm HS} = 200$, $\varepsilon_{\rm P} = 0.7$, $\varepsilon_{\rm S} = 0.2$, $\gamma_{\rm P} = 0.08$, $\gamma_{\rm S} = 0.03$, $\alpha = 1$ and $\beta = 0$.

N	Least stable mode
20	1.381714977153-0.001363069077i
25	1.382332575796-0.001675627942i
30	1.382331740470-0.001669739266i
40	1.382331654595-0.001669726083i
45	1.382331990285-0.001669694091i
50	1.382331733296-0.001669754193i
51	1.382331725969-0.001669747977i
55	1.382331722677-0.001669748729i
60	1.382331726960-0.001669749819i

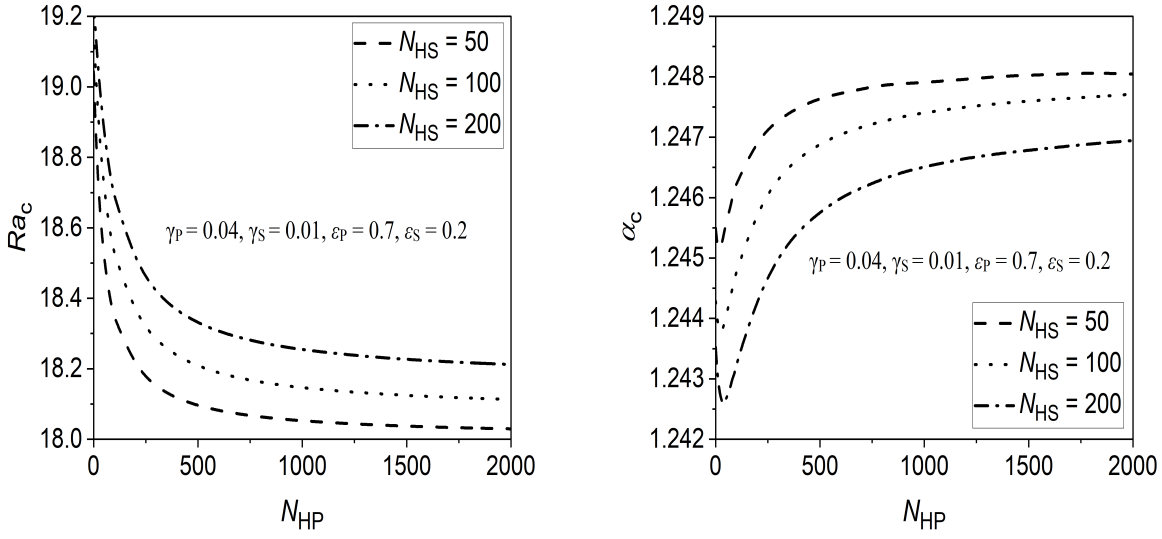

(a) (b)

Figure 8.2: Influence of N_{HS} on instability boundaries in (a) $(N_{\mathrm{HP}}, Ra_{\mathrm{c}})$-plane and (b) $(N_{\mathrm{HP}}, \alpha_{\mathrm{c}})$-plane.

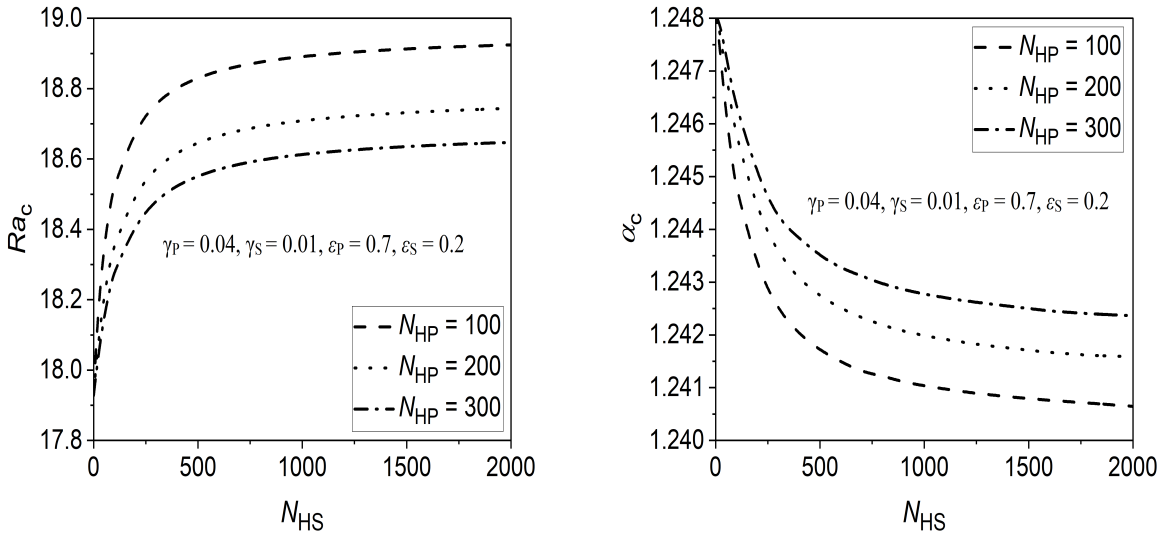

(a) (b)

Figure 8.3: Influence of N_{HP} on instability boundaries in (a) $(N_{\mathrm{HS}}, Ra_{\mathrm{c}})$-plane and (b) $(N_{\mathrm{HS}}, \alpha_{\mathrm{c}})$-plane.

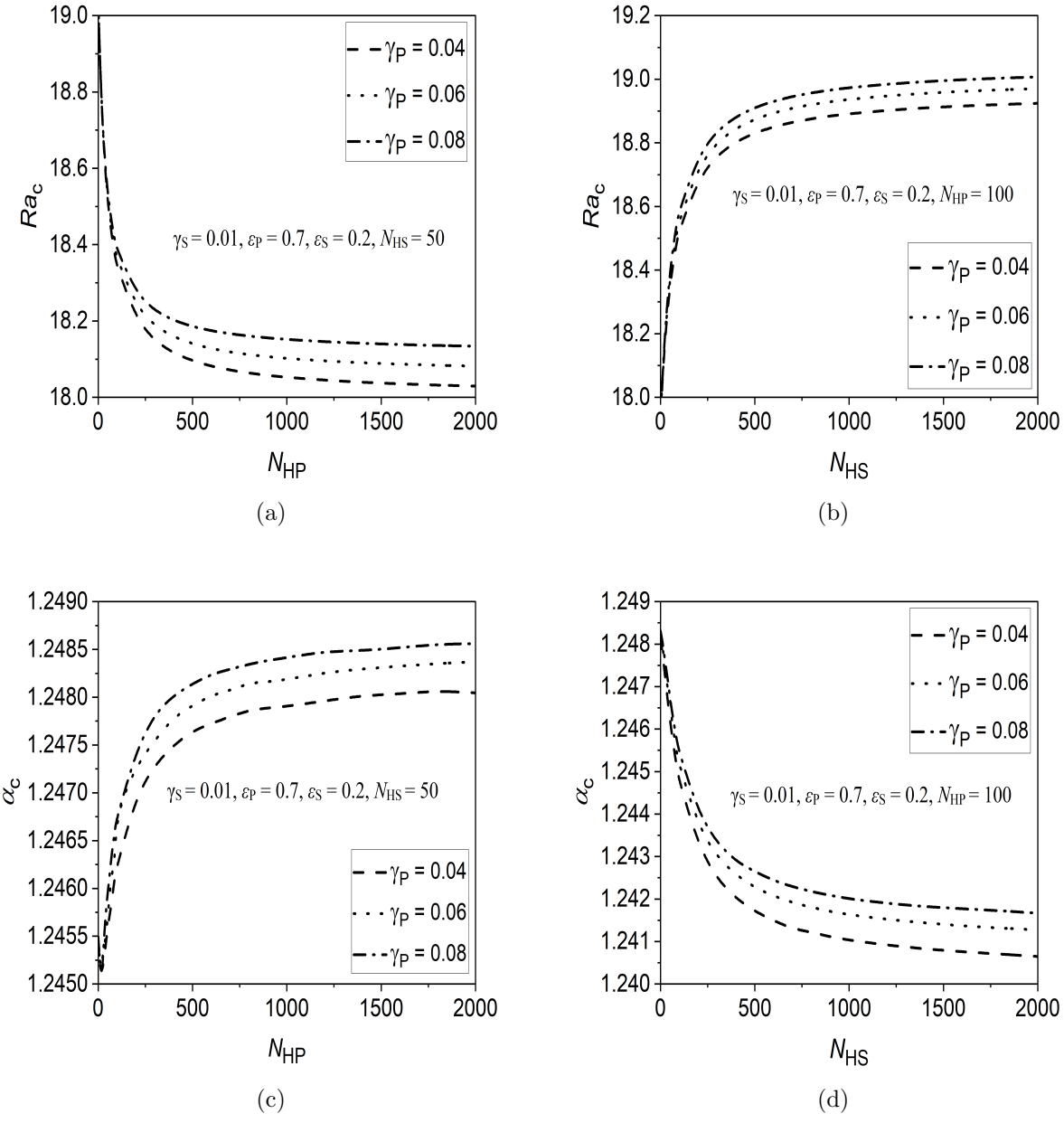

Figure 8.4: Influence of γ_{P} on instability boundaries in (a) $(N_{\mathrm{HP}}, Ra_{\mathrm{c}})$-plane, (b) $(N_{\mathrm{HS}}, Ra_{\mathrm{c}})$-plane, (c) $(N_{\mathrm{HP}}, \alpha_{\mathrm{c}})$-plane and, (d) $(N_{\mathrm{HS}}, \alpha_{\mathrm{c}})$-plane.

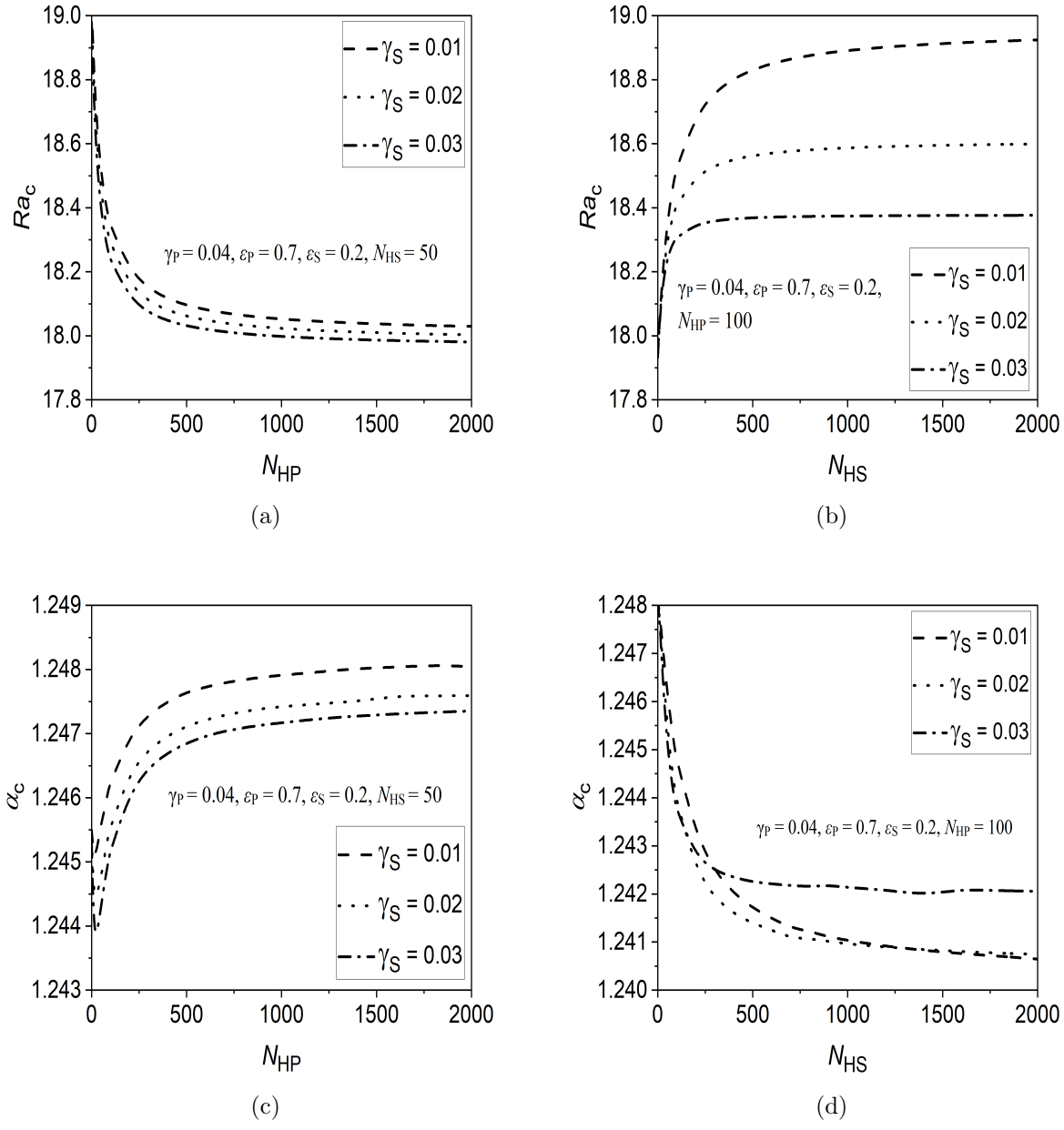

Figure 8.5: Influence of γ_S on instability boundaries in (a) (N_{HP}, Ra_c)-plane, (b) (N_{HS}, Ra_c)-plane, (c) (N_{HP}, α_c)-plane and, (d) (N_{HS}, α_c)-plane.

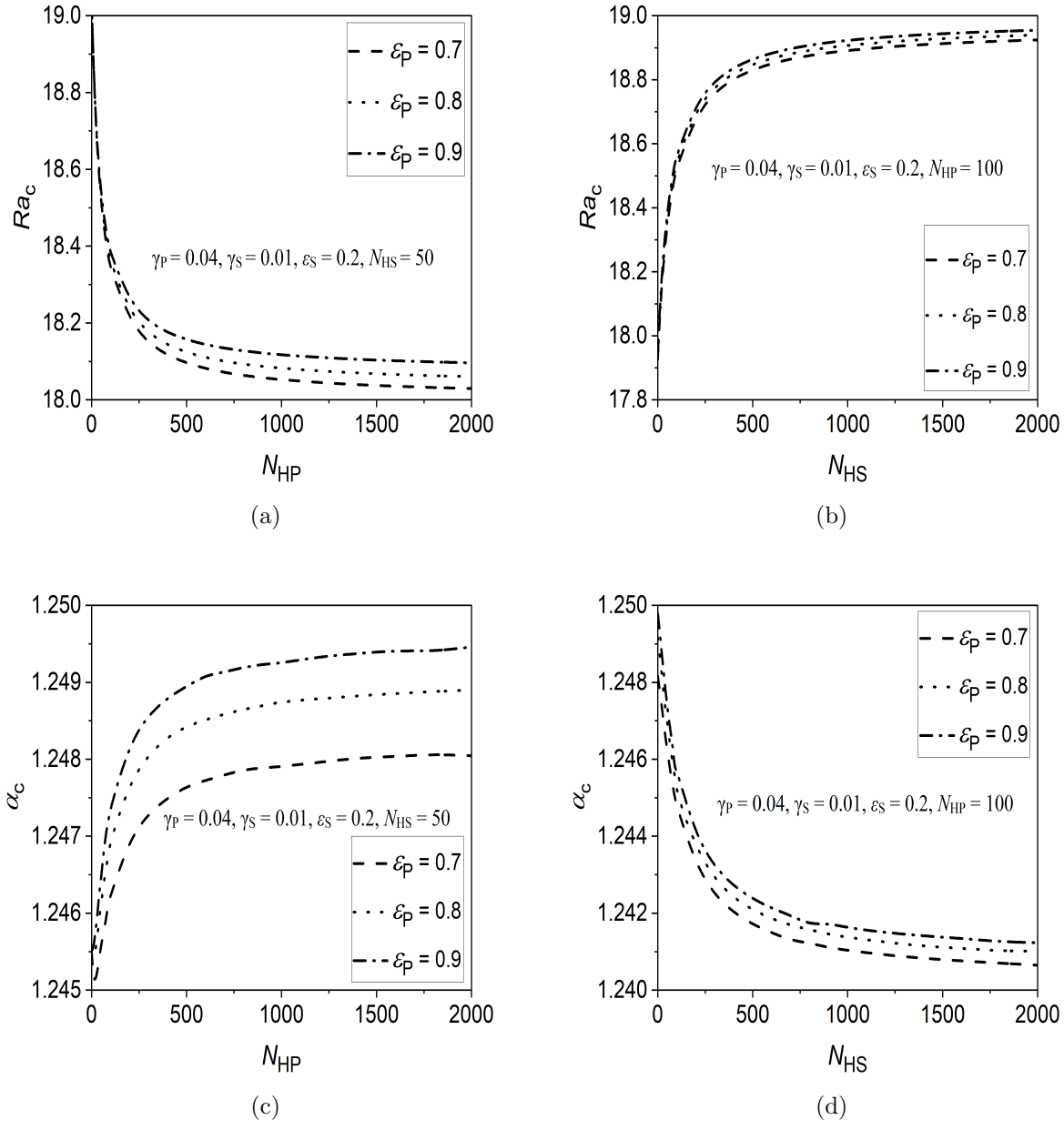

Figure 8.6: Influence of ε_{P} on instability boundaries in (a) $(N_{\mathrm{HP}}, Ra_{\mathrm{c}})$-plane, (b) $(N_{\mathrm{HS}}, Ra_{\mathrm{c}})$-plane, (c) $(N_{\mathrm{HP}}, \alpha_{\mathrm{c}})$-plane and, (d) $(N_{\mathrm{HS}}, \alpha_{\mathrm{c}})$-plane.

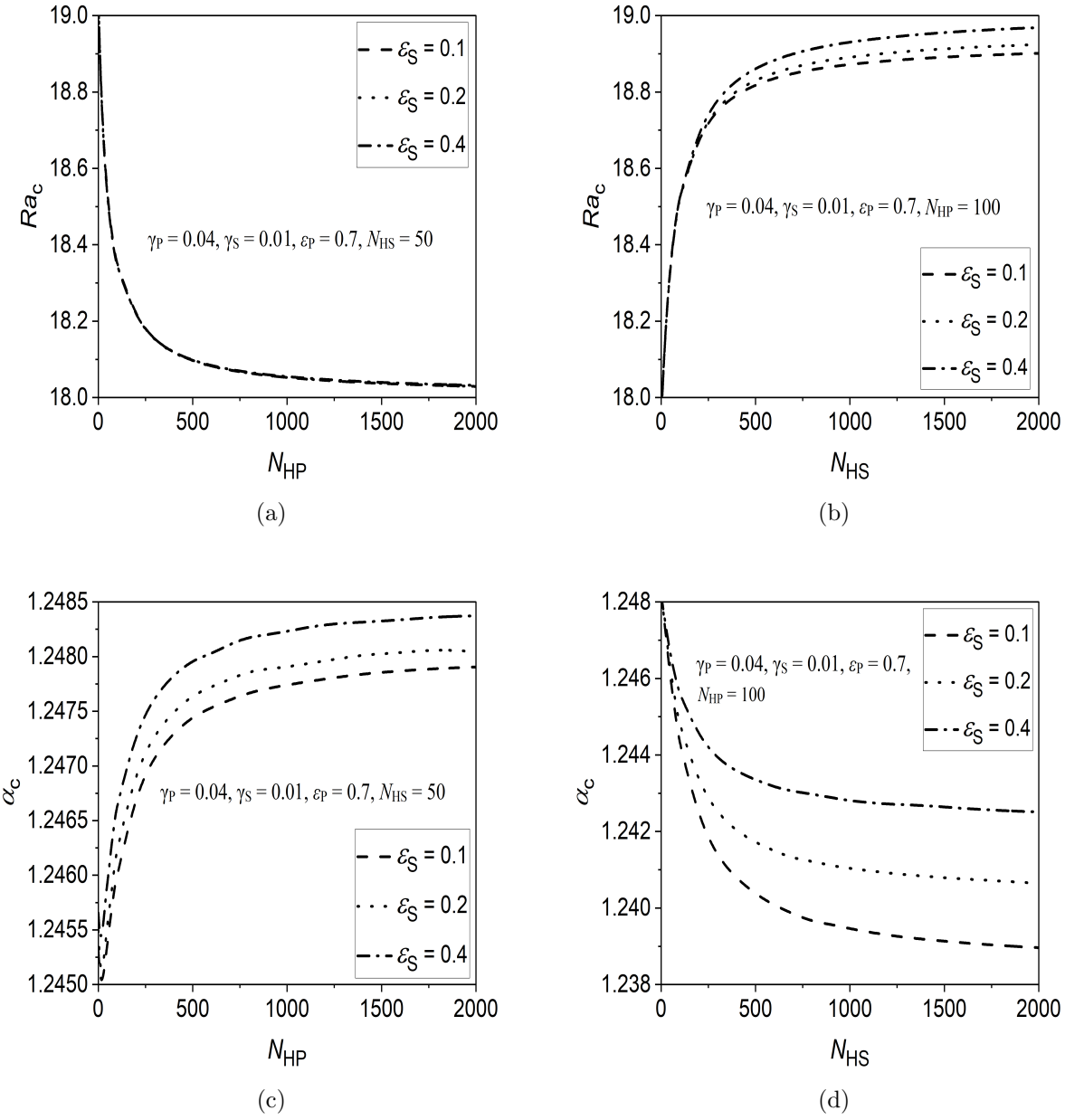

Figure 8.7: Influence of ε_S on instability boundaries in (a) (N_{HP}, Ra_c)-plane, (b) (N_{HP}, α_c)-plane, (c) (N_{HS}, Ra_c)-plane and, (d) (N_{HS}, α_c)-plane.

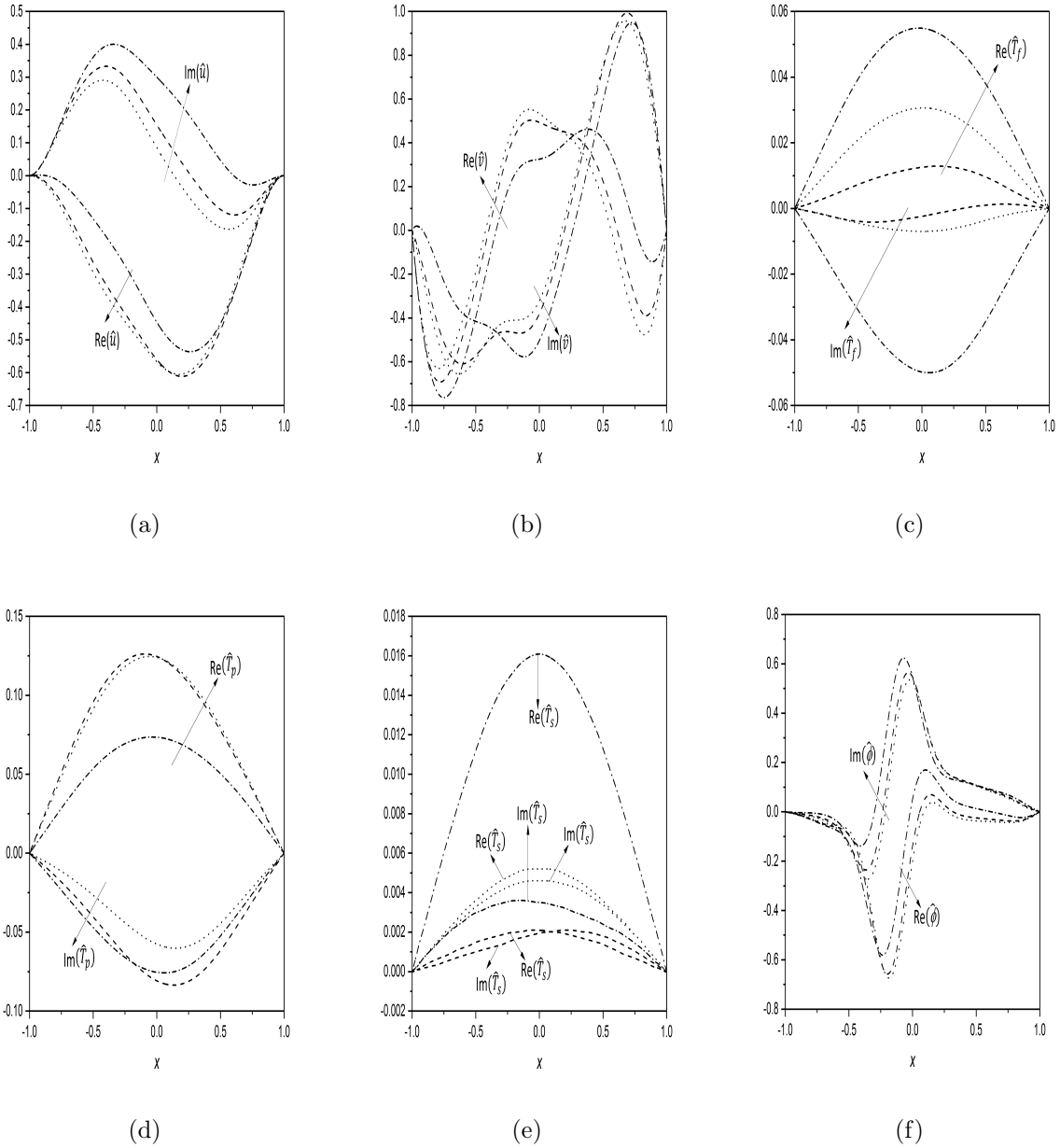

Figure 8.8: Eigenfunctions of (a) $\hat{u}$, (b) $\hat{v}$, (c) $\hat{T}_{\rm f}$, (d) $\hat{T}_{\rm p}$, (e) $\hat{T}_{\rm s}$ and (f) $\hat{\phi}$ for $N_{\rm HP} = 1$ ('--'), $N_{\rm HP} = 10$ ('$\cdots$') and $N_{\rm HP} = 100$ ('-·-') when $\gamma_{\rm P} = 0.04$, $\gamma_{\rm S} = 0.01$, $\varepsilon_{\rm P} = 0.7$, $\varepsilon_{\rm S} = 0.2$ and $N_{\rm HS} = 50$.

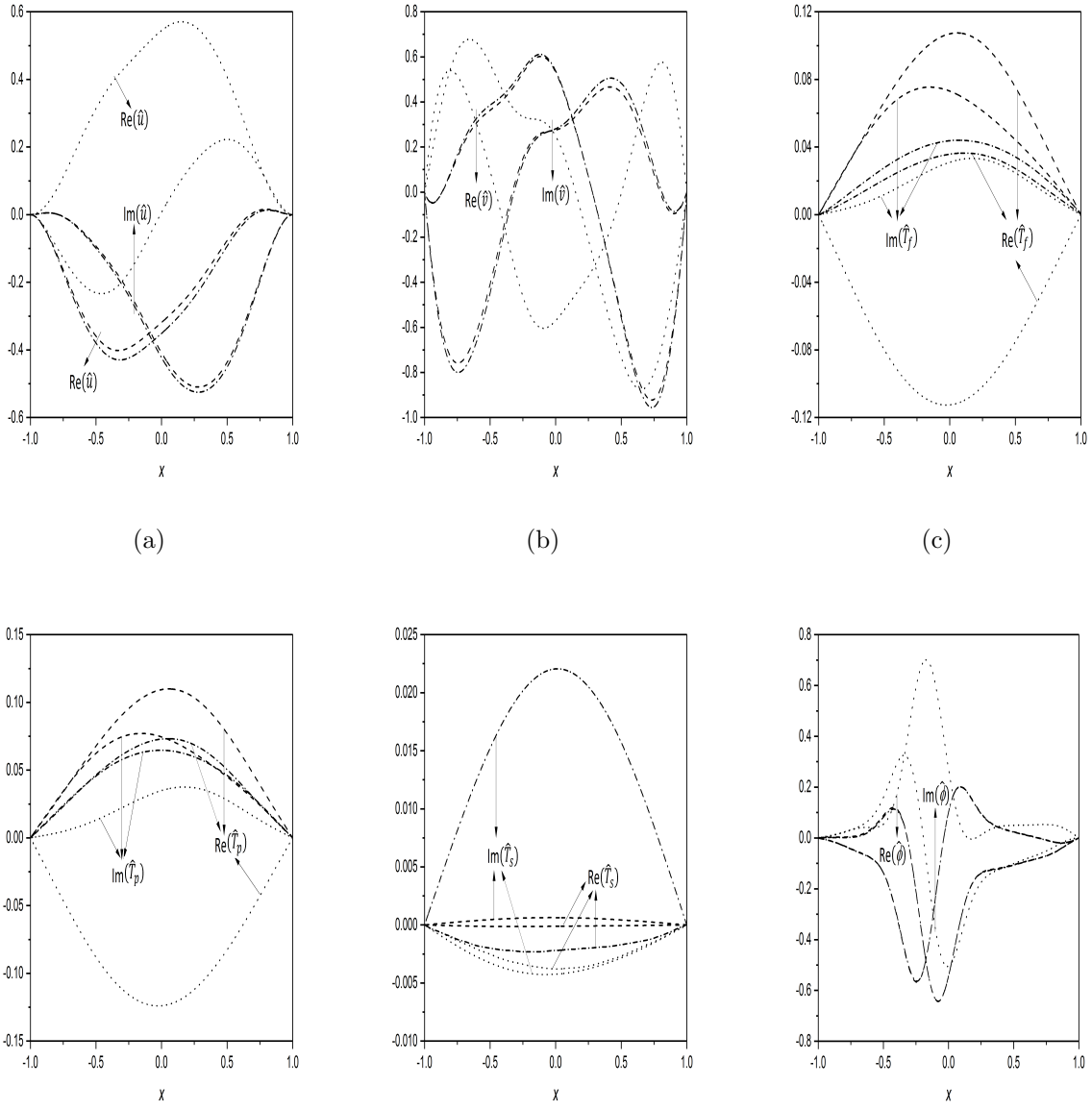

(a) (b) (c)

(d) (e) (f)

Figure 8.9: Eigenfunctions of (a) $\hat{u}$, (b) $\hat{v}$, (c) $\hat{T}_{\rm f}$, (d) $\hat{T}_{\rm p}$, (e) $\hat{T}_{\rm s}$ and (f) $\hat{\phi}$ for $N_{\rm HS} = 1$ ('- -'), $N_{\rm HS} = 10$ ('$\cdots$') and $N_{\rm HS} = 100$ ('-·-') when $\gamma_{\rm P} = 0.04$, $\gamma_{\rm S} = 0.01$, $\varepsilon_{\rm P} = 0.7$, $\varepsilon_{\rm S} = 0.2$ and $N_{\rm HP} = 100$.

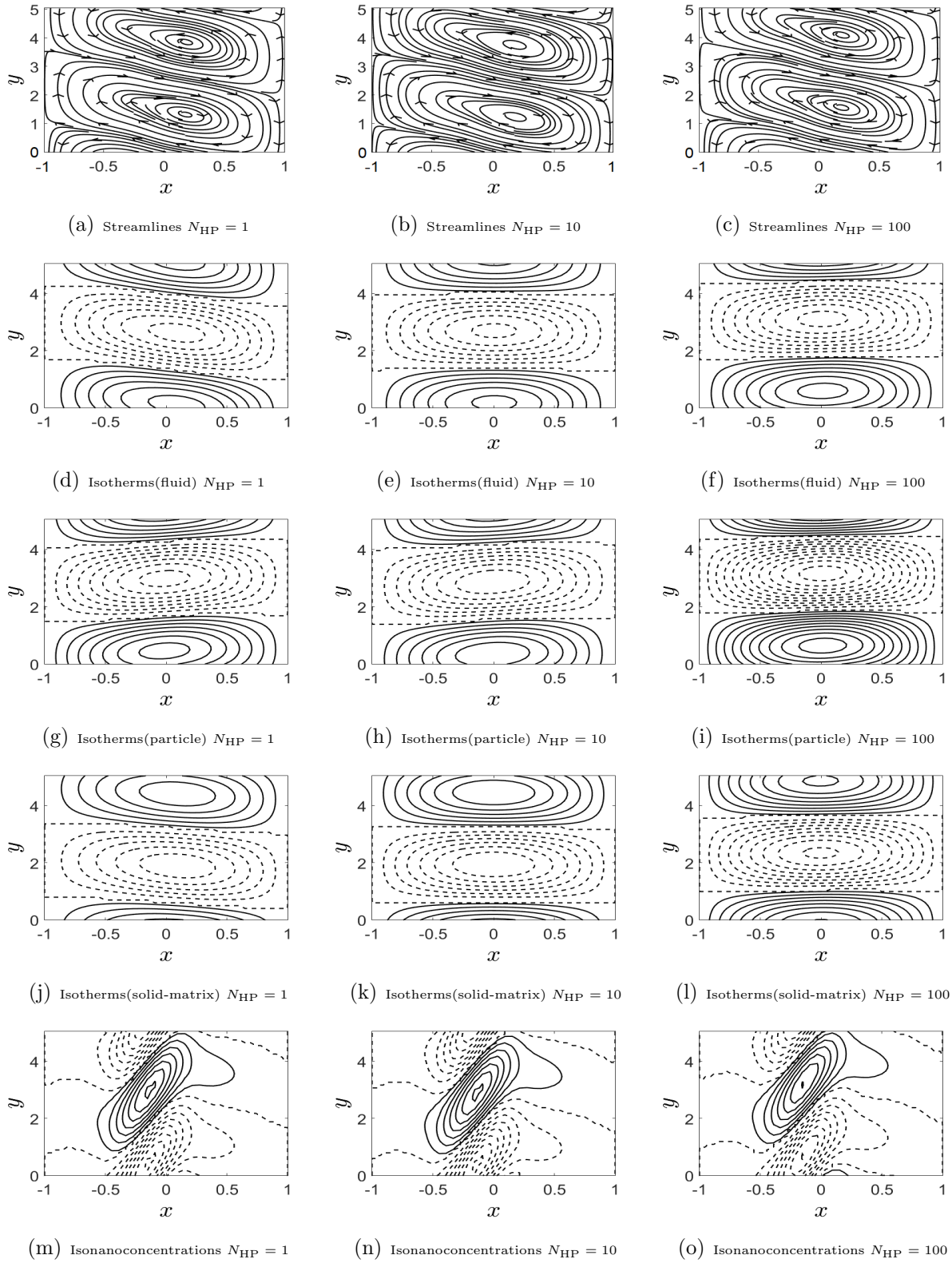

(a) Streamlines $N_{\mathrm{HP}} = 1$ (b) Streamlines $N_{\mathrm{HP}} = 10$ (c) Streamlines $N_{\mathrm{HP}} = 100$

(d) Isotherms(fluid) $N_{\mathrm{HP}} = 1$ (e) Isotherms(fluid) $N_{\mathrm{HP}} = 10$ (f) Isotherms(fluid) $N_{\mathrm{HP}} = 100$

(g) Isotherms(particle) $N_{\mathrm{HP}} = 1$ (h) Isotherms(particle) $N_{\mathrm{HP}} = 10$ (i) Isotherms(particle) $N_{\mathrm{HP}} = 100$

(j) Isotherms(solid-matrix) $N_{\mathrm{HP}} = 1$ (k) Isotherms(solid-matrix) $N_{\mathrm{HP}} = 10$ (l) Isotherms(solid-matrix) $N_{\mathrm{HP}} = 100$

(m) Isonanoconcentrations $N_{\mathrm{HP}} = 1$ (n) Isonanoconcentrations $N_{\mathrm{HP}} = 10$ (o) Isonanoconcentrations $N_{\mathrm{HP}} = 100$

Figure 8.10: The disturbance of streamlines ((a) to (c)), isotherms(fluid) ((d) to (f)), isotherms(particle) ((g) to (i)), isotherms(solid) ((j) to (l)) and isonanoconcentrations ((m) to (o)) for various values of N_{HP} over one period.

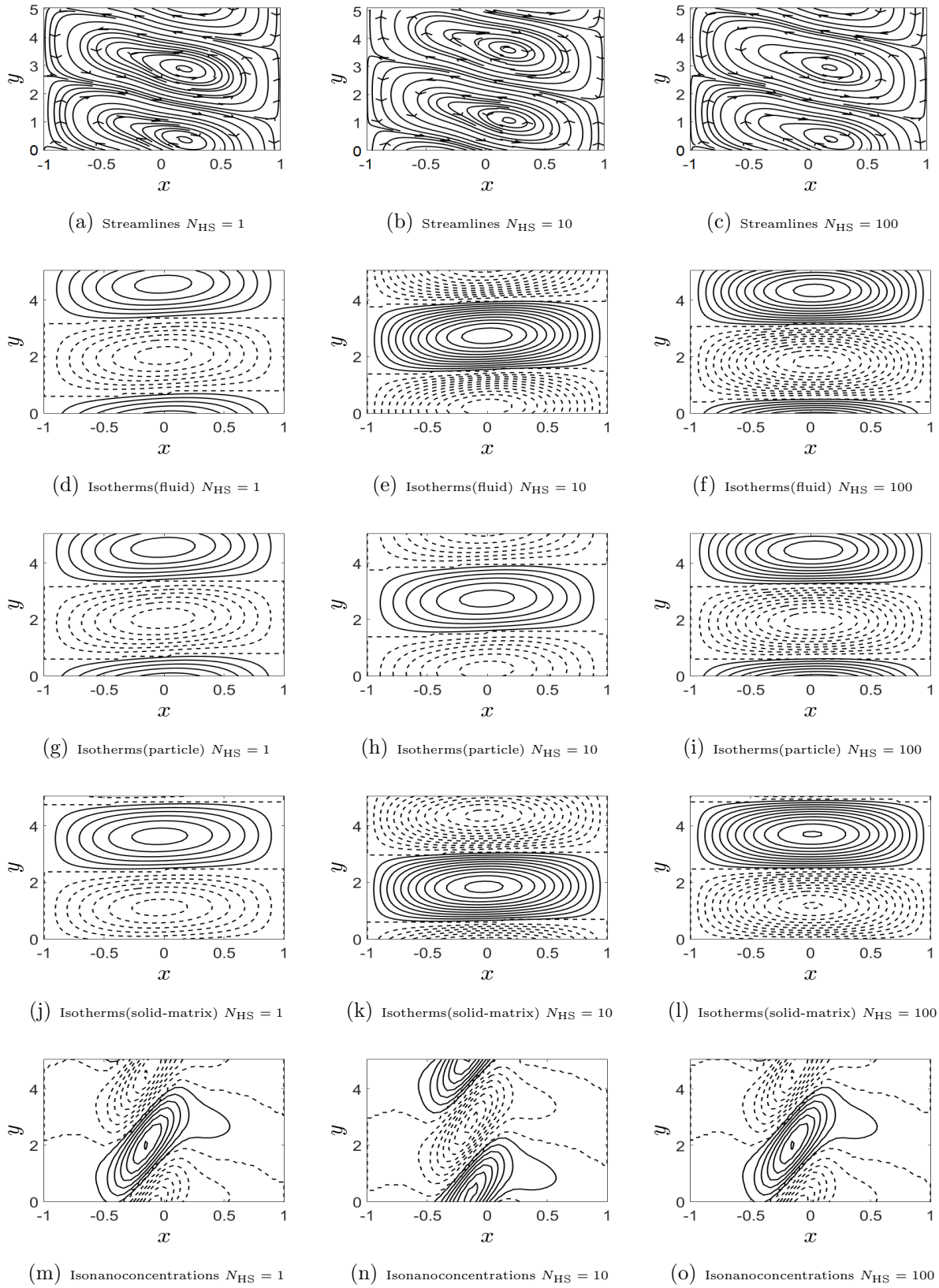

(a) Streamlines $N_{\mathrm{HS}} = 1$ (b) Streamlines $N_{\mathrm{HS}} = 10$ (c) Streamlines $N_{\mathrm{HS}} = 100$

(d) Isotherms(fluid) $N_{\mathrm{HS}} = 1$ (e) Isotherms(fluid) $N_{\mathrm{HS}} = 10$ (f) Isotherms(fluid) $N_{\mathrm{HS}} = 100$

(g) Isotherms(particle) $N_{\mathrm{HS}} = 1$ (h) Isotherms(particle) $N_{\mathrm{HS}} = 10$ (i) Isotherms(particle) $N_{\mathrm{HS}} = 100$

(j) Isotherms(solid-matrix) $N_{\mathrm{HS}} = 1$ (k) Isotherms(solid-matrix) $N_{\mathrm{HS}} = 10$ (l) Isotherms(solid-matrix) $N_{\mathrm{HS}} = 100$

(m) Isonanoconcentrations $N_{\mathrm{HS}} = 1$ (n) Isonanoconcentrations $N_{\mathrm{HS}} = 10$ (o) Isonanoconcentrations $N_{\mathrm{HS}} = 100$

Figure 8.11: The disturbance of streamlines ((a) to (c)), isotherms(fluid) ((d) to (f)), isotherms(particle) ((g) to (i)), isotherms(solid) ((j) to (l)) and isonanoconcentrations ((m) to (o)) for various values of N_{HS} over one period.

8.6 Conclusions

The impact of local thermal non-equilibrium (LTNE) state on the onset convection of nanofluid flow in a vertical porous-medium channel is investigated. The Darcy-Brinkman model for the porous medium and three medium temperature treatment has been taken for the energy equation. Stability of the flow is analysed using normal mode technique. The main observations from the obtained results are:

- The rising effect of N_{HS}, γ_{P} and ε_{P} delay the convective motion, while γ_{S} and N_{HP} give the onset convection quickly.
- Enhancing the effect of ε_{S} postpones the convection when N_{HP} dominated by N_{HS}, but in the opposite case, the effect of ε_{S} is insignificant on the convective motion. However, the destabilizing characteristic of N_{HP} and stabilizing characteristic of N_{HS} die out when they converge to zero and beyond sufficiently large values of them, where system behaves as in LTE state.
- The size of the convective cells reduces on rising the values of γ_{P}, ε_{P} and ε_{S}, while dual character has been observed for increasing values of γ_{S} and N_{HS} when N_{HS} dominates to N_{HP}, otherwise cells size increases.
- The size of the cell decreases with enhancing the value of N_{HP}, while N_{HS} is more than N_{HP}, otherwise it has a dual character on it.

Chapter 9

Local thermal non-equilibrium effect on the convective instability in a vertical channel filled with nanofluid in the presence of transverse magnetic field [1]

9.1 Introduction

The study of LTNE for nanofluid saturated porous media turns to be an important research area due to its interesting applications in Engineering and science. Several reserchers considered the stability of the fluid flow in porous layer /channel with different physical situations. Although the influence of the magnetic field on the flow of nanofluids is important, relatively little attention was paid in the literature [7, 8]. Hudoba and Molokov [59] studied the effect of internal heat sources and a transverse magnetic field of a buoyancy convective flow in a channel. Mahajan and Sharma [70] considered the effect of LTNE on the onset of convection in a magnetic nanofluid layer.

In this chapter, the stability characteristics of nanofluid flow in a vertical channel under LTNE mode for fluid and solid particle are examined. The linear disturbance equations are solved by applying the spectral method and obtained results are verified with existing results in the literature.

[1] Communicated in "***Special Topics & Reviews in Porous Medium - An international journal***"

9.2 Mathematical Formulation

Consider an unsteady, incompressible, electrically conducting nanofluid flow in a vertical channel of width $2L$ bounded by two impermeable and perfectly thermally conducting walls. Assume that the nanofluid is modelled by the Buongiorno [25] model and under LTNE mode. The coordinate system is shown in Fig. 9.1. Let $\hat{\mathbf{e}}_\mathbf{x}$, $\hat{\mathbf{e}}_\mathbf{y}$ and $\hat{\mathbf{e}}_\mathbf{z}$ be the unit vector along $x-$, $y-$ and $z-$ direction. The heat flow is described using two temperature equations model by considering the LTNE between the particle and fluid phase. Also, a uniform magnetic field $\mathbf{B}_0 = B\hat{\mathbf{e}}_\mathbf{x}$, where B is the strength of the magnetic field, is applied normal to the channel. The assumption that the neglect of induced magnetic field in comparison with the applied magnetic field gives the magnetic Reynolds to be small. With these assumptions, the governing equations are

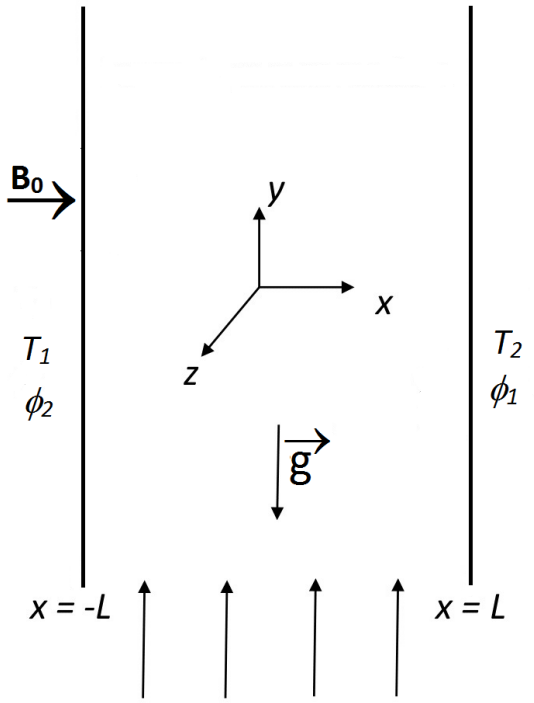

Figure 9.1: Graphical representation of the problem.

$$\nabla \cdot \mathbf{v} = 0, \tag{9.1}$$

$$\rho_{\rm f}\left[\frac{\partial \mathbf{v}}{\partial t}+(\mathbf{v}\cdot\nabla)\mathbf{v}\right]=-\nabla p+\tilde{\mu}\nabla^2\mathbf{v}+\mathbf{j}\times\mathbf{B_0}+[\phi\rho_{\rm p}+(1-\phi)\rho_{\rm f}\{1-\beta_{\rm T}(T_{\rm f}-T_1)\}]\mathbf{g}, \quad (9.2)$$

$$(\rho c)_{\rm f}\left[\frac{\partial T_{\rm f}}{\partial t}+\mathbf{v}\cdot\nabla T_{\rm f}\right]=k_{\rm f}\nabla^2 T_{\rm f}+(\rho c)_{\rm p}\left[D_{\rm B}\nabla\phi\cdot\nabla T_{\rm f}+\frac{D_{\rm T}}{T_2}\nabla T_{\rm f}\cdot\nabla T_{\rm f}\right]+\frac{h_{\rm fp}}{(1-\phi_1)}(T_{\rm p}-T_{\rm f}), \quad (9.3)$$

$$(\rho c)_{\rm p}\left[\frac{\partial T_{\rm p}}{\partial t}+\mathbf{v}\cdot\nabla T_{\rm p}\right]=k_{\rm p}\nabla^2 T_{\rm p}+\frac{h_{\rm fp}}{\phi_1}(T_{\rm f}-T_{\rm p}), \quad (9.4)$$

$$\frac{\partial \phi}{\partial t}+\mathbf{v}\cdot\nabla\phi=D_{\rm B}\nabla^2\phi+\frac{D_{\rm T}}{T_2}\nabla^2 T_{\rm f}, \quad (9.5)$$

where $\mathbf{v}(=(u,v,w))$ is the nanofluid velocity vector and other quantities are defined in previous chapters.

The conditions on the walls of the channel are

$$\mathbf{v}=0, \quad T_{\rm f}=T_1, \quad T_{\rm p}=T_1, \quad \phi=\phi_2 \quad \text{at} \quad x=-L, \quad (9.6a)$$

$$\mathbf{v}=0, \quad T_{\rm f}=T_2, \quad T_{\rm p}=T_2, \quad \phi=\phi_1 \quad \text{at} \quad x=L. \quad (9.6b)$$

Substituting Eq. (8.8) in the governing Eqs. (9.1)-(9.5) and the boundary conditions Eq. (9.6) and dropping tildes, we get

$$\nabla\cdot\mathbf{v}=0, \quad (9.7)$$

$$\frac{1}{Pr}\left[\frac{\partial \mathbf{v}}{\partial t}+(\mathbf{v}\cdot\nabla)\mathbf{v}\right]=-\nabla p+\Lambda\nabla^2\mathbf{v}+Ha^2(\mathbf{v}\times\hat{\mathbf{e}}_{\mathbf{x}})\times\hat{\mathbf{e}}_{\mathbf{x}}+RaT_{\rm f}\hat{\mathbf{e}}_{\rm y}-Rn\phi\hat{\mathbf{e}}_{\rm y}-Rm\hat{\mathbf{e}}_{\rm y}, \quad (9.8)$$

$$\frac{\partial T_{\rm f}}{\partial t}+\mathbf{v}\cdot\nabla T_{\rm f}=\nabla^2 T_{\rm f}+\frac{N_{\rm B}}{Le}\nabla\phi\cdot\nabla T_{\rm f}+\frac{N_{\rm A}N_{\rm B}}{Le}\nabla T_{\rm f}\cdot\nabla T_{\rm f}+N_{\rm HP}(T_{\rm p}-T_{\rm f}), \quad (9.9)$$

$$\frac{\partial T_{\rm p}}{\partial t}+\mathbf{v}\cdot\nabla T_{\rm p}=\varepsilon_{\rm P}\nabla^2 T_{\rm p}+\gamma_{\rm P}N_{\rm HP}(T_{\rm f}-T_{\rm p}), \quad (9.10)$$

$$Le\left[\frac{\partial \phi}{\partial t}+\mathbf{v}\cdot\nabla\phi\right]=\nabla^2\phi+N_{\rm A}\nabla^2 T_{\rm f}, \quad (9.11)$$

$$\mathbf{v}=0, \quad T_{\rm f}=0, \quad T_{\rm p}=0, \quad \phi=1 \quad \text{at} \quad x=-1, \quad (9.12a)$$

$$\mathbf{v}=0, \quad T_{\rm f}=1, \quad T_{\rm p}=1, \quad \phi=0 \quad \text{at} \quad x=1, \quad (9.12b)$$

where $\gamma_{\rm P}=\dfrac{(1-\phi_1)}{\phi_1}\dfrac{(\rho c)_{\rm f}}{(\rho c)_{\rm p}}$ is the modified thermal capacity ratio, and $\varepsilon_{\rm P}=\frac{\alpha_{\rm p}}{\alpha_{\rm f}}$ is the thermal diffusivity ratio. The remaining parameters are already defined in the previous chapters.

9.3 Basic state solution

In the basic state, the flow is considered to be steady, unidirectional and fully developed and the corresponding form are as mentioned in the previous chapter. With these considerations, the Eqs. (9.7)-(9.11) reduce to

$$\frac{d^2V_0}{dx^2} - Ha^2V_0 = \frac{dp_0}{dy} - RaT_{\mathrm{f0}} + Rn\phi_0 + Rm, \tag{9.13}$$

$$\frac{d^2T_{\mathrm{f0}}}{dx^2} + \frac{N_{\mathrm{B}}}{Le}\frac{d\phi_0}{dx}\frac{dT_{\mathrm{f0}}}{dx} + \frac{N_{\mathrm{A}}N_{\mathrm{B}}}{Le}\left(\frac{dT_{\mathrm{f0}}}{dx}\right)^2 + N_{\mathrm{HP}}(T_{\mathrm{p0}} - T_{\mathrm{f0}}) = 0, \tag{9.14}$$

$$\varepsilon_{\mathrm{P}}\frac{d^2T_{\mathrm{p0}}}{dx^2} + \gamma_{\mathrm{P}}N_{\mathrm{HP}}(T_{\mathrm{f0}} - T_{\mathrm{p0}}) = 0, \tag{9.15}$$

$$\frac{d^2\phi_0}{dx^2} + N_{\mathrm{A}}\frac{d^2T_{\mathrm{f0}}}{dx^2} = 0. \tag{9.16}$$

Following Chapter - 8, the basic state solutions are given by

$$T_{\mathrm{f0}} \;=\; T_{\mathrm{p0}} \;=\; \frac{1+x}{2} \quad \text{and} \quad \phi_0 = \frac{1-x}{2}, \tag{9.17}$$

$$V_0 = r\left[1 - \frac{\cosh(Hax)}{\cosh(Ha)}\right] + \frac{(Ra+Rn)}{2Ha^2}\left[x - \frac{\sinh(Hax)}{\sinh(Ha)}\right], \tag{9.18}$$

where $r = Ha\left(\dfrac{\sinh(2Ha)}{Ha(\sinh(2Ha)) - \cosh(2Ha) + 1}\right)$.

9.4 Linear stability analysis

As in Chapter - 6, imposing the infinitesimal disturbances (δ) on the basic state solutions, neglecting δ^2 and higher order terms and then using the usual normal mode form to express infinitesimal disturbances of corresponding field variables, and eliminating pressure terms from the resulting equations, the linearized stability equations become

$$\left[\frac{d^4\hat{u}}{dx^4} - 2(\alpha^2+\beta^2)\frac{d^2\hat{u}}{dx^2} + (\alpha^2+\beta^2)^2\hat{u}\right] - \frac{i\alpha V_0}{Pr}\left[\frac{d^2\hat{u}}{dx^2} - (\alpha^2+\beta^2)\hat{u}\right] + \frac{i\alpha}{Pr}\frac{d^2V_0}{dx^2}\hat{u}$$
$$-Ha^2\frac{d^2\hat{u}}{dx^2} - i\alpha Ra\frac{d\hat{T}_{\mathrm{f}}}{dx} + i\alpha Rn\frac{d\hat{\phi}}{dx} = -\frac{i\alpha c}{Pr}\left[\frac{d^2\hat{u}}{dx^2} - (\alpha^2+\beta^2)\hat{u}\right], \tag{9.19}$$

$$\frac{\beta}{Pr}\frac{dV_0}{dx}\hat{u} + \frac{i\alpha V_0}{Pr}\hat{\eta} - \left[\frac{d^2\hat{\eta}}{dx^2} - (\alpha^2+\beta^2)\hat{\eta}\right] + Ha^2\hat{\eta} - \beta Ra\hat{T}_{\mathrm{f}} + \beta Rn\hat{\phi} = \frac{i\alpha c}{Pr}\hat{\eta}, \tag{9.20}$$

$$\frac{dT_{\mathrm{f0}}}{dx}\hat{u} + i\alpha V_0 \hat{T}_{\mathrm{f}} - \left[\frac{d^2\hat{T}_{\mathrm{f}}}{dx^2} - (\alpha^2+\beta^2)\hat{T}_{\mathrm{f}}\right] - \frac{N_{\mathrm{B}}}{Le}\frac{dT_{\mathrm{f0}}}{dx}\left(\frac{d\hat{\phi}}{dx} + 2N_{\mathrm{A}}\frac{d\hat{T}_{\mathrm{f}}}{dx}\right) - \frac{N_{\mathrm{B}}}{Le}\frac{d\phi_0}{dx}\frac{d\hat{T}_{\mathrm{f}}}{dx}$$
$$-N_{\mathrm{HP}}(\hat{T}_{\mathrm{p}} - \hat{T}_{\mathrm{f}}) = i\alpha c\hat{T}_{\mathrm{f}}, \qquad (9.21)$$

$$\frac{dT_{\mathrm{p0}}}{dx}\hat{u} + i\alpha V_0 \hat{T}_{\mathrm{p}} - \varepsilon_{\mathrm{P}}\left[\frac{d^2\hat{T}_{\mathrm{p}}}{dx^2} - (\alpha^2+\beta^2)\hat{T}_{\mathrm{p}}\right] - \gamma_{\mathrm{P}}N_{\mathrm{HP}}(\hat{T}_{\mathrm{f}} - \hat{T}_{\mathrm{p}}) = i\alpha c\hat{T}_{\mathrm{p}}, \qquad (9.22)$$

$$\frac{d\phi_0}{dx}\hat{u} + i\alpha V_0\hat{\phi} - \frac{1}{Le}\left[\frac{d^2\hat{\phi}}{dx^2} - (\alpha^2+\beta^2)\hat{\phi}\right] - \frac{N_{\mathrm{A}}}{Le}\left[\frac{d^2\hat{T}_{\mathrm{f}}}{dx^2} - (\alpha^2+\beta^2)\hat{T}_{\mathrm{f}}\right] = i\alpha c\hat{\phi}, \qquad (9.23)$$

where $\hat{\eta} = \beta\hat{v} - \alpha\hat{w}$ and $\hat{\mathbf{v}} = (\hat{u}, \hat{v}, \hat{w})$.

The associated boundary conditions are

$$\hat{u} = \frac{d\hat{u}}{dx} = \hat{\eta} = \hat{T}_{\mathrm{f}} = \hat{T}_{\mathrm{p}} = \hat{\phi} = 0 \quad \text{at} \quad x = \mp 1. \qquad (9.24)$$

9.5 Results and discussion

The system of differential equations (9.19)-(9.23) together with Eq. (9.24) form a generalized eigenvalue problem with $c = c_r + ic_i$ as the eigenvalue. This eigenvalue problem is solved using spectral collocation method.

To check the convergence, the least stable eigenvalues are computed varying the number of collocation points (N) as 10, 20, 30, 40, 45, 50, 51, 55 and 60 as shown in Table 9.1. In each case, we found very good agreement between them. The same tendency is witnessed by changing the values of the parameters. Hence, a grid size of $N = 51$ is adopted to be satisfactory for the convergence criterion of 10^{-7}.

The results obtained from the current study are checked by comparing the published channel flow results for the local thermal equilibrium state. The critical Reynolds number Re_{c} and critical wavenumber α_{c} for the isothermal channel are obtained as $Re_{\mathrm{c}} = 3848.278$ (in this paper $1/Pr$) and $\alpha_{\mathrm{c}} = 1.0205$ from the current study by taking $Ra = 0$, $Rn = 0$, $Ha = 0$, $\beta = 0$, $\varepsilon_{\mathrm{P}} = 1$, $N_{\mathrm{A}} = 0$, $N_{\mathrm{B}} = 0$, $Le = 10^7$, $N_{\mathrm{HP}} = 0$. These values are well in line with those given by Orszag [84].

The influence of local thermal non-equilibrium (LTNE) state on the instability mechanism studied in a vertical channel filled with nanofluid. The computations are carried out by taking the viscosity ratio $\Lambda = 1$ and Prandtl number $\mathrm{Pr} = 7$. The critical values of Ra and α have

been represented by Ra_c and α_c, respectively, throughout this section, and the variations of them with different values of the governing parameters is shown on the (N_{HP}, Ra_c) and (N_{HP}, α_c)-planes . Further, it is observed that the two dimensional mode is most unstable for convective motion as shown in Fig. 9.2. Therefore, in the entire section, $\beta = 0$ has been taken.

Fig. 9.3 represents the comparative neutral stability curves for different states of fluid. It is observed that Rayleigh number Ra is less in the case of non-equilibrium mode than equilibrium mode as shown in Fig. 9.3(a). Which indicates that LTNE mode is found to quick the onset of convective motion than LTE mode. This observation can be explained by the fact that the energy transfer occurs between fluid and particle phases due to the temperature difference between them. Also, from Fig. 9.3(b), it is noticed that Ra is less for nanofluids than clear fluids, or to say convection postpones in clear fluids than nanofluids. Therefore, Fig. 9.3 exhibits that onset of convection sets in earlier when the nanofluids is an under LTNE mode.

The influence of the magnetic paramter Ha, concentration Rayleigh number Rn, the thermal diffusivity ratio ε_P, the modified thermal capacity ratio γ_P, the inter-phase heat transfer parameter (Nield number) N_{HP}, Lewis number Le and the modified diffusivity ratio N_A on the neutral stability curves for the least stable mode is depicted in Fig. 9.4. It is evident from Figs. 9.4(a), 9.4(c), 9.4(d) and 9.4(f) that, an increase in the Ha, ε_P, γ_P, and Le leads to an increase in the Rayleigh number Ra. With an increase in these parameters, the stability area increases. Hence, these parameters stabilizes the system. Similarly, it is perceived from Figs. 9.4(b), 9.4(e) and 9.4(g) that the Rayleigh number Ra is decreasing for increasing values of Rn, N_{HP} and N_A. The influence of N_B on the Rayleigh number is almost insignificant as shown in the Fig. 9.4(h). The variation of critical Rayleigh number (Ra_c) and the corresponding critical wavenumber (α_c) calculated as function of inter-phase heat transfer parameter or Nield numbers (N_{HP}) for various values of the governing parameters and plotted in Figs. 9.5–9.10. Since it is to be noted that the increase of N_{HP} intensifies the heat release from the nanoparticle to fluid or from the fluid to nanoparticles . Therefore, the variance of Rayleigh number is assumed to be significant up to a certain value of N_{HP}, beyond that they have almost the same temperatures and behave as a single phase, i.e. it will achieve local thermal equilibrium state. This is because, the temperature differ by an amount which is of order 1/(inter-phase heat transfer parameter) when $N_{HP} \to \infty$. The values of the parameters are taken as $Ha = 1$, $Rn = 15$, $Le = 50$, $N_A = 8$, $N_B = 0.2$ and $\gamma_P = 0.01$ unless and otherwise specified.

The variation of critical Rayleigh number Ra_c and corresponding wavenumber α_c with

Nield number N_{HP} are presented Figs. 9.5 and 9.6 for different values of Hartmann number Ha and concentration Rayleigh number Rn, respectively. Figs. 9.5(a) and 9.6(a) indicate that the critical Rayleigh number is decreasing with N_{HP}. Further, it is observed that the variation of Ra_{c} is insignificant when N_{HP} is very small. This is happening because, at $N_{\mathrm{HP}} \to 0$, i.e., occurrence of heat transfer between fluid/nanoparticle inter-phase is almost zero. Thus, the convective instability does not affected in this situation. Also, it is recognized that the variation of the critical Rayleigh number is almost uniform when $N_{\mathrm{HP}} \to \infty$. Therefore, the system behaves like LTE state for both the limiting case of N_{HP}. Also, the same trend has been observed for all the critical plots. Further, it is distinguished that the system shows a destabilizing nature for the intermediate values of N_{HP}. Also, Ra_{c} increases with an increased values of Ha indicates that Ha has a stabilizing effect in the flow field as shown in Fig. 9.5(a). Since the applied magnetic field is perpendicular to the direction of flow, there is a tendency to produce a drag called the Lorentz force. As a consequence, the system uses a great deal of energy to overcome this resistance and thus delays convection, giving rise to a stabilizing effect. Thus magnetic field can be effectively used to regulate convection of nanofluid in a channel flow. On the other hand, it has been observed that the convection comes earlier due to the rising effect of Rn and it displayed in Fig. 9.6(a). After that, the variation of critical wavenumber are displayed in Figs. 9.5(b) and 9.6(b) for the effect of Ha and Rn, respectively. We observe that alternation of α_{c} is almost negligible when $N_{\mathrm{HP}} \to 0$, and $N_{\mathrm{HP}} \to \infty$. Therefore, α_{c} approaches to its LTE value for both the limiting case, i.e., $N_{\mathrm{HP}} \to 0$ and $N_{\mathrm{HP}} \to \infty$. It is noticed that α_{c} increases quickly in the intermediate value of N_{HP} and beyond that it has a uniform nature. Also, it has been seen that α_{c} increase with Hartmann number (Ha) and concentration Rayleigh number (Rn) in the case of LTNE mode.

The influence of the thermal diffusivity ratio ε_{P} and modified thermal capacity ratio γ_{P}, on Ra_{c} and corresponding α_{c} are depicted in the Figs. 9.7 and 9.8 with inter-phase heat transfer parameter, respectively. It is noticed that Ra_{c} increases with ε_{P} and γ_{P} as shown in Figs. 9.7(a) and 9.8(a), respectively. Thus, ε_{P} and γ_{P} have a stabilizing effect on the flow field under non-equilibrium mode. Also, α_{c} decreases with ε_{P} and γ_{P} as pictured in Figs. 9.7(b) and 9.8(b). Thus, the size of the convective cells increase with the enhancing values of ε_{P} and γ_{P}.

Figs. 9.9 and 9.10 are presented the impact of Lewis number Le and modified diffusivity ratio N_{A} on the critical Rayleigh number and corresponding wavenumber with inter-phase heat transfer parameter by fixing the other governing parameters. It is noticed that Ra_{c} increases with Le, while it decreases with N_{A} as shown in Figs. 9.9(a) and 9.10(a), respec-

tively. Thus, convection sets delay due to the rising effect of Lewis number, while it comes earlier for the enhanced value of modified diffusivity ratio in the LTNE mode. Also, the dimension of the convective cells decrease with the increased values of Le and N_{A}.

The impact of inter-phase heat transfer parameter N_{HP} on the instability boundary curves in Figs. 9.5–9.10 could be further enlightened through the plots of eigenfunctions $\hat{u}$, $\hat{v}$, $\hat{T}_{\mathrm{f}}$, $\hat{T}_{\mathrm{p}}$ and $\hat{\phi}$ at the critical position. In Fig. 9.11 represents the disturbance eigenfunction curve for $N_{\mathrm{HP}} = 10, 100$ and 1000 at $Ha = 1, Rn = 15, \varepsilon_{\mathrm{P}} = 0.04, \gamma_{\mathrm{P}} = 0.01, Le = 50, N_{\mathrm{A}} = 8, N_{\mathrm{B}} = 0.2$. The figures reveal that the magnitude of the eigenfunctions for the velocities is greater than the magnitude of the eigenfunctions for the fluid phase temperature, the particle phase temperature, and the volume fraction. We observed that the magnitude of the eigenfunction for the temperatures disturbance for fluid phase and particle phase and the volume fraction disturbance increase with N_{HP} increases, while it shows a decreasing nature for the velocity disturbance of the x-axis and y-axis. Also, we have examined the the variations of eigenfunctions in the absence and presence of the magnetic parameter in Fig. 9.12. It is observed that the magnitude of the eigenfunctions decrease with the rising effect of magnetic field.

In addition to the variations of Ra_{c} and α_{c} with governing parameters, the contour plots of streamlines, isotherms and isonanoconcentration at the critical level for various values of inter-phase heat transfer parameter (N_{HP}) and magnetic parameter (Ha) are shown in Figs. 9.13 and 9.14 by fixing the other governing parameters are at $Ha = 1, Rn = 15, Le = 50, \varepsilon_{\mathrm{P}} = 0.04, \gamma_{\mathrm{P}} = 0.01$, $N_{\mathrm{A}} = 8$ and $N_{\mathrm{B}} = 0.2$. The positive contours are associated with clockwise rotation in the case of streamline contour, while the negative contours are associated with anti-clockwise rotation. The solid lines indicate the positive values for isotherms and isonanoconcentration contours, while the negative values are shown by the dotted line.

The pattern of streamlines, isotherms and isonanoconcentrations for various values of N_{HP} are shown in the Fig. 9.13 for $Ha = 1$ over a period. From Figs. 9.13(a)–9.13(c), The flow is mainly regulated by bi-cellular structure i.e. two asymmetric cells, where one cell (primary cell) rotates clockwise and the other cell (secondary cell) rotates clockwise. The form of the inner contour of this bi-cellular configuration is modified by enhancing the value of the heat transfer parameter N_{HP}. As shown in Figs. 9.13(d)–9.13(i), the isotherm cells are mainly belongs to the right part of the channel for all values of N_{HP}, while only shiffting arrangement has been seen with alternation of the inter-phase heat transfer parameter. This is because the transfer of the temperature receives mainly by diffusion, indicating to disturbances into flow configuration. Further noticed that the patterns of the isotherms for fluid and particle

phases are same when $N_{\mathrm{HP}} = 1000$, which indicates that temperature phases are coinciding in a single phase as N_{HP} takes higher value. The isonanoconcentration contours for the flow are depicted in Figs. 9.13(j)—9.13(l) and shows that for different values of N_{HP}, the two-cell configuration moves to the right wall of the channel over a period. In addition, it is noted that with an enhancement of N_{HP}, the dimension of the isonanoconcentration cells reduces.

Further, we have drawn the patterns of the contours in the absence and presence of magnetic effect over a period when $N_{\mathrm{HP}} = 10$. Here also, it is noticed that the streamline disturbances of the primary and secondary cells are moving along the y-direction as shown in Figs. 9.14(a)–9.14(c). Also, it is seen in Figs. 9.14(d)–9.14(l) that isotherms and isonanoconcentrations contours are shifting towards the right wall of the channel.

Table 9.1: Convergence of the least stable eigenvalue by Chebyshev collocation method. Here $Ha = 1.2$, $Pr = 7$, $Ra = 50$, $Rn = 12$, $\varepsilon_{\mathrm{P}} = 0.05$, $\gamma_{\mathrm{P}} = 0.001$, $Le = 30$, $N_{\mathrm{A}} = 4$, $N_{\mathrm{B}} = 0.007$, $N_{\mathrm{HP}} = 100$, $\alpha = 1$ and $\beta = 0$.

N (terms)	Least stable eigenvalue
10	2.842701938014-0.235831679574i
20	2.836571699188-0.237082808997i
30	2.836571686677-0.237082760143i
40	2.836571683491-0.237082753044i
45	2.836571721854-0.237082740183i
50	2.836571699924-0.237082760318i
51	2.836571715071-0.237082763647i
55	2.836571718023-0.237082765104i
60	2.836571711764-0.237082764102i

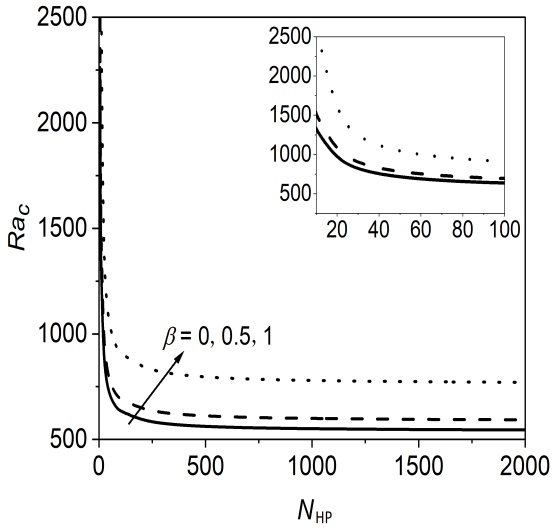

Figure 9.2: Visual representation for the effect of β on the instabilities boundary $(N_{\mathrm{HP}}, Ra_{\mathrm{c}})$-plane at $Ha = 1, Rn = 15, Le = 50, N_{\mathrm{A}} = 8,\ N_{\mathrm{B}} = 0.2,\ \varepsilon_{\mathrm{P}} = 0.04$ and $\gamma_{\mathrm{P}} = 0.01$.

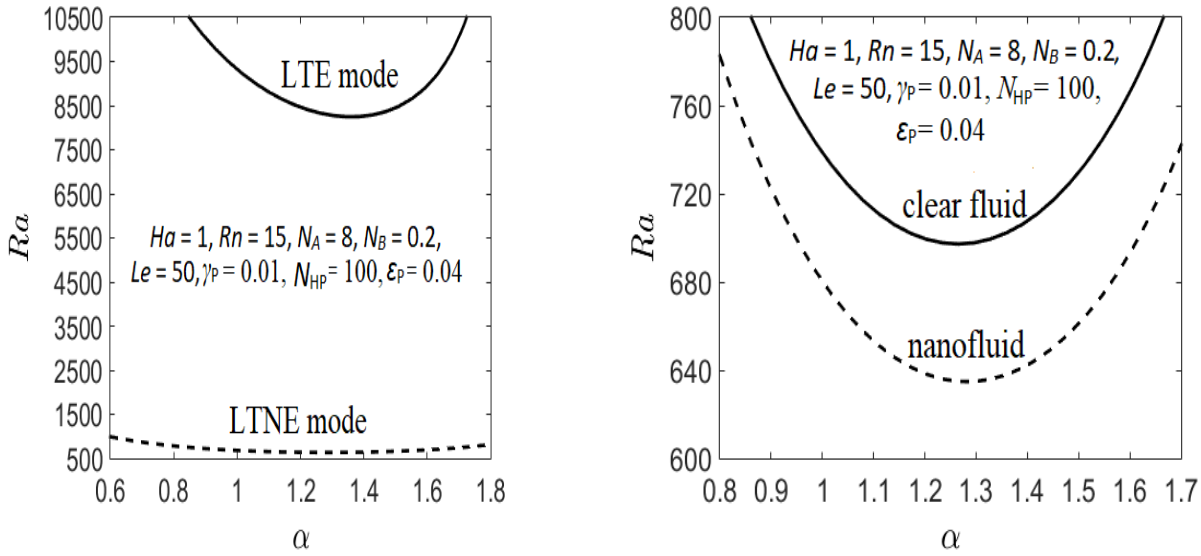

Figure 9.3: Comparisons of Rayleigh number Ra against wavenumber α for (a) LTNE mode and LTE mode and (b) clear fluid and nanofluid.

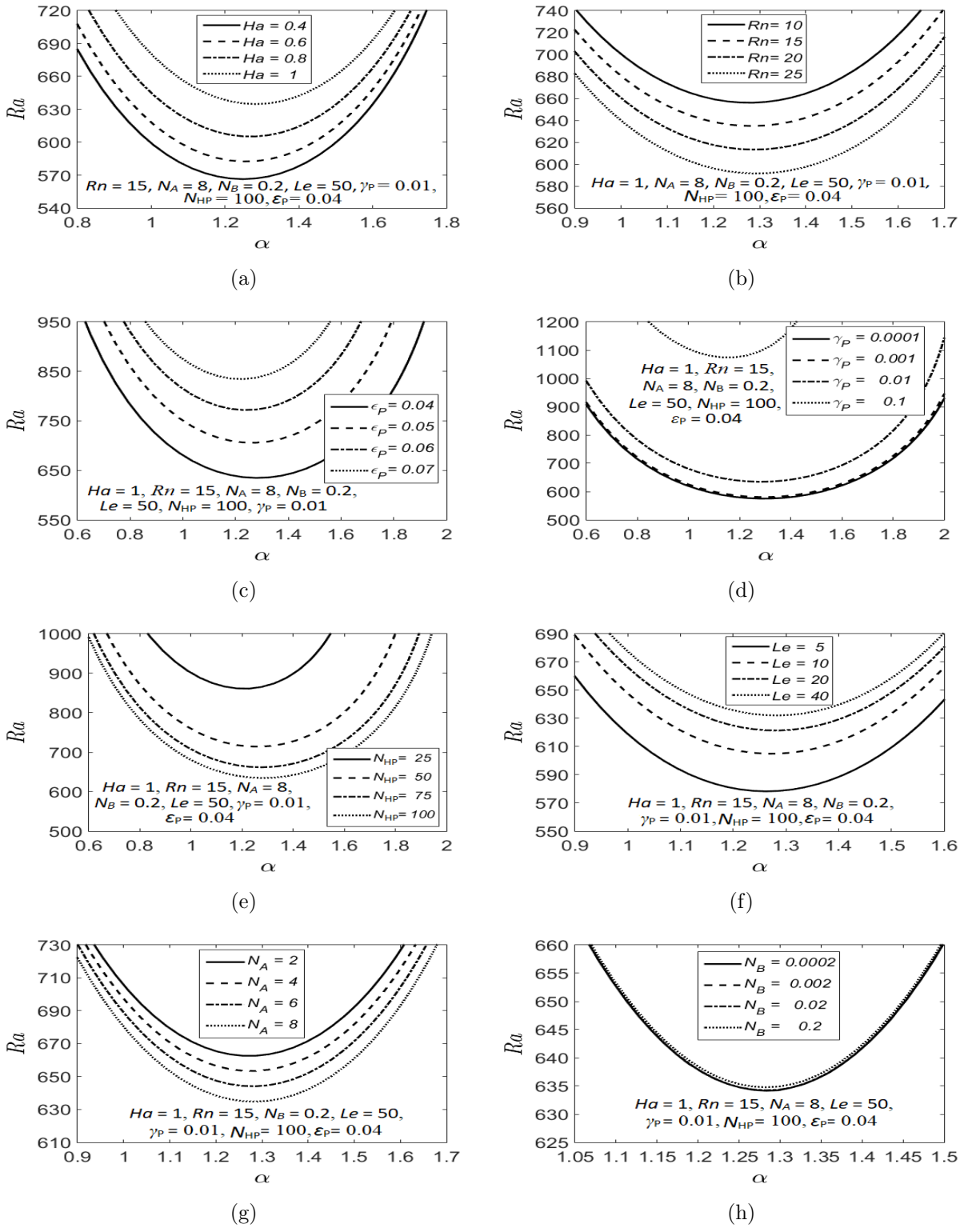

Figure 9.4: Neutral stability curves for different values of (a) Ha, (b) Rn, (c) ε_{P}, (d) γ_{P}, (e) N_{HP}, (f) Le, (g) N_{A} and (h) N_{B}.

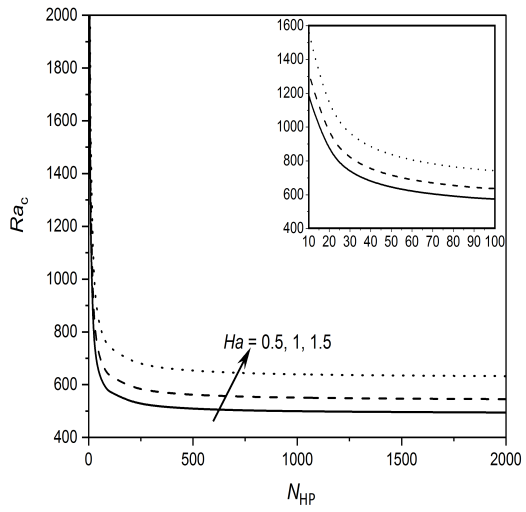

(a)

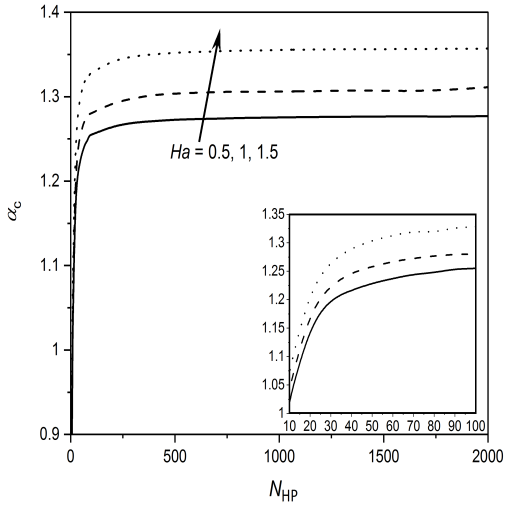

(b)

Figure 9.5: The instability curves for (a) Ra_c (b) α_c with N_{HP} for varying values of Ha.

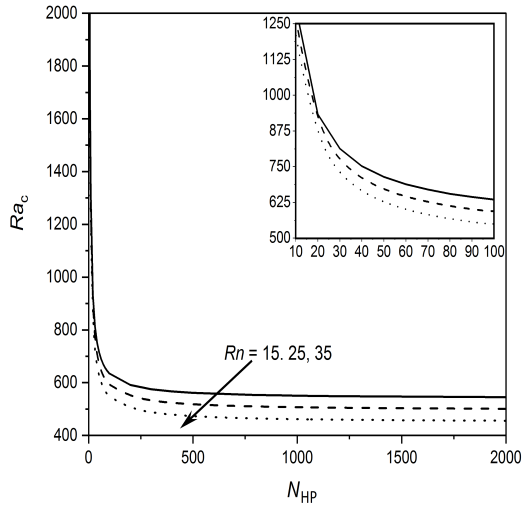

(a)

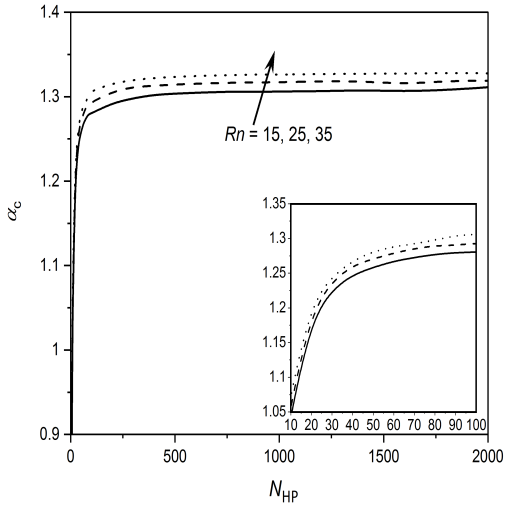

(b)

Figure 9.6: The instability curves for (a) Ra_c (b) α_c with N_{HP} for varying values of Rn.

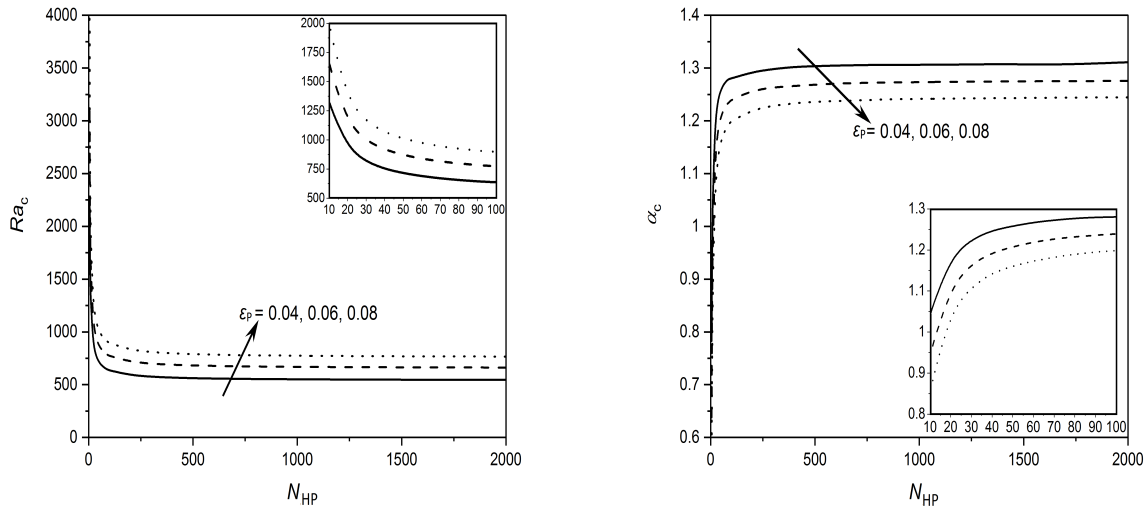

(a) (b)

Figure 9.7: The instability curves for (a) Ra_c (b) α_c with N_{HP} for varying values of ε_P .

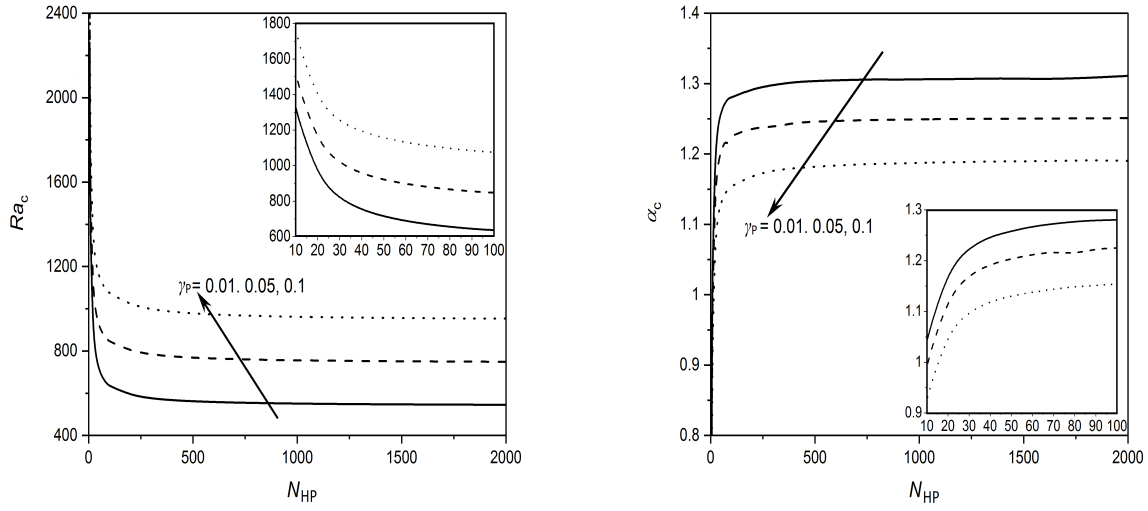

(a) (b)

Figure 9.8: The instability curves for (a) Ra_c (b) α_c with N_{HP} for varying values of γ_P.

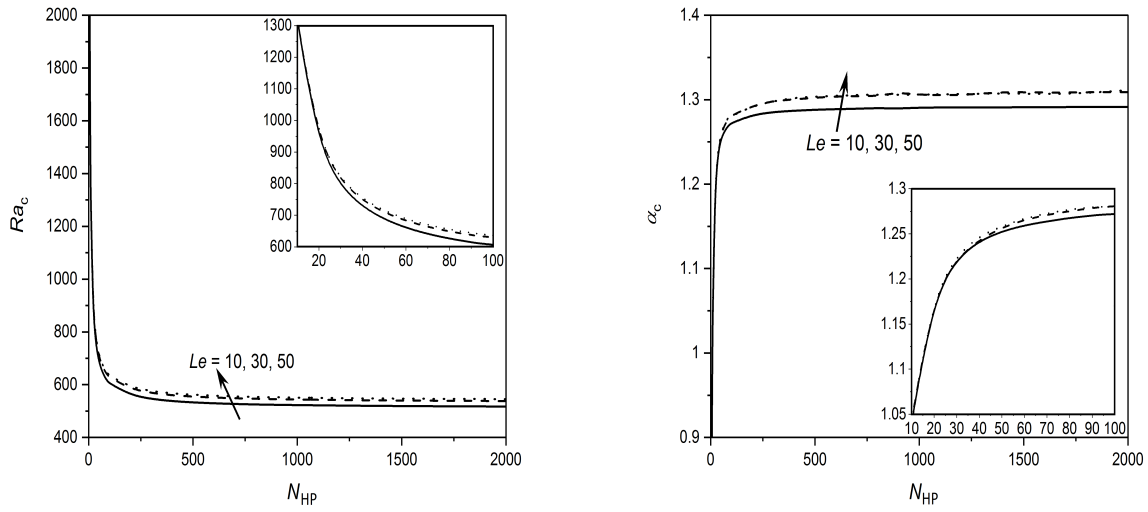

(a) (b)

Figure 9.9: The instability curves for (a) Ra_{c} (b) α_{c} with N_{HP} for varying values of Le.

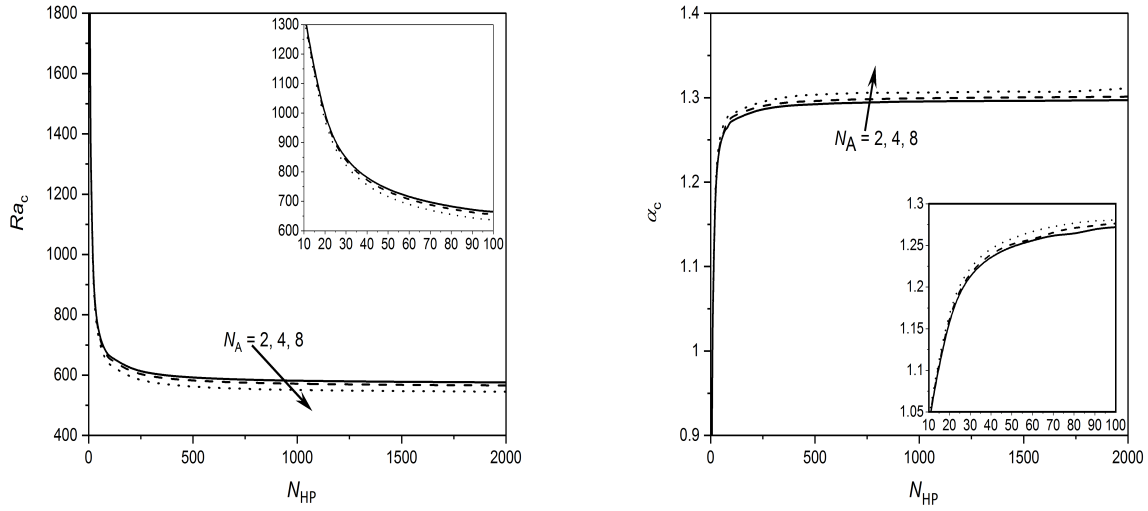

(a) (b)

Figure 9.10: The instability curves for (a) Ra_{c} (b) α_{c} with N_{HP} for varying values of N_{A}.

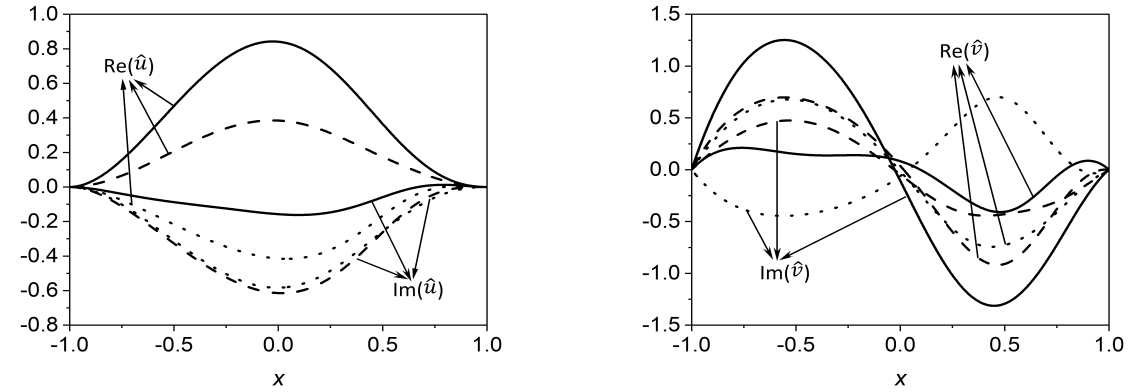

(a)

(b)

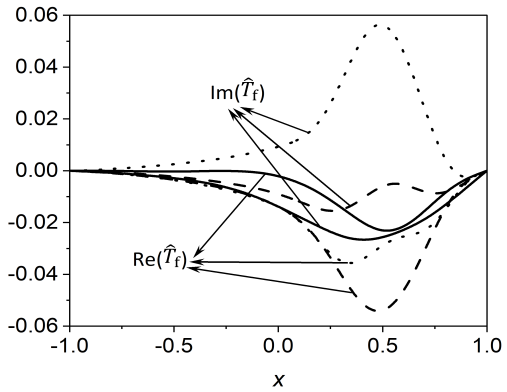

(c)

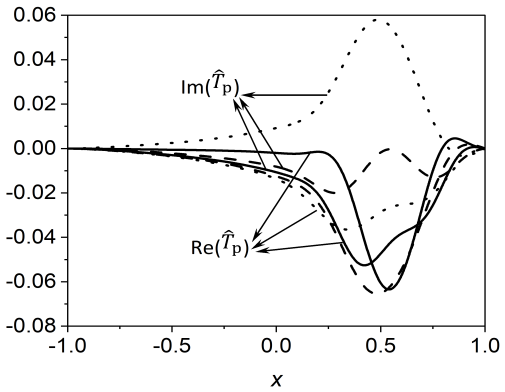

(d)

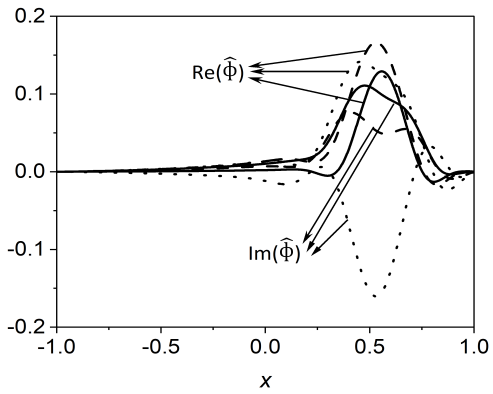

(e)

Figure 9.11: Eigenfunctions of (a) $\hat{u}$, (b) $\hat{v}$, (c) $\hat{T}_{\rm f}$, (d) $\hat{T}_{\rm p}$ (e) $\hat{\phi}$ with $Ha = 1, Rn = 15, \varepsilon_{\rm P} = 0.04, \gamma_{\rm P} = 0.01, Le = 50, N_{\rm A} = 8, N_{\rm B} = 0.2$ for $N_{\rm HP} = 10$ ('$-$'), $N_{\rm HP} = 100$ ('$--$') and $N_{\rm HP} = 1000$ ('$\cdots$').

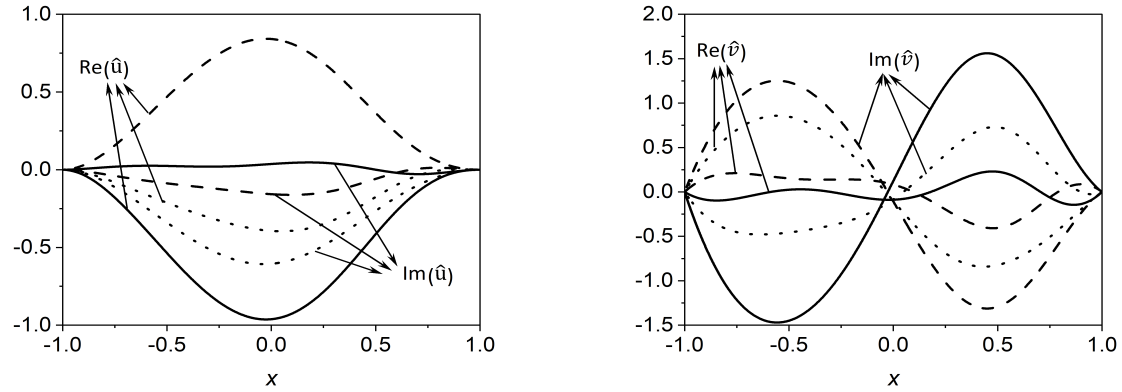

(a)

(b)

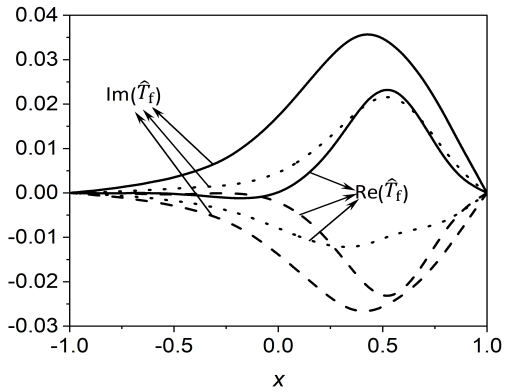

(c)

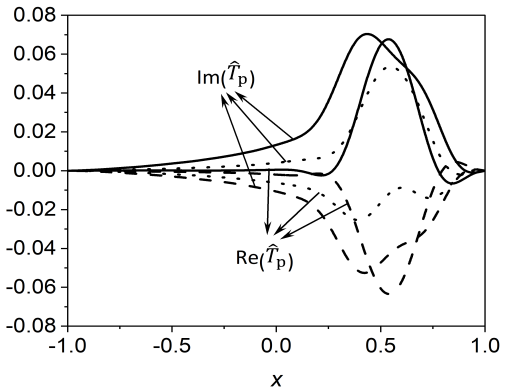

(d)

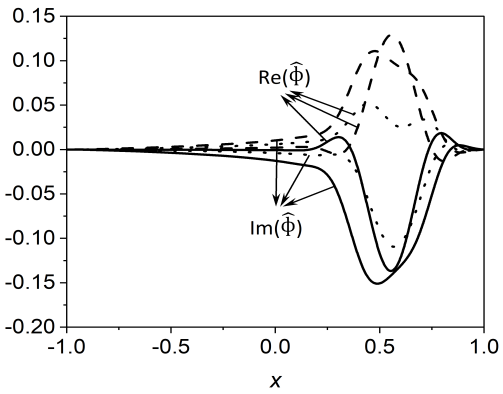

(e)

Figure 9.12: Eigenfunctions of (a) $\hat{u}$, (b) $\hat{v}$, (c) $\hat{T}_{\rm f}$, (d) $\hat{T}_{\rm p}$ (e) $\hat{\phi}$ for $N_{\rm HP} = 10, Rn = 15, \varepsilon_{\rm P} = 0.04, \gamma_{\rm P} = 0.01, Le = 50, N_{\rm A} = 8, N_{\rm B} = 0.2$ with $Ha = 0$ ('$-$'), $Ha = 1$ ('$--$') and $Ha = 2$ ('$\cdots$').

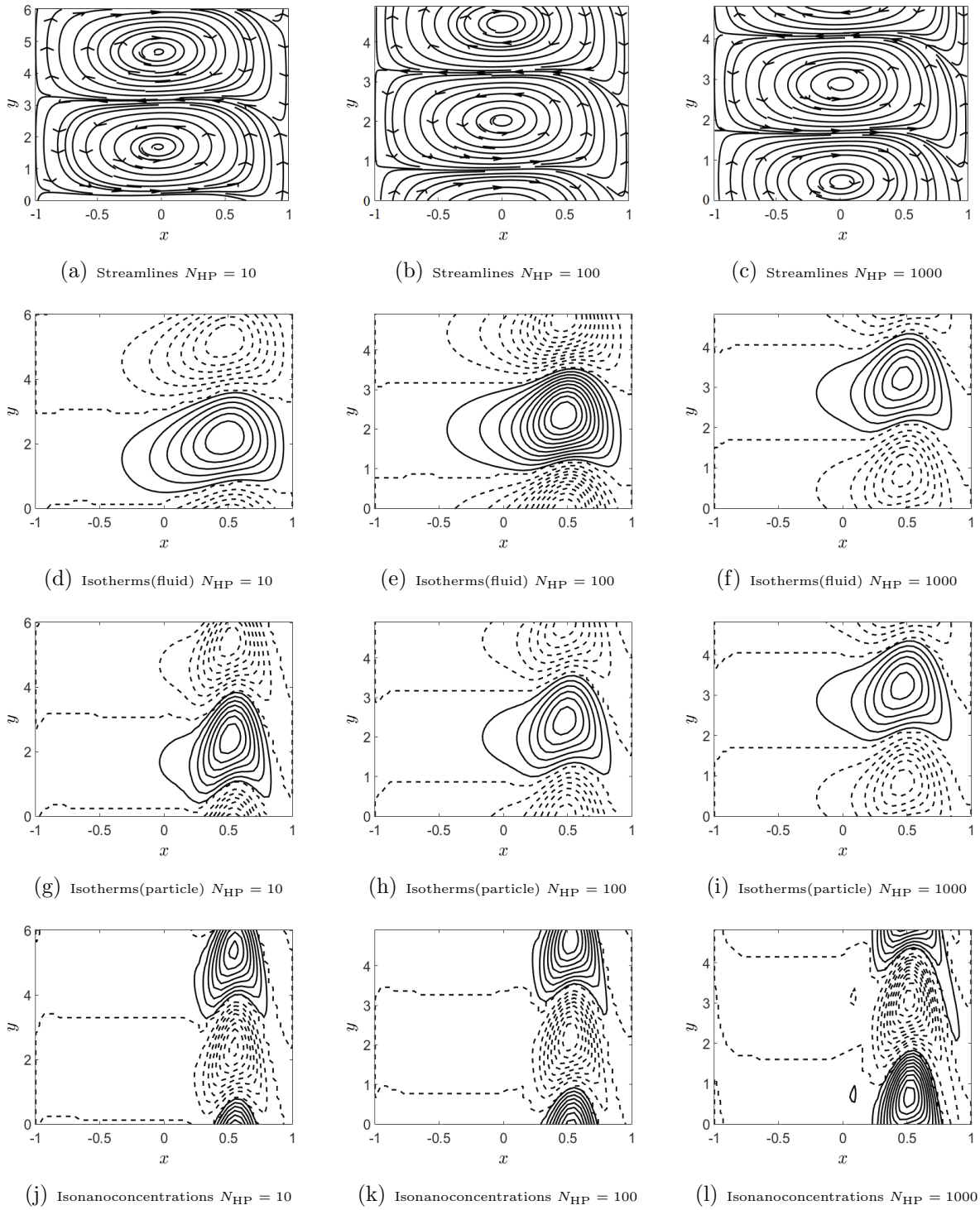

(a) Streamlines $N_{\mathrm{HP}} = 10$ (b) Streamlines $N_{\mathrm{HP}} = 100$ (c) Streamlines $N_{\mathrm{HP}} = 1000$

(d) Isotherms(fluid) $N_{\mathrm{HP}} = 10$ (e) Isotherms(fluid) $N_{\mathrm{HP}} = 100$ (f) Isotherms(fluid) $N_{\mathrm{HP}} = 1000$

(g) Isotherms(particle) $N_{\mathrm{HP}} = 10$ (h) Isotherms(particle) $N_{\mathrm{HP}} = 100$ (i) Isotherms(particle) $N_{\mathrm{HP}} = 1000$

(j) Isonanoconcentrations $N_{\mathrm{HP}} = 10$ (k) Isonanoconcentrations $N_{\mathrm{HP}} = 100$ (l) Isonanoconcentrations $N_{\mathrm{HP}} = 1000$

Figure 9.13: The pattern of streamlines ((a) to (c)), isotherms(fluid) ((d) to (f)), isotherms(particle) ((g) to (i)) and isonanoconcentrations ((j) to (l)) for different values of N_{HP}.

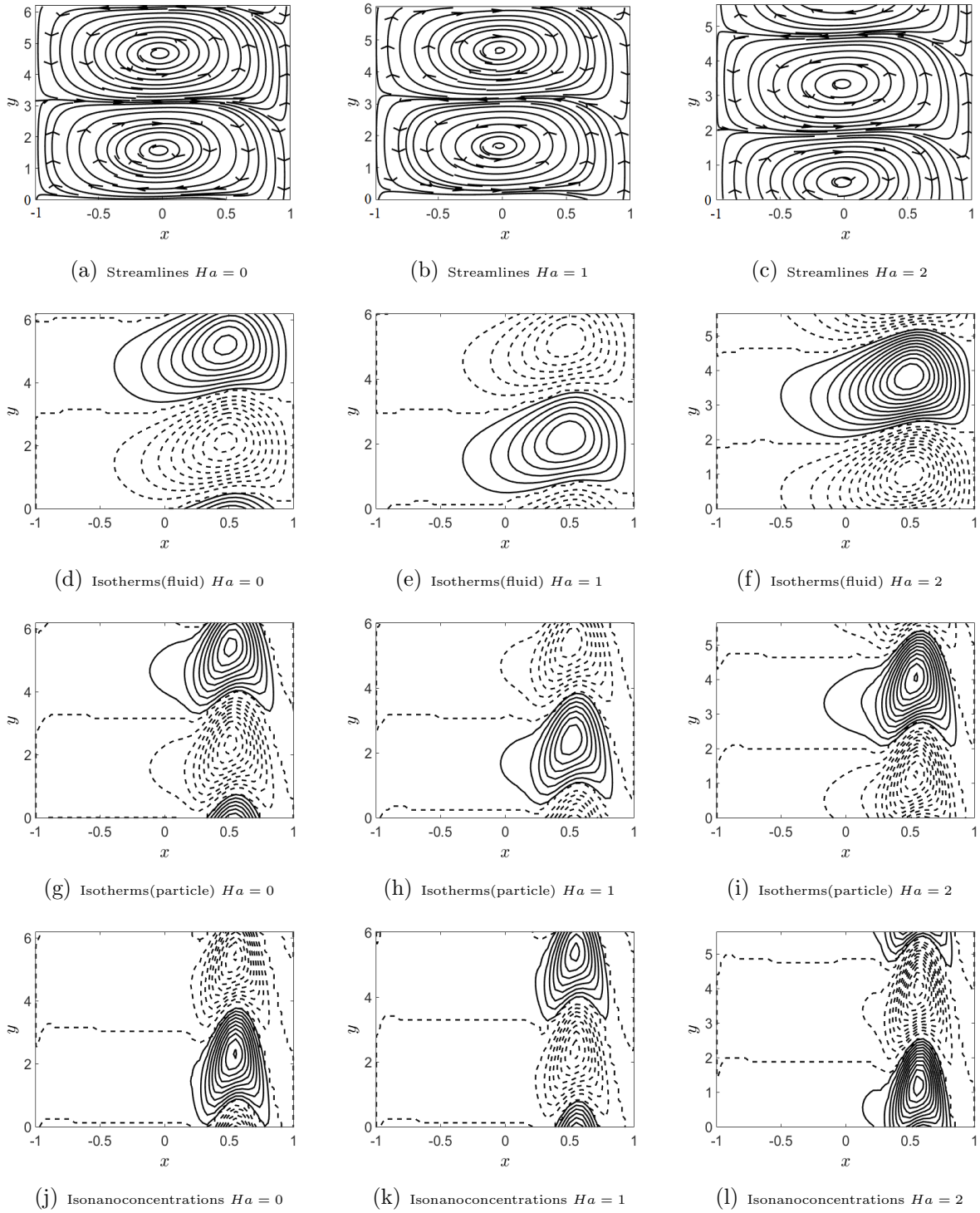

(a) Streamlines $Ha = 0$ (b) Streamlines $Ha = 1$ (c) Streamlines $Ha = 2$

(d) Isotherms(fluid) $Ha = 0$ (e) Isotherms(fluid) $Ha = 1$ (f) Isotherms(fluid) $Ha = 2$

(g) Isotherms(particle) $Ha = 0$ (h) Isotherms(particle) $Ha = 1$ (i) Isotherms(particle) $Ha = 2$

(j) Isonanoconcentrations $Ha = 0$ (k) Isonanoconcentrations $Ha = 1$ (l) Isonanoconcentrations $Ha = 2$

Figure 9.14: The pattern of streamlines ((a) to (c)), isotherms(fluid) ((d) to (f)), isotherms(particle) ((g) to (i)) and isonanoconcentrations ((j) to (l)) for different values of Ha.

9.6 Conclusions

The linear stability of nanofluid flow in a vertical channel has been investigated under the influence of local thermal non-equilibrium (LTNE) mode in the presence of transverse magnetic effect. The model incorporates the effect of Brownian motion and thermophoresis has been used into the momentum equation, under non-equilibrium conditions. The eigenvalue problem solved numerically using spectral method and the effect of the various parameter on the instability boundary has been calculated and presented them graphically. The following conclusions are drawn.

- The system shows more unstable when the flow is two dimensional, i.e., when spanwise wavenumber $\beta = 0$.
- System becomes more unstable for LTNE as compared to LTE.
- Convection sets in earlier for nanofluid than clear fluid under LTNE mode.
- The effect of Rn and N_{A} advances the onset of convective motion, while convection delays due to the effect of $Ha, \varepsilon_{\mathrm{P}}$, γ_{P} Le, and N_{B}.
- For small and large values of N_{HP}, LTNE converges to LTE. However, N_{HP} has a destabilizing nature in the intermediate range.
- Dimension of the convective cells amplifies on rising ε_{P} and γ_{P} while Ha, Rn, Le and N_{A} have no significant effect on the size of the convection cells.

Chapter 10

The effect of changeable gravity field on the stability of convection in a porous layer filled with nanofluid: Brinkman model [1]

10.1 Introduction

Due to fascinating uses in modern chemistry, chemical and nuclear industries, engineering and technology and biomechanics, a massive number of papers have appeared in the literature on nanofluid flow for the last few decades. In 1995, Choi [36] proposed the term "nanofluids", which are the mixtures of nanoparticles (ranged between 1nm and 100 nm) in a base fluid-like water, kerosene, ethylene glycol, etc. The selection of the base fluid and nanoparticle for nanofluid depends on the application is intended.

Recently, the heat transfer and fluid flow in a horizontal porous layer filled with nanofluids is an active research area for convection problem because of its wide area of applications such as chemical technology, geophysics, engineering and nuclear industries, food processing and oceanography. The works of Horton and Rogers Jr. [58] and Lapwood [66] were extended for nanofluid saturated in a porous medium based on the transport equations of Buongiorno's model by Kuznetsov and Nield [63], Chand and Rana [29], Nield and Kuznetsov [83], Rana and Chand [88] etc.

It is understood that the concept of a uniform gravitational field is not true for large-scale flows, such as the flow in the sea or the veil of the earth, as the gravitational field of the

[1] Published in "***Computational Thermal Sciences: An International Journal***", 13(6), 1-17, 2021

earth varies with altitude from the surface. Thus, a changeable gravity field with height is to be considered for such problems. Pradhan and Samal [87] analyzed the instability mechanism between two horizontal plates under the action of varying gravity field. Later, several authors, to mention a few, Chand *et al.* [31], Yadav [123, 124] (see the references therein) analysed the effect of gravity field variations on the instability mechanism in an anisotropic porous layer filled with nanofluid

After reviewing the literature, it is noted that very lack attention has been paid on the onset of convection due to the effect of the variable gravity field on the stability analysis of the horizontal porous layer filled with the nanofluid using Darcy extended Brinkman model, taking into account the effects of Brownian diffusion and thermophoresis. Such investigations may be very useful to execute problem connected with the fluid flows for large-scale, such as saturated soils, petroleum drilling, atmosphere, ocean, fuel piercing and space science.

In this chapter, linear, quadratic, cubic and exponential varying gravity has been considered to study the region of instabilities in a porous layer filled with nanofluid for rigid-rigid, free-free and rigid-free boundaries.

10.2 Mathematical Formulation

Consider an incompressible nanofluid saturated in a horizontal porous layer of width L. The geometry and coordinates system is shown in Fig. 2.1. The changeable gravity $\mathbf{g}$ is acting toward negative $z-$direction.

Using the Oberbeck−Boussinesq approximation, the equations governing the flow are

$$\nabla \cdot \mathbf{u} = 0, \tag{10.1}$$

$$\frac{\rho_{\mathrm{f}}}{\epsilon}\frac{\partial \mathbf{u}}{\partial t} = -\nabla p + \tilde{\mu}\nabla^2\mathbf{u} - \frac{\mu}{K}\mathbf{u} - [\phi\rho_{\mathrm{p}} + (1-\phi)\rho_{\mathrm{f}}\{1-\beta_{\mathrm{T}}(T-T_2)\}]\mathrm{g}(z)\hat{\mathbf{e}}_{\mathrm{z}}, \tag{10.2}$$

$$(\rho c)_{\mathrm{m}}\frac{\partial T}{\partial t} + (\rho c)_{\mathrm{f}}\mathbf{u}\cdot\nabla T = k_{\mathrm{m}}\nabla^2 T + \epsilon(\rho c)_{\mathrm{p}}\left[D_{\mathrm{B}}\nabla\phi\cdot\nabla T + \frac{D_{\mathrm{T}}}{T_1}\nabla T\cdot\nabla T\right], \tag{10.3}$$

$$\frac{\partial \phi}{\partial t} + \frac{1}{\epsilon}\mathbf{u}\cdot\nabla\phi = D_{\mathrm{B}}\nabla^2\phi + \frac{D_{\mathrm{T}}}{T_1}\nabla^2 T. \tag{10.4}$$

The gravity field is assumed as a function of z i.e., $\mathrm{g}(z) = \mathrm{g}_0(1+\lambda G(z))$, where g_0 is the reference gravity and λ is the gravity variation parameter.

It is assumed that the isothermal boundaries are either rigid or free with constant temper-

atures and the nanoparticle flux is zero on the boundaries, which is physically more realistic. Hence,

$$w = 0, \quad \frac{\partial w}{\partial z} + \kappa_1 L \frac{\partial^2 w}{\partial z^2} = 0, \quad T = T_1, \quad D_{\mathrm{B}} \frac{\partial \phi}{\partial z} + \frac{D_{\mathrm{T}}}{T_1} \frac{\partial T}{\partial z} = 0 \quad \text{at} \quad z = 0, \tag{10.5a}$$

$$w = 0, \quad \frac{\partial w}{\partial z} - \kappa_2 L \frac{\partial^2 w}{\partial z^2} = 0, \quad T = T_2, \quad D_{\mathrm{B}} \frac{\partial \phi}{\partial z} + \frac{D_{\mathrm{T}}}{T_1} \frac{\partial T}{\partial z} = 0 \quad \text{at} \quad z = L, \tag{10.5b}$$

where κ_1 and κ_2 are parameters which take the values 0 and ∞ for the rigid boundary and free boundary cases, respectively.

The non-dimensional scheme is defined as follows:

$$(x^*, y^*, z^*) = \frac{(x, y, z)}{L}, \quad \mathbf{u}^* = \frac{\mathbf{u} L (\rho c)_{\mathrm{f}}}{k_{\mathrm{m}}}, \quad p^* = \frac{K p (\rho c)_{\mathrm{f}}}{\mu k_{\mathrm{m}}},$$
$$t^* = \frac{\alpha_{\mathrm{m}} t}{\epsilon L^2}, \quad T^* = \frac{T - T_2}{T_1 - T_2}, \quad \phi^* = \frac{\phi - \phi_1}{\phi_1}. \tag{10.6}$$

Eliminating pressure term from Eq. (10.2), substituting Eq. (10.6) in Eqs. (10.1)-(10.4) and dropping asterisk, we get

$$\frac{Da}{Pr_{\mathrm{m}}} \frac{\partial}{\partial t} \left(\nabla^2 w \right) = \Lambda Da \nabla^4 w - \nabla^2 w + \left(Ra \nabla_{\mathrm{H}}^2 T - Rn \nabla_{\mathrm{H}}^2 \phi \right) (1 + \lambda G(z)), \tag{10.7}$$

$$\gamma \frac{\partial T}{\partial t} + \mathbf{u} \cdot \nabla T = \nabla^2 T + \frac{N_{\mathrm{B}}}{Le_{\mathrm{m}}} \nabla \phi \cdot \nabla T + \frac{N_{\mathrm{A}} N_{\mathrm{B}}}{Le_{\mathrm{m}}} \nabla T \cdot \nabla T, \tag{10.8}$$

$$\frac{\partial \phi}{\partial t} + \mathbf{u} \cdot \nabla \phi = \frac{1}{Le_{\mathrm{m}}} \nabla^2 \phi + \frac{N_{\mathrm{A}}}{Le_{\mathrm{m}}} \nabla^2 T. \tag{10.9}$$

All the parameters are already defined in the previous chapters. The conditions Eq. (10.5) in dimensionless form are

$$w = 0, \quad \frac{\partial w}{\partial z} + \kappa_1 \frac{\partial^2 w}{\partial z^2} = 0, \quad T = 1, \quad \frac{\partial \phi}{\partial z} + N_{\mathrm{A}} \frac{\partial T}{\partial z} = 0 \quad \text{at} \quad z = 0, \tag{10.10a}$$

$$w = 0, \quad \frac{\partial w}{\partial z} - \kappa_2 \frac{\partial^2 w}{\partial z^2} = 0, \quad T = 0, \quad \frac{\partial \phi}{\partial z} + N_{\mathrm{A}} \frac{\partial T}{\partial z} = 0 \quad \text{at} \quad z = 1. \tag{10.10b}$$

10.3 Basic state solution

We look for a time independent, unidirectional and fully developed solution of the nanofluid, which is of the form

$$\mathbf{u}_0 = 0, \quad T_0 = T_0(z), \quad \phi_0 = \phi_0(z). \tag{10.11}$$

Then Eqs. (10.8)-(10.9) can be written as:

$$\frac{d^2T_0}{dx^2} + \frac{N_\mathrm{B}}{Le_\mathrm{m}}\frac{dT_0}{dx}\left(\frac{d\phi_0}{dx} + N_\mathrm{A}\frac{dT_0}{dx}\right) = 0, \tag{10.12}$$

$$\frac{d^2\phi_0}{dx^2} + N_\mathrm{A}\frac{d^2T_0}{dx^2} = 0. \tag{10.13}$$

The boundary conditions for $T_0(z)$ and $\phi_0(z)$ are:

$$T_0 = 1, \quad \frac{\partial\phi_0}{\partial z} + N_\mathrm{A}\frac{\partial T_0}{\partial z} = 0 \quad \text{at} \quad z = 0, \tag{10.14a}$$

$$T_0 = 0, \quad \frac{\partial\phi_0}{\partial z} + N_\mathrm{A}\frac{\partial T_0}{\partial z} = 0 \quad \text{at} \quad z = 1. \tag{10.14b}$$

On solving Eqs. (10.12)-(10.13) with the boundary conditions Eq. (10.14), the basic temperature and volume fraction fields found that, respectively:

$$T_0(z) = 1 - z \qquad \text{and} \qquad \phi_0(z) = \phi_* + N_\mathrm{A}z, \tag{10.15}$$

where ϕ_* is the reference value for nanoparticle volume fraction.

10.4 Linear stability analysis

As in Chapter - 6 (or Chapter - 2), imposing the infinitesimal disturbances (δ) on the basic state solutions, neglecting δ^2 and higher order terms and then using the usual normal mode form to express infinitesimal disturbances of corresponding field variables, and by putting $\eta = 0$, the equations for neutral stability modes are

$$[Da(D^2 - a^2)^2 - (D^2 - a^2)]\hat{w} - a^2(Ra\hat{T} - Rn\hat{\phi})(1 + \lambda G(z)) = 0, \tag{10.16}$$

$$\hat{w} + \left(D^2 - a^2 - \frac{N_\mathrm{A}N_\mathrm{B}}{Le_\mathrm{m}}D\right)\hat{T} - \frac{N_\mathrm{B}}{Le_\mathrm{m}}D\hat{\phi} = 0, \tag{10.17}$$

$$-N_\mathrm{A}\hat{w} + \frac{N_\mathrm{A}}{Le_\mathrm{m}}(D^2 - a^2)\hat{T} + \frac{1}{Le_\mathrm{m}}(D^2 - a^2)\hat{\phi} = 0, \tag{10.18}$$

where $D = \frac{d}{dz}$ and $a = \sqrt{a_x^2 + a_y^2}$ is the wavenumber.

The solution of the system of Eqs. (10.16)-(10.18) is to be obtained subject to the three types of boundary conditions given below:

Type - a (Free-Free): Both upper and lower boundaries are stress-free:

$$\hat{w} = \frac{d^2\hat{w}}{dz^2} = \hat{T} = \frac{d\hat{\phi}}{dz} + N_{\mathrm{A}}\frac{d\hat{T}}{dz} = 0, \quad \text{at} \quad z = 0, 1. \tag{10.19}$$

Type - b (Rigid-Free): Lower boundary is rigid and upper boundary is stress free:

$$\begin{aligned} \hat{w} = \frac{d\hat{w}}{dz} = \hat{T} = \frac{d\hat{\phi}}{dz}\phi + N_{\mathrm{A}}\frac{d\hat{T}}{dz} = 0, \quad \text{at} \quad z = 0, \\ \hat{w} = \frac{d^2\hat{w}}{dz^2} = \hat{T} = \frac{d\hat{\phi}}{dz} + N_{\mathrm{A}}\frac{d\hat{T}}{dz} = 0, \quad \text{at} \quad z = 1. \end{aligned} \tag{10.20}$$

Type - c (Rigid-Rigid): Both upper and lower boundaries are rigid (no-slip boundaries):

$$\hat{w} = \frac{d\hat{w}}{dz} = \hat{T} = \frac{d\hat{\phi}}{dz} + N_{\mathrm{A}}\frac{d\hat{T}}{dz} = 0, \quad \text{at} \quad z = 0, 1. \tag{10.21}$$

10.5 Results and discussion

The eigenvalue problem defined by the Eqs. (10.16)-(10.18) is solved using the *bvp4c* routine in MATLAB.

In this investigation, four forms of gravitational force functions are considered.They are linear i.e. $G(z) = -z$ (designated by Case $-$ A), quadratic i.e. $G(z) = -z^2$ (designated by Case $-$ B), cubic i.e. $G(z) = -z^3$ (designated by Case $-$ C) and exponential i.e., $G(z) = -(e^z - 1)$ (designated by Case $-$ D).

The critical Rayleigh number and corresponding wavenumber calculated for stationary convection from the present study by taking $Rn = 0$, $N_{\mathrm{A}} = 0$ and $N_{\mathrm{B}} = 0$ are compared with the results of Rionero and Straughan [91] for variable gravity and Chandrasekhar [32] for constant gravity fields of clear fluid and tabulated in Table 10.1 and Table 10.2 to confirm the accuracy of our code. It can be observed from these tables that the findings are in strong agreement with Rionero and Straughan [91] and Chandrasekhar [32] results.

The variation of (Ra_{c}) and (a_{c}) as a function of gravity variation parameter λ are presented in the Table 10.3 and shown in the Figs. 10.1 and 10.2 for four forms of the gravity field with different values of Darcy number (Da). From Fig. 10.1, it is distinguished that λ and Da, i.e., both the parameters have a stabilizing impact on the convective instability. This is happening since the disturbances of the system regain due to the increment of λ, which states to delay in the gravity field. This is the reason to postpone the convective with augment of λ. Also, Ra_{c} increases with Da. This is happening because the viscous effect

becomes more strong in the presence of Brinkman term with rising the values of the Darcy number and it leads to increase the values of Ra_c. Further, it is perceived that the critical wavenumber rises with increasing the values of both λ and Da. Thus, the convective cells dimension decrease in the estimate of both λ and Da.

The impact of basic density Rayleigh number on (Ra_c) and (a_c) are presented in the Figs. 10.3 and 10.4, respectively. It is noticed that with an enhancement in the value of Rn, the critical Rayleigh number decreases, suggesting that Rn has a destabilizing effect on the flow region. With the top-heavy distribution of nanoparticles, too, the scale of the convective cells increases.

Figs. 10.5 and 10.6 illustrate the influence of Lewis number and Figs. 10.7 and 10.8 demonstrate the impact of modified diffusivity ratio on the instability boundaries for four forms of gravity field with different boundary conditions. From Figs. 10.5 and 10.7, it is noticed that the critical Rayleigh number reduces with the enhancing values of Le_m and N_A. Thus, Le_m and N_A has a destabilizing effect on the stability of the scheme. Also, size of the convective cells increases with augmenting values of Le_m and N_A as shown in Figs. 10.6 and 10.8, respectively.

The deviation of the critical Rayleigh number for various values of N_B has shown in the Fig. 10.9 and Table 10.4 for linear, quadratic, cubic and exponential gravity fields. From this figure, it is clear that N_B has a stabilizing effect when both the boundaries are free-free or rigid-rigid, while it shows a destabilizing effect when lower boundary is rigid and upper one is free. It indicates that convection is postponing or advancing for the effect of N_B under different boundary of the planes. Also, it is seen that the critical wavenumber increases for rigid-rigid boundaries, while decreases for Type - a and Type - b boundary conditions as shown in Fig. 10.10.

In addition, it is noted that the convection for the cubic varying gravity field arrives faster, while the convection is more delayed by the exponential varying gravity field. It is also found that when both boundaries are rigid due to the removal of disruptions, the structure becomes more stable, although more unstable for free-free boundaries.

Table 10.1: Comparison of Ra_c and a_c^2 with the results of Rionero and Straughan [91] for $Rn = 0$, $N_A = 0$, $N_B = 0$, $Le_m = 1$ and $Da = 0$.

$G(z)$	λ	Rionero and Straughan [91]		Present results	
		Ra_c	a_c^2	Ra_c	a_c^2
Case - A	0	39.478	9.870	39.478	9.870
	1	77.020	10.209	77.020	10.209
	1.5	132.020	12.314	132.021	12.314
	1.8	189.908	17.198	189.908	17.198
	1.9	212.280	19.477	212.284	19.477
Case - B	0	39.478	9.870	39.478	9.870
	0.2	41.832	9.874	41.832	9.874
	0.4	44.455	9.887	44.455	9.887
	0.6	47.389	9.915	47.389	9.915
	0.8	50.682	9.961	50.682	9.961
	1	54.390	10.034	54.390	10.034
Case - D	0	39.478	9.870	39.478	9.870
	0.1	42.331	9.872	42.331	9.872
	0.2	45.607	9.883	45.607	9.883
	0.3	49.398	9.904	49.398	9.904
	0.4	53.828	9.942	53.828	9.942
	0.5	59.053	10.005	59.053	10.005

Table 10.2: Comparison of Ra_c, a_c and $2\pi/a_c$ with the results of Chandrasekhar [32] for $Rn = 0$, $N_A = 0$, $N_B = 0$, $\lambda = 0$, $Le_m = 1$ and $Da \to \infty$.

Boundary status	Chandrasekhar [32]			Present results		
	Ra_c	a_c	$2\pi/\alpha_c$	Ra_c	a_c	$2\pi/\alpha_c$
Type - a	657.511	2.2214	2.828	657.511365	2.221441	2.8284
Type - b	1100.65	2.682	2.342	1100.64978	2.682321	2.3424
Type - c	1707.762	3.117	2.016	1707.76178	3.116324	2.0162

Table 10.3: Influence of Da and λ on Ra_c and a_c for Type - a, Type - b and Type - c boundaries when $Le_m = 5$, $N_A = 6$, $N_B = 0.5$ and $Rn = 2$.

$G(z)$	Da	λ	Type - a		Type - b		Type - c	
			Ra_c	a_c	Ra_c	a_c	Ra_c	a_c
Case - A	0.6	0	257.905	1.718	532.074	2.438	967.589	3.034
		0.4	375.839	1.886	715.998	2.489	1235.281	3.060
		0.8	564.313	2.015	1036.433	2.544	1675.565	3.088
		1.2	926.366	2.130	1726.061	2.620	2521.748	3.138
Case - B		0	257.905	1.718	532.074	2.438	967.589	3.034
		0.4	320.097	1.825	631.408	2.472	1100.366	3.049
		0.8	397.678	1.914	763.588	2.508	1268.557	3.067
		1.2	498.640	1.994	947.294	2.549	1487.378	3.089
Case - C		0	257.905	1.718	532.074	2.438	967.589	3.034
		0.4	295.797	1.791	592.931	2.462	1042.843	3.044
		0.8	338.588	1.855	664.976	2.487	1128.495	3.055
		1.2	387.647	1.914	751.413	2.514	1226.634	3.068
Case - D		0	257.905	1.718	532.074	2.438	967.589	3.034
		0.4	432.074	1.938	813.363	2.512	1358.084	3.069
		0.8	788.092	2.106	1477.908	2.612	2164.848	3.129
		1.2	1892.228	2.356	4054.363	3.063	4459.790	3.352
Case - A	0.7	0	328.241	1.822	635.348	2.463	1139.515	3.046
		0.4	460.652	1.946	847.419	2.507	1449.807	3.067
		0.8	675.235	2.049	1217.212	2.554	1960.198	3.094
		1.2	1089.836	2.146	2013.714	2.625	2941.232	3.141
Case - B		0	328.241	1.822	635.348	2.463	1139.515	3.046
		0.4	397.469	1.900	749.678	2.492	1293.332	3.060
		0.8	484.872	1.968	901.904	2.524	1488.180	3.076
		1.2	599.399	2.032	1113.615	2.560	1741.708	3.096
Case - C		0	328.241	1.822	635.348	2.463	1139.515	3.046
		0.4	370.085	1.874	705.250	2.484	1226.630	3.055
		0.8	417.802	1.923	788.043	2.505	1325.785	3.065
		1.2	472.879	1.968	887.423	2.529	1439.400	3.077
Case - D		0	328.241	1.822	635.348	2.463	1139.515	3.046
		0.4	524.244	1.987	959.577	2.527	1592.076	3.078
		0.8	930.718	2.125	1726.536	2.617	2527.205	3.133
		1.2	2198.943	2.355	4711.012	3.059	5189.330	3.352
Case - A	0.8	0	396.994	1.889	738.484	2.481	1311.398	3.055
		0.4	544.717	1.987	978.752	2.519	1664.299	3.074
		0.8	785.816	2.073	1397.939	2.562	2244.808	3.099
		1.2	1253.183	2.157	2301.317	2.628	3360.701	3.144
Case - B		0	396.994	1.889	738.484	2.481	1311.398	3.055
		0.4	473.840	1.950	867.842	2.507	1486.262	3.067
		0.8	571.427	2.006	1040.157	2.535	1707.671	3.082
		1.2	699.761	2.059	1279.882	2.568	1996.013	3.102
Case - C		0	396.994	1.889	738.484	2.481	1311.398	3.055
		0.4	443.207	1.930	817.453	2.500	1410.398	3.063
		0.8	496.157	1.969	911.017	2.519	1523.041	3.073
		1.2	557.479	2.006	1023.359	2.540	1652.135	3.084
Case - D		0	396.994	1.889	738.484	2.481	1311.398	3.055
		0.4	615.856	2.021	1105.718	2.538	1826.039	3.084
		0.8	1073.183	2.139	1975.133	2.621	2889.546	3.137
		1.2	2505.628	2.354	5367.581	3.056	5918.853	3.352

Table 10.4: Influence of N_B and λ on Ra_c and a_c for Type - a, Type - b and Type - c boundaries when $Le_m = 5$, $N_A = 6$, $Da = 0.8$ and $Rn = 2$.

$G(z)$	N_B	λ	Type - a		Type - b		Type - c	
			Ra_c	a_c	Ra_c	a_c	Ra_c	a_c
Case - A	0.5	0	396.994	1.889	738.484	2.481	1311.398	3.055
		0.3	501.585	1.964	907.207	2.510	1560.792	3.069
		0.5	593.357	2.009	1060.723	2.529	1781.270	3.079
		1	975.230	2.114	1749.564	2.589	2699.608	3.117
Case - B		0	396.994	1.889	738.484	2.481	1311.398	3.055
		0.3	452.974	1.935	832.153	2.501	1438.774	3.064
		0.5	495.983	1.964	906.168	2.514	1536.632	3.071
		1	630.908	2.033	1149.436	2.551	1841.911	3.091
Case - C		0	396.994	1.889	738.484	2.481	1311.398	3.055
		0.3	431.075	1.920	796.479	2.495	1384.445	3.061
		0.5	455.757	1.940	839.335	2.504	1437.164	3.066
		1	525.651	1.988	964.525	2.529	1585.337	3.078
Case - D		0	396.994	1.889	738.484	2.481	1311.398	3.055
		0.3	547.941	1.990	988.208	2.523	1666.058	3.072
		0.5	696.945	2.051	1250.001	2.554	2016.758	3.093
		1	1552.245	2.213	3026.392	2.724	3957.834	3.199
Case - A	1.5	0	405.620	1.874	653.108	2.351	1375.952	3.061
		0.3	514.264	1.950	805.058	2.379	1636.319	3.081
		0.5	609.620	1.996	943.374	2.399	1865.215	3.098
		1	1004.760	2.104	1563.145	2.464	2800.817	3.161
Case - B		0	405.620	1.874	653.108	2.351	1375.952	3.061
		0.3	463.888	1.921	737.517	2.371	1507.326	3.076
		0.5	508.612	1.951	804.186	2.385	1607.520	3.087
		1	648.423	2.022	1022.853	2.425	1915.272	3.123
Case - C		0	405.620	1.874	653.108	2.351	1375.952	3.061
		0.3	441.151	1.906	705.360	2.365	1450.297	3.071
		0.5	466.847	1.927	743.941	2.375	1503.575	3.079
		1	539.408	1.977	856.413	2.403	1651.453	3.102
Case - D		0	405.620	1.874	653.108	2.351	1375.952	3.061
		0.3	562.478	1.977	878.023	2.393	1743.678	3.094
		0.5	716.982	2.040	1113.598	2.426	2102.160	3.124
		1	1573.518	2.217	2674.911	2.620	3951.178	3.273
Case - A	2.5	0	425.183	1.838	590.534	2.243	1563.332	3.072
		0.3	542.846	1.914	730.682	2.270	1857.360	3.109
		0.5	646.178	1.960	858.347	2.289	2111.549	3.139
		1	1068.946	2.075	1428.666	2.357	3093.845	3.239
Case - B		0	425.183	1.838	590.534	2.243	1563.332	3.072
		0.3	488.243	1.886	668.395	2.262	1706.156	3.101
		0.5	536.525	1.917	729.840	2.277	1812.514	3.122
		1	685.870	1.993	930.582	2.319	2123.915	3.181
Case - C		0	425.183	1.838	590.534	2.243	1563.332	3.072
		0.3	463.591	1.871	638.677	2.258	1640.440	3.094
		0.5	491.275	1.893	674.168	2.268	1694.384	3.108
		1	568.788	1.947	777.246	2.297	1838.230	3.147
Case - D		0	425.183	1.838	590.534	2.243	1563.332	3.072
		0.3	594.898	1.942	797.939	2.284	1969.800	3.131
		0.5	760.935	2.007	1014.786	2.318	2348.928	3.181
		1	1601.793	2.217	2389.786	2.540	3998.814	3.346

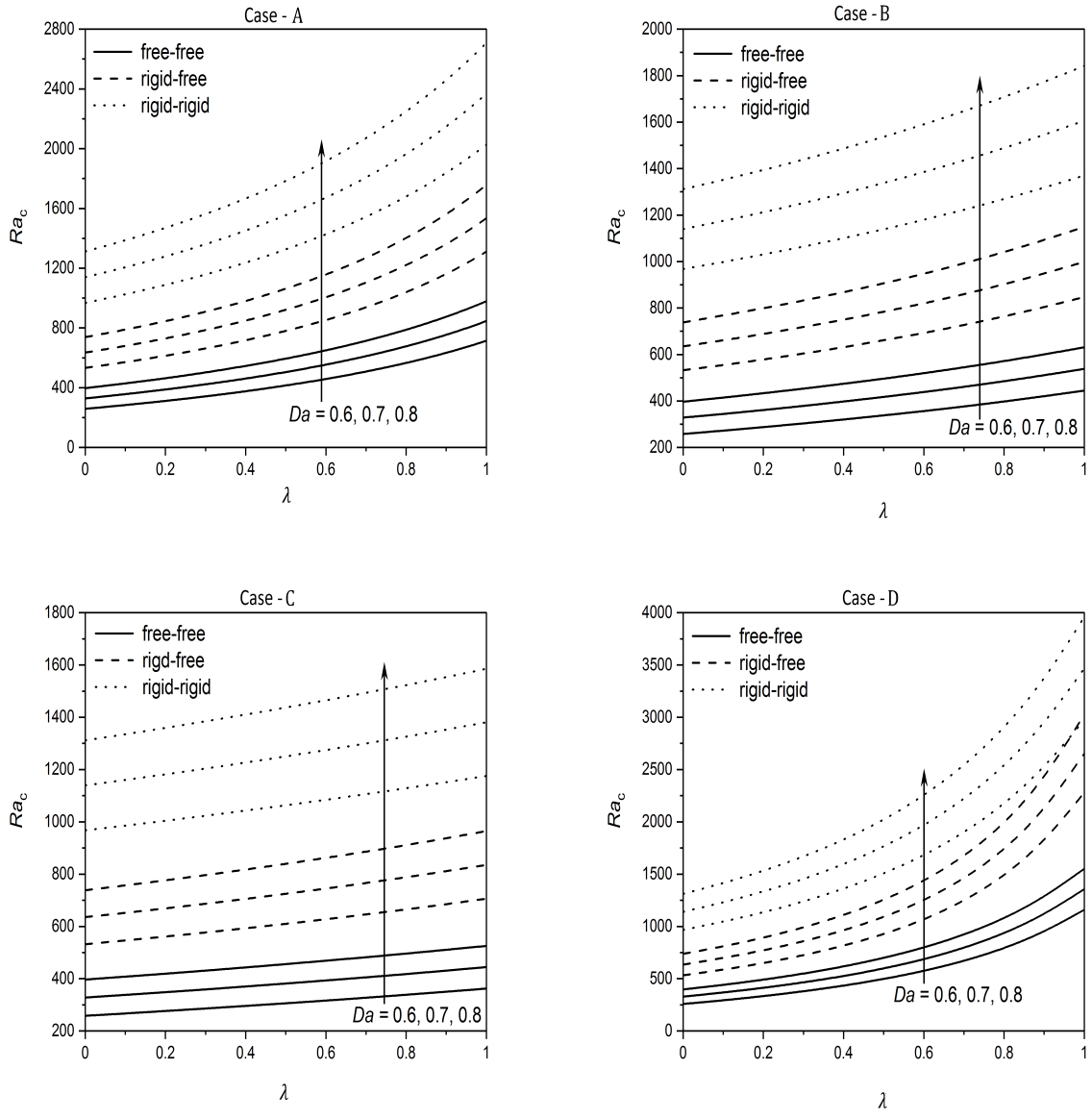

Figure 10.1: Effect of the Da on Ra_{c} for $Rn = 2$, $Le_{\mathrm{m}} = 5$, $N_{\mathrm{A}} = 6$ and $N_{\mathrm{B}} = 0.5$.

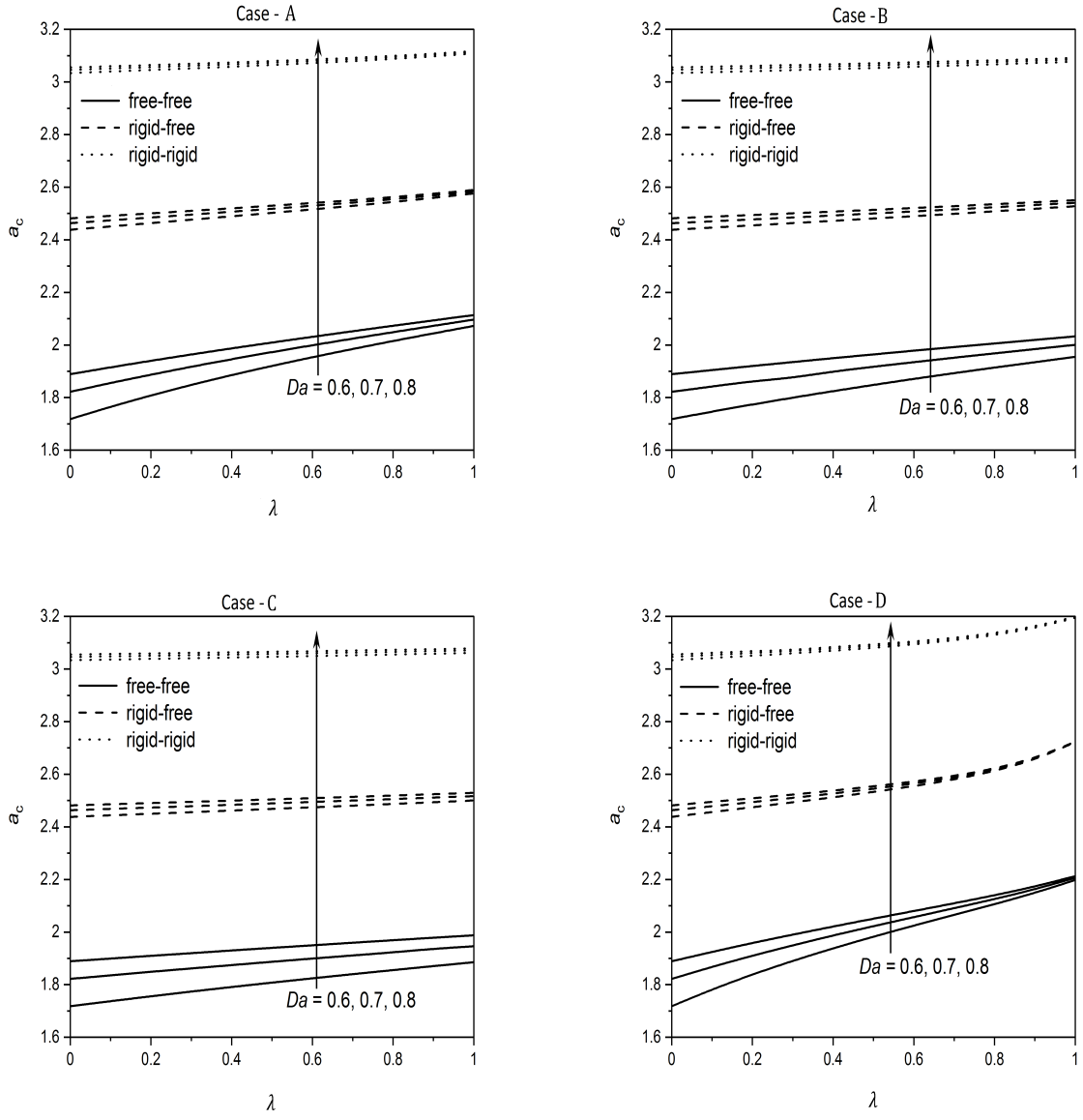

Figure 10.2: Effect of the Da on a_c for $Rn = 2$, $Le_m = 5$, $N_A = 6$ and $N_B = 0.5$.

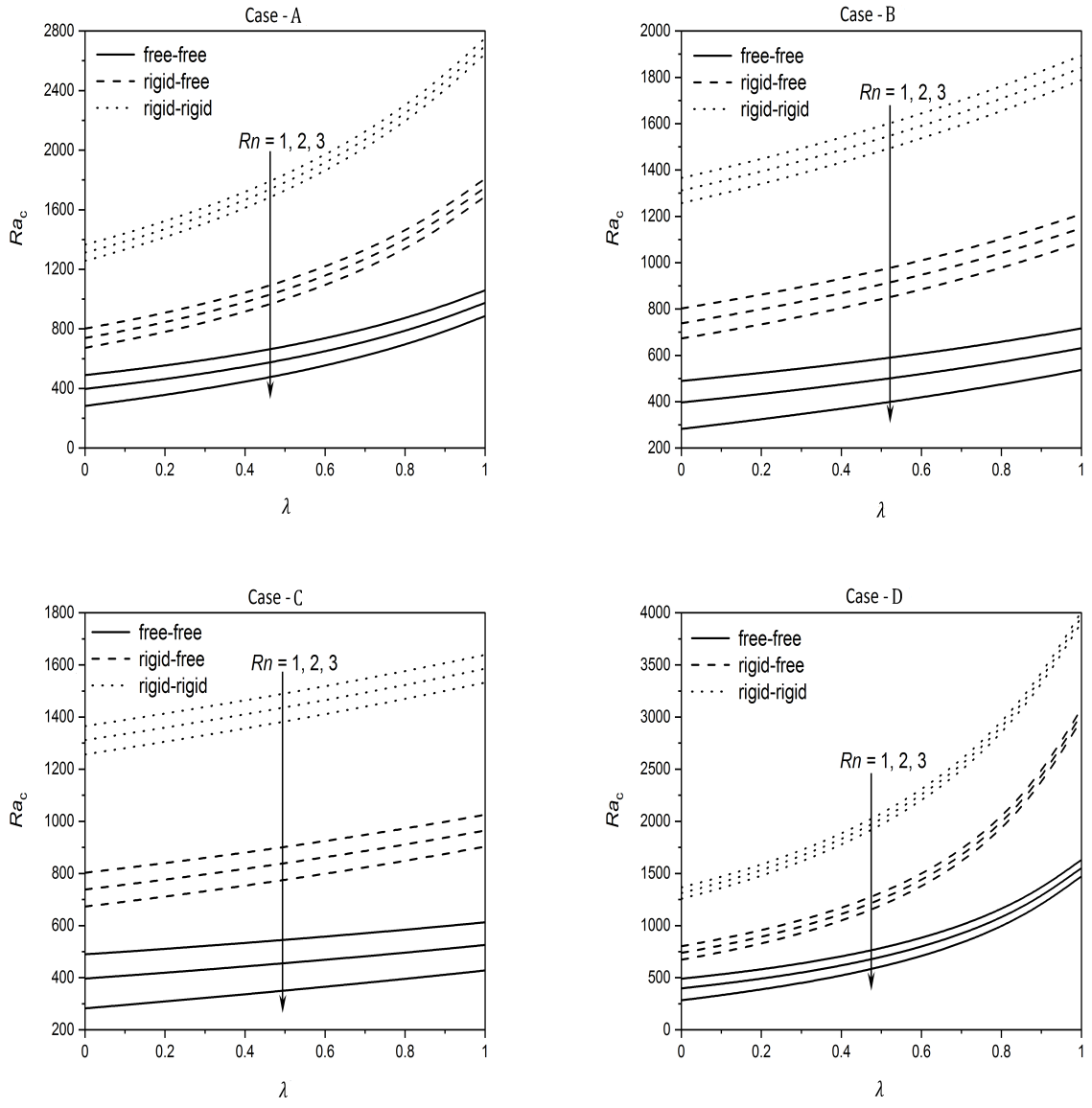

Figure 10.3: Effect of the Rn on Ra_{c} for $Da = 0.8$, $Le_{\mathrm{m}} = 5$, $N_{\mathrm{A}} = 6$ and $N_{\mathrm{B}} = 0.5$.

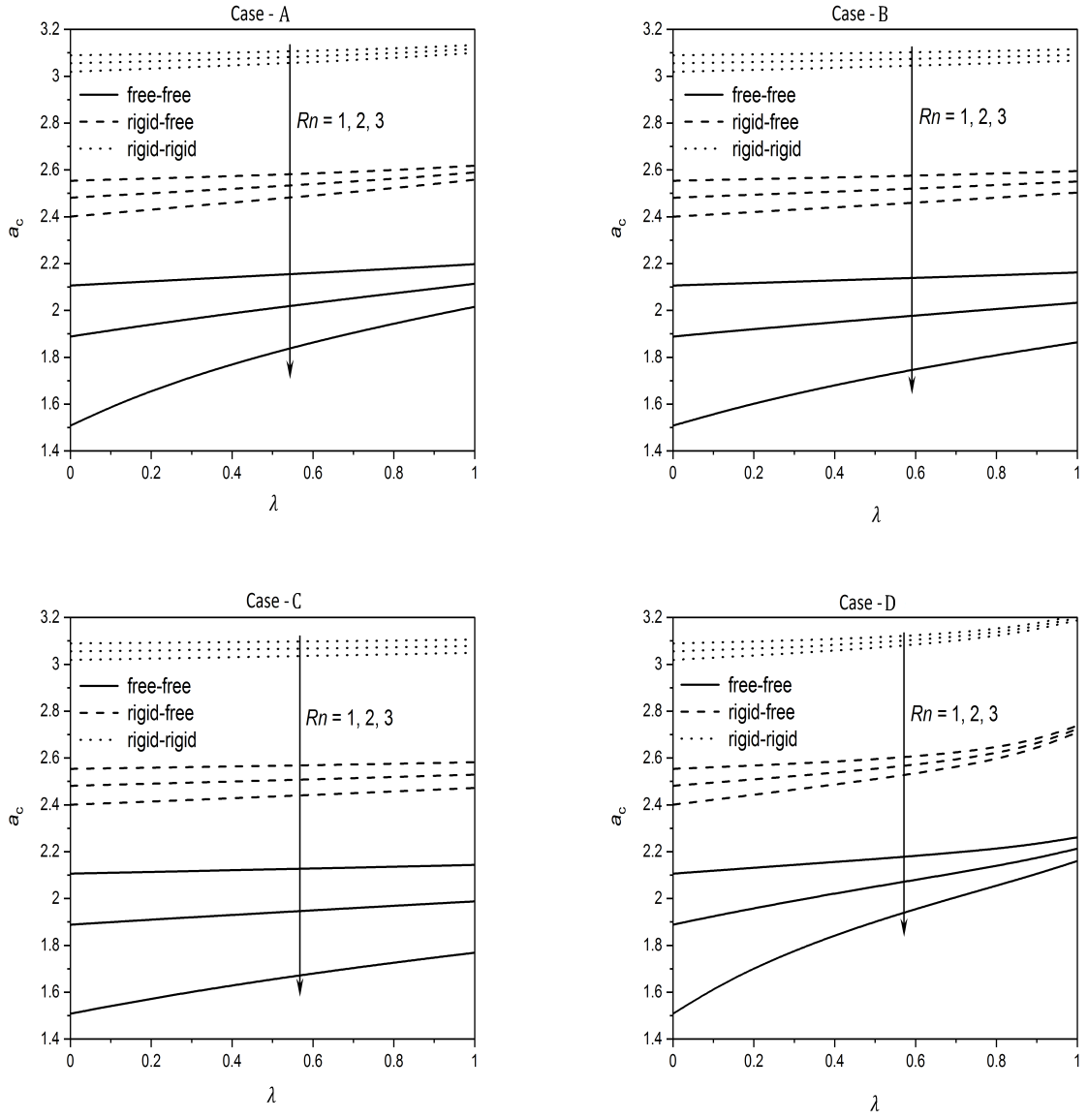

Figure 10.4: Effect of the Rn on a_c for $Da = 0.8$, $Le_m = 5$, $N_A = 6$ and $N_B = 0.5$.

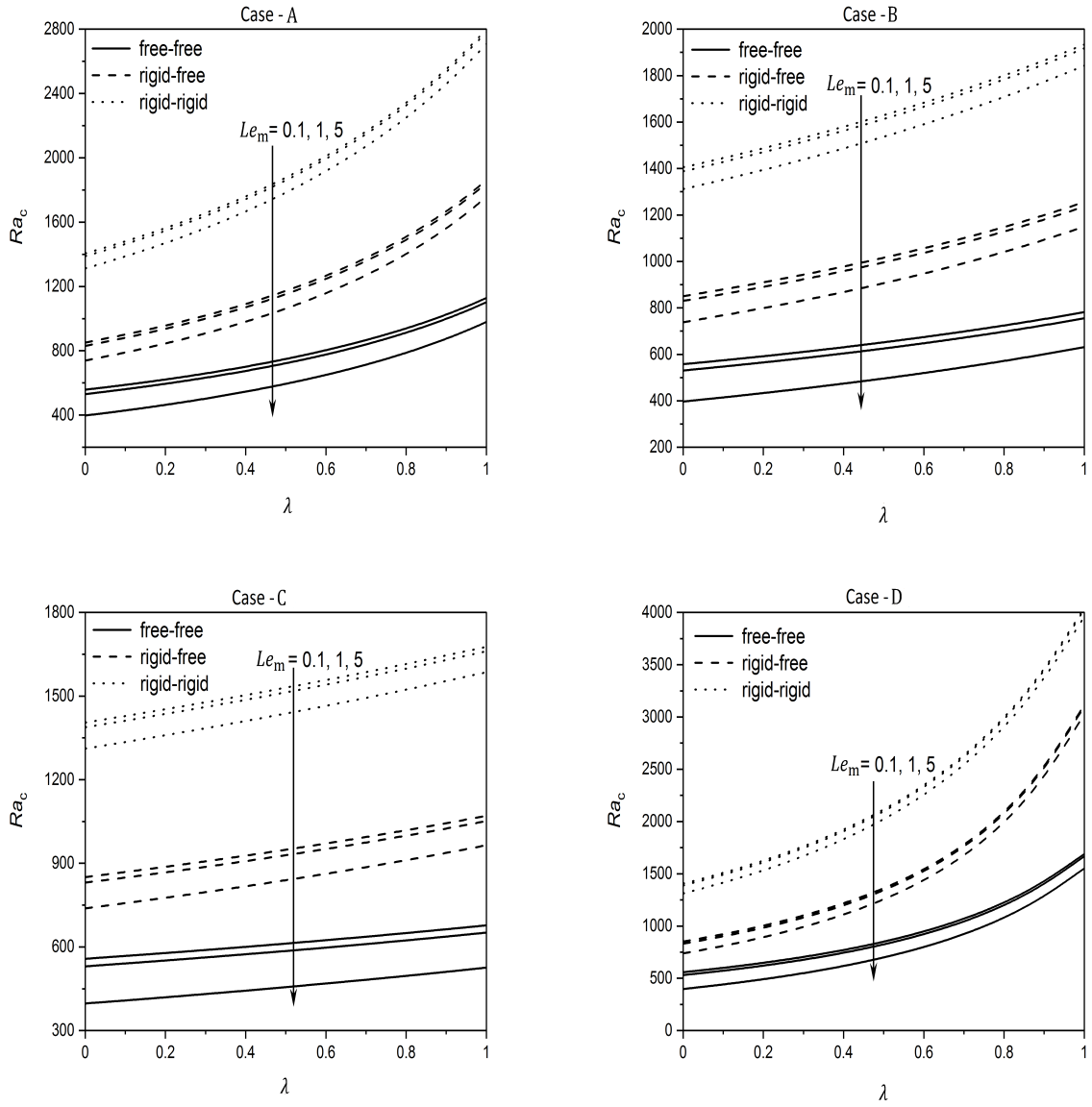

Figure 10.5: Effect of Le_{m} on Ra_{c} for $Da = 0.8$, $Rn = 2$, $N_{\mathrm{A}} = 6$ and $N_{\mathrm{B}} = 0.5$.

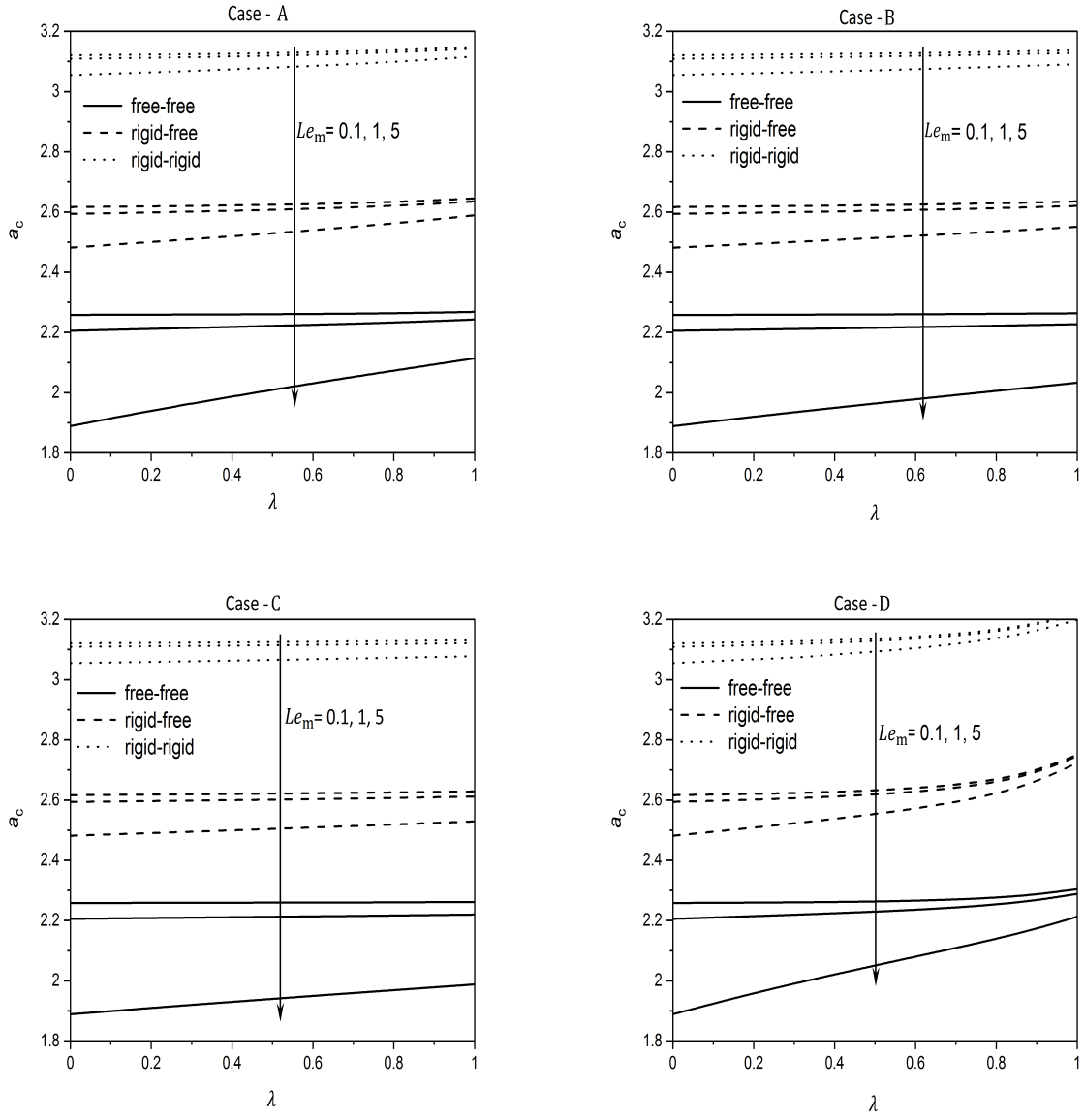

Figure 10.6: Effect of Le_{m} on a_{c} for $Da = 0.8$, $Rn = 2$, $N_{\mathrm{A}} = 6$ and $N_{\mathrm{B}} = 0.5$.

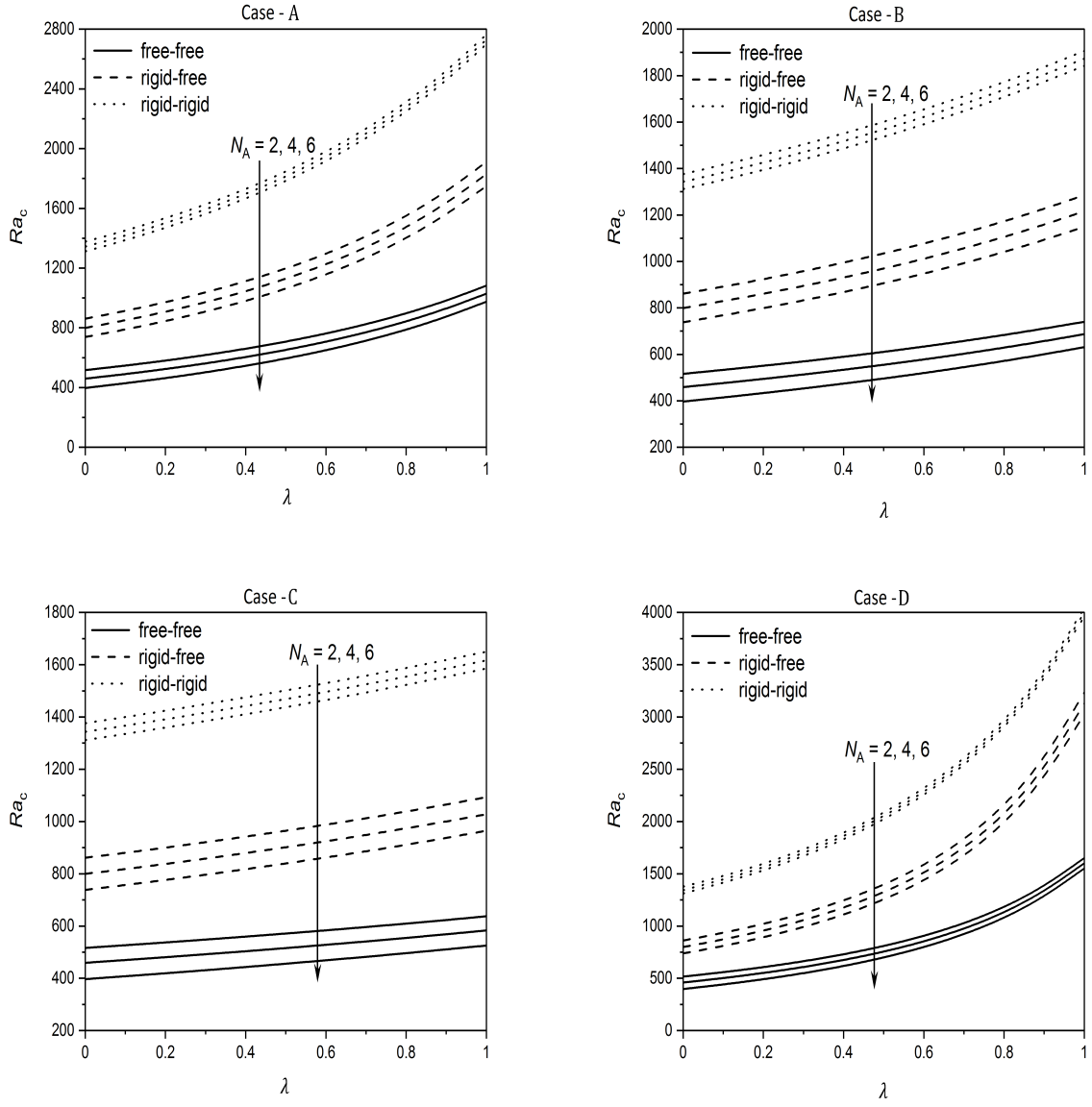

Figure 10.7: Effect of N_{A} on Ra_{c} for $Da = 0.8$, $Rn = 2$, $Le_{\mathrm{m}} = 5$ and $N_{\mathrm{B}} = 0.5$.

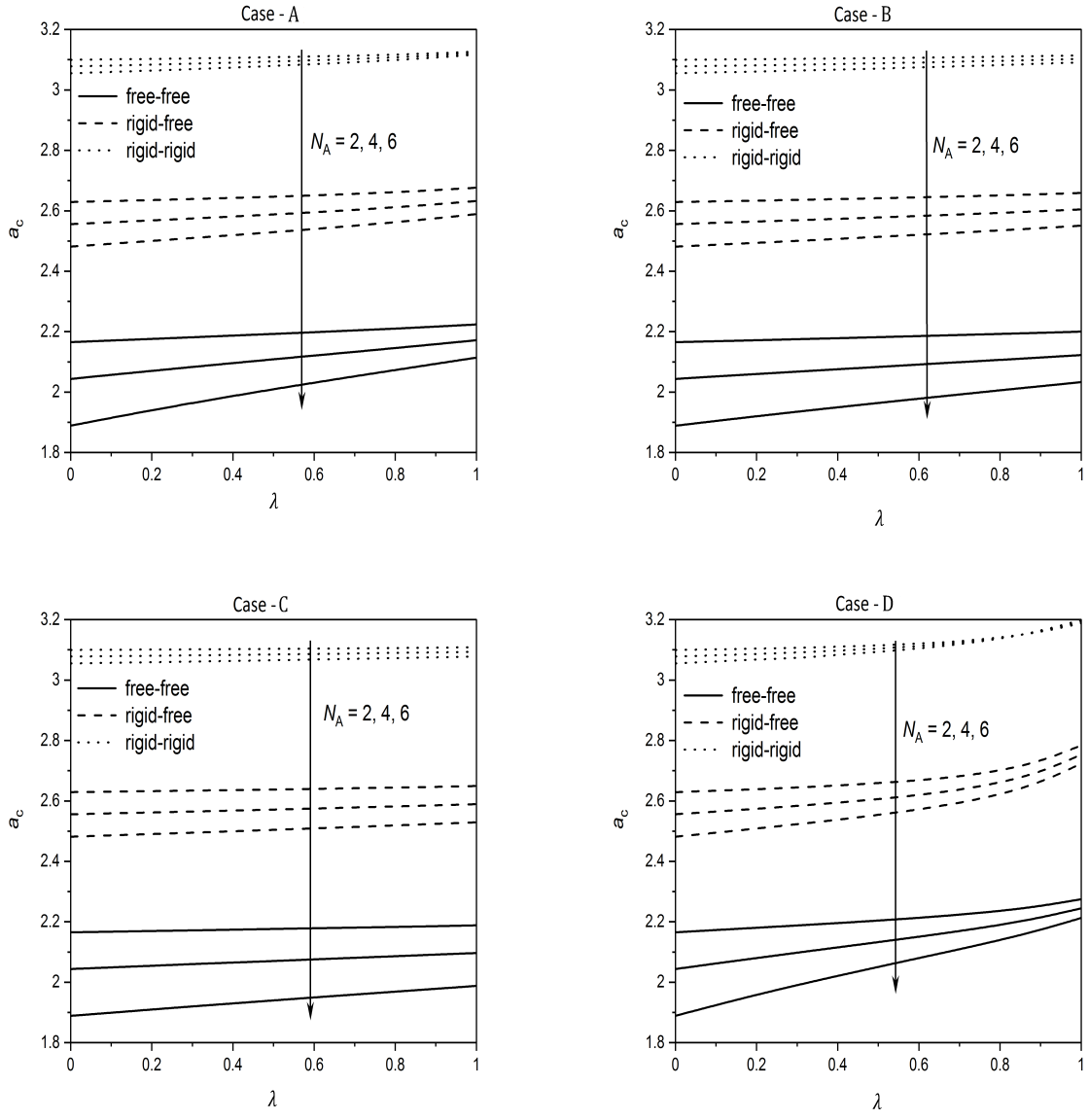

Figure 10.8: Effect of N_{A} on a_{c} for $Da = 0.8$, $Rn = 2$, $Le_{\mathrm{m}} = 5$ and $N_{\mathrm{B}} = 0.5$.

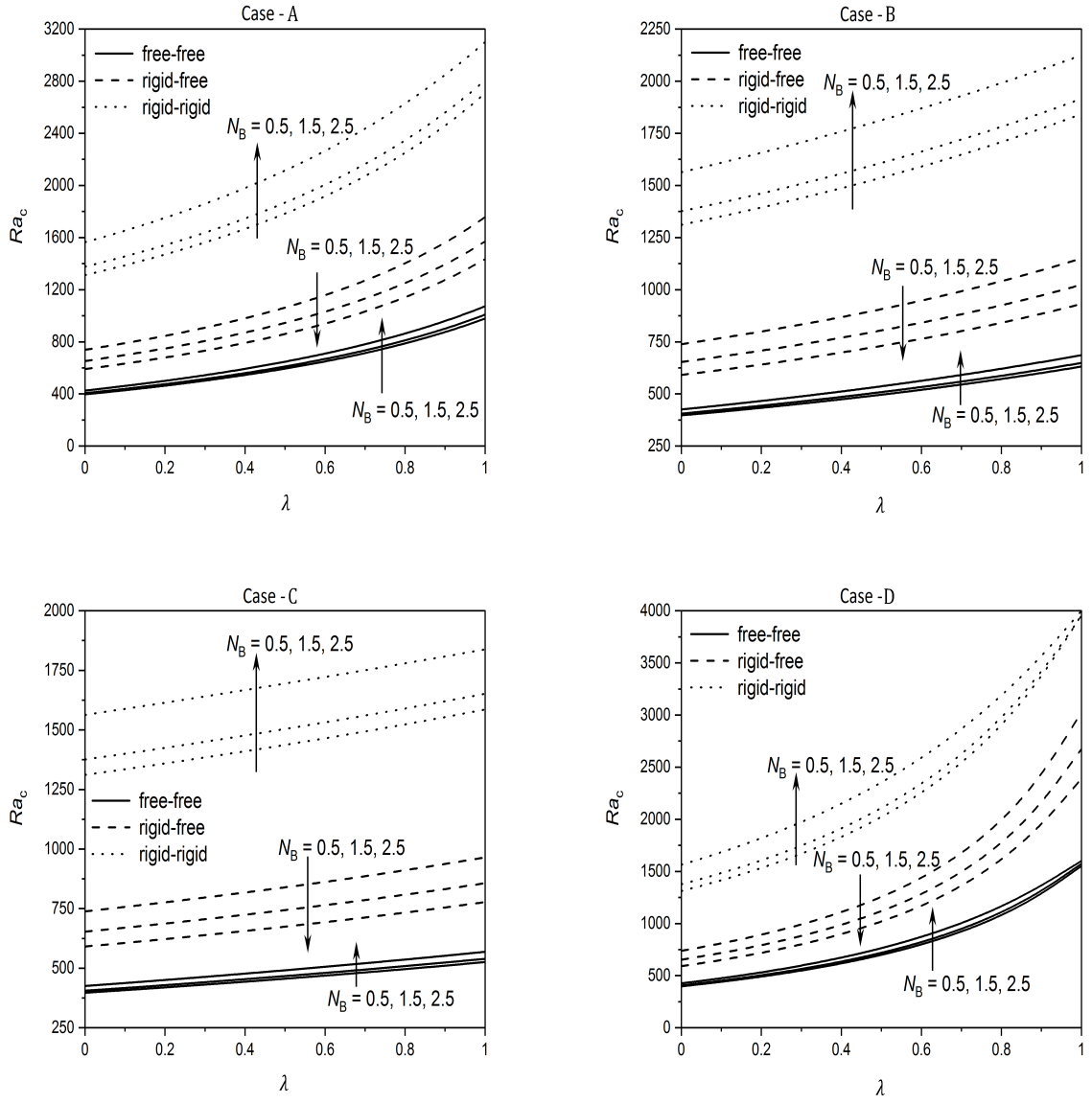

Figure 10.9: Effect of the N_{B} on Ra_{c} for $Da = 0.8$, $Rn = 2$, $Le_{\mathrm{m}} = 5$ and $N_{\mathrm{A}} = 6$.

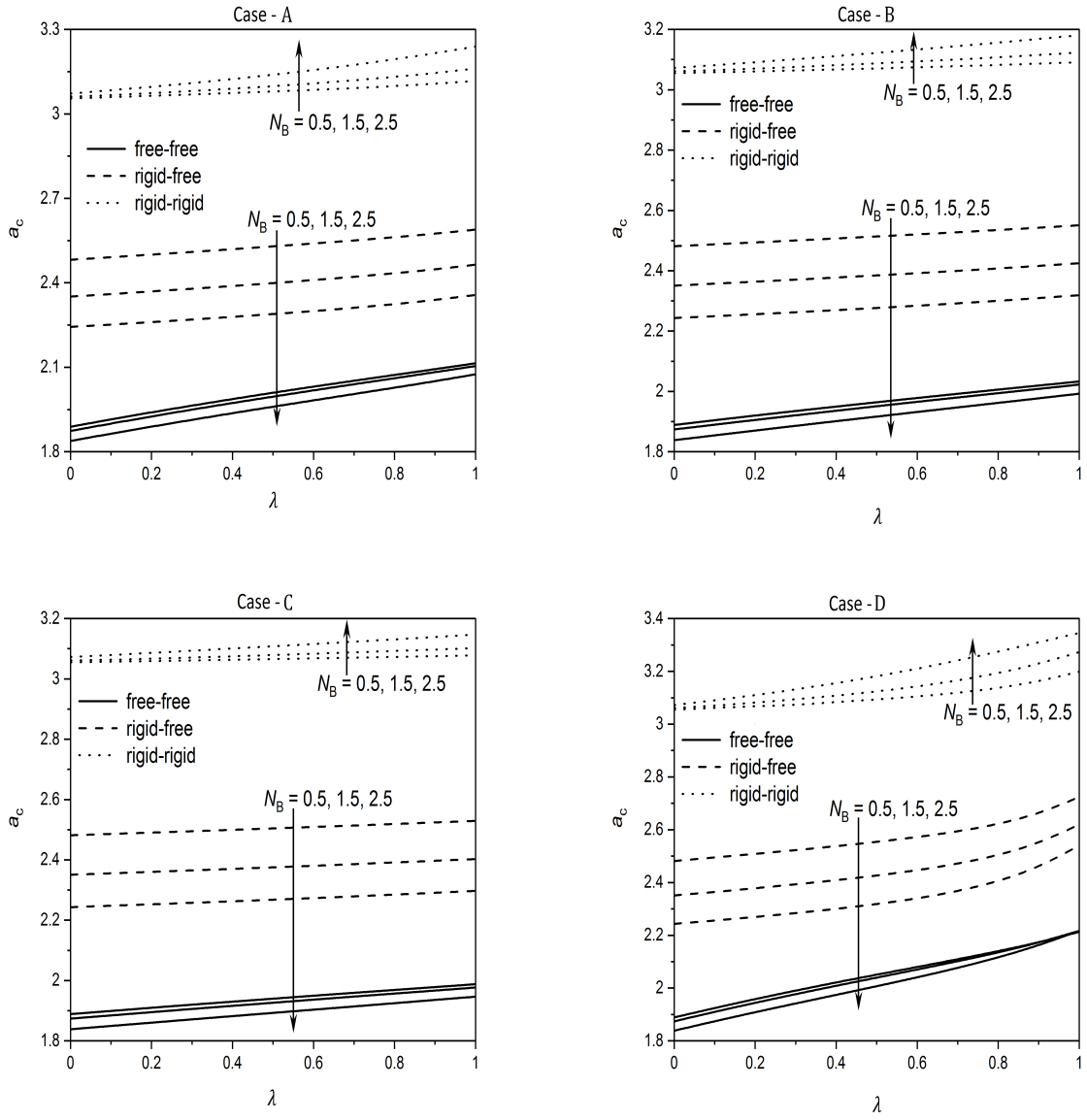

Figure 10.10: Effect of N_{B} on a_{c} for $Da = 0.8$, $Rn = 2$, $Le_{\mathrm{m}} = 5$ and $N_{\mathrm{A}} = 6$.

10.6 Conclusions

The effect of changeable gravity field on the onset of convection in an infinite horizontal porous filled with nanofluid was investigated for three types of boundaries under Brinkman-extended Darcy model. This study has been carried out for four different forms of gravity field variations. The impact of the governing parameters on the instability mechanism has been investigated numerically using *bvp4c* routine in MATLAB. The main observations drawn from the analysis are as follows:

- The influence of rising the values of λ and Da is found to be delay of the convection motion, while Rn, N_{A} and Le react to fast the onset of convective motion.
- With Da and λ, the size of the convective cells decreases, while Rn, N_{A} and Le amplify the size of the convective cells.
- The impact of rising N_{B} shows stabilizing effect for Type - a and Type - c boundaries, while it shows destabilizing effect for Type - b boundaries. Also, the size of the convective cells amplify for Type - a and Type - b boundaries, while reduces for Type - c boundaries for the rising effect of N_{B}.
- The system becomes more unstable for the exponential gravity field and more stable for cubic gravity field.
- It is observed that the system is more stable for Type - c boundaries and more unstable for Type - a boundaries, i.e., $(Ra_{\mathrm{c}})_{\text{rigid–rigid}} > (Ra_{\mathrm{c}})_{\text{rigid–free}} > (Ra_{\mathrm{c}})_{\text{free–free}}$. Also, size of the convection cells is more for Type - a boundaries compared to other types of boundaries, i.e., $(a_{\mathrm{c}})_{\text{rigid–rigid}} > (a_{\mathrm{c}})_{\text{rigid–free}} > (a_{\mathrm{c}})_{\text{free–free}}$.

Chapter 11

Linear stability of longitudinal convective rolls in a non-Darcy porous layer filled with nanofluid due to viscous dissipation effect [1]

11.1 Introduction

In most of the earlier investigations of convection, the contribution of the viscous dissipation effect has been ignored in the energy balance of a fluid saturated porous medium. However, it has a significant effect in the mixed and natural convection flows in a porous medium when the fluid has both a high viscosity and a low thermal conductivity. The importance of viscous dissipation effect on the natural convection was discussed firstly by Gebhart [48]. This dissipation number does not depend on Prantdl number and Grashof number. Turcotte *et al.* [113] has been reported the effect of the viscous dissipation parameter on the finite amplitude Bénard convection. He noticed that viscous dissipation can play a significant role on thermal convection. Later, Rees *et al.* [90] analyzed the instability mechanism in a parallel external flow solution in the presence of viscous dissipation for the boundary layer around an inclined cold surface embedded in a porous medium. Barletta *et al.* [12] investigated the effect of viscous dissipation on parallel Darcy flow in a horizontal porous layer. In this observation, they have taken lower boundary as adiabatic and the upper one as an isothermal. The extension of this has been disclosed by Barletta *et al.* [13] for Brinkman model. Recently, the viscous dissipation effect on the double diffusion convection in a porous medium discussed by Roy and Murthy [93] by taking the Soret effect.

In this chapter, we investigate the onset of convective instability due to viscous heating

[1] Communicated in "***Thermal Science and Engineering Progress***"

in a horizontal porous layer filled with nanofluid. The Brinkman-extended Darcy law is used to formulate the momentum balance equation and viscous dissipation in the medium. The governing parameter is taken as $R = GePe^2$ (introduced by Barletta *et al.* [11, 12, 13]), where Ge is the Gebhart number and Pe is the Péclet number. The basic state solution is obtained analytically. The resulting eigenvalue problem for stability is solved using *bvp4c* routine in MATLAB.

11.2 Mathematical Formulation

Consider an incompressible fluid saturated in a horizontal porous layer of thickness L, bounded by a isothermal impermeable upper wall and a thermally insulated impermeable lower wall as shown in Fig. 2.1. The Darcy–Brinkman model is adopted in order to derive the equations governing flow in the porous layer along with the effect of viscous dissipation. Applying Oberbeck-Boussinesq approximation conservation equations for the total mass, momentum, thermal energy and nanoparticles volume fraction are given below.

$$\nabla \cdot \mathbf{u} = 0, \tag{11.1}$$

$$\frac{\mu}{K}\mathbf{u} - \tilde{\mu}\nabla^2\mathbf{u} = -\nabla p + \left[\phi\rho_{\mathrm{p}} + (1-\phi)\rho_{\mathrm{f}}\{1 - \beta_{\mathrm{T}}(T - T_2)\}\right]\mathbf{g}, \tag{11.2}$$

$$\sigma\frac{\partial T}{\partial t} + \mathbf{u}\cdot\nabla T = \alpha_{\mathrm{m}}\nabla^2 T + \epsilon\frac{(\rho c)_{\mathrm{p}}}{(\rho c)_{\mathrm{f}}}\left[D_{\mathrm{B}}\nabla\phi\cdot\nabla T + \frac{D_{\mathrm{T}}}{T_2}\nabla T\cdot\nabla T\right] + \frac{\nu}{Kc_{\mathrm{p}}}\mathbf{u}\cdot\left(\mathbf{u} - \frac{\tilde{\mu}K}{\mu}\nabla^2\mathbf{u}\right), \tag{11.3}$$

$$\frac{\partial\phi}{\partial t} + \frac{1}{\epsilon}\mathbf{u}\cdot\nabla\phi = D_{\mathrm{B}}\nabla^2\phi + \frac{D_{\mathrm{T}}}{T_2}\nabla^2 T. \tag{11.4}$$

The corresponding boundary conditions are written as

$$z = 0: \quad \mathbf{u} = 0, \quad \frac{\partial T}{\partial z} = 0, \quad D_{\mathrm{B}}\frac{\partial\phi}{\partial z} + \frac{D_{\mathrm{T}}}{T_2}\frac{\partial T}{\partial z} = 0, \tag{11.5a}$$

$$z = L: \quad \mathbf{u} = 0, \quad T = T_2, \quad D_{\mathrm{B}}\frac{\partial\phi}{\partial z} + \frac{D_{\mathrm{T}}}{T_2}\frac{\partial T}{\partial z} = 0. \tag{11.5b}$$

Substituting the non-dimensional variables given in Eq. (10.6) into Eqs. (11.1)-(11.4) (after eliminating pressure term from the Eq. (11.2), we get (after dropping asterisk)

$$\nabla \cdot \mathbf{u} = 0, \tag{11.6}$$

$$\nabla \times \left(Da^{-1}\mathbf{u} - \Lambda\nabla^2\mathbf{u}\right) = \nabla \times \left[\left(\Lambda T - RnDa^{-1}\phi\right)\hat{\mathbf{e}}_{\mathrm{z}}\right], \tag{11.7}$$

$$\frac{\partial T}{\partial t}+\mathbf{u}\cdot\nabla T=\nabla^2 T+\frac{N_{\mathrm{B}}}{Le_{\mathrm{m}}}\nabla\phi\cdot\nabla T+\frac{N_{\mathrm{A}}N_{\mathrm{B}}Da}{Le_{\mathrm{m}}}\nabla T\cdot\nabla T+Ge\mathbf{u}\cdot\left(Da^{-1}\mathbf{u}-\Lambda\nabla^2\mathbf{u}\right), \quad (11.8)$$

$$\chi\frac{\partial\phi}{\partial t}+\mathbf{u}\cdot\nabla\phi=\frac{1}{Le_{\mathrm{m}}}\nabla^2\phi+\frac{N_{\mathrm{A}}Da}{Le_{\mathrm{m}}}\nabla^2 T. \quad (11.9)$$

The dimensionless conditions on the boundary are

$$z=0: \quad \mathbf{u}=0, \quad \frac{\partial T}{\partial z}=0, \quad \frac{\partial\phi}{\partial z}+N_{\mathrm{A}}\Lambda Da\frac{\partial T}{\partial z}=0, \quad (11.10a)$$

$$z=1: \quad \mathbf{u}=0, \quad T=0, \quad \frac{\partial\phi}{\partial z}+N_{\mathrm{A}}\Lambda Da\frac{\partial T}{\partial z}=0. \quad (11.10b)$$

To avoid too many parameter studies, we have taken $\Lambda=1$ and $\chi=1$ in this investigation.

11.3 Basic state solution

The magnitude of the horizontal mass flow is obtained by

$$\int_0^1 \mathbf{u_0}\cdot\mathbf{s}\,dz=Pe, \quad (11.11)$$

where Pe is the Péclet number and $\mathbf{s}=(\cos\varphi,\sin\varphi,0)$. Further, $\mathbf{u_0}$ is the dimensionless basic velocity, which is defined as

$$\mathbf{u}_0=u_0\ \mathbf{s}, \quad (11.12)$$

where u_0 is the magnitude of the basic velocity.

Under the above situations, the governing equations for u_0, T_0 and ϕ_0 can be reduced from Eqs. (11.6)-(11.9) and are given the following set of coupled ordinary differential equations as

$$\frac{d^3u_0(z)}{dz^3}-Da^{-1}\frac{du_0(z)}{dz}=0, \quad (11.13)$$

$$\frac{d^2T_0(z)}{dz^2}+\frac{N_{\mathrm{B}}}{Le}\frac{d\phi_0(z)}{dz}\frac{dT_0(z)}{dz}+\frac{N_{\mathrm{A}}N_{\mathrm{B}}Da}{Le}\left(\frac{dT_0(z)}{dz}\right)^2 + Ge\left(Da^{-1}u_0^2(z)-u_0(z)\frac{d^2u_0(z)}{dz^2}\right)=0, \quad (11.14)$$

$$\frac{d^2\phi_0(z)}{dz^2}+N_{\mathrm{A}}Da\frac{d^2T_0(z)}{dz^2}=0. \quad (11.15)$$

The solution of the base flow Eqs. (11.13)-(11.15) admits the boundary conditions:

$$z=0: \quad u_0=0, \quad \frac{dT_0(z)}{dz}=0, \quad \frac{d\phi_0(z)}{dz}+N_{\mathrm{A}}Da\frac{dT_0(z)}{dz}=0, \quad (11.16a)$$

$$z=1: \quad u_0=0, \quad T_0(z)=0, \quad \frac{d\phi_0(z)}{dz}+N_{\mathrm{A}}Da\frac{dT_0(z)}{dz}=0, \quad (11.16b)$$

where suffix '0' represents the base flow.
On solving Eqs. (11.13)-(11.15), the basic velocity, temperature and volume fraction profiles are obtained as

$$u_0(z) = \frac{Pe\xi}{\xi\cosh(\xi) - \sinh(\xi)}\Big\{\cosh(\xi) - \cosh[\xi(1-2z)]\Big\}, \tag{11.17}$$

$$T_0(z) = \frac{\xi^2 R\,\cosh(\xi)}{[\xi\cosh(\xi) - \sinh(\xi)]^2}\Big\{\left[2\xi^2(1-z^2) - 1\right]\cosh(\xi) - 2(1-z)\xi\,\sinh(\xi) + \cosh[\xi(1-2z)]\Big\}, \tag{11.18}$$

and

$$\phi_0(z) = \phi_* - \frac{0.25N_{\rm A}R\,\cosh(\xi)}{[\xi\cosh(\xi) - \sinh(\xi)]^2}\Big\{\left[2\xi^2(1-z^2) - 1\right]\cosh(\xi) - 2(1-z)\xi\,\sinh(\xi) + \cosh[\xi(1-2z)]\Big\}, \tag{11.19}$$

where Pe is the Péclet number related to the average basic velocity and ϕ_* is the reference value for nanoparticle volume fraction. Also,

$$\xi = \frac{1}{2\sqrt{Da}} \quad \text{and} \quad R = GePe^2. \tag{11.20}$$

Here, ξ is related to the permeability of the medium, which can be referred as the Brinkman parameter. Here, $\xi \to 0$ refers to the clear fluid regime, while $\xi \to \infty$ refers to the Darcy flow regime. Also the basic velocity and temperature profiles are exactly matches with the one obtained by Barletta *et al.* [13] for viscous fluid. Further, the parameter R is considered by Barletta *et al.* [11, 12], Barletta *et al.* [13] and Dubey and Murthy [45], which governs the threshold curve of the marginal stability beyond which the flow is definitely unstable.

11.4 Linear stability analysis

The instability of this system is investigated by imposing the infinitesimal disturbances on the basic state solution. Thus the velocity, temperature and volume fraction can be written as

$$(\mathbf{u}, T, \phi) = (u_0, T_0, \phi_0) + \delta(\mathbf{U}, \theta, \Phi), \tag{11.21}$$

where $\delta \ll 1$ is a small disturbance parameter and $\mathbf{U} = (U, V, W)$, θ and Φ are the infinitesimal disturbance for velocity, temperature and concentration fields. Substituting Eq. (11.21) into Eqs. (11.6)-(11.10) and neglecting δ^2 and higher order terms, the linearized continuity, momentum, thermal energy and nanoparticle volume fraction equations for the disturbed

quantities become

$$\nabla \cdot \mathbf{U} = 0, \tag{11.22}$$

$$\nabla \times \left(4\xi^2 \mathbf{U} - \nabla^2 \mathbf{U}\right) = \nabla \times \left\{(\theta - 4Rn\xi^2\Phi)\hat{\mathbf{e}}_z\right\}, \tag{11.23}$$

$$\frac{\partial \theta}{\partial t} + \mathbf{u}_0 \cdot \nabla\theta + \mathbf{U} \cdot \nabla T_0 = \nabla^2\theta + \frac{N_B}{Le_m}\left(\nabla\phi_0 \cdot \nabla\theta + \nabla T_0 \cdot \nabla\Phi\right) + \frac{N_A N_B}{2Le_m\xi^2}\nabla T_0 \cdot \nabla\theta$$
$$+Ge\mathbf{u}_0 \cdot \left(4\xi^2\mathbf{U} - \nabla^2\mathbf{U}\right) + Ge\mathbf{U} \cdot \left(4\xi^2\mathbf{u}_0 - \nabla^2\mathbf{u}_0\right), \tag{11.24}$$

$$\frac{\partial \Phi}{\partial t} + \mathbf{u}_0 \cdot \nabla\Phi + \mathbf{U} \cdot \nabla\phi_0 = \frac{1}{Le_m}\nabla^2\Phi + \frac{N_A}{4Le_m\xi^2}\nabla^2\theta. \tag{11.25}$$

The corresponding boundary condition becomes

$$z = 0: \quad \mathbf{U} = 0, \quad \frac{\partial\theta}{\partial z} = 0, \quad \frac{\partial\Phi}{\partial z} + \frac{N_A}{4\xi^2}\frac{\partial\theta}{\partial z} = 0, \tag{11.26a}$$

$$z = 1: \quad \mathbf{U} = 0, \quad \theta = 0, \quad \frac{\partial\Phi}{\partial z} + \frac{N_A}{4\xi^2}\frac{\partial\theta}{\partial z} = 0. \tag{11.26b}$$

The values of the Gebhart number is usually very small for some of the typical fluids in most general cases as it discussed by Barletta *et al.* [13], except for the case when there is a relatively high flow rate. Thus, $R = GePe^2$ is of $\mathcal{O}(1)$ when $|Pe| \gg 1$ and $Ge \ll 1$. Hence all terms are of , then the fourth and fifth term on the the right hand side of Eq. (11.24) are negligible with respect to other terms, since both are of $\mathcal{O}(|Pe|^{-1})$. Under this consideration, the simplified form of Eq. (11.24) is

$$\frac{\partial \theta}{\partial t} + \mathbf{u}_0 \cdot \nabla\theta + \mathbf{U} \cdot \nabla T_0 = \nabla^2\theta + \frac{N_B}{Le_m}\left(\nabla\phi_0 \cdot \nabla\theta + \nabla T_0 \cdot \nabla\Phi\right) + \frac{N_A N_B}{2Le_m\xi^2}\nabla T_0 \cdot \nabla\theta. \tag{11.27}$$

Expand the above equations to get

$$4\xi^2\left(\frac{\partial W}{\partial y} - \frac{\partial V}{\partial z}\right) - \nabla^2\left(\frac{\partial W}{\partial y} - \frac{\partial V}{\partial z}\right) = \frac{\partial\theta}{\partial y} - 4Rn\xi^2\frac{\partial\Phi}{\partial y}, \tag{11.28}$$

$$4\xi^2\left(\frac{\partial U}{\partial z} - \frac{\partial W}{\partial x}\right) - \nabla^2\left(\frac{\partial U}{\partial z} - \frac{\partial W}{\partial x}\right) = -\left(\frac{\partial\theta}{\partial x} - 4Rn\xi^2\frac{\partial\Phi}{\partial x}\right), \tag{11.29}$$

$$4\xi^2\left(\frac{\partial V}{\partial x} - \frac{\partial U}{\partial y}\right) - \nabla^2\left(\frac{\partial V}{\partial x} - \frac{\partial U}{\partial y}\right) = 0, \tag{11.30}$$

$$\frac{\partial\theta}{\partial t} + W\frac{dT_0}{dz} + u_0\frac{\partial\theta}{\partial x} = \nabla^2\theta + \frac{N_B}{Le_m}\frac{dT_0}{dz}\frac{\partial\Phi}{\partial z} + \frac{N_A N_B}{4Le_m\xi^2}\frac{dT_0}{dz}\frac{\partial\theta}{\partial z}, \tag{11.31}$$

$$\frac{\partial\Phi}{\partial t} + W\frac{d\phi_0}{dz} + u_0\frac{\partial\Phi}{\partial x} = \frac{1}{Le_m}\nabla^2\Phi + \frac{N_A}{4Le_m\xi^2}\nabla^2\theta. \tag{11.32}$$

The longitudinal rolls and transverse rolls occur with the parallel and perpendicular axes to the basic flow, which have been discussed in the rest of the section.

It is assumed that the disturbances are in the two dimensional oblique structures inclined to the base flow at an angle, $\varphi \in \left[0, \frac{\pi}{2}\right]$. Hence, the disturbance functions can be defined as the functions of x, z and t and are given as

$$U = U(x,z,t), \quad V = 0, \quad W = W(x,z,t), \quad \theta = \theta(x,z,t), \tag{11.33}$$
$$\Phi = \Phi(x,z,t), \quad \text{and} \quad \nabla = \left(\frac{\partial}{\partial x}, 0, \frac{\partial}{\partial z}\right).$$

Introducing the stream function formulation, the velocity components can be written as

$$U = \frac{\partial \psi}{\partial z}, \quad W = -\frac{\partial \psi}{\partial x}. \tag{11.34}$$

Thus, Eqs. (11.22)-(11.26) can be reduced as

$$\nabla^4 \psi - 4\xi^2 \nabla^2 \psi - \frac{\partial \theta}{\partial x} + 4Rn\xi^2 \frac{\partial \Phi}{\partial x} = 0, \tag{11.35}$$

$$\frac{\partial \theta}{\partial t} + PF(z,\xi)\frac{\partial \theta}{\partial x} - RG(z,\xi)\frac{\partial \psi}{\partial x} = \nabla^2 \theta + \frac{N_{\mathrm{B}}}{Le} RG(z,\xi)\left(\frac{\partial \Phi}{\partial z} + \frac{N_{\mathrm{A}}}{4\xi^2}\frac{\partial \theta}{\partial z}\right), \tag{11.36}$$

$$\frac{\partial \Phi}{\partial t} + PF(z,\xi)\frac{\partial \Phi}{\partial x} + \frac{N_{\mathrm{A}}}{4\xi^2} RG(z,\xi)\frac{\partial \psi}{\partial x} = \frac{1}{Le_{\mathrm{m}}}\left(\nabla^2 \Phi + \frac{N_{\mathrm{A}}}{4\xi^2}\nabla^2 \theta\right). \tag{11.37}$$

The corresponding boundary conditions are

$$z = 0: \quad \psi = 0, \quad \frac{\partial \psi}{\partial z} = 0, \quad \frac{\partial \theta}{\partial z} = 0, \quad \frac{\partial \Phi}{\partial z} + \frac{N_{\mathrm{A}}}{4\xi^2}\frac{\partial \theta}{\partial z} = 0, \tag{11.38a}$$

$$z = 1: \quad \psi = 0, \quad \frac{\partial \psi}{\partial z} = 0, \quad \theta = 0, \quad \frac{\partial \Phi}{\partial z} + \frac{N_{\mathrm{A}}}{4\xi^2}\frac{\partial \theta}{\partial z} = 0, \tag{11.38b}$$

where

$$P = Pe\,\cos\gamma, \tag{11.39}$$

$$F(z,\xi) = \frac{\xi}{\xi\cosh(\xi) - \sinh(\xi)}\Big\{\cosh(\xi) - \cosh[\xi(1-2z)]\Big\}, \tag{11.40}$$

and

$$G(z,\xi) = \frac{-2\xi^3\cosh(\xi)}{\left[\xi\,\cosh(\xi) - \sinh(\xi)\right]^2}\big\{2z\xi\cosh(\xi) - \sinh(\xi) + \sinh[\xi(1-2z)]\big\}. \tag{11.41}$$

The plane wave solutions are expressed as

$$\psi(x,z,t) = \Re\big\{if(z)e^{i(ax-\eta t)}\big\}, \quad \theta(x,z,t) = \Re\big\{h(z)e^{i(ax-\eta t)}\big\},$$
$$\Phi(x,z,t) = \Re\big\{q(z)e^{i(ax-\eta t)}\big\}. \tag{11.42}$$

Here, $\Re$ indicates the real part of the expression and a is the wave number. Further, $\eta = \eta_{\mathrm{r}} + i\eta_{\mathrm{i}}$ is the growth rate, where η_{r} and η_{i} describes the real and imaginary part of η, respectively, where $\eta_{\mathrm{i}} > 0$ leads to instability of the system, $\eta_{\mathrm{i}} < 0$ leads to stability of

the system and $\eta_{\rm i} = 0$ leads to the neutral or marginal stability. Since, we are very much interested in studying the marginal stability, so that we assume $\eta_{\rm i} = 0$ and $\eta_{\rm r} = \omega$. Also, $f(z), h(z)$ and $q(z)$ are complex valued functions. After applying Eq. (11.42) in Eqs. (11.35)-(11.38), the final set of governing equations with corresponding boundary conditions for the general oblique structures is given as

$$\left[(D^2 - a^2)^2 - 4\xi^2(D^2 - a^2)\right] f - ah + 4aRn\xi^2 q = 0, \tag{11.43}$$

$$\left[D^2 + \frac{N_{\rm A}N_{\rm B}}{4\xi^2 Le_{\rm m}} RG(z,\xi)D - a^2 - i(aPF(z,\xi) - \omega)\right] h + \frac{N_{\rm B}}{Le_{\rm m}} RG(z,\xi)Dq - aRG(z,\xi)f = 0, \tag{11.44}$$

$$\left[D^2 - a^2 - iLe_{\rm m}\left(aPF(z,\xi) - \omega\right)\right] q + \frac{N_{\rm A}}{4\xi^2}(D^2 - a^2)h + \frac{N_{\rm A}Le_{\rm m}}{4\xi^2} aRG(z,\xi)f = 0, \tag{11.45}$$

$$z = 0: \quad f = 0, \quad \frac{df}{dz} = 0, \quad \frac{dh}{dz} = 0, \quad \frac{dq}{dz} + \frac{N_{\rm A}}{4\xi^2}\frac{dh}{dz} = 0, \tag{11.46a}$$

$$z = 1: \quad f = 0, \quad \frac{df}{dz} = 0, \quad h = 0, \quad \frac{dq}{dz} + \frac{N_{\rm A}}{4\xi^2}\frac{dh}{dz} = 0. \tag{11.46b}$$

where $D \equiv \dfrac{d}{dz}$.

11.5 Results and discussion

The set of Eqs. (11.43)-(11.45) defines a real valued eigenvalue problem when and R is the only eigenvalue (as ω is set to zero) for longitudinal role i.e., when $\gamma = \pi/2$ or $P = 0$. Then we solved this problem using *bvp4c* routine in MATLAB.

In this work, we investigated the onset of longitudinal convective rolls with viscous dissipation effect inside a porous region filled by nanofluid. The impact of the governing parameters, $Rn, Le, N_{\rm A}, N_{\rm B}$ and ξ has been calculated throughout the paper and shown them graphically.

Fig. 11.1 shows the influence of concentration Rayleigh number, Lewis number, modified diffusivity ratio and modified particle density increment on critical R at $Rn = 0.1, Le = 5, N_{\rm A} = 3$ and $N_{\rm B} = 0.01$. It is observed that the values of $R_{\rm c}$ decreases as $Rn, Le, N_{\rm A}$ and $N_{\rm B}$ decreases, which indicates that all the parameters have a destabilizing effect. Thus, convection comes earlier for $Rn, Le, N_{\rm A}$ and $N_{\rm B}$. Further noticed that, switching parameter

(ξ) has a dual character, i.e., R_c increases for small increment of ξ and attained its maximum value for some ξ and finally bounces back. Also, the impact on R_c is invisible for large values of ξ.

11.5.1 Convective rolls

The pattern of streamlines, isotherms and isonanoconcentrations for longitudinal rolls are plotted in this section for different values of ξ and N_A. The region of the disturbance lines are shown $x \in \left[0, \frac{\pi}{a}\right]$ for streamlines and $x \in \left[-\frac{\pi}{2a}, \frac{\pi}{2a}\right]$ for isotherms and isonanoconcentrations.

Fig. 11.2 represents the effect of ξ on streamlines, isotherms and isonanoconcentrations for fixed values of $Rn = 0.1, N_A = 2, N_B = 0.01$ and $Le = 5$ at the critical label. The streamlines, isotherms and isonanoconcentrations are asymmetric with respect to the mid-plane $z = 1/2$. The streamlines are in fact slightly more compressed to the central part of channel when ξ is large. The isotherms lines are more closer near the adiabatic boundary for the small ξ. Further, the isonanoconcentrations lines are more dense inside the channel when $\xi = 0.5$.

Fig. 11.3 describe the changes in the streamlines, isotherms and isonanoconcentrations due to modified diffusivity ratio (N_A) or fixed values of $Rn = 0.1, \xi = 0.5, N_B = 0.01$ and $Le = 5$ at the critical label. There are no marked qualitative differences on the streamlines due to modified diffusivity ratio effect. The density of the isotherms curves is less near the upper boundary when modified diffusivity ratio more. This change is more prominent when N_A is large, whereas isonanoconcentrations lines are not affected due to N_A effect.

Table 11.1: Comparison of a_c and R_c between the results obtained by Barletta *et al.* [13] and Dubey and Murthy [45] with present results when $N_A = 0$, $N_B = 0$, $Rn = 0$ and $Le_m = 1$.

ξ	Barletta *et al.* [13]		Dubey and Murthy [45]		Present results	
	a_c	R_c	a_c	R_c	a_c	R_c
0	2.665502	235.3163	2.665501	235.3163	2.665502	235.3163
0.001	2.665502	235.3162	2.665501	235.3162	2.665502	235.3162
0.01	2.665502	235.3094	2.665503	235.3094	2.665502	235.3094
0.1	2.665538	234.6241	2.665537	234.6241	2.665538	234.6241
0.2	2.665647	232.5806	2.665649	232.5806	2.665647	232.5806
0.3	2.665826	229.2814	2.665825	229.2814	2.665826	229.2814
0.4	2.666072	224.8738	2.666074	224.8738	2.666073	224.8736
0.5	2.666380	219.5407	2.666379	219.5407	2.666380	219.5407
1	2.668627	185.8752	2.668628	185.8752	2.668627	185.8752
1.5	2.671296	153.5797	2.671298	153.5797	2.671296	153.5797
2	2.673358	129.3689	2.673354	129.3689	2.673358	129.3689
2.470719	2.674075	113.3695	2.674075	113.3695	2.674075	113.3695
3	2.673120	100.9718	2.673126	100.9718	2.673120	100.9718
4	2.666550	87.07186	2.666549	87.07186	2.666550	87.07186
5	2.655707	79.58888	2.655707	79.58888	2.655707	79.58888
6	2.642980	75.15759	2.642976	75.15759	2.642980	75.15759
7	2.629979	72.32003	2.629976	72.32003	2.629979	72.32003
8	2.617557	70.38715	2.617561	70.38715	2.617557	70.38716
9	2.606083	69.00467	2.606088	69.00467	2.606083	69.00467
10	2.595662	67.97654	2.595668	67.97654	2.595662	67.97654
∞	2.448266	61.86657	2.448255	61.86657	2.448266	61.86657

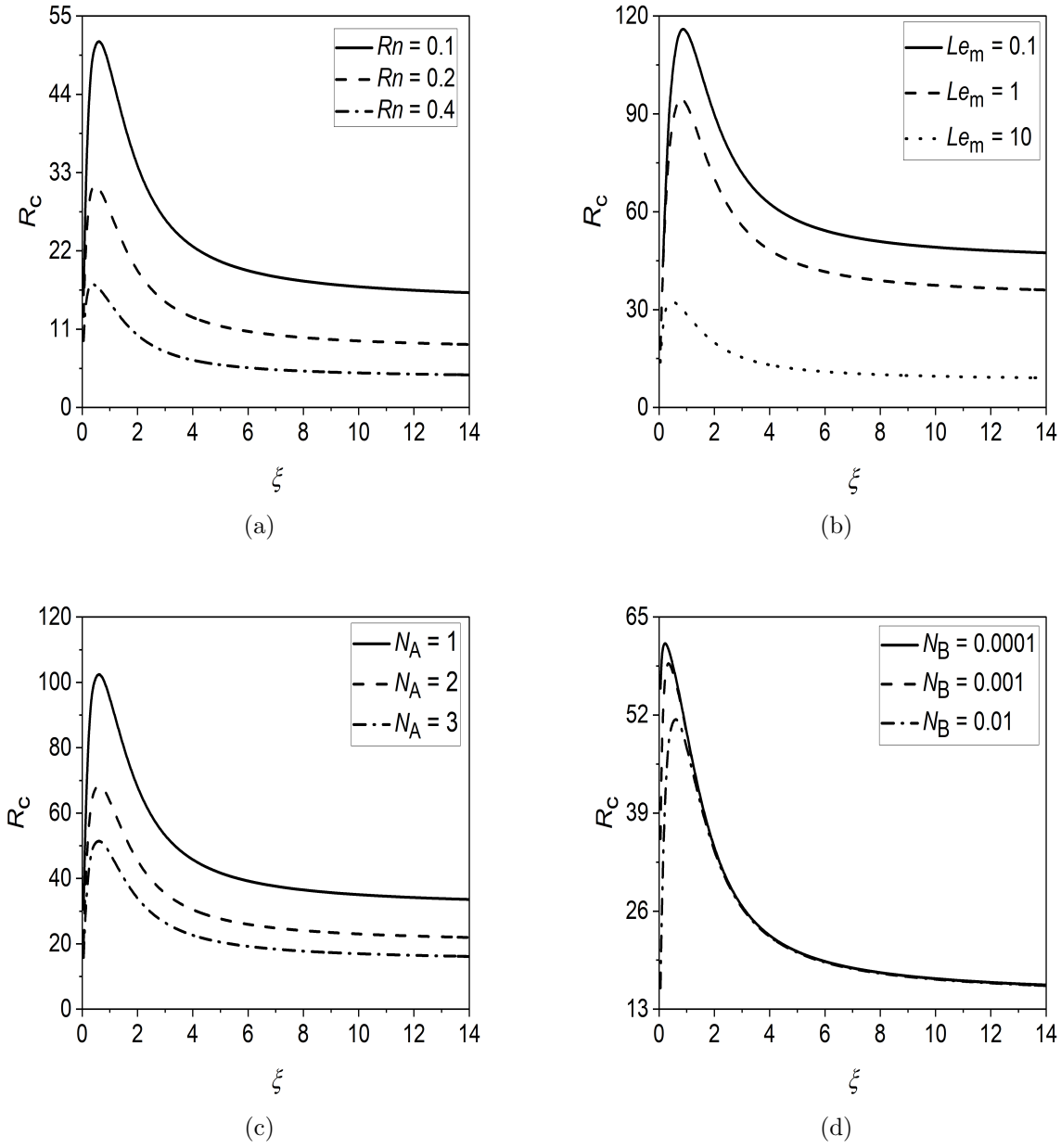

Figure 11.1: Longitudinal rolls: effect of (a) Rn, (b) Le_{m}, (c) N_{A} and (d) N_{B} on R_{c} for longitudinal rolls at $Rn = 0.1, Le_{\mathrm{m}} = 5, N_{\mathrm{A}} = 3$ and $N_{\mathrm{B}} = 0.01$.

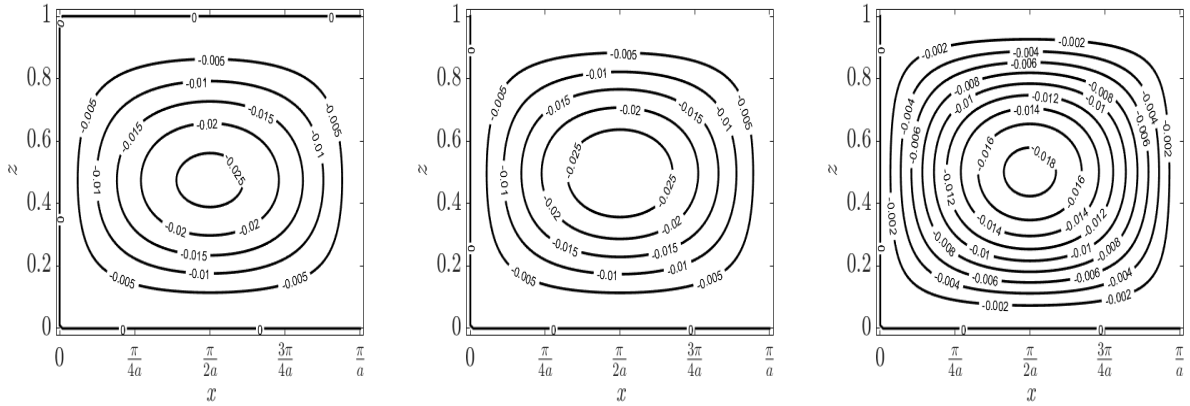

(a) $\xi = 0.05$ (b) $\xi = 0.5$ (c) $\xi = 5$

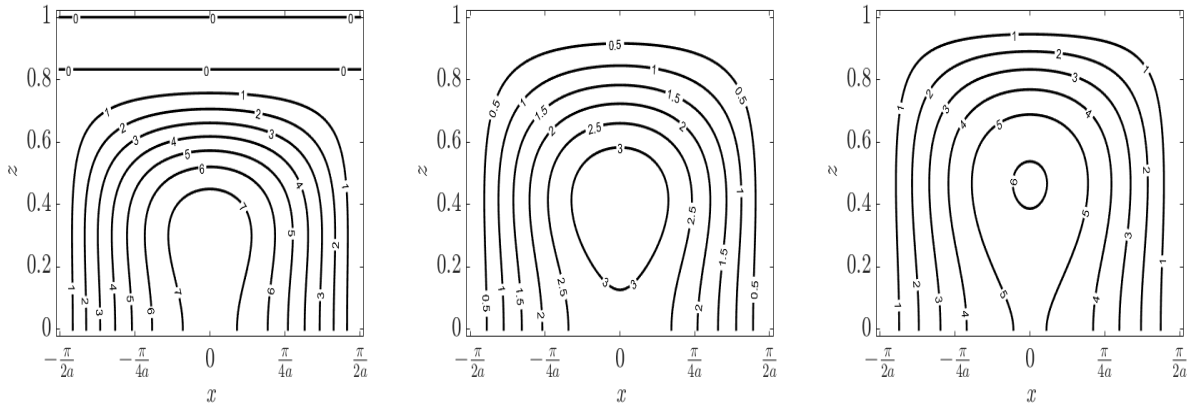

(d) $\xi = 0.05$ (e) $\xi = 0.5$ (f) $\xi = 5$

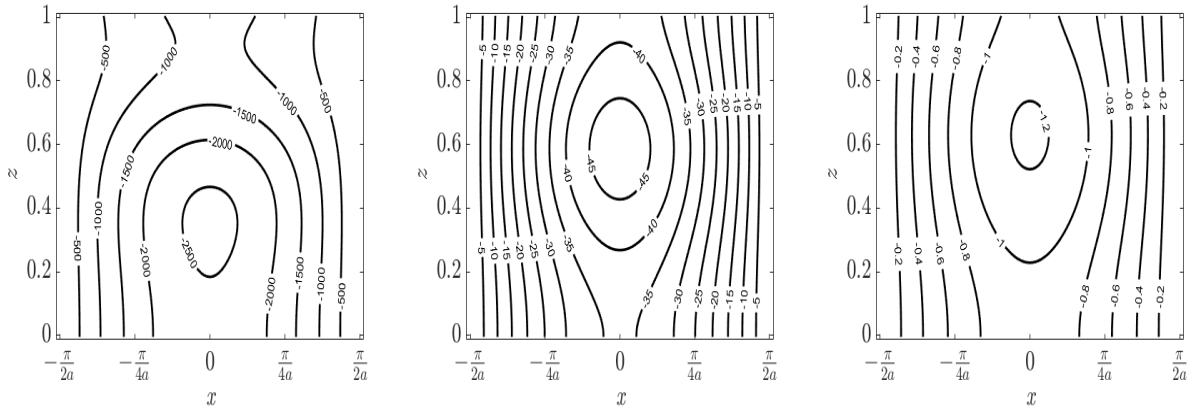

(g) $\xi = 0.05$ (h) $\xi = 0.5$ (i) $\xi = 5$

Figure 11.2: Convective rolls: effect of ξ on streamlines ($\psi = constant$) ((a) to (c)), isotherms ($\theta = constant$) ((d) to (f)) and isonanoconcentrations ($\Phi = constant$) ((g) to (i)) for longitudinal rolls at critical situation.

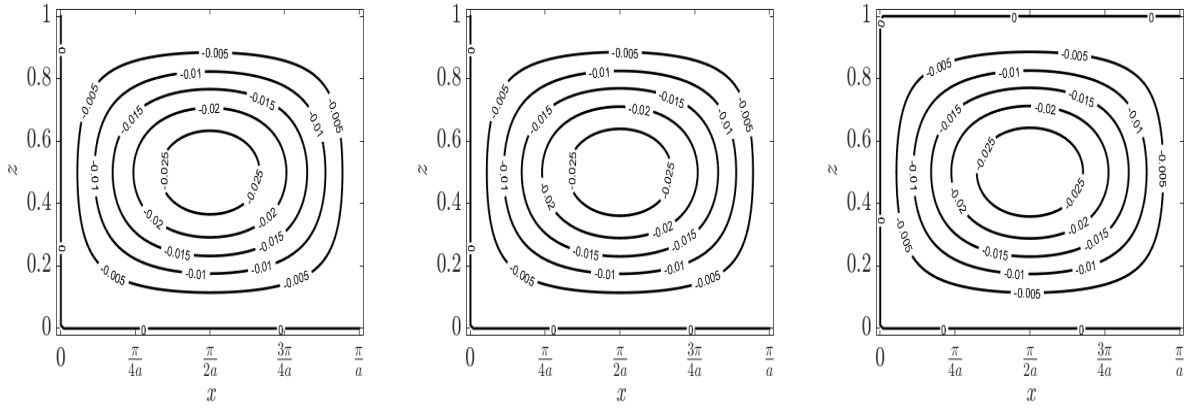

(a) $N_{\mathrm{A}} = 1$ (b) $N_{\mathrm{A}} = 2$ (c) $N_{\mathrm{A}} = 3$

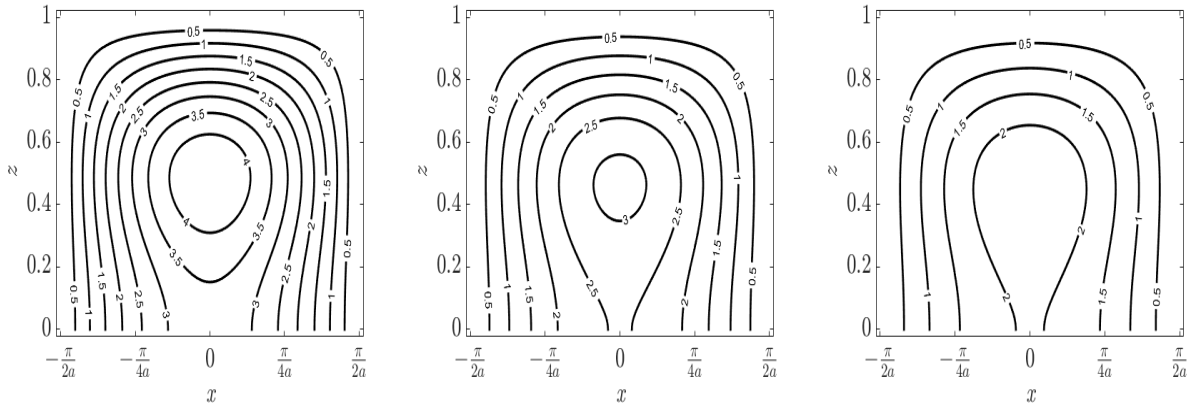

(d) $N_{\mathrm{A}} = 1$ (e) $N_{\mathrm{A}} = 2$ (f) $N_{\mathrm{A}} = 3$

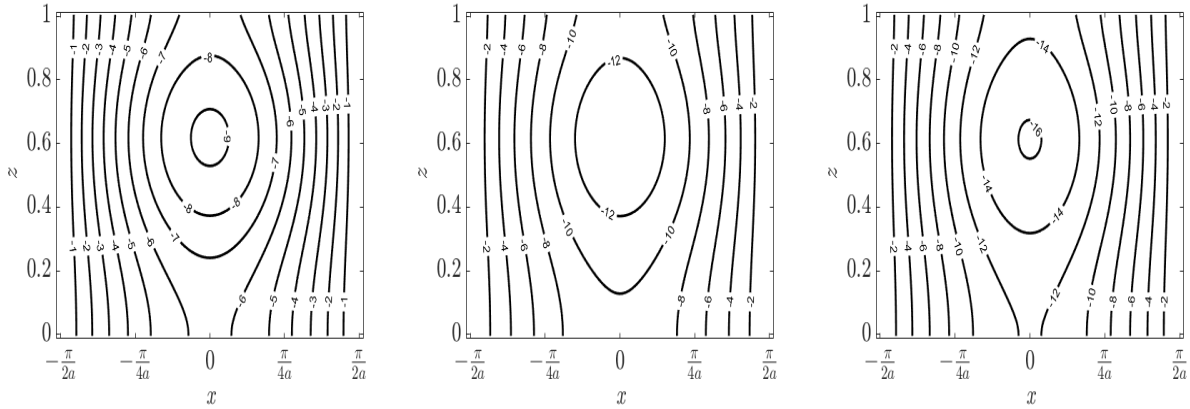

(g) $N_{\mathrm{A}} = 1$ (h) $N_{\mathrm{A}} = 2$ (i) $N_{\mathrm{A}} = 3$

Figure 11.3: Convective rolls: effect of N_{A} on streamlines $\psi = constant$ ((a) to (c)), isotherms $\theta = constant$ ((d) to (f)) and isonanoconcentrations $\Phi = constant$ ((g) to (i)) for longitudinal rolls at critical situation.

11.6 Conclusions

In this study, we have analyzed the stability analysis of longitudinal convective rolls with viscous dissipation effect in a horizontal porous layer filled with nanofluid.

- It is observed that R_{c} decreases when the values of $Rn, N_{\mathrm{A}}, N_{\mathrm{B}}$ and Le increase, whereas R_{c} follows dual nature due to the effect of ξ, i.e., R_{c} increases for small values of ξ, but it decreases for further values of ξ.
- The convection comes earlier for the rising effect of $Rn, N_{\mathrm{A}}, N_{\mathrm{B}}$ and Le, whereas it delays before some particular values of ξ.

Part IV

SUMMARY AND CONCLUSIONS

Chapter 12

Summary and Conclusions

Linear stability analysis of viscous and nanofluid flows in horizontal/vertical channels has been investigated in this thesis. The effect of double diffusion, Magnetic effect, interphase heat transfer parameter (LTNE parameter), viscous dissipation, variable gravity effect, Biots number (convective boundary conditions parameter), Soret number, Dufour number are studied to the beginning of convection

The governing partial differential equations of the flow in the Chapters - 2 through Chapters - 11 are transformed into a system of nonlinear ordinary differential equations using suitable transformations. The resulting non-linear ordinary differential equations were linearized using perturbation technique and converted them ordinary differential equations using normal mode analysis. The eigenvalue problem equations together with corresponding boundary conditions were solved using either Chebyshev spectral collocation method or boundary value problem solver *bvp4c* routine in MATLAB. The effects of various geometrical and fluid parameters on the onset of convection is presented through graphs and discussed. The important observations made from this study are listed below:

- The impact of increasing throughflow parameter (Q), gravity variation parameter (λ) are found to lag the onset of convection, whereas Gebhart number (Ge) is react to elevate the onset of convective motion.
- The flow field is more stable for Brinkam model as compared with the Darcy model.
- The convection comes earlier for quadratic varying gravity field compare to linear varying gravity field when the external heat supplies on both the boundaries. The same nature of quadratic varying gravity field has been observed one boundary maintains

a constant heat flux while another one is an isothermal condition or external heat supplies from the boundaries exchange their role.

- The Brinkman flow regime shows more stability when two the boundaries are subjected to the external heating for both the gravity fields.

- The size of the convective cells decreases with rising the effect of gravity field parameter, Lewis number and Soret parameter, while solutal Rayleigh number and Gebhart number has a dual character on the dimension of convection cells.

- It is distinguished that the flow is more stable for exponential varying gravity field whereas more unstable for cubic varying gravity field.

- The rise in the heat supplied both the boundaries stabilize the flow field. Further, the flow shows more stable when the external heating on the lower boundaries is higher than at the top boundary.

- The stability of the flow increases when the upper boundary maintain constant heat flux and lower one as at isothermal state compare to the lower boundary maintain constant heat flux and upper one as at isothermal state.

- Soret parameter (Sr) has a stabilizing effect for horizontal flow of viscous fluid in the presence of variable gravity field, whereas it has a destabilizing effect for nanofluid flow in vertical channel for constant gravity field. Further, Lewis number (Le) shows a stabilizing nature for both the cases.

- The disturbance is least stable for two dimensional flows.

- Interphase heat transfer parameter (H) shows the stabilizing nature inside the intermediate range, while the system acts like an LTE model when $H \to 0$ and $H \to \infty$ for horizontal flow of viscous fluid with inconstant gravity field. On the other hand, interphase heat transfer parameter for fluid/nanoparticle has a destabilizing nature, whereas interphase heat transfer parameter for fluid/solid-matrix has a stabilizing nature inside the intermediate range but these effects die out when they converge to zero and beyond sufficiently large values of them, where system behaves as in LTE state for constant varying gravity filled filled with nanofluid.

- Convection delays due to the rising effect of Hartmann number (Ha) and Prandtl number (Pr) and it comes earlier for growing values of concentration Rayleigh number (Rn), thermo-solutal Lewis number (Ln) and Dufour number (D_{f}), whereas no

significant effect has been detected for the enhance values of modified diffusivity ratio (N_{A}), modified particle density increment (N_{B}) and solutal Rayleigh number (Rs) for constant gravity field. But, both N_{A} and N_{B} shows significant impact on stability analysis when the flow is controlled by variable gravity fields.

- The dimension of the convective cells displays dual nature for the rising effect of Darcy number Da and λ when two the boundaries are subjected to the external heating for both the gravity fields. But, the cell size decreases due to the augmenting values of B_0 and B_1 (Biots number). On the other hand, the cells size increases when $B_0 = 0$ and $B_1 \to \infty$, but it decreases when $B_0 \to \infty$ and $B_1 = 0$ for both the gravity fields.

The work presented in the thesis can be extended by studying the analysis in various non-Newtonian fluids like Micropolar fluids, Couple stress fluids, Power-law fluids and the geometry can be changed to pipe, inclined channel, through annulus and an inclined pipe. This work can also be extended to porous media. Further, this work can be extended to study the analysis on nonlinear stability.

Bibliography

[1] S. Agarwal and P. Rana. Analysis of periodic and aperiodic convective stability of double diffusive nanofluid convection in rotating porous layer. *Applied Mathematics and Mechanics*, 37(2):215–226, 2016.

[2] S. Agarwal, P. Rana, and B. S. Bhadauria. Rayleigh–Bénard convection in a nanofluid layer using a thermal nonequilibrium model. *Journal of Heat Transfer*, 136(12):122501, 2014.

[3] J. Ahuja and J. Sharma. Rayleigh—Bénard instability in nanofluids: a comprehensive review. *Micro and Nano Syst. Lett.*, 8(21):https://doi.org/10.1186/s40486–020–00123–y, 2020.

[4] T. Alboussiere, J. P. Garandet, and R. Moreau. Buoyancy-driven convection with a uniform magnetic field. part 1. Asymptotic analysis. *Journal of Fluid Mechanics*, 253:545–563, 1993.

[5] S. M. Alex and P. R. Patil. Effect of a variable gravity field on convection in an anisotropic porous medium with internal heat source and inclined temperature gradient. *Journal of Heat Transfer*, 124(1):144–150, 2002.

[6] S. M. Alex, P. R. Patil, and K. S. Venkatakrishnan. Variable gravity effects on thermal instability in a porous medium with internal heat source and inclined temperature gradient. *Fluid Dynamics Research*, 29(1):1–6, 2001.

[7] K. Ali, S. Ahmad, S. Ahmad, M. Ashraf, and M. Asif. On the interaction between the external magnetic field and nanofluid inside a vertical square duct. *AIP Advances*, 5(10):107–120, 2015.

[8] N. Alsoy-Akgün. Effect of an uniform magnetic field on unsteady natural convection of nanofluid. *Journal of Taibah University for Science*, 13(1):1073–1086, 2019.

[9] N. Banu and D. A. S. Rees. Onset of Darcy–Bénard convection using a thermal non-equilibrium model. *International Journal of Heat and Mass Transfer*, 45(11):2221–2228, 2002.

[10] A. Barletta, M. Celli, and H. Lagziri. Instability of a horizontal porous layer with local thermal non-equilibrium: effects of free surface and convective boundary conditions. *International Journal of Heat and Mass Transfer*, 89:75–89, 2015.

[11] A. Barletta, M. Celli, and D. A. S. Rees. Darcy–Forchheimer flow with viscous dissipation in a horizontal porous layer: onset of convective instabilities. *Journal of Heat Transfer*, 131(7):072602, 2009.

[12] A. Barletta, M. Celli, and D. A. S. Rees. The onset of convection in a porous layer induced by viscous dissipation: a linear stability analysis. *International Journal of Heat and Mass Transfer*, 52(1-2):337–344, 2009.

[13] A. Barletta, E. R. di Schio, and M. Celli. Instability and viscous dissipation in the horizontal Brinkman flow through a porous medium. *Transport in Porous Media*, 87(1):105–119, 2011.

[14] A. Barletta, E. R. di Schio, and L. Storesletten. Convective roll instabilities of vertical throughflow with viscous dissipation in a horizontal porous layer. *Transport in Porous Media*, 81(3):461–477, 2010.

[15] A. Barletta and D. A. Nield. Thermosolutal convective instability and viscous dissipation effect in a fluid-saturated porous medium. *International Journal of Heat and Mass Transfer*, 54(7-8):1641–1648, 2011.

[16] A. Barletta and D. A. S. Rees. Local thermal non-equilibrium analysis of the thermo-convective instability in an inclined porous layer. *International Journal of Heat and Mass Transfer*, 83:327–336, 2015.

[17] H. Bénard. Les tourbillions cellularies dans une nappe liquide transportant de la chaleut par convection en regime permanent. *Ann. Che. Phys.*, 23:62, 1901.

[18] P. Bera and A. Khalili. Stability of mixed convection in an anisotropic vertical porous channel. *Physics of Fluids*, 14(5):1617–1630, 2002.

[19] P. Bera and M. K. Khandelwal. A thermal non-equilibrium perspective on instability mechanism of non-isothermal Poiseuille flow in a vertical porous-medium channel. *International Journal of Thermal Sciences*, 105:159–173, 2016.

[20] B. S. Bhadauria and S. Agarwal. Convective transport in a nanofluid saturated porous layer with thermal non equilibrium model. *Transport in Porous Media*, 88(1):107–131, 2011.

[21] B. S. Bhadauria and S. Agarwal. Natural convection in a nanofluid saturated rotating porous layer: a nonlinear study. *Transport in Porous Media*, 87(2):585–602, 2011.

[22] B. S. Bhadauria and A. Singh. Throughflow and G-jitter effects on chaotic convection in an anisotropic porous medium. *Ain Shams Engineering Journal*, 9(4):1999–2013, 2018.

[23] N. R. Braga Jr, P. V. Brandão, L. S. de B. Alves, and A. Barletta. Convective instability induced by internal and external heating in a fluid saturated porous medium. *International Journal of Heat and Mass Transfer*, 108:2393–2402, 2017.

[24] H. C. Brinkman. A calculation of the viscous force exerted by a flowing fluid on a dense swarm of particles. *Applied Scientific Research*, 1(1):27–34, 1949.

[25] J. Buongiorno. Convective transport in nanofluids. *ASME Journal of Heat Transfer*, 128(3):240–250, 2006.

[26] J. Buongiorno, D. C. Venerus, N. Prabhat, T. McKrell, J. Townsend, R. Christianson, Y. V. Tolmachev, P. Keblinski, Lin-wen Hu, J. L. Alvarado, et al. A benchmark study on the thermal conductivity of nanofluids. *Journal of Applied Physics*, 106(9):094312, 2009.

[27] C. Caruto, M. Y. Hussaini, A. Quarteroni, and T. A. Zang. *Spectral Method in Fluid Dynamics*. Springer-Verlag Berlin Heidelberg, 1988.

[28] M. Celli, H. Lagziri, and M. Bezzazi. Local thermal non-equilibrium effects in the Horton-Rogers-Lapwood problem with a free surface. *International Journal of Thermal Sciences*, 116:254–264, 2017.

[29] R. Chand and G. C. Rana. On the onset of thermal convection in rotating nanofluid layer saturating a Darcy–Brinkman porous medium. *International Journal of Heat and Mass Transfer*, 55(21-22):5417–5424, 2012.

[30] R. Chand and G. C. Rana. Oscillating convection of nanofluid in porous medium. *Transport in Porous Media*, 95(2):269–284, 2012.

[31] R. Chand, G. C. Rana, and S. Kumar. Variable gravity effects on thermal instability of nanofluid in anisotropic porous medium. *International Journal of Applied Mechanics and Engineering*, 18(3):631–642, 2013.

[32] S. Chandrasekhar. *Hydrodynamic and Hydromagnetic Stability*. New York, NY: Dover Publication, 2013.

[33] F. Chen. Throughflow effects on convective instability in superposed fluid and porous layers. *Journal of Fluid Mechanics*, 231:113–133, 1991.

[34] Y. C. Chen. Non-Darcy flow stability of mixed convection in a vertical channel filled with a porous medium. *International Journal of Heat and Mass Transfer*, 47(6-7):1257–1266, 2004.

[35] Y. C. Chen and J. N. Chung. The linear stability of mixed convection in a vertical channel flow. *Journal of Fluid Mechanics*, 325:29–51, 1996.

[36] S. U. S. Choi and J. A. Eastman. Enhancing thermal conductivity of fluids with nanoparticles. *ASME FED*, 231/MD-Vol. 66:99–105, 1995.

[37] L. Cordell. Gravity analysis using an exponential density-depth function; san jacinto graben, california. *Geophysics*, 38(4):684–690, 1973.

[38] H. P. G. Darcy. *Les fontaines publiques de la ville de Dijon*. Victor Dalmont, Paris, 1856.

[39] S. K. Das, S. U. S. Choi, W. Yu, and T. Pradeep. *Nanofluids: Science and Technology*. Wiley, New Jersey, USA, 2007.

[40] L. Davoust, M. D. Cowley, R. Moreau, and R. Bolcato. Buoyancy-driven convection with a uniform magnetic field. part 2. Experimental investigation. *Journal of Fluid Mechanics*, 400:59–90, 1999.

[41] N. Deepika. Linear and nonlinear stability of double-diffusive convection with the Soret effect. *Transport in Porous Media*, 121(1):93–108, 2018.

[42] P. G. Drazin and W. H. Reid. *Hydrodynamic Stability*. Cambridge University Press, 2004.

[43] R. Dubey and P. V. S. N. Murthy. The onset of convective instability of horizontal throughflow in a porous layer with inclined thermal and solutal gradients. *Physics of Fluids*, 30(7):074104, 2018.

[44] R. Dubey and P. V. S. N. Murthy. Linear stability of horizontal throughflow in a Brinkman porous medium with mixed thermal boundary conditions. *International Journal of Thermal Sciences*, 145:105923, 2019.

[45] R. Dubey and P. V. S. N. Murthy. Linear stability of horizontal throughflow in a Brinkman porous medium with viscous dissipation and Soret effect. *Transport in Porous Media*, 126(2):275–294, 2019.

[46] R. Dubey and P. V. S. N. Murthy. The onset of double–diffusive convection in a Brinkman porous layer with convective thermal boundary conditions. *AIP Advances*, 9(4):045322, 2019.

[47] P. Forchheimer. Wasserbewegung durch boden. *Zeitschrift des Verines Deutscher Ingenieure*, 45:1782–1788, 1901.

[48] B. Gebhart. Effects of viscous dissipation in natural convection. *Journal of Fluid Mechanics*, 14(2):225–232, 1962.

[49] B. Gebhart and J. Mollendorf. Viscous dissipation in external natural convection flows. *Journal of Fluid Mechanics*, 38(1):97–107, 1969.

[50] U. Gupta, J. Ahuja, and R. K. Wanchoo. Magneto convection in a nanofluid layer. *International Journal of Heat and Mass Transfer*, 64:1163–1171, 2013.

[51] A. Halder, A. Dhall, and A. K. Datta. Modeling transport in porous media with phase change: applications to food processing. *Journal of Heat Transfer*, 133(3):031010, 2011.

[52] A. J. Harfash. Convection in a porous medium with variable gravity field and magnetic field effects. *Transport in Porous Media*, 103(3):361–379, 2014.

[53] A. J. Harfash. Three-dimensional simulations for convection in a porous medium with internal heat source and variable gravity effects. *Transport in Porous Media*, 101(2):281–297, 2014.

[54] A. J. Harfash. Three-dimensional simulations for convection problem in anisotropic porous media with nonhomogeneous porosity, thermal diffusivity, and variable gravity effects. *Transport in Porous Media*, 102(1):43–57, 2014.

[55] A. J. Harfash. Magnetic effect on convection in a porous medium with chemical reaction effect. *Transport in Porous Media*, 106(1):163–179, 2015.

[56] A. J. Harfash and A. K. Alshara. Chemical reaction effect on double diffusive convection in porous media with magnetic and variable gravity effects. *Korean Journal of Chemical Engineering*, 32(6):1046–1059, 2015.

[57] C. Hirt, S. Claessens, T. Fecher, M. Kuhn, R. Pail, and M. Rexer. New ultrahigh-resolution picture of Earth's gravity field. *Geophysical Research Letters*, 40(16):4279–4283, 2013.

[58] C. W. Horton and F. T. Rogers Jr. Convection currents in a porous medium. *Journal of Applied Physics*, 16(6):367–370, 1945.

[59] A. Hudoba and S. Molokov. Linear stability of buoyant convective flow in a vertical channel with internal heat sources and a transverse magnetic field. *Physics of Fluids*, 28(11):114103, 2016.

[60] P. Kiran. Throughflow and gravity modulation effects on heat transport in a porous medium. *Journal of Applied Fluid Mechanics*, 9(3):1105–1113, 2016.

[61] S. Kumari and P. V. S. N. Murthy. Stability of the horizontal throughflow of a power–law fluid in a double-diffusive porous layer under convective boundary conditions. *International Journal of Thermal Sciences*, 146:106098, 2019.

[62] A. V. Kuznetsov and D. A. Nield. Effect of local thermal non-equilibrium on the onset of convection in a porous medium layer saturated by a nanofluid. *Transport in Porous Media*, 83(2):425–436, 2010.

[63] A. V. Kuznetsov and D. A. Nield. The onset of double-diffusive nanofluid convection in a layer of a saturated porous medium. *Transport in Porous Media*, 85(3):941–951, 2010.

[64] A. V. Kuznetsov and D. A. Nield. Thermal instability in a porous medium layer saturated by a nanofluid: Brinkman model. *Transport in Porous Media*, 81(3):409–422, 2010.

[65] A. V. Kuznetsov and D. A. Nield. Local thermal non-equilibrium effects on the onset of convection in an internally heated layered porous medium with vertical throughflow. *International Journal of Thermal Sciences*, 92:97–105, 2015.

[66] E. R. Lapwood. Convection of a fluid in a porous medium. *Mathematical Proceedings of the Cambridge Philosophical Society*, 44(4):508–521, 1948.

[67] Q. Li, J. Wang, J. Wang, J. Baleta, C. Min, and B. Sundén. Effects of gravity and variable thermal properties on nanofluid convective heat transfer using connected and unconnected walls. *Energy Conversion and Management*, 171:1440–1448, 2018.

[68] L. Liu and O. Zikanov. Elevator mode convection in flows with strong magnetic fields. *Physics of Fluids*, 27(4):044103, 2015.

[69] A. Mahajan and M. K. Sharma. Double-diffusive convection in a magnetic nanofluid layer with cross diffusion effects. *Journal of Engineering Mathematics*, 115(1):67–87, 2019.

[70] A. Mahajan and M. K. Sharma. Effects of local thermal nonequilibrium on the onset of convection in a magnetic nanofluid layer. *Heat Transfer Research*, 51(7):689–705, 2020.

[71] A. Mahajan and V. K. Tripathi. Effects of spatially varying gravity, temperature and concentration fields on the stability of a chemically reacting fluid layer. *Journal of Engineering Mathematics*, 125(1):23–45, 2020.

[72] M. S. Malashetty, I. S. Shivakumara, and S. Kulkarni. The onset of Lapwood–Brinkman convection using a thermal non-equilibrium model. *International Journal of Heat and Mass Transfer*, 48(6):1155–1163, 2005.

[73] M. S. Malashetty, M. Swamy, and R. Heera. Double diffusive convection in a porous layer using a thermal non-equilibrium model. *International Journal of Thermal Sciences*, 47(9):1131–1147, 2008.

[74] I. Manna. Synthesis, characterization and application of nanofluid—an overview. *Journal of the Indian Institute of Science*, 89(1):21–33, 2009.

[75] D. A. Nield. Onset of thermohaline convection in a porous medium. *Water Resources Research*, 4(3):553–560, 1968.

[76] D. A. Nield. The boundary correction for the Rayleigh–Darcy problem: limitations of the Brinkman equation. *Journal of Fluid Mechanics*, 128:37–46, 1983.

[77] D. A. Nield. Convection in a porous medium with inclined temperature gradient and vertical throughflow. *International Journal of Heat and Mass Transfer*, 41(1):241–243, 1998.

[78] D. A. Nield and A. Bejan. *Convection in Porous Media*, volume 5th edn. Springer, New York, NY, 2017.

[79] D. A. Nield and A. V. Kuznetsov. Thermal instability in a porous medium layer saturated by a nanofluid. *International Journal of Heat and Mass Transfer*, 52(25-26):5796–5801, 2009.

[80] D. A. Nield and A. V. Kuznetsov. The effect of local thermal nonequilibrium on the onset of convection in a nanofluid. *Journal of Heat Transfer*, 132(5):052405, 2010.

[81] D. A. Nield and A. V. Kuznetsov. The onset of double-diffusive convection in a nanofluid layer. *International Journal of Heat and Fluid Flow*, 32(4):771–776, 2011.

[82] D. A. Nield and A. V. Kuznetsov. Onset of convection with internal heating in a porous medium saturated by a nanofluid. *Transport in Porous Media*, 99(1):73–83, 2013.

[83] D. A. Nield and A. V. Kuznetsov. Thermal instability in a porous medium layer saturated by a nanofluid: a revised model. *International Journal of Heat and Mass Transfer*, 68:211–214, 2014.

[84] S. A. Orszag. Accurate solution of the Orr–Sommerfeld stability equation. *Journal of Fluid Mechanics*, 50(4):689–703, 1971.

[85] A. Postelnicu. The onset of a Darcy–Brinkman convection using a thermal nonequilibrium model. part ii. *International Journal of Thermal Sciences*, 47(12):1587–1594, 2008.

[86] A. Postelnicu and D. A. S. Rees. The onset of Darcy–Brinkman convection in a porous layer using a thermal nonequlibrium model—part i: stress-free boundaries. *International Journal of Energy Research*, 27(10):961–973, 2003.

[87] G. K. Pradhan and P. C. Samal. Thermal stability of a fluid layer under variable body forces. *Journal of Mathematical Analysis and Applications*, 122(2):487–495, 1987.

[88] G. C. Rana and R. Chand. Onset of thermal convection in a rotating nanofluid layer saturating a Darcy–Brinkman porous medium: a more realistic model. *Journal of Porous Media*, 18(6):629–635, 2015.

[89] L. Rayleigh. On convection currents in a horizontal layer of fluid when the higher temperature is on the under side. *Phil. Mag.*, 32:529, 1916.

[90] D. A. S. Rees, E. Magyari, and B. Keller. Vortex instability of the asymptotic dissipation profile in a porous medium. *Transport in Porous Media*, 61(1):1–14, 2005.

[91] S. Rionero and B. Straughan. Convection in a porous medium with internal heat source and variable gravity effects. *International Journal of Engineering Science*, 28(6):497–503, 1990.

[92] H. Rodot and A. M. Regel, L. L.and Turtchaninov. Crystal growth of iv–vi semiconductors in a centrifuge. *J. Cryst. Growth*, 104:280–284, 1990.

[93] K. Roy and P. V. S. N. Murthy. Soret effect on the double diffusive convection instability due to viscous dissipation in a horizontal porous channel. *International Journal of Heat and Mass Transfer*, 91:700–710, 2015.

[94] K. Roy and P. V. S. N. Murthy. Effect of variable gravity on Darcy flow with impressed horizontal gradient and viscous dissipation. *Journal of Applied Fluid Mechanics*, 9(5):2621–2628, 2016.

[95] K. Roy and P. V. S. N. Murthy. Effect of viscous dissipation on the convective instability induced by inclined temperature gradients in a non-Darcy porous medium with horizontal throughflow. *Physics of Fluids*, 29(4):044104, 2017.

[96] K. Roy and P. V. S. N. Murthy. Linear stability of the double-diffusive convection in a horizontal porous layer with open top: Soret and viscous dissipation effects. *Transport in Porous Media*, 122(3):693–712, 2018.

[97] V. C. Santanna, A. C. M. Silva, H. M. Lopes, and F. A. S. Neto. Microemulsion flow in porous medium for enhanced oil recovery. *Journal of Petroleum Science and Engineering*, 105:116–120, 2013.

[98] B. M. Shankar, J. Kumar, and I. S. Shivakumara. Magnetohydrodynamic instability of mixed convection in a differentially heated vertical channel. *The European Physical Journal Plus*, 134(2):53, 2019.

[99] A. K. Sharma, M. K. Khandelwal, and P. Bera. Finite amplitude analysis of non-isothermal parallel flow in a vertical channel filled with a highly permeable porous medium. *Journal of Fluid Mechanics*, 857:469–507, 2018.

[100] J. Sharma and U. Gupta. Nanofluid convection under Hall currents and LTNE effects. *Materials Today: Proceedings*, 26:3369–3377, 2020.

[101] L. Shi, Y Li, and E. E. Zhang. A new approach for density contrast interface inversion based on the parabolic density function in the frequency domain. *J. Appl. Geophys*, 116:1–9, 2015.

[102] I. S. Shivakumara, A. L. Mamatha, and M. Ravisha. Effects of variable viscosity and density maximum on the onset of Darcy-Bénard convection using a thermal nonequilibrium model. *Journal of Porous Media*, 13(7):613–622, 2010.

[103] A. J. Shneiderov. The exponential law of gravitation and its effects on seismological and tectonic phenomena: a preliminary expositi. *Eos Transac. Am. Geophys. Union.*, 24(1):61–88, 1943.

[104] H. B. Squire. On the stability for three-dimensional disturbances of viscous fluid flow between parallel walls. *Proceedings of the Royal Society of London. Series A, Containing Papers of a Mathematical and Physical Character*, 142(847):621–628, 1933.

[105] L. Storesletten and A. Barletta. Linear instability of mixed convection of cold water in a porous layer induced by viscous dissipation. *International Journal of Thermal Sciences*, 48(4):655–664, 2009.

[106] B. Straughan. Convection in a variable gravity field. *Journal of Mathematical Analysis and Applications*, 140(2):467–475, 1989.

[107] B. Straughan. Global nonlinear stability in porous convection with a thermal nonequilibrium model. *Proceedings of the Royal Society A: Mathematical, Physical and Engineering Sciences*, 462(2066):409–418, 2006.

[108] B. Straughan. *Convection with Local Thermal Non-Equilibrium and Microfluidic Effects*, volume 32. Springer, Switzerland, 2015.

[109] F. M. Sutton. Onset of convection in a porous channel with net through flow. *Physics of Fluids*, 13(8):1931–1934, 1970.

[110] B. D. Tapley, S. Bettadpur, J. C. Ries, P. F. Thompson, and M. M. Watkins. GRACE measurements of mass variability in the Earth system. *Science*, 305(5683):503–505, 2004.

[111] R. K. Tiwari and M. K. Das. Heat transfer augmentation in a two-sided lid-driven differentially heated square cavity utilizing nanofluids. *International Journal of Heat and Mass Transfer*, 50:2002–2018, 2007.

[112] D. J. Tritton. *Physical Fluid Dynamics*. Van Nostrand Reinhold(U.K.) Co.Ltd, England, 1985.

[113] D. L. Turcotte, A. T. Hsui, K. E. Torrance, and G. Schubert. Influence of viscous dissipation on Bénard convection. *Journal of Fluid Mechanics*, 64(2):369–374, 1974.

[114] D. Y. Tzou. Instability of nanofluids in natural convection. *Journal of Heat Transfer*, 130(7):072401, 2008.

[115] D. Y. Tzou. Thermal instability of nanofluids in natural convection. *International Journal of Heat and Mass Transfer*, 51(11-12):2967–2979, 2008.

[116] J. C. Umavathi, M. A. Sheremet, O. Ojjela, and G. J. Reddy. The onset of double-diffusive convection in a nanofluid saturated porous layer: Cross-diffusion effects. *European Journal of Mechanics-B/Fluids*, 65:70–87, 2017.

[117] P. Vadasz. Heat conduction in nanofluid suspensions. *ASME Journal of Heat Transfer*, 128:465–477, 2006.

[118] K Vafai. *Handbook of Porous Media*. CRC Press, 2015.

[119] R. K. Vanishree. Effects of through-flow and internal heat generation on a thermo convective instability in an anisotropic porous medium. *Journal of Applied Fluid Mechanics*, 7(4):581–590, 2014.

[120] C. Visweswara Rao, V. Chakravarthi, and M. L. Raju. Forward modeling: gravity anomalies of two-dimensional bodies of arbitrary shape with hyperbolic and parabolic density functions. *Comput. Geosci.*, 20(5):873–880, 1994.

[121] S. Wang and W. Tan. The onset of Darcy–Brinkman thermosolutal convection in a horizontal porous media. *Physics Letters A*, 373(7):776–780, 2009.

[122] R. A. Wooding. Rayleigh instability of a thermal boundary layer in flow through a porous medium. *Journal of Fluid Mechanics*, 9(2):183–192, 1960.

[123] D. Yadav. Numerical investigation of the combined impact of variable gravity field and throughflow on the onset of convective motion in a porous medium layer. *International Communications in Heat and Mass Transfer*, 108:104274, 2019.

[124] D. Yadav. Effects of rotation and varying gravity on the onset of convection in a porous medium layer: a numerical study. *World Journal of Engineering*, 17(6):785–793, 2020.

[125] D. Yadav. Numerical examination of the thermal instability in an anisotropic porous medium layer subjected to rotation and variable gravity field. *Special Topics & Reviews in Porous Media: An International Journal*, 11(4):395–407, 2020.

[126] D. Yadav, R. Bhargava, and G. S. Agrawal. Boundary and internal heat source effects on the onset of Darcy–Brinkman convection in a porous layer saturated by nanofluid. *International Journal of Thermal Sciences*, 60:244–254, 2012.

[127] D. Yadav, R. Bhargava, and G. S. Agrawal. Thermal instability in a nanofluid layer with a vertical magnetic field. *Journal of Engineering Mathematics*, 80(1):147–164, 2013.

[128] D. Yadav, D. Lee, H.-H. Cho, and J. Lee. The onset of double-diffusive nanofluid convection in a rotating porous medium layer with thermal conductivity and viscosity variation: a revised model. *Journal of Porous Media*, 19(1):31–46, 2016.